Input and State Estimation for Discrete-Time Linear Systems with Application to Target Tracking and Fault Detection

by

Ahmad A. Ansari

A dissertation submitted in partial fulfillment
of the requirements for the degree of
Doctor of Philosophy
(Aerospace Engineering)
in The University of Michigan
2018

Doctoral Committee:

Professor Dennis S. Bernstein, Chair
Professor Ella M. Atkins
Assistant Professor Alex Gorodetsky
Professor Jeff Stein

Ahmad A. Ansari
ansahmad@umich.edu
ORCID ID: 0000-0002-9011-7901

To my parents and fiancée Naureen

ACKNOWLEDGEMENTS

First of all, I would like to thank my advisor, Professor Dennis S. Bernstein for all of his guidance and support during the past five years. His helpful advises, discussions, comments, and critiques have greatly improved this work. Also, I would like to thank my committee members Professor Ella M. Atkins, Professor Jeff Stein, and Professor Alex Gorodetsky for their helpful comments and suggestions. I am grateful for all the hard work of the professors at the University of Michigan, that helped me along the way in graduate school.

Next, I would like to thank Mr. Khawar M. Butt, Chairman English Biscuit Manufacturers, Pakistan, for his support and helpful discussions. I'd also like to appreciate my friends and colleagues at the University of Michigan: Pedro Di Donato, Khaled Aljanaideh, Yousaf Rahman, Ankit Goel, Yasir Ahmed, Akbar Ali, Alauddin Ahmed, Evan Hilgemann, Nitika Yadav, Ray Yu, Antai Xie, Shicong Dai, Syed Aseem Ul Islam, Robert Zidek, Sweewarman Balachandran, Wei Ding, Gianluca Kapiris, Christian Spiess, Ningyuan Zhang, Alireza Nafari, Nouman Khan, Muhammad Abdullah.

Finally, I would like to thank my family. Very special thanks goes to my parents for their love, support, and encouragement. My fiancée Naureen for her love, patience, and support. Without her, this dissertation would not be a possibility. My siblings Muhammad Ali, Madiha Hassan, and Maliha Hassan. My fiancée parents, and her sisters Ambereen Khattak and Uswa Khattak. I am very grateful for the love and support I am surrounded by from all of you.

TABLE OF CONTENTS

LIST OF FIGURES

Figure

LIST OF TABLES

Table

LIST OF APPENDICES

Appendix

ABSTRACT

This dissertation first presents a deterministic treatment of discrete-time input reconstruction and state estimation without assuming the existence of a full-rank Markov parameter. Algorithms based on the generalized inverse of a block-Toeplitz matrix are given for 1) input reconstruction in the case where the initial state is known; 2) state estimation in the case where the initial state is unknown, the system has no invariant zeros, and the input is unknown; and 3) input reconstruction and state estimation in the case where the initial state is unknown and the system has no invariant zeros. In all cases, the unknown input is an arbitrary deterministic or stochastic signal. In addition, the reconstruction/estimation algorithm is deadbeat, which means that, in the absence of sensor noise, exact input reconstruction and state estimation are achieved in a finite number of steps.

Next, asymptotic input and state estimation for systems with invariant zeros is considered. Although this problem has been widely studied, existing techniques are confined to the case where the system is minimum phase. This dissertation presents retrospective cost input estimation (RCIE), which is based on retrospective cost optimization. It is shown that RCIE automatically develops an internal model of the unknown input. This internal model provides an asymptotic estimate of the unknown input regardless of the location of the zeros of the plant, including the case of nonminimum-phase dynamics.

The input and state estimation method developed in this dissertation provides a novel approach to a longstanding problem in target tracking, namely, estimation of the inertial acceleration of a body using only position measurements. It turns out

that, for this problem, the discretized kinematics have invariant zeros on the unit circle, and thus the dynamics is nonminimum-phase. Using optical position data for a UAV, RCIE estimates the inertial acceleration, which is modeled as an unknown input. The acceleration estimates are compared to IMU data from onboard sensors.

Finally, based on exact kinematic models for input and state estimation, this dissertation presents a method for detecting sensor faults. A numerical investigation using the NASA Generic Transport Model shows that the method can detect stuck, bias, drift, and deadzone sensor faults. Furthermore, a laboratory experiment shows that RCIE can estimate the inertial acceleration (3-axis accelerometer measurements) and angular velocity (3-axis rate-gyro measurements) of a quadrotor using vision data; comparing these estimates to the actual accelerometer and rate-gyro measurements provide the means for assessing the health of the accelerometer and rate gyro.

CHAPTER 1

Introduction

1.1 What is Input Reconstruction?

State estimation uses measurements of the output of a system to produce statistically optimal estimates of the states of the system [1–3]. These estimates assume that the exogenous input consists of a known deterministic component, which is replicated in the estimator, and an unknown stochastic disturbance, which is assumed to be white and zero mean. If the deterministic input is unknown, then it cannot be replicated in the observer, and thus the state estimates may be biased. To remedy this problem, state estimators have been developed to provide unbiased state estimates in the presence of unknown, deterministic inputs [4–8].

An alternative approach is to extend state estimation to include input estimation, where the goal is to estimate the deterministic component of the exogenous input [9–31]. In many applications, knowledge of the input signal is of independent interest and, in some cases, may be of greater interest than the estimates of the states [32]. The terminology *input reconstruction* is used in the case of deterministic analysis, just as an observer is the deterministic analogue of an estimator.

In light of state estimation, which assumes a known deterministic input and an unknown zero-mean stochastic input, it may be somewhat surprising that it is indeed possible to estimate not only the states but also, in many cases, the unknown

deterministic input. The benefit of state and input estimation is the fact that the deterministic component can often vastly improve the accuracy of the state estimates. To illustrate this point, consider the mass-spring-damper system shown in Figure 1.1, where $m_1 = m_2 = 1$ kg, $k_1 = k_2 = 10$ N/m, and $c_1 = c_2 = 5$ kg/sec, and the sample time is $T_s = 0.1$ sec. The position and velocity of m_1 are measured, and the position and velocity of m_2 are estimated using the Kalman filter in the case where d is unknown. The signal-to-noise-ratio for both measurements is 25 dB. Alternatively, Theorem 4 in Section 3.6 is applied to this problem, and the estimated input is replicated in the Kalman filter. Figure 1.2 shows that the estimates of the position and velocity of m_2 are significantly more accurate in the case where the estimated input is used.

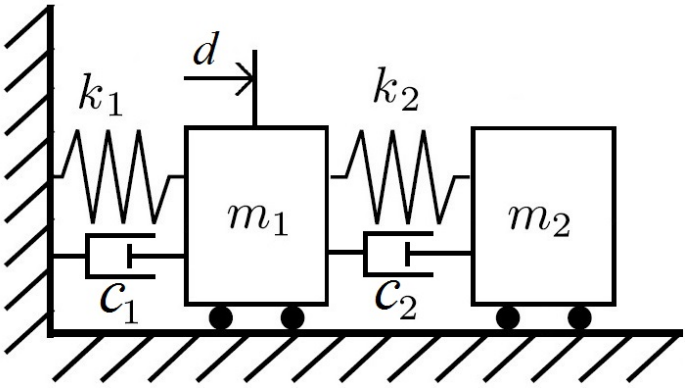

Figure 1.1: Mass-spring-damper system, where d is the unknown input force.

1.2 Deadbeat Input Reconstruction and State Estimation

Input reconstruction without assuming the existence of a full-column-rank Markov parameter is considered in this dissertation. In [17, 29] it is assumed that the first Markov parameter H_1 has full column rank, which implies that the plant has relative degree 1. Likewise, the approach of [24] is limited to the case where at least one Markov parameter has full column rank. A more general case where no Markov

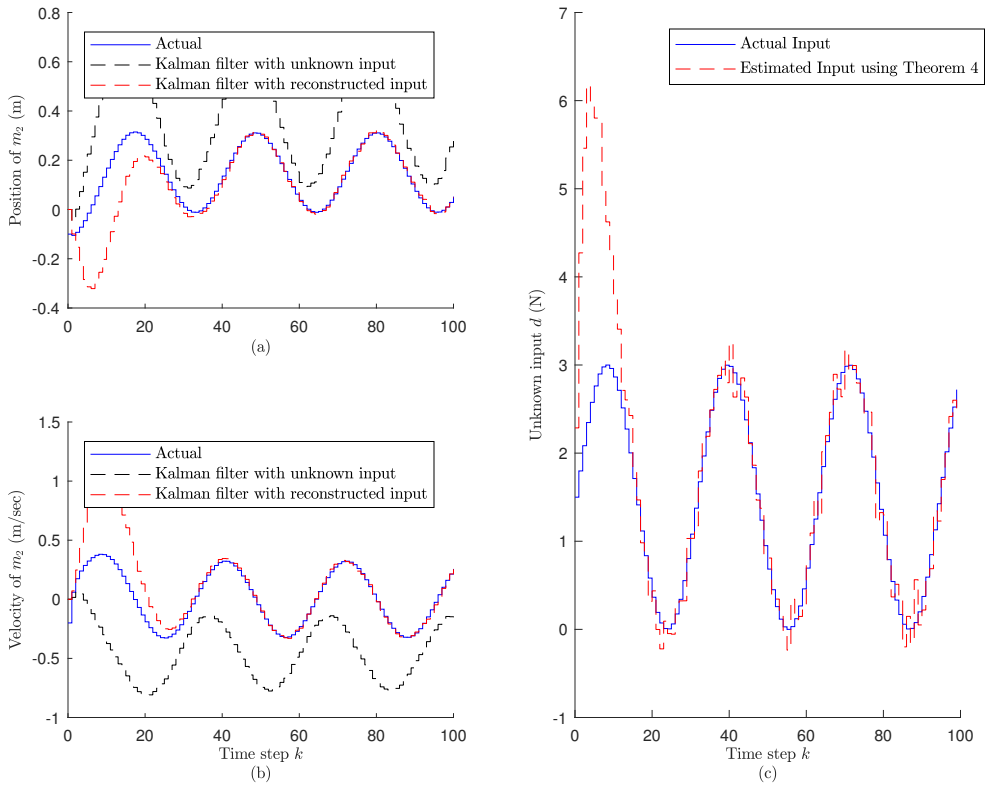

Figure 1.2: (a) and (b) show that the accuracy of the state estimates is enhanced by replicating the estimated input in the estimator. After 15 steps, (c) shows that the estimated input is close to the actual input.

parameter is required to have full column rank is considered in this work.

In addition to considering a more general case, this dissertation presents a simplified input reconstruction algorithm as compared to the inversion algorithms given in earlier works. Assuming that the initial condition is known, techniques for constructing system inverses were considered in [9, 33]. These techniques are based on sequential constructive algorithms that entail the decomposition of various matrices until a full-rank condition is attained. For the case of known initial conditions, Theorem 2 provides a simplified input-reconstruction algorithm with a delay of η steps, where η is defined in [9] and further studied in [11]. The input observer given by Theorem 2 is deadbeat in the sense that exact input reconstruction is achieved in η steps,

and the number of required measurements is $\eta+1$. Deadbeat estimation is considered in [34]. Since the initial condition is known, the input reconstruction algorithm given by Theorem 2 is applicable whether or not the system has any invariant zeros.

Next, this dissertation considers deadbeat input reconstruction and state estimation algorithms without assuming that the initial condition is known. In this case, the presence of an invariant zero makes it impossible to distinguish the zero input with zero initial condition from a nonzero input with a specific initial condition that yields zero response. This case is considered in [13], where an algorithm is given for constructing an input-reconstruction filter. Although zeros are not explicitly mentioned in [13], the assumption that u is observable rules out the presence of invariant zeros. For the case where $x(0)$ is unknown and (A, B, C, D) has no invariant zeros, Theorem 3 provides a deadbeat state-estimation algorithm despite the presence of an unknown, arbitrary input. Although this performance is better than the Kalman filter in the absence of sensor noise, it has to be kept in mind that the estimates are obtained with a delay, which means that the estimator is effectively a smoother. The estimation delay is given by the integer μ, which is guaranteed to be finite, and the number of required measurements is $\mu + 1$. Furthermore, for the case where η is finite, $x(0)$ is unknown, and (A, B, C, D) has no invariant zeros, Theorem 4 provides a deadbeat input-reconstruction and state-estimation algorithm. In this case, the input reconstruction delay is η, and the number of required measurements is $\max\{\mu, \eta\} + 1$.

Theorems 2, 3, and 4 are each given in terms of the generalized inverse of a block-Toeplitz matrix. This unified formulation provides a direct and simplified presentation of all three results. However, these input-reconstruction and state-estimation algorithms are not given in the form of linear time-invariant (LTI) systems. Consequently, Theorem 3 and Theorem 4 are recast in terms of LTI deadbeat systems for input reconstruction and state estimation. Theorem 2 can be recast in a similar manner, but is awkward due to the need to propagate the free response, and thus an LTI version

is not given.

The assumption invoked in Theorems 3 and 4 that the system has no invariant zeros is clearly restrictive in the SISO case, since it is unusual for an nth-order SISO system to have relative degree n. Furthermore, since the transmission zeros of a square MIMO transfer function with full normal rank are the roots of the numerator of the determinant, it would be unusual for the system to have no transmission zeros. The situation is different, however, for rectangular systems. For example, a MIMO system with two inputs and four outputs and full normal rank possesses a transmission zero if and only if all six 2×2 embedded transfer functions possess a common transmission zero. Consequently, input reconstruction based on Theorem 4 may be useful for a large class of rectangular systems.

1.3 Input Estimation for Nonminimum-Phase Systems

Deadbeat input reconstruction for a system with *any* zeros is impossible. This can easily be seen by noting that the presence of an invariant zero implies the existence of an initial condition and input for which the output is identically zero. These details are related to the *unobservable input subspace* [24] Hence, in the case where the system has one or more invariant zeros, asymptotic input reconstruction of the component of the input that resides in the orthogonal complement of the unobservable input subspace must be considered, with careful attention paid to the presence of nonmimimum-phase zeros.

Most of the techniques for state and input estimation [12, 14–31, 35–39] are confined to minimum-phase systems, that is, systems with invariant zeros contained in the open unit disk. In particular, the approach of [29], which extends the method of [17], explicitly invokes a minimum-phase assumption.

The case of nonminimum-phase (NMP) zeros, that is, zeros that are either on the unit circle or outside the closed unit disk, is much more challenging. As shown

in [24], a naive attempt to estimate the input for a NMP system with zeros outside the closed unit disk yields a reconstruction error that is unbounded; in the case of zeros on the unit circle, the input-reconstruction error is bounded but nonzero. In contrast, in the case of minimum-phase systems, the input-reconstruction error vanishes asymptotically. Unlike most of the references cited above, [39] considers the case of NMP zeros, but the method is not applicable to the case of zeros on the unit circle.

This dissertation aims at the case where the system is NMP. In particular, this dissertation considers state and input estimation based on retrospective cost optimization [38, 40–46]. Based on this technique, the dissertation develops retrospective cost input estimation (RCIE), which is a technique for state and input estimation that is effective for NMP systems. This approach uses an estimator whose coefficients are recursively updated at each time step so as to minimize a retrospective cost function. Motivation for this approach is discussed within the context of adaptive control in [47–54].

1.4 Target Tracking

The input estimation method developed in this dissertation provides a novel approach to a longstanding problem in target tracking, namely, estimation of the inertial acceleration of a body using only position measurements. This problem is motivated by the need to estimate acceleration in order to predict future motion and distinguish ballistic vehicles from maneuvering vehicles. The extensive literature and diverse methods developed for this problem attests to its importance [20, 41, 55–60]. It turns out that, for this problem, the discretized kinematics have invariant zeros on the unit circle, and thus the approach of [39] is not applicable. A more restricted version of RCIE confined to LTI systems is applied to this problem for planar target tracking in [43]. The approach of [43], however, is not applicable to LTV systems, such as the

kinematics of a 3D maneuvering vehicle resolved in the body frame. In addition, [43] does not recognize or address the NMP features of the problem.

1.5 Sensor Fault Detection

Sensor health is crucial to the operation of every feedback control system. Consequently, extensive research has been devoted to developing techniques for detecting and diagnosing sensor faults [61–70]. One approach is to search for anomalies in the sensor signal [67], while another approach is to compute sensor residuals based on the assumed model and measured input signals [61]. Yet another approach is to empirically identify transmissibilities between pairs of sensors under healthy conditions and then use these relations during subsequent operation to compute sensor residuals [71].

This dissertation formulates the problem of diagnosing sensor faults for a flight vehicle as a problem of input and state estimation. In particular, an exact model of the kinematics of the vehicle is considered, which circumvents the need to measure forces and moments on the vehicle as well as the need to know the vehicle inertia and stability derivatives. Instead, the kinematics model views suspect sensor-measurement as the input or state. A related formulation is considered in [44, 45, 70]. It turns out, that the kinematics based models can be nonlinear, and thus, this dissertation extends the approach in [72] to nonlinear systems by combining the unscented Kalman filter [73, 74] and retrospective cost input estimation [38, 44, 72].

To detect sensor faults using state and input estimation techniques, this dissertation uses combinations of inertial and aerodynamic sensors. This work is motivated by [68, 70], which uses rate-gyro, accelerometer, GPS, angle-of-attack, and sideslip measurements to estimate forward velocity relative to the air in order to assess the health of the pitot tube. This dissertation extends the approach of [68, 70] in several ways. First, for pitot-tube fault detection, this work apply the unscented Kalman

filter with augmented bias states in order to deal with biased accelerometer measurements. Unlike [68, 70], this work does not use GPS to assess the health of the pitot tube. Next, four scenarios that are not considered in [68, 70] are addressed by this work, two of which depends on state estimation and the other two on input estimation.

In the first scenario, the pitot tube, rate gyros, accelerometers, α-sensor, and β-sensor are used to assess the health of the vertical gyros. In the second scenario, the pitot tube, vertical gyro, rate gyros, accelerometers, and β-sensor are used to assess the health of the α-sensor. In the third scenario, the pitot tube, rate gyros, vertical gyro, α-sensor, and β-sensor are used to assess the health of the accelerometers. In the fourth scenario, vertical gyro and magnetometer are used to assess the health of the rate gyros. For input estimation in the third and fourth scenarios, a variation of retrospective cost input estimation is used as described in [45, 72].

1.6 Contributions

Tables 1.1 and 1.2 summarize the various cases that can occur in the context of input and state estimation, the relevant literature in each case, and the contribution (highlighted in blue) of this dissertation.

Table 1.3 summarizes the sensor fault detection cases considered in this dissertation. The table lists the suspect sensors as well as the sensors used for diagnosing faults. The last column of the table gives the method used for diagnosing sensor faults, distinguishing between cases of state estimation alone or combined input and state estimation.

$x(0)$ \ u	**Known**	**Unknown**
Known	N/A	[9–11] • defines the inherent delay η for system inversion • gives necessary and sufficient conditions for existence of η • gives bounds on η • allows rank-deficient Markov parameters Theorem 2 • deadbeat FIR filter for input reconstruction • the inherent delay is η • requires $\eta + 1$ measurements • allows invariant zeros and rank-deficient Markov parameters
Unknown	Equation (3.8)	See Table 1.2

Table 1.1: State estimation and input reconstruction with known or unknown $x(0)$.

1.7 Publications

The following is the list of publications relevant to the research presented in this dissertation.

1.7.1 Journal Articles

- Ahmad Ansari and Dennis Bernstein, "Input Estimation for Nonminimum-Phase Systems with Application to Acceleration Estimation for a Maneuvering Vehicle", *IEEE Transactions on Control System Technology*, 2018 March 6.

- Ahmad Ansari and Dennis Bernstein, "Deadbeat State Estimation and Input Reconstruction for Discrete-Time Linear Systems", *Automatica*, under review.

- Ahmad Ansari and Dennis Bernstein, "Aircraft Sensor Fault Diagnosis Using Combined Input and State Estimation", *Journal of Guidance, Control, and Dynamics*, under review.

	Asymptotic Estimation	Deadbeat Estimation
State Estimation	[5] • unbiased minimum variance filter • assumes that H_1 has full column rank • allows minimum-phase zeros	Theorem 3 • deadbeat FIR filter for state estimation • the inherent delay is μ • requires $\mu + 1$ measurements • allows rank-deficient Markov parameters • assumes no invariant zeros
State and Input Estimation	[17, 29] • unbiased minimum variance filter • assumes that H_1 has full column rank • allows minimum-phase zeros [75, 76] • unbiased minimum variance filter with a delay • H_1 need not have full column rank • allows minimum-phase zeros [77] • reduced-order state observers • allows rank-deficient Markov parameters • allows minimum-phase zeros Retrospective Cost Input Estimation • modified Kalman filter with adaptive input estimation • allows rank-deficient Markov parameters • allows zeros at any location	Theorem 4 • deadbeat FIR filter for input reconstruction • the inherent delay is η • requires $\max(\eta, \mu) + 1$ measurements • allows rank-deficient Markov parameters • assumes no invariant zeros

Table 1.2: State estimation and input reconstruction with unknown $x(0)$.

1.7.2 Peer–reviewed Conference Papers

- Ahmad Ansari and Dennis Bernstein, "Satellite Drag Estimation Using Retrospective Cost Input Estimation", *57th IEEE Conference on Decision and Control*, Miami, FL, 2018, under review.

- Ahmad Ansari and Dennis Bernstein, "Estimation of Angular Velocity and Rate-Gyro Noise for Sensor Health Monitoring", *Proceedings of American Control Conference*, pp. 1159-1164, Seattle, 2017.

- Ahmad Ansari and Dennis Bernstein, "Adaptive Input Estimation for Nonminimum-Phase Discrete-Time Systems", *55th IEEE Conference on Decision and Control*, pp. 1159-1164, Las Vegas, 2016.

Faulty Sensors \ Sensors Used	Pitot Tube	Vertical Gyro	α Sensor	3-axis Acceler–ometer	3-axis Rate-Gyro	β Sensor	Method
Pitot Tube		✓	✓	✓	✓	✓	UKF
Vertical Gyro	✓		✓	✓	✓	✓	UKF
α Sensor	✓	✓		✓	✓	✓	UKF
3-axis Accelerometer	✓	✓	✓		✓	✓	ERCIE with UKF
3-axis Rate-Gyro		✓ with Ψ sensor					ERCIE with UKF

Table 1.3: Sensor fault detection cases considered in this dissertation.

- Ahmad Ansari and Dennis Bernstein, "Aircraft Sensor Fault Detection Using State and Input Estimation", *Proceedings of American Control Conference*, pp. 5951-5956, Boston, 2016.

1.8 Dissertation Outline

This dissertation is organized as follows.

Chapter 2 Summary

Chapter 2 first presents the problem of input reconstruction for a discrete-time linear system. Next, it defines *input and initial state observable* (IISO) systems, and then gives Proposition 2 which links IISO with the left invertibility of a matrix consisting of system matrices. Next, it provides Proposition 3 which shows that if the system has at least one invariant zero then the system is not IISO. Finally, it gives necessary and sufficient conditions (Theorem 1) for a system to be IISO.

Chapter 3 Summary

Chapter 3 first gives preliminaries on the invertibility of a linear system with an input reconstruction delay η. Next, it provides Theorem 2 for η-delay input reconstruction with known $x(0)$. Next, it gives Theorems 3 and 4 for μ-delay state estimation and η-delay input reconstruction, respectively. Next, it investigates the effect of disturbance and sensor noise on the reconstructed input. Then, it shows that Theorem 4 yields an unbiased input estimator. Finally, it gives Theorem 5 for deadbeat input and state estimation for linear time-varying systems.

Chapter 4 Summary

Chapter 4 first numerically investigates the effect of invariant zeros either inside or outside the unit circle on the projected input sequence onto the orthogonal complement of unobservable input subspace. Then, using the projection, it gives Property 4.1 for asymptotic input estimation, and demonstrates it numerically in Example 4.4.1. Proof of this property is outside the scope of this dissertation.

Chapter 5 Summary

Chapter 5 introduces state and input estimation problem along with the retrospective cost input estimation (RCIE) algorithm. Next, it gives the details of the input-estimation subsystem. Then, it shows how RCIE can asymptotically reconstruct an unknown input to NMP systems by embedding an internal model of the unknown input in the input-estimation subsystem. Then, it numerically illustrates the effect of the unobservable input subspace on RCIE estimates. Finally, it compares RCIE with the filter presented in [29].

Chapter 6 Summary

Chapter 6, based on kinematics, formulates state-space models for acceleration estimation. Then, it describes an experimental setup, and then presents the application of RCIE to estimation of inertial acceleration. Using optical position data for a UAV, RCIE estimates the inertial acceleration, which is modeled as an unknown input. The acceleration estimates are compared to IMU data from onboard sensors.

Chapter 7 Summary

Chapter 7 focuses on the problem of drag estimation of a satellite without assuming knowledge of the nominal orbit of the satellite. The contribution of this chapter is the novel application of input estimation to the problem of estimating drag acceleration. The approach used in this chapter is based on the retrospective cost optimization.

Chapter 8 Summary

Chapter 8 formulates the problem of diagnosing sensor faults for a flight vehicle as a problem of input and state estimation. In particular, it considers an exact model of the kinematics of the vehicle, which circumvents the need to measure forces and moments on the vehicle as well as the need to know the vehicle inertia and stability derivatives. Instead, the kinematics model views suspect sensor-measurement as the input or state. To detect sensor faults using state and input estimation techniques, Chapter 8 uses combinations of inertial and aerodynamic sensors. Various sensor faults are considered, including stuck, bias, drift, and deadzone sensor faults.

Finally, conclusions and future work are presented in Chapter 9.

CHAPTER 2

Input and Initial-State Observability

2.1 Introduction

State estimation uses measurements of the output of a system to produce statistically optimal estimates of the states of the system [1–3]. It is well known that an asymptotic estimator design is possible, if and only if, the underlying system is *observable* or *stabilizable* [3, 78]. A notion similar to *observabiliy*, called as *input and initial-state observability*, is developed in this chapter for systems with unknown input and initial state.

The contents of this chapter are as follows. First, we present the problem of input reconstruction for a discrete-time linear system. Next, we define *input and initial state observable* (IISO) systems, and then give Proposition 2 which links IISO with the left invertibility of a matrix consisting of system matrices. Next, we provide Proposition 3 which shows that if the system has at least one invariant zero then the system is not IISO. Finally, we give necessary and sufficient conditions (Theorem 1) for a system to be IISO.

2.2 Problem Statement

Let $A \in \mathbb{R}^{l_x \times l_x}$, $G \in \mathbb{R}^{l_x \times l_d}$, and $C \in \mathbb{R}^{l_y \times l_x}$, assume that (A, G, C) is minimal, and consider

$$x(k) = Ax(k-1) + Gd(k-1), \tag{2.1}$$

$$y(k) = Cx(k), \tag{2.2}$$

where, for all $k \geq 0$, $x(k) \in \mathbb{R}^{l_x}$, $d(k) \in \mathbb{R}^{l_d}$, and $y(k) \in \mathbb{R}^{l_y}$, The goal is to develop necessary and sufficient conditions on the system [(2.1), (2.2)] such that the knowledge of $y(k)$ uniquely determines the unknown input $d(k)$.

2.3 Analysis of the Output Measurement Equation

Let r denote a positive integer, and define

$$\mathcal{Y}_r \triangleq \begin{bmatrix} y(0) \\ y(1) \\ \vdots \\ y(r) \end{bmatrix} \in \mathbb{R}^{(r+1)l_y}, \; \mathcal{D}_r \triangleq \begin{bmatrix} d(0) \\ d(1) \\ \vdots \\ d(r) \end{bmatrix} \in \mathbb{R}^{(r+1)l_d}, \; \Gamma_r \triangleq \begin{bmatrix} C \\ CA \\ \vdots \\ CA^r \end{bmatrix} \in \mathbb{R}^{(r+1)l_y \times l_x}, \tag{2.3}$$

$$M_r \triangleq \begin{bmatrix} 0 & 0 & \cdots & 0 \\ CG & 0 & \cdots & 0 \\ CAG & CG & \cdots & 0 \\ \vdots & \vdots & \ddots & \vdots \\ CA^{r-1}G & CA^{r-2}G & \cdots & CG \end{bmatrix} \in \mathbb{R}^{(r+1)l_y \times rl_d}. \tag{2.4}$$

It follows from (2.1), (2.2) that

$$\mathcal{Y}_r = \Gamma_r x(0) + M_r \mathcal{D}_{r-1} = \Psi_r \begin{bmatrix} x(0) \\ \mathcal{D}_{r-1} \end{bmatrix}, \tag{2.5}$$

where

$$\Psi_r \stackrel{\triangle}{=} \begin{bmatrix} \Gamma_r & M_r \end{bmatrix} \in \mathbb{R}^{(r+1)l_y \times (l_x + rl_d)}. \tag{2.6}$$

The existence of an initial state $x(0)$ and input sequence $\mathcal{D}_{r-1}$ satisfying (2.5) is guaranteed by [(2.1),(2.2)]. For exact input reconstruction, uniqueness is required. Note that $x(0)$ and $\mathcal{D}_{r-1}$ satisfying (2.5) are unique if and only if Ψ_r has full column rank. Suppose that $l_y \leq l_d$. Then, for all $r \geq 1$, if Ψ_r has full column rank, then $l_x \leq l_y$. In practice, $l_y < l_x$, and thus $l_y \leq l_d$ precludes exact input reconstruction. In particular, exact input reconstruction is not possible in the SISO case $l_y = l_d = 1$. For the remainder of this chapter, we assume that $l_d < l_y < l_x$. Consequently, (A, G, C) represents a tall system.

In the special case where $x(0)$ is known, the situation is greatly simplified. For example, if CG has full column rank and $x(0) = 0$, then, since, for all $r \geq 1$, M_r is left invertible, $\mathcal{D}_{r-1}$ can be exactly reconstructed.

Note that there exists $r \geq 1$ such that Γ_r has full column rank if and only if (A, C) is observable. Furthermore, for all $r \geq 1$, M_r has full column rank if and only if CG has full column rank.

2.4 Input and Initial-State Observable (IISO) Systems

Now define the positive integer

$$r_0 \stackrel{\triangle}{=} \left\lceil \frac{l_x - l_y}{l_y - l_d} \right\rceil, \tag{2.7}$$

where $\lceil a \rceil$ denotes the smallest integer greater than or equal to a. Note that $1 \leq r_0 \leq l_x - 1$.

Proposition 1. The following statements are equivalent:

i) There exists $r \geq 1$ such that Ψ_r has full column rank.

ii) For all $r \geq r_0$, Ψ_r has full column rank.

Proof. This is a restatement of the equivalence of statements 3) and 4) of Theorem 2.1 of [22]. □

Definition 1. [(2.1),(2.2)] is input and initial state observable (IISO) if *i*) and *ii*) of Proposition 1 hold.

Proposition 2. [(2.1),(2.2)] is IISO if and only if, for all $r \geq r_0$, Ψ_r is left invertible.

If (A, G, C) is IISO, then Proposition 2 implies that, for all $r \geq r_0$, Ψ_r is left invertible. It thus follows that, for all $r \geq r_0$,

$$\begin{bmatrix} x(0) \\ \mathcal{D}_{r-1} \end{bmatrix} = \Psi_r^+ \mathcal{Y}_r, \tag{2.8}$$

where the generalized inverse Ψ_r^+ of Ψ_r is a left inverse of Ψ_r.

2.5 Effect of an Invariant Zero on Input and Initial-State Observability

Definition 2. For all $\mathrm{z} \in \mathbb{C}$, define $\mathcal{Z} \in \mathbb{R}^{(l_x+l_y)\times(l_x+l_d)}[\mathrm{z}]$ by

$$\mathcal{Z}(\mathrm{z}) \triangleq \begin{bmatrix} \mathrm{z}I - A & -G \\ C & 0 \end{bmatrix}. \tag{2.9}$$

Then $\xi \in \mathbb{C}$ is an *invariant zero* of [(2.1),(2.2)] if

$$\mathrm{rank}\mathcal{Z}(\xi) < \mathrm{normal\,rank}\,\mathcal{Z}. \tag{2.10}$$

Since $l_d < l_y$, $\mathcal{Z}(\mathrm{z})$ is a tall matrix. Proposition 12.10.3 in [79, p. 817] states that

$$\mathrm{normal\,rank}\,\mathcal{Z} = l_x + \mathrm{normal\,rank}\,\mathcal{G}, \tag{2.11}$$

where $\mathcal{G}(\mathrm{z}) \triangleq C(\mathrm{z}I - A)^{-1}G \in \mathbb{R}^{l_y \times l_d}(\mathrm{z})$ is also a tall matrix. To avoid the degenerate case of redundant inputs, we assume henceforth that $\mathrm{normal\,rank}\,\mathcal{G} = l_d$. Therefore, $\xi \in \mathbb{C}$ is an invariant zero of [(2.1),(2.2)] if and only if $\mathrm{rank}\mathcal{Z}(\xi) < l_x + l_d$.

Definition 3. Let $r \geq 1$. Then the input sequence $\mathcal{D}_{r-1} \in \mathbb{R}^{rl_d}$ is unobservable if it is nonzero and there exists an initial state $x(0) \in \mathbb{R}^n$ such that $\begin{bmatrix} x(0) \\ \mathcal{D}_{r-1} \end{bmatrix} \in \mathcal{N}(\Psi_r)$.

The following result shows that, if [(2.1),(2.2)] has an invariant zero, then [(2.1),(2.2)] is not IISO. This result is the contrapositive of (ii) $\Rightarrow$ (i) of Theorem 6.1 of [22] along with an explicit expression for the unobservable input sequence and the cor-

responding initial state. Note that the assumption that the possibly complex vector $\begin{bmatrix} \bar{x} \\ \bar{d} \end{bmatrix} \in \mathcal{N}(\mathcal{Z}(\xi))$ has nonzero real part entails no loss of generality since otherwise $\bar{x}$ and $\bar{d}$ could be replaced by $\jmath\bar{x}$ and $\jmath\bar{d}$, respectively. In the case where $\xi = 0$ and $k = 0$, ξ^k is interpreted as 1.

Proposition 3. Assume that (A, G, C) has an invariant zero $\xi \in \mathbb{C}$, let $\begin{bmatrix} \bar{x} \\ \bar{d} \end{bmatrix} \in \mathcal{N}(\mathcal{Z}(\xi))$ be nonzero with nonzero real part, define the initial state

$$x(0) \stackrel{\triangle}{=} \mathrm{Re}(\bar{x}), \tag{2.12}$$

and, for all $k \geq 0$, define the input sequence

$$d(k) \stackrel{\triangle}{=} \mathrm{Re}(\xi^k \bar{d}). \tag{2.13}$$

Then, for all $r \geq 1$, $\begin{bmatrix} x(0)^{\mathrm{T}} & \mathcal{D}_{r-1}^{\mathrm{T}} \end{bmatrix}^{\mathrm{T}} \in \mathcal{N}(\Psi_r)$, and thus [(2.1),(2.2)] is not IISO.

Proof. By assumption,

$$\begin{bmatrix} \xi I - A & -G \\ C & 0 \end{bmatrix} \begin{bmatrix} \bar{x} \\ \bar{d} \end{bmatrix} = 0, \tag{2.14}$$

and thus

$$(\xi I - A)\bar{x} = G\bar{d}. \tag{2.15}$$

Hence

$$\mathrm{Re}((\xi I - A)\bar{x}) = G\,\mathrm{Re}(\bar{d}). \tag{2.16}$$

Using (2.12), (2.13), and (2.16), it follows from (2.1) that

$$x(1) = A\,\mathrm{Re}(\bar{x}) + \mathrm{Re}(\xi\bar{x}) - A\,\mathrm{Re}(\bar{x}) = \mathrm{Re}(\xi\bar{x}). \tag{2.17}$$

Proceeding similarly, it follows that, for all $k \geq 0$,

$$x(k) = \mathrm{Re}(\xi^k\bar{x}). \tag{2.18}$$

Substituting (2.18) into (2.2) yields, for all $k \geq 0$,

$$y(k) = C\,\mathrm{Re}(\xi^k\bar{x}) = \mathrm{Re}(\xi^k C\bar{x}). \tag{2.19}$$

Since, by (2.14), $C\bar{x} = 0$, (2.19) implies that, for all $k \geq 0$, $y(k) = 0$. Hence, for all $r \geq 0$, $\mathcal{Y}_r = 0$. Note that, since for all $r \geq 0$, $\mathcal{Y}_r = 0$, it follows that $\Psi_r \begin{bmatrix} x(0)^{\mathrm{T}} & \mathcal{D}_{r-1}^{\mathrm{T}} \end{bmatrix}^{\mathrm{T}} = 0$, and thus [(2.1),(2.2)] is not IISO. □

The following result shows that, if [(2.1),(2.2)] has no invariant zeros and CG has full column rank, then [(2.1),(2.2)] is IISO. This result corrects (i) ⇒ (ii) of Theorem 6.1 of [22], which omits the assumption on rankCG.

Let "$\mathcal{R}$" denote range.

Proposition 4. If CG has full column rank and (A, G, C) has no invariant zeros, then [(2.1),(2.2)] is IISO.

Proof. Since (A, G, C) has no invariant zeros, it follows that, for all $\xi \in \mathbb{C}$,

$$\mathrm{rank}\mathcal{Z}(\xi) = l_x + l_d. \tag{2.20}$$

Using (2.20), Theorem A.1 of [24] implies that, there exists $r \geq l_x$ such that

$$\mathcal{R}(\Gamma_r) \cap \mathcal{R}(M_r) = \{0\}. \tag{2.21}$$

Since (A, C) is observable, it follows that

$$\text{rank}\Gamma_r = l_x. \tag{2.22}$$

Furthermore, since CG has full column rank, it follows that

$$\text{rank}M_r = rl_d. \tag{2.23}$$

Using (2.21)–(2.23), Fact 2.11.9 in [79, p. 131] implies that

$$\begin{aligned}
\text{rank}\Psi_r &= \text{rank}\begin{bmatrix}\Gamma_r & M_r\end{bmatrix} \\
&= \text{rank}\Gamma_r + \text{rank}M_r - \dim[\mathcal{R}(\Gamma_r) \cap \mathcal{R}(M_r)] \\
&= \text{rank}\Gamma_r + \text{rank}M_r = l_x + rl_d.
\end{aligned}$$

Therefore, Ψ_r has full column rank. Hence, Proposition 1 implies, that, for all $l \geq r_0$, Ψ_l has full column rank. Proposition 2 thus implies [(2.1),(2.2)] is IISO. □

2.6 Necessary and Sufficient Conditions

The following theorem combines Proposition 3 and Proposition 4 to give necessary and sufficient conditions for [(2.1),(2.2)] to be IISO.

Theorem 1. The following statements are equivalent:

i) CG has full column rank, and (A, G, C) has no invariant zeros.

ii) For all $r \geq r_0$, $\text{rank}\Psi_r = l_x + rl_d$.

Example 2.6.1. Consider [(2.1),(2.2)] with

$$A = \begin{bmatrix} 0.1 & 0.2 & 0.3 \\ 0.4 & 0 & 0 \\ 0 & 0.5 & 0 \end{bmatrix}, G = \begin{bmatrix} 1 \\ 0 \\ 0 \end{bmatrix}, C = \begin{bmatrix} 1 & 3 & 5 \\ 1 & 7 & 9 \end{bmatrix}, \tag{2.24}$$

where $l_d = 1 < l_y = 2 < l_x = 3$. Note that $\text{rank}CG = l_d = 1$ and (A, G, C) has no invariant zeros. Thus, *i*) of Theorem 1 is satisfied. It then follows from *ii*) of Theorem 1 that, for all $r \geq 3$, $\text{rank}\Psi_r = 3 + r$, which can be confirmed numerically. $\diamond$

2.7 Conclusions

This chapter defined and developed theory for input and initial-state observability for systems with no direct feedthrough matrix in (2.2). It is shown that if the system has at least one invariant zero then the system is not IISO. Theorem 1 gives the necessary and sufficient conditions for a system to be IISO.

In the next chapter, we reconsider system [(2.1), (2.2)] but with direct feedthrough matrix. We then provide an algorithm for reconstructing the unknown input and state based on the generalized inverse of a block-Toeplitz matrix.

CHAPTER 3

Deadbeat Input Reconstruction and State Estimation

3.1 Introduction

State estimation uses measurements of the output of a system to produce statistically optimal estimates of the states of the system [1–3]. These estimates assume that the exogenous input consists of a known deterministic component, which is replicated in the estimator, and an unknown stochastic disturbance, which is assumed to be white and zero mean. If the deterministic input is unknown, then it cannot be replicated in the observer, and thus the state estimates may be biased. To remedy this problem, state estimators have been developed to provide unbiased state estimates in the presence of unknown, deterministic inputs [4–8].

An alternative approach is to extend state estimation to include input estimation, where the goal is to estimate the deterministic component of the exogenous input [9–31]. In many applications, knowledge of the input signal is of independent interest and, in some cases, may be of greater interest than the estimates of the states [32]. The terminology *input reconstruction* is used in the case of deterministic analysis, just as an observer is the deterministic analogue of an estimator.

In light of state estimation, which assumes a known deterministic input and an

unknown zero-mean stochastic input, it may be somewhat surprising that it is indeed possible to estimate not only the states but also, in many cases, the unknown deterministic input. The benefit of state and input estimation is the fact that the deterministic component can often vastly improve the accuracy of the state estimates.

The present chapter considers input reconstruction within a deterministic discrete-time setting. The first contribution of the present chapter is to consider input reconstruction without assuming the existence of a full-column-rank Markov parameter. In [17, 29] it is assumed that the first Markov parameter H_1 has full column rank, which implies that the plant has relative degree 1. Likewise, the approach of [24] is limited to the case where at least one Markov parameter has full column rank. The present chapter considers a more general case where no Markov parameter is required to have full column rank.

The second contribution of the present chapter is a simplified input reconstruction algorithm as compared to the inversion algorithms given in earlier works. Assuming that the initial condition is known, techniques for constructing system inverses were considered in [9, 33]. These techniques are based on sequential constructive algorithms that entail the decomposition of various matrices until a full-rank condition is attained. For the case of known initial conditions, Theorem 2 provides a simplified input-reconstruction algorithm with a delay of η steps, where η is defined in [9] and further studied in [11]. The input observer given by Theorem 2 is deadbeat in the sense that exact input reconstruction is achieved in η steps, and the number of required measurements is $\eta + 1$. Deadbeat estimation is considered in [34]. Since the initial condition is known, the input reconstruction algorithm given by Theorem 2 is applicable whether or not the system has any invariant zeros.

The third contribution of the present chapter is the construction of deadbeat input reconstruction and state estimation algorithms without assuming that the initial condition is known. In this case, the presence of an invariant zero makes it impossible to

distinguish the zero input with zero initial condition from a nonzero input with a specific initial condition that yields zero response. This case is considered in [13], where an algorithm is given for constructing an input-reconstruction filter. Although zeros are not explicitly mentioned in [13], the assumption that u is observable rules out the presence of invariant zeros. For the case where $x(0)$ is unknown and (A, B, C, D) has no invariant zeros, Theorem 3 provides a deadbeat state-estimation algorithm despite the presence of an unknown, arbitrary input. Although this performance is better than the Kalman filter in the absence of sensor noise, it has to be kept in mind that the estimates are obtained with a delay, which means that the estimator is effectively a smoother. The estimation delay is given by the integer μ, which is guaranteed to be finite, and the number of required measurements is $\mu + 1$. Furthermore, for the case where η is finite, $x(0)$ is unknown, and (A, B, C, D) has no invariant zeros, Theorem 4 provides a deadbeat input-reconstruction and state-estimation algorithm. In this case, the reconstruction delay is η, and the number of required measurements is $\max\{\mu, \eta\} + 1$.

Theorems 2, 3, and 4 are each given in terms of the generalized inverse of a block-Toeplitz matrix. This unified formulation provides a direct and simplified presentation of all three results. However, these input-reconstruction and state-estimation algorithms are not given in the form of linear time-invariant (LTI) systems. Consequently, Theorem 7 and Theorem 8 are recast in terms of LTI deadbeat systems for input reconstruction and state estimation. Theorem 5 can be recast in a similar manner, but is awkward due to the need to propagate the free response, and thus an LTI version is not given.

If the initial condition is unknown and the system has at least one invariant zero, then deadbeat input reconstruction is not possible. In this case, asymptotic input reconstruction must be considered, with careful attention paid to the presence of nonmimimum-phase zeros. The assumption invoked in Theorems 3 and 4 that

the system has no invariant zeros is clearly restrictive in the SISO case, since it is unusual for an nth-order SISO system to have relative degree n. Furthermore, since the transmission zeros of a square MIMO transfer function with full normal rank are the roots of the numerator of the determinant, it would be unusual for the system to have no transmission zeros. The situation is different, however, for rectangular systems. For example, a MIMO system with two inputs and four outputs and full normal rank possesses a transmission zero if and only if all six 2×2 embedded transfer functions possess a common transmission zero. Consequently, input reconstruction based on Theorem 4 may be useful for a large class of rectangular systems.

The contents of the chapter are as follows. The next section presents the input-reconstruction problem for discrete-time linear systems. Section 3.3 gives preliminaries on the invertibility of a linear system with an input reconstruction delay η. Section 3.4 provides Theorem 2 for η-delay input reconstruction with known $x(0)$. Sections 3.5 and 3.6 provide Theorems 3 and 4 for μ-delay state estimation and η-delay input reconstruction, respectively. In Section 3.7, we investigate the effect of disturbance and sensor noise on the reconstructed input. Finally, in Section 3.8, we show that Theorem 4 yields an unbiased input estimator.

3.2 Problem Statement

Let $A \in \mathbb{R}^{n \times n}$, $B \in \mathbb{R}^{n \times m}$, $C \in \mathbb{R}^{p \times n}$, and $D \in \mathbb{R}^{p \times m}$, assume that (A, B, C, D) is minimal, and consider

$$x(k+1) = Ax(k) + Bu(k), \tag{3.1}$$

$$y(k) = Cx(k) + Du(k), \tag{3.2}$$

where, for all $k \geq 0$, $x(k) \in \mathbb{R}^n$, $u(k) \in \mathbb{R}^m$, and $y(k) \in \mathbb{R}^p$. The goal is to use knowledge of $y(k)$ to estimate the unknown input $u(k)$. The initial condition $x(0)$

may be known or unknown.

For all $l \geq 0$, define the lth Markov parameter

$$H_l \triangleq \begin{cases} D, & l = 0, \\ CA^{l-1}B, & l \geq 1. \end{cases} \tag{3.3}$$

Let r denote a nonnegative integer, and define

$$\mathcal{Y}_r \triangleq \begin{bmatrix} y(0) \\ y(1) \\ \vdots \\ y(r) \end{bmatrix} \in \mathbb{R}^{(r+1)p}, \; \mathcal{U}_r \triangleq \begin{bmatrix} u(0) \\ u(1) \\ \vdots \\ u(r) \end{bmatrix} \in \mathbb{R}^{(r+1)m}, \; \Gamma_r \triangleq \begin{bmatrix} C \\ CA \\ \vdots \\ CA^r \end{bmatrix} \in \mathbb{R}^{(r+1)p \times n}, \tag{3.4}$$

$$M_r \triangleq \begin{bmatrix} H_0 & 0 & 0 & \cdots & 0 \\ H_1 & H_0 & 0 & \cdots & 0 \\ H_2 & H_1 & H_0 & \cdots & 0 \\ \vdots & \vdots & \ddots & \ddots & \vdots \\ H_r & H_{r-1} & \cdots & H_1 & H_0 \end{bmatrix} \in \mathbb{R}^{(r+1)p \times (r+1)m}. \tag{3.5}$$

It follows from (3.1), (3.2) that

$$\mathcal{Y}_r = \Gamma_r x(0) + M_r \mathcal{U}_r = \Psi_r \begin{bmatrix} x(0) \\ \mathcal{U}_r \end{bmatrix}, \tag{3.6}$$

where

$$\Psi_r \triangleq \begin{bmatrix} \Gamma_r & M_r \end{bmatrix} \in \mathbb{R}^{(r+1)p \times [n+(r+1)m]}. \tag{3.7}$$

Note that, since (A, C) is observable, it follows that

$$x(0) = \Gamma_n^+(\mathcal{Y}_n - M_n\mathcal{U}_n), \tag{3.8}$$

where the generalized inverse Γ_n^+ of Γ_n is a left inverse of Γ_n. For $r \geq s \geq 0$, it is convenient to partition M_r as

$$M_r = \left[\begin{array}{ccc|cc} H_0 & 0 & \cdots & \cdots & 0 \\ \vdots & \ddots & \ddots & \vdots & \vdots \\ H_s & \ddots & \ddots & \ddots & \vdots \\ \vdots & \ddots & \ddots & \ddots & 0 \\ \underbrace{H_r \quad \cdots \quad H_s}_{N_{r,s}} & & & \underbrace{\cdots \quad H_0}_{Q_{r,s}} & \end{array}\right] = \left[\begin{array}{c|c} \underbrace{C_r \quad \cdots \quad C_s}_{N_{r,s}} & \underbrace{\cdots \quad C_0}_{Q_{r,s}} \end{array}\right], \tag{3.9}$$

where $N_{r,s} \in \mathbb{R}^{(r+1)p\times(r-s+1)m}$, $Q_{r,s} \in \mathbb{R}^{(r+1)p\times sm}$, and, for all $i \in \{0, \ldots, r\}$, C_i denotes the $(i+1)^{\text{th}}$ block column of M_r labeled right to left. Furthermore, since, for all $r \geq 0$,

$$M_r = \left[\begin{array}{c|c} H_0 & 0 \\ \hline H_1 & \\ \vdots & M_{r-1} \\ H_r & \end{array}\right] = \left[\begin{array}{ccc|c} & M_{r-1} & & 0 \\ \hline H_r & \cdots & H_1 & H_0 \end{array}\right], \tag{3.10}$$

it follows that, for all $r \geq 0$,

$$\begin{aligned} \text{rank}M_{r-1} &\leq \text{rank}M_r && (3.11)\\ &\leq \min\{\text{rank}C_r, \text{rank}R_r\} \\ &\quad + \text{rank}M_{r-1} && (3.12)\\ &\leq m + \text{rank}M_{r-1}, && (3.13) \end{aligned}$$

where $R_r \stackrel{\triangle}{=} [H_r \ \cdots \ H_0]$ is the last block row of M_r and M_{-1} is an empty matrix

whose rank is 0 and range is $\{0\}$. Finally, note that, if $r > s \geq 0$ and $N_{r,s}$ has full column rank, then, for all $s' \in \{s+1, \ldots, r\}$, $N_{r,s'}$ has full column rank.

3.3 Preliminaries on d-Delay Invertibility

Let $G \in \mathbb{R}(z)^{p \times m}$ be the $p \times m$ proper rational transfer function corresponding to (3.1) and (3.2).

Definition 4. Let d be a nonnegative integer. Then G is d-delay invertible if there exists $\hat{G} \in \mathbb{R}(z)^{m \times p}$ such that $\hat{G}(z)G(z) = z^{-d}I_m$. $\hat{G}$ is a d-delay left inverse of G.

Note that, if G is d-delay invertible, then G must have full normal column rank, and thus $m \leq p$, that is, G must be square or tall. Furthermore, if G is d-delay invertible, then, for all $r > d$, G is r-delay invertible.

It follows from (3.11) and (3.13) that $\text{rank}M_r \leq m + \text{rank}M_{r-1}$. The following result shows that equality in either the case $r = d$ or $r = n$ is necessary and sufficient for invertibility.

Proposition 5. The following conditions are equivalent:

i) There exists $d \geq 0$ such that G is d-delay invertible.

ii) G has full column normal rank.

iii) $\text{rank}N_{2n,n} = (n+1)m$.

iv) There exists $d \geq 0$ such that $\text{rank}M_d - \text{rank}M_{d-1} = m$.

v) $\text{rank}M_n - \text{rank}M_{n-1} = m$.

If these conditions hold, then there exists $d \geq 0$ such that $(1/\mathbf{z}^d)[G(\mathbf{z})^{\mathrm{T}}G(\mathbf{z})]^{-1}G(\mathbf{z})^{\mathrm{T}}$ is a d-delay inverse of G.

Proof. The equivalence of *i*) and *ii*) is immediate. The equivalence of *i*) and *iii*) is given by Theorem 3 of [9]. The equivalence of *i*) and *iv*) is given by Theorem 2 of [9] and Theorem 4 of [10]. The equivalence of *i*) and *v*) is given by Corollary 1 of [9]. □

It is desirable to achieve the smallest possible delay d such that G is d-delay invertible. We thus define

$$\eta \stackrel{\triangle}{=} \min\{l \geq 0 : \text{rank}M_l = m + \text{rank}M_{l-1}\}. \tag{3.14}$$

Note that G is d-delay invertible if and only if η is finite. Furthermore, the equivalence of *i*) and *iv*) of Proposition 5 implies that, if G is d-delay invertible, then η is the smallest delay d such that G is d-delay invertible. Finally, *v*) of Proposition 5 implies that $\eta \leq n$. A sharper bound is given in the next section.

3.4 Input Reconstruction with Known Initial State

The existence of a d-delay left inverse of G implies that, if $x(0) = 0$, then the output of the cascaded system $\hat{G}G$ is exactly the input sequence $u(0), u(1), \ldots$ delayed by d steps. However, for several reasons, the d-delay inverse $\hat{G}(\mathbf{z}) = (1/\mathbf{z}^d)[G(\mathbf{z})^{\mathrm{T}}G(\mathbf{z})]^{-1}G(\mathbf{z})^{\mathrm{T}}$ given by Proposition 5 may be deficient. In particular, $\hat{G}$ may be unstable; the cascade $\hat{G}G$ may entail nonminimum-phase pole-zero cancellation; and the McMillan degree of $\hat{G}$ may not be the smallest possible value. In this section, we construct a deadbeat (finite-impulse response (FIR)) inverse with minimal delay η.

We first focus on sufficient or necessary conditions under which η is finite. In the following result, the first three statements are immediate, and the last statement is given by Corollary 1 of [11].

Proposition 6. The following statements hold:

i) Let $q \geq 0$ be the smallest nonnegative integer such that H_q is nonzero, and assume that H_q has full column rank. Then $\eta = q$.

ii) If $p < m$, then η is infinite.

iii) Assume that, for all $r \geq 0$, either $\operatorname{rank} R_r < p$ or $\operatorname{rank} C_r < m$. Then η is infinite.

iv) If η is finite, then $\eta \leq \min\{n, n+1-m+\operatorname{rank} D\}$.

i) implies that, if $m = 1$, then η is the index of the first nonzero Markov parameter. Therefore, in the SISO case $m = p = 1$, η is the relative degree of G. *ii*) shows that η is finite only if G is either square or tall. *iii*) implies that, if η is finite, then there exists a nonnegative integer r such that either R_r has full row rank or C_r has full column rank. However, Example 1 below shows that the converse of this statement is not true. The second bound in *iv*) is given in [11].

The following example illustrates the range of possible values of η in the case $p = 3$ and $m = 2$.

Example 3.4.1. Let $p = 3$ and $m = 2$, and consider $G(\mathbf{z}) = C(\mathbf{z}I - A)^{-1}B + D$ given by

$$G(\mathbf{z}) = \frac{1}{\mathbf{z}^4}(H_4 + H_3\mathbf{z} + H_2\mathbf{z}^2 + H_1\mathbf{z}^3). \tag{3.15}$$

Note that $D = H_0 = 0_{3\times 2}$, and thus $\text{rank}M_0 = 0 < m$. If

$$H_1 = \begin{bmatrix} 0 & 1 \\ 1 & 2 \\ 0 & 1 \end{bmatrix}, H_2 = \begin{bmatrix} 0 & 0 \\ 0 & 1 \\ 0 & 0 \end{bmatrix}, H_3 = \begin{bmatrix} 1 & 0 \\ 1 & 0 \\ 1 & 0 \end{bmatrix}, H_4 = \begin{bmatrix} 0 & 1 \\ 0 & 1 \\ 0 & 2 \end{bmatrix}, \tag{3.16}$$

then $\text{rank}M_1 = 2 = m$, and thus $\eta = 1$. Alternatively, if

$$H_1 = \begin{bmatrix} 1 & 0 \\ 1 & 0 \\ 1 & 0 \end{bmatrix}, H_2 = \begin{bmatrix} 1 & 0 \\ 0 & 1 \\ 1 & 0 \end{bmatrix}, H_3 = \begin{bmatrix} 0 & 0 \\ 0 & 1 \\ 0 & 0 \end{bmatrix}, H_4 = \begin{bmatrix} 0 & 1 \\ 0 & 1 \\ 0 & 2 \end{bmatrix}, \tag{3.17}$$

then $\text{rank}M_1 = 1 < m$, and, for all $l \geq 2$, $\text{rank}M_l - \text{rank}M_{l-1} = 2 = m$, and thus $\eta = 2$. Next, if

$$H_1 = \begin{bmatrix} 0 & 0 \\ 1 & 0 \\ 0 & 0 \end{bmatrix}, H_2 = \begin{bmatrix} 0 & 0 \\ 0 & 1 \\ 0 & 0 \end{bmatrix}, H_3 = \begin{bmatrix} 1 & 0 \\ 1 & 0 \\ 1 & 0 \end{bmatrix}, H_4 = \begin{bmatrix} 0 & 1 \\ 0 & 1 \\ 0 & 2 \end{bmatrix}, \tag{3.18}$$

then, for all $l \leq 3$, $\text{rank}M_l - \text{rank}M_{l-1} = 1 < m$, and, for all $l \geq 4$, $\text{rank}M_l - \text{rank}M_{l-1} = 2 = m$, and thus $\eta = 4$. Finally, if

$$H_1 = \begin{bmatrix} 0 & 0 \\ 1 & 0 \\ 0 & 0 \end{bmatrix}, H_2 = \begin{bmatrix} 0 & 0 \\ 0 & 1 \\ 0 & 0 \end{bmatrix}, H_3 = \begin{bmatrix} 1 & 0 \\ 1 & 0 \\ 1 & 0 \end{bmatrix}, H_4 = \begin{bmatrix} 0 & 1 \\ 0 & 1 \\ 0 & 1 \end{bmatrix}, \tag{3.19}$$

then, for all $l \geq 1$, $\text{rank}M_l - \text{rank}M_{l-1} = 1 \neq m$, and thus η is infinite. $\diamond$

The cases (3.16)–(3.18) show that η may be finite whether or not at least one Markov parameter has full column rank. Furthermore, the cases (3.18) and (3.19) show that, if no Markov parameter has full column rank, then η may be finite or

infinite.

The following result, which assumes that η is finite, is used in the proof of Theorem 2. The proof depends on Lemma 2. Note that, since, by *iv*) of Proposition 6, $\eta \leq n$, it follows that the first result of Proposition 7 generalizes *i*) $\Longrightarrow$ *iii*) of Proposition 5.

Proposition 7. Assume that η is finite, and let $r \geq \eta$. Then, $N_{r,\eta}$ has full column rank, and

$$\mathcal{R}(N_{r,\eta}) \cap \mathcal{R}(Q_{r,\eta}) = \{0\}. \tag{3.20}$$

Proof. First, consider the case $\eta = 0$. Then $M_0 = N_0 = H_0$ and $\text{rank}M_0 = \text{rank}N_0 = \text{rank}H_0 = m$. Since H_0 has full column rank, it follows that $N_{r,\eta}$ has full column rank, and, since $Q_{r,\eta}$ is an empty matrix, (3.20) holds.

Next, let $r = \eta = 1$ so that

$$\text{rank}M_1 = m + \text{rank}M_0. \tag{3.21}$$

Since

$$M_1 = \left[\begin{array}{c|c} C_1 & \begin{array}{c} 0 \\ M_0 \end{array} \end{array}\right] = \left[\begin{array}{c|c} C_1 & C_0 \end{array}\right] = \left[\begin{array}{c|c} N_{1,1} & Q_{1,1} \end{array}\right], \tag{3.22}$$

it follows that

$$\begin{aligned} \text{rank}M_1 &= \text{rank}C_1 + \text{rank}C_0 - \dim\left(\mathcal{R}(C_1) \cap \mathcal{R}(C_0)\right) \\ &= \text{rank}N_{1,1} + \text{rank}M_0 - \dim\left(\mathcal{R}(N_{1,1}) \cap \mathcal{R}(Q_{1,1})\right). \end{aligned} \tag{3.23}$$

Combining (3.21) with (3.23) yields

$$0 \leq \dim\left(\mathcal{R}(N_{1,1}) \cap \mathcal{R}(Q_{1,1})\right) = \operatorname{rank} N_{1,1} - m \leq 0,$$

which implies that $N_{1,1}$ has full column rank and $\mathcal{R}(N_{1,1}) \cap \mathcal{R}(Q_{1,1}) = \{0\}$.

Next, let $r \geq 2$ and $\eta \in \{1, \ldots, r\}$ so that

$$\operatorname{rank} M_\eta = m + \operatorname{rank} M_{\eta-1}. \tag{3.24}$$

Noting

$$M_\eta = \left[\begin{array}{c|c} C_\eta & \begin{array}{c} 0 \\ \\ M_{\eta-1} \end{array} \end{array}\right] = \left[\begin{array}{c|ccc} C_\eta & C_{\eta-1} & \cdots & C_0 \end{array}\right], \tag{3.25}$$

it follows that

$$\begin{aligned} \operatorname{rank} M_\eta &= \operatorname{rank} C_\eta + \operatorname{rank}\left[C_{\eta-1} \ \cdots \ C_0\right] - \dim\left(\mathcal{R}(C_\eta) \cap \mathcal{R}([C_{\eta-1} \ \cdots \ C_0])\right) \\ &= \operatorname{rank} C_\eta + \operatorname{rank} M_{\eta-1} - \dim\left(\mathcal{R}(C_\eta) \cap \mathcal{R}([C_{\eta-1} \ \cdots \ C_0])\right). \end{aligned} \tag{3.26}$$

Combining (3.24) with (3.26) yields

$$0 \leq \dim\left(\mathcal{R}(C_\eta) \cap \mathcal{R}([C_{\eta-1} \ \cdots \ C_0])\right) = \operatorname{rank} C_\eta - m \leq 0,$$

which implies that C_η has full column rank and

$$\mathcal{R}(C_\eta) \cap \mathcal{R}([C_{\eta-1} \ \cdots \ C_0]) = \{0\}. \tag{3.27}$$

It thus follows from Lemma 2 that $N_{r,\eta} = [C_r \ \cdots \ C_\eta]$ has full column rank and

$$\mathcal{R}(N_{r,\eta}) \cap \mathcal{R}(Q_{r,\eta}) = \mathcal{R}([C_r \ \cdots \ C_\eta]) \cap \mathcal{R}([C_{\eta-1} \ \cdots \ C_0]) = \{0\}. \qquad \square$$

The following result shows that, if $x(0)$ is known and η is finite, then deadbeat input reconstruction is possible with a delay of η steps whether or not (A, B, C, D) has any invariant zeros. The proof depends on Proposition 7 and Lemma 3.

Theorem 2. Assume that the initial state $x(0)$ is known and η is finite. Then, for all $r \geq \eta$,

$$\mathcal{U}_{r-\eta} = \begin{bmatrix} I_{(r-\eta+1)m} & 0_{[(r-\eta+1)m]\times\eta m} \end{bmatrix} M_r^+ \left(\mathcal{Y}_r - \Gamma_r \, x(0)\right). \tag{3.28}$$

Proof. Let $r \geq \eta$. Multiplying (3.6) by M_r^+ and rearranging terms yields

$$M_r^+ M_r \mathcal{U}_r = M_r^+ \left(\mathcal{Y}_r - \Gamma_r \, x(0)\right). \tag{3.29}$$

Proposition 7 implies that $N_{r,\eta}$ has full column rank and $\mathcal{R}(N_{r,\eta}) \cap \mathcal{R}(Q_{r,\eta}) = \{0\}$. It thus follows from Lemma 3 that

$$\begin{aligned} M_r^+ M_r &= [N_{r,\eta} \ Q_{r,\eta}]^+ [N_{r,\eta} \ Q_{r,\eta}] \\ &= \begin{bmatrix} I_{(r-\eta+1)m} & 0 \\ 0 & Q_{r,\eta}^+ Q_{r,\eta} \end{bmatrix} \in \mathbb{R}^{(r+1)m\times(r+1)m}. \end{aligned} \tag{3.30}$$

Substituting (3.30) into (3.29) yields

$$\begin{bmatrix} I_{(r-\eta+1)m} & 0 \\ 0 & Q_{r,\eta}^{+} Q_{r,\eta} \end{bmatrix} \mathcal{U}_r = M_r^{+} \left(\mathcal{Y}_r - \Gamma_r \, x(0) \right). \tag{3.31}$$

Multiplying (3.31) by $[I_{(r-\eta+1)m} \; 0_{[(r-\eta+1)m]\times\eta m}]$ implies that (3.28) holds. □

Note that (3.28) shows that the unknown input u is reconstructed with a delay of η steps. Furthermore, note that the condition that η is finite is a necessary and sufficient condition for the application of (3.28).

The following example illustrates Theorem 2 for a system with an invariant zero and column-rank-deficient Markov parameter.

Example 3.4.2. Consider $G(\mathbf{z}) = C(\mathbf{z}I - A)^{-1}B + D$ given by

$$G(\mathbf{z}) = \frac{\mathbf{z} - 1.2}{(\mathbf{z} - 0.9)^2(\mathbf{z} - 0.6)^2} \begin{bmatrix} 1 \\ \mathbf{z} - 0.85 \end{bmatrix}. \tag{3.32}$$

Note that (A, B, C, D) has an invariant zero at 1.2, $H_0 = H_1 = 0_{2\times1}$, and $\eta = 2$. Assume that the initial state $x(0) = [5 \;\; 6 \;\; 2 \;\; 1]^{\mathrm{T}}$ is known, and for all $k \geq 0$, let the unknown input $u(k)$ be sampled Gaussian white noise with variance 1. To apply Theorem 2, we choose $r = 40$ and compute M_r^{+} using the Matlab function "pinv" with the default machine constant. Figure 3.1 shows that, for all $0 \leq k \leq r - \eta = 38$, the reconstructed input using Theorem 2 is equal to the actual input u, which confirms (3.28). ◇

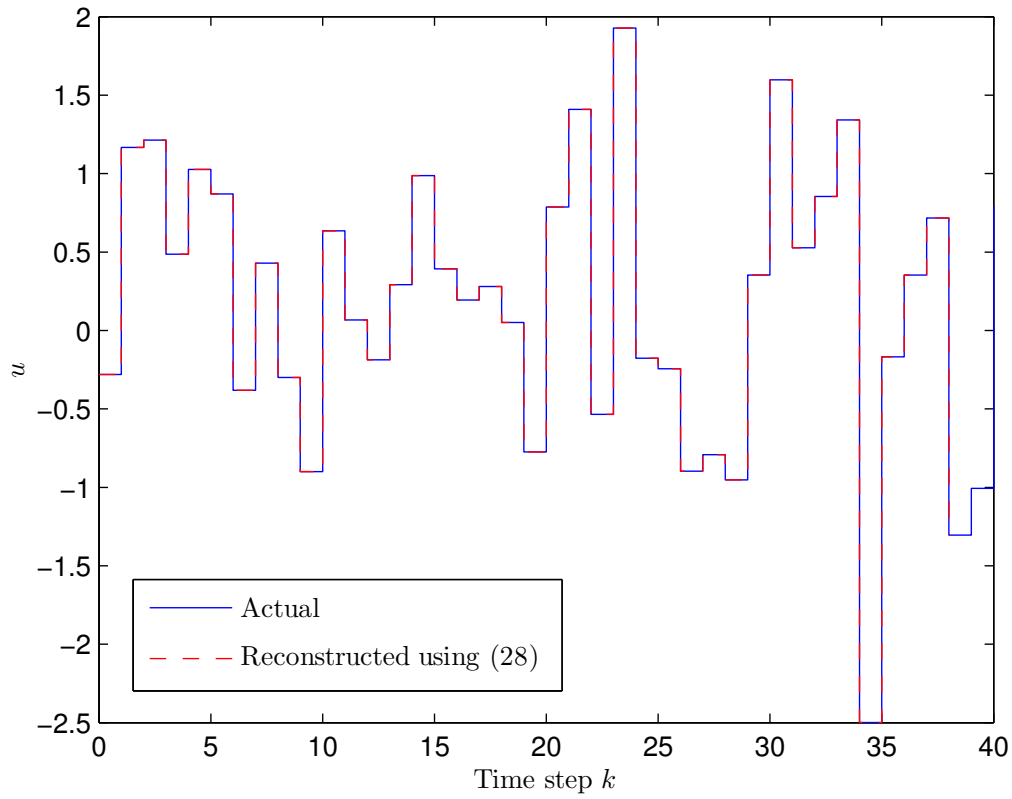

Figure 3.1: Application of Theorem 2 to Example 3.4.2. For all $0 \leq k \leq r - \eta = 38$, the reconstructed input is equal to the actual input, which confirms (3.28).

3.5 Deadbeat State Estimation for Systems without Invariant Zeros

Define

$$\mu \stackrel{\triangle}{=} \min\{l \geq 0 : \text{rank}\Psi_l = n + \text{rank}M_l\}. \tag{3.33}$$

The index μ is the smallest integer such that Γ_μ has full column rank and the disjointness condition (3.34) is valid.

The following result is used in the proof of Theorem 3.

Proposition 8. Assume that (A, B, C, D) has no invariant zeros. Then μ is finite, and, for all $r \geq \mu$, Γ_r has full column rank and

$$\mathcal{R}(\Gamma_r) \cap \mathcal{R}(M_r) = \{0\}. \tag{3.34}$$

Proof. Since (A, B, C, D) has no invariant zeros, Theorem A.1 of [24] implies that there exists $l \geq n$ such that

$$\mathcal{R}(\Gamma_l) \cap \mathcal{R}(M_l) = \{0\}. \tag{3.35}$$

Since (A, C) is observable, it follows that

$$\text{rank}\Gamma_l = n. \tag{3.36}$$

Noting $\Psi_l = [\Gamma_l \; M_l]$ and using (3.35), (3.36), and Fact 2.11.9 in [79, p. 131], it follows that

$$\begin{aligned} \text{rank}\Psi_l &= \text{rank}\Gamma_l + \text{rank}M_l - \dim(\mathcal{R}(\Gamma_l) \cap \mathcal{R}(M_l)) \\ &= n + \text{rank}M_l. \end{aligned} \tag{3.37}$$

It thus follows from (3.37) that μ is finite and satisfies $0 \leq \mu \leq l$. Next, note that

$$\text{rank}\Psi_\mu = n + \text{rank}M_\mu. \tag{3.38}$$

Furthermore, noting $\Psi_\mu = [\Gamma_\mu \; M_\mu]$ and using Fact 2.11.9 in [79, p. 131] yields

$$\text{rank}\Psi_\mu = \text{rank}\Gamma_\mu + \text{rank}M_\mu - \dim(\mathcal{R}(\Gamma_\mu) \cap \mathcal{R}(M_\mu)). \tag{3.39}$$

Combining (3.38) with (3.39) yields

$$0 \leq \dim\left(\mathcal{R}(\Gamma_\mu) \cap \mathcal{R}(M_\mu)\right) = \operatorname{rank}\Gamma_\mu - n \leq 0,$$

which implies that Γ_μ has full column rank and

$$\mathcal{R}(\Gamma_\mu) \cap \mathcal{R}(M_\mu) = \{0\}. \tag{3.40}$$

Since Γ_μ has full column rank, it thus follows from (3.5) that, for all $r \geq \mu$, Γ_r has full column rank. Finally, note that

$$\mathcal{R}(\Gamma_{\mu+1}) \cap \mathcal{R}(M_{\mu+1}) = \mathcal{R}\left(\begin{bmatrix} \Gamma_\mu \\ CA^{\mu+1} \end{bmatrix}\right) \cap \left(\left[\begin{array}{ccc|c} & M_\mu & & 0 \\ \hline H_{\mu+1} & \cdots & H_1 & H_0 \end{array}\right]\right). \tag{3.41}$$

Since Γ_μ has full column rank and $\mathcal{R}(\Gamma_\mu) \cap \mathcal{R}(M_\mu) = \{0\}$, it follows from (3.41) and Lemma 1 that

$$\mathcal{R}(\Gamma_{\mu+1}) \cap \mathcal{R}(M_{\mu+1}) = \{0\}.$$

By similar arguments, it follows that, for all $r \geq \mu$, $\mathcal{R}(\Gamma_r) \cap \mathcal{R}(M_r) = \{0\}$. □

The following example compares μ and η for a system that has no invariant zeros.

Example 3.5.1. Since (3.15) has no invariant zeros for (3.16)–(3.18), Proposition 8 implies that μ is finite for each of these cases. For (3.16), numerical computation shows that $n = 7$, $\text{rank}\Psi_0 - \text{rank}M_0 = 3 < n$, $\text{rank}\Psi_1 - \text{rank}M_1 = 4 < n$, $\text{rank}\Psi_2 - \text{rank}M_2 = 5 < n$, $\text{rank}\Psi_3 - \text{rank}M_3 = 6 < n$, and, for all $l \geq 4$, $\text{rank}\Psi_l - \text{rank}M_l = 7 = n$. Hence, $\mu = 4 > \eta = 1$.

For (3.17), numerical computation shows that $n = 6$, $\text{rank}\Psi_0 - \text{rank}M_0 = 3 < n$, $\text{rank}\Psi_1 - \text{rank}M_1 = 5 < n$, and, for all $l \geq 2$, $\text{rank}\Psi_l - \text{rank}M_l = 6 = n$. Hence, $\mu = \eta = 2$.

For (3.18), numerical computation shows that $n = 7$, $\text{rank}\Psi_0 - \text{rank}M_0 = 3 < n$, $\text{rank}\Psi_1 - \text{rank}M_1 = 5 < n$, $\text{rank}\Psi_2 - \text{rank}M_2 = 6 < n$, and, for all $l \geq 3$, $\text{rank}\Psi_l - \text{rank}M_l = 7 = n$. Hence, $\mu = 3 < \eta = 4$.

Finally, for (3.19), (A, B, C, D) has an invariant zero at 0, and thus Proposition 8 is not applicable. $\diamond$

The following result shows that, if (A, B, C, D) has no invariant zeros, then deadbeat state estimation is possible with a delay of μ steps without knowledge of u. Unlike Theorem 2, the initial condition is unknown, but the system is assumed to have no invariant zeros. The proof depends on Proposition 8 and Lemma 3.

Theorem 3. Assume that (A, B, C, D) has no invariant zeros. Then, for all $k \geq 0$ and $r \geq \mu$,

$$x(k) = \begin{bmatrix} I_n & 0_{n\times(r+1)m} \end{bmatrix} \Psi_r^+ \begin{bmatrix} y(k) \\ y(k+1) \\ \vdots \\ y(k+r) \end{bmatrix}. \tag{3.42}$$

Proof. Let $k \geq 0$. Since (A, B, C, D) has no invariant zeros, it follows from Proposition 8 that, for all $r \geq \mu$, Γ_r has full column rank, and

$$\mathcal{R}(\Gamma_r) \cap \mathcal{R}(M_r) = \{0\}. \tag{3.43}$$

Using (3.43), it follows from Lemma 3 that, for all $r \geq \mu$,

$$\Psi_r^+ \Psi_r = \begin{bmatrix} \Gamma_r^+ \Gamma_r & 0 \\ 0 & M_r^+ M_r \end{bmatrix} = \begin{bmatrix} I_n & 0 \\ 0 & M_r^+ M_r \end{bmatrix}. \tag{3.44}$$

Next, multiplying (3.44) by $[x^{\mathrm{T}}(k)\ u^{\mathrm{T}}(k)\ \cdots\ u^{\mathrm{T}}(k+r)]^{\mathrm{T}}$ implies that, for all $r \geq \mu$,

$$\begin{bmatrix} I_n & 0 \\ 0 & M_r^+ M_r \end{bmatrix} \begin{bmatrix} x(k) \\ u(k) \\ \vdots \\ u(k+r) \end{bmatrix} = \Psi_r^+ \begin{bmatrix} y(k) \\ y(k+1) \\ \vdots \\ y(k+r) \end{bmatrix}. \tag{3.45}$$

Finally, multiplying (3.45) by $[I_n\ 0_{n\times(r+1)m}]$ implies that, for all $r \geq \mu$, (3.42) holds. □

3.5.1 Deadbeat State Estimator Based on Theorem 3

We now construct a deadbeat state estimator based on Theorem 3. Defining

$$G_{yu}(\mathbf{z}) \stackrel{\triangle}{=} G(\mathbf{z}) = C(\mathbf{z}I_n - A)B + D, \tag{3.46}$$

$$G_{xu}(\mathbf{z}) \stackrel{\triangle}{=} (\mathbf{z}I_n - A)B, \tag{3.47}$$

and taking the $\mathcal{Z}$-transform of (3.42) with $r = \mu$ yields

$$\mathbf{z}^{-\mu} X(\mathbf{z}) = \underbrace{\begin{bmatrix} I_n & 0_{n\times(\mu+1)m} \end{bmatrix} \Psi_\mu^+ \begin{bmatrix} \mathbf{z}^{-\mu} I_p \\ \mathbf{z}^{-\mu+1} I_p \\ \vdots \\ I_p \end{bmatrix}}_{\hat{G}_{xy,\mu}(\mathbf{z})} Y(\mathbf{z}). \tag{3.48}$$

Note that $\hat{G}_{xy,\mu} \in \mathbb{R}(\mathbf{z})^{n\times p}$ is an FIR filter. Substituting $Y(\mathbf{z}) = G_{yu}(\mathbf{z})U(\mathbf{z})$ and $X(\mathbf{z}) = G_{xu}(\mathbf{z})U(\mathbf{z})$ into (3.48) yields

$$\mathbf{z}^{-\mu} G_{xu}(\mathbf{z})U(\mathbf{z}) = \hat{G}_{xy,\mu}(\mathbf{z}) G_{yu}(\mathbf{z})U(\mathbf{z}). \tag{3.49}$$

It follows from (3.49) that

$$\hat{G}_{xy,\mu}(\mathbf{z})G_{yu}(\mathbf{z}) = \mathbf{z}^{-\mu}G_{xu}(\mathbf{z}), \tag{3.50}$$

which shows that $\hat{G}_{xy,\mu}$ is a deadbeat μ-delay FIR state estimator. It should be noted that the deadbeat estimator does not invoke the assumption that H_1 has full column rank as assumed in [5].

3.5.2 Numerical Example

Example 3.5.2. Consider the mass-spring-damper system with masses m_1, m_2 and unknown input force u applied to m_1, as shown in Figure 3.2. The dynamics are given by

$$\dot{x} = A_{\mathrm{c}}x + B_{\mathrm{c}}u, \tag{3.51}$$

where

$$A_{\mathrm{c}} \triangleq \begin{bmatrix} 0_{2\times 2} & I_{2\times 2} \\ \Omega_1 & \Omega_2 \end{bmatrix}, B_{\mathrm{c}} \triangleq \begin{bmatrix} 0_{2\times 1} \\ \Omega_3 \end{bmatrix}, \Omega_1 \triangleq \begin{bmatrix} -\frac{k_1+k_2}{m_1} & \frac{k_2}{m_1} \\ \frac{k_2}{m_2} & -\frac{k_2}{m_2} \end{bmatrix},$$
$$\Omega_2 \triangleq \begin{bmatrix} -\frac{c_1+c_2}{m_1} & \frac{c_2}{m_1} \\ \frac{c_2}{m_2} & -\frac{c_2}{m_2} \end{bmatrix}, \Omega_3 \triangleq \begin{bmatrix} \frac{1}{m_1} \\ 0 \end{bmatrix},$$

x_1 and x_2 are the displacements and x_3 and x_4 are the velocities of m_1 and m_2, respectively. Letting $m_1 = m_2 = 1\,\mathrm{kg}$, $k_1 = k_2 = 10\,\mathrm{N/m}$, and $c_1 = c_2 = 5\,\mathrm{kg/sec}$, we discretize (3.51) as

$$A = e^{A_{\mathrm{c}}T_{\mathrm{s}}}, \quad B = A_{\mathrm{c}}^{-1}(A_{\mathrm{c}} - I)B_{\mathrm{c}}, \tag{3.52}$$

where $T_{\mathrm{s}} = 1$ sec is the sampling time. Letting

$$C = \begin{bmatrix} 1 & 0 & 0 & 0 \\ 0 & 0 & 1 & 0 \end{bmatrix}, \quad D = \begin{bmatrix} 0 \\ 0 \end{bmatrix},$$

the measurements are the position x_1 and velocity x_3 of m_1. The system (A, B, C, D) has no invariant zeros, and thus we use Theorem 3 to estimate the position and velocity of m_2. Furthermore, $\mu = 2$. Let the unknown initial condition be $x(0) = [-6\,1\,4\,4]^{\mathrm{T}}$, and let the unknown input be $u(k) = 1 + w(k) + \sin(kT_{\mathrm{s}})$, where w is zero-mean Gaussian white noise with variance 0.1. Furthermore, let the available measurement be $[y^{\mathrm{T}}(0) \ \cdots \ y^{\mathrm{T}}(40)]^{\mathrm{T}}$.

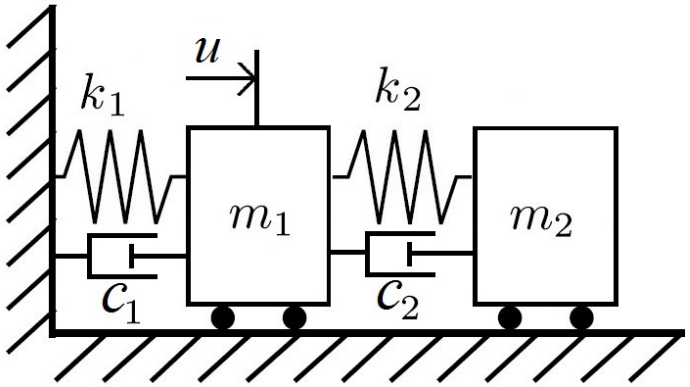

Figure 3.2: Mass-spring-damper system, where the disturbance u is the unknown input force.

We estimate x_2 and x_4 in two different ways, namely, 1) by using (3.42), and 2) by using the filter $\hat{G}_{xy,2}$ given by (3.48). To apply (3.42), we choose $r = \mu = 2$. The

computed $\hat{G}_{xy,2}$ is given by

$$\hat{G}_{xy,2}(\mathbf{z}) = \begin{bmatrix} \frac{1}{\mathbf{z}^2} & 0 \\ \frac{-18.96\mathbf{z}^2+19.86\mathbf{z}+0.098}{\mathbf{z}^2} & \frac{23.3\mathbf{z}^2+8.05\mathbf{z}+0.067}{\mathbf{z}^2} \\ 0 & \frac{1}{\mathbf{z}^2} \\ \frac{28.6\mathbf{z}^2-25.5\mathbf{z}-3.05}{\mathbf{z}^2} & \frac{-35.14\mathbf{z}^2-17.55\mathbf{z}-0.9}{\mathbf{z}^2} \end{bmatrix}. \tag{3.53}$$

Figure 3.3 shows that, for all $0 \leq k \leq 40 - \mu = 38$, the estimated state is equal to the actual state, which confirms (3.42) and (3.48). $\diamond$

3.6 Deadbeat Input Reconstruction for Systems without Invariant Zeros

The following result shows that, if (A, B, C, D) has no invariant zeros and η is finite, then deadbeat input reconstruction is possible with a delay of η steps, whether or not $x(0)$ is known. The proof depends on Proposition 7, Proposition 8, and Lemma 3.

Theorem 4. Assume that (A, B, C, D) has no invariant zeros and η is finite. Then, for all $k \geq 0$ and $r \geq \max\{\mu, \eta\}$,

$$\begin{bmatrix} x(k) \\ u(k) \\ \vdots \\ u(k+r-\eta) \end{bmatrix} = \begin{bmatrix} I_{n+(r-\eta+1)m} & 0_{[n+(r-\eta+1)m]\times\eta m} \end{bmatrix} \Psi_r^+ \begin{bmatrix} y(k) \\ y(k+1) \\ \vdots \\ y(k+r) \end{bmatrix}. \tag{3.54}$$

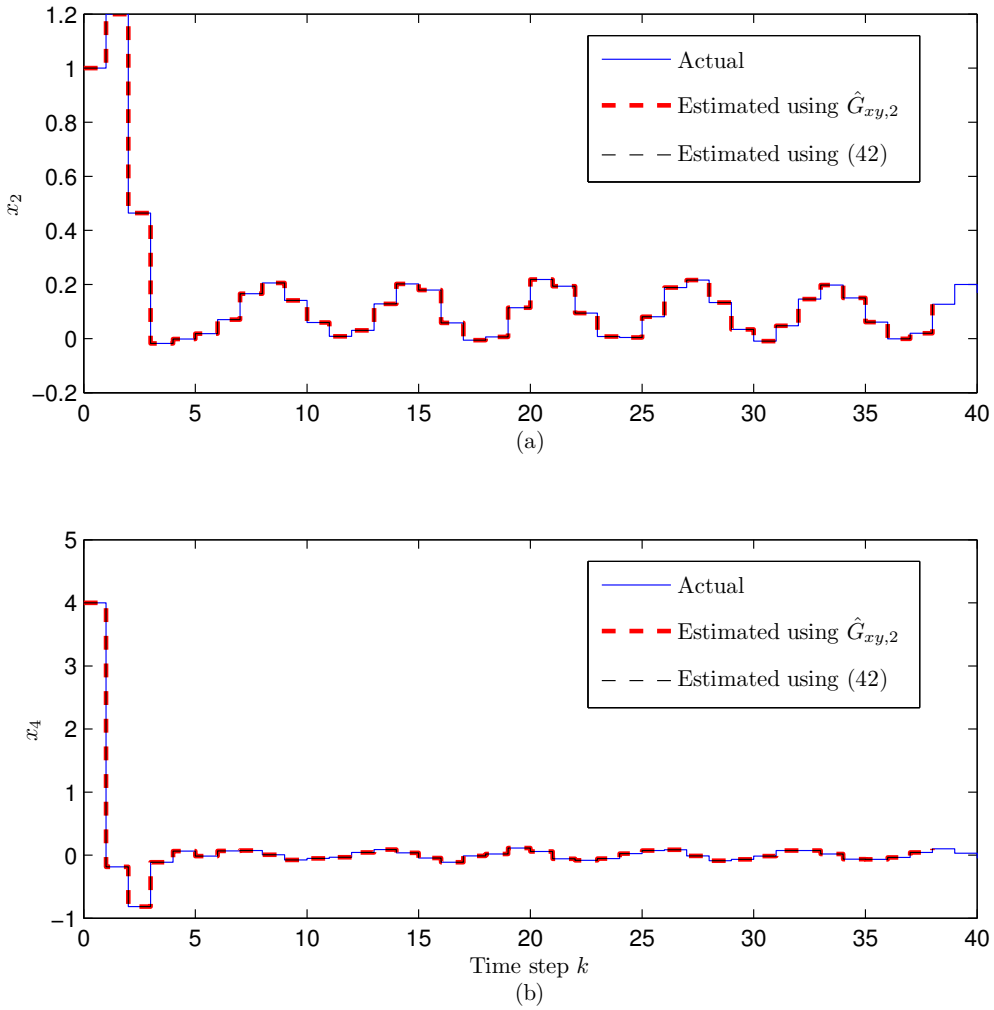

Figure 3.3: Application of Theorem 3 to Example 3.5.2. For all $0 \leq k \leq 40 - \mu = 38$, the estimated state is equal to the actual state, which confirms (3.42) and (3.48).

Proof. Let $k \geq 0$. Since, η exists, it follows from Proposition 7 that, for all $r \geq \eta$,

$$\mathcal{R}(N_{r,\eta}) \cap \mathcal{R}(Q_{r,\eta}) = \{0\}. \tag{3.55}$$

Noting $M_r = [N_{r,\eta}\ Q_{r,\eta}]$ and using (3.55) and Fact 2.11.9 in [79, p. 131], it follows that, for all $r \geq \eta$,

$$\text{rank}M_r = \text{rank}N_{r,\eta} + \text{rank}Q_{r,\eta}. \tag{3.56}$$

Since (A, B, C, D) has no invariant zeros, it follows from Proposition 8 that, for all $r \geq \mu$,

$$\mathcal{R}(\Gamma_r) \cap \mathcal{R}(M_r) = \{0\}. \tag{3.57}$$

Noting $\Psi_r = [\Gamma_r\ M_r]$ and using (3.57) and Fact 2.11.9 in [79, p. 131], it follows that, for all $r \geq \mu$,

$$\text{rank}\Psi_r = \text{rank}\Gamma_r + \text{rank}M_r. \tag{3.58}$$

Substituting (3.56) into (3.58) yields, for all $r \geq \max\{\mu, \eta\}$,

$$\text{rank}\Psi_r = \text{rank}\Gamma_r + \text{rank}N_{r,\eta} + \text{rank}Q_{r,\eta}. \tag{3.59}$$

Next, noting $\Psi_r = [\Gamma_r\ N_{r,\eta}\ Q_{r,\eta}]$ and using Fact 2.11.9 in [79, p. 131], it follows that, for all $r \geq 0$,

$$\begin{aligned}\text{rank}\Psi_r &= \text{rank}\,[\Gamma_r\ N_{r,\eta}] + \text{rank}Q_{r,\eta} - \dim[\mathcal{R}([\Gamma_r\ N_{r,\eta}]) \cap \mathcal{R}(Q_{r,\eta})] \\ &= \text{rank}\Gamma_r + \text{rank}N_{r,\eta} + \text{rank}Q_{r,\eta} - \dim[\mathcal{R}(\Gamma_r) \cap \mathcal{R}(N_{r,\eta})] \\ &\qquad - \dim[\mathcal{R}([\Gamma_r\ N_{r,\eta}]) \cap \mathcal{R}(Q_{r,\eta})]. \end{aligned} \tag{3.60}$$

Subtracting (3.60) from (3.59) yields, for all $r \geq \max\{\mu, \eta\}$,

$$\dim[\mathcal{R}(\Gamma_r) \cap \mathcal{R}(N_{r,\eta})] + \dim[\mathcal{R}([\Gamma_r \ N_{r,\eta}]) \cap \mathcal{R}(Q_{r,\eta})] = 0. \tag{3.61}$$

Since both terms in (3.61) are nonnegative, it follows that, for all $r \geq \max\{\mu, \eta\}$,

$$\mathcal{R}(\Gamma_r) \cap \mathcal{R}(N_{r,\eta}) = \{0\}, \tag{3.62}$$

$$\mathcal{R}([\Gamma_r \ N_{r,\eta}]) \cap \mathcal{R}(Q_{r,\eta}) = \{0\}. \tag{3.63}$$

Using (3.63), it follows from Lemma 3 that, for all $r \geq \max\{\mu, \eta\}$,

$$\Psi_r^+ \Psi_r = \begin{bmatrix} [\Gamma_r \ N_{r,\eta}]^+ [\Gamma_r \ N_{r,\eta}] & 0 \\ 0 & Q_{r,\eta}^+ Q_{r,\eta} \end{bmatrix}. \tag{3.64}$$

Next, Proposition 8 implies that, for all $r \geq \mu$, Γ_r has full column rank. Furthermore, Proposition 7 implies that, for all $r \geq \eta$, $N_{r,\eta}$ has full column rank. Therefore, using (3.62) it follows that

$$\begin{aligned} \operatorname{rank} [\Gamma_r \ N_{r,\eta}] &= \operatorname{rank}\Gamma_r + \operatorname{rank} N_{r,\eta} - \dim[\mathcal{R}(\Gamma_r) \cap \mathcal{R}(N_{r,\eta})] \\ &= \operatorname{rank}\Gamma_r + \operatorname{rank} N_{r,\eta}. \end{aligned} \tag{3.65}$$

Therefore, for all $r \geq \max\{\mu, \eta\}$, $[\Gamma_r \ N_{r,\eta}]$ has full column rank, and thus $[\Gamma_r \ N_{r,\eta}]^+$ is a left inverse of $[\Gamma_r \ N_{r,\eta}]$. Hence, for all $r \geq \max\{\mu, \eta\}$,

$$\Psi_r^+ \Psi_r = \begin{bmatrix} I_{n+(r-\eta+1)m} & 0 \\ 0 & Q_{r,\eta}^+ Q_{r,\eta} \end{bmatrix}. \tag{3.66}$$

Next, multiplying (3.66) by $[x^{\mathrm{T}}(k)\ u^{\mathrm{T}}(k)\ \cdots\ u^{\mathrm{T}}(k{+}r)]^{\mathrm{T}}$ implies that, for all $r \geq \max\{\mu, \eta\}$,

$$\begin{bmatrix} I_{n+(r-\eta+1)m} & 0 \\ 0 & Q_{r,\eta}^{+} Q_{r,\eta} \end{bmatrix} \begin{bmatrix} x(k) \\ u(k) \\ \vdots \\ u(k{+}r) \end{bmatrix} = \Psi_r^{+} \begin{bmatrix} y(k) \\ y(k{+}1) \\ \vdots \\ y(k{+}r) \end{bmatrix}. \tag{3.67}$$

Finally, multiplying (3.67) by $[I_{n+(r-\eta+1)m}\ 0_{[n+(r-\eta+1)m]\times\eta m}]$ implies that, for all $r \geq \max\{\mu, \eta\}$, (3.54) holds. □

In order to minimize the size of Ψ_r, we specialize Theorem 4 with $r = \max\{\mu, \eta\}$. In the case $\mu \leq \eta$, it follows that $r = \eta$ and (3.54) specializes to

$$\begin{bmatrix} x(k) \\ u(k) \end{bmatrix} = \begin{bmatrix} I_{n+m} & 0_{(n+m)\times\eta m} \end{bmatrix} \Psi_\eta^{+} \begin{bmatrix} y(k) \\ y(k+1) \\ \vdots \\ y(k+\eta) \end{bmatrix}. \tag{3.68}$$

Similarly, in the case $\mu > \eta$, it follows that $r = \mu$ and (3.54) specializes to

$$\begin{bmatrix} x(k) \\ u(k) \\ \vdots \\ u(k{+}\mu{-}\eta) \end{bmatrix} = \begin{bmatrix} I_{n+(\mu-\eta+1)m} & 0_{[n+(\mu-\eta+1)m]\times\eta m} \end{bmatrix} \Psi_\mu^{+} \begin{bmatrix} y(k) \\ y(k+1) \\ \vdots \\ y(k+\mu) \end{bmatrix}. \tag{3.69}$$

Note that (3.68) and (3.69), starting at time step k, require $\eta{+}1$ and $\mu{+}1$ measurements, respectively.

3.6.1 Deadbeat Left Inverse Based on Theorem 4

We now derive a transfer matrix corresponding to Theorem 4, and show that it provides an η-delay left inverse of G_{yu}. Define $\gamma \triangleq \max\{\mu, \eta\}$ and the matrix

$$P_{r,\eta,m,n} \triangleq \begin{bmatrix} I_{n+(r-\eta+1)m} & 0_{[n+(r-\eta+1)m]\times\eta m} \end{bmatrix}. \tag{3.70}$$

Then, with $r = \gamma$, (3.54) implies

$$\begin{bmatrix} x(k) \\ u(k) \\ \vdots \\ u(k+\gamma-\eta) \end{bmatrix} = P_{\gamma,\eta,m,n}\, \Psi_\gamma^+ \begin{bmatrix} y(k) \\ y(k+1) \\ \vdots \\ y(k+\gamma) \end{bmatrix}. \tag{3.71}$$

Taking the $\mathcal{Z}$-transform of (3.71) yields

$$\begin{bmatrix} \mathbf{z}^{-\gamma}X(\mathbf{z}) \\ \mathbf{z}^{-\gamma}U(\mathbf{z}) \\ \mathbf{z}^{-\gamma+1}U(\mathbf{z}) \\ \vdots \\ \mathbf{z}^{-\eta}U(\mathbf{z}) \end{bmatrix} = \underbrace{P_{\gamma,\eta,m,n}\, \Psi_\gamma^+ \begin{bmatrix} \mathbf{z}^{-\gamma}I_p \\ \mathbf{z}^{-\gamma+1}I_p \\ \vdots \\ I_p \end{bmatrix}}_{\hat{G}(\mathbf{z})} Y(\mathbf{z}). \tag{3.72}$$

Note that $\hat{G} \in \mathbb{R}(\mathbf{z})^{[n+(\gamma-\eta+1)m]\times p}$ is an FIR filter. Partition $\hat{G}$ as

$$\hat{G} = \begin{bmatrix} \hat{G}_{xy,\gamma} \\ \hat{G}_{uy,\gamma} \\ \hat{G}_{uy,\gamma-1} \\ \vdots \\ \hat{G}_{uy,\eta} \end{bmatrix}, \tag{3.73}$$

such that

$$\mathbf{z}^{-\gamma}X(\mathbf{z}) = \hat{G}_{xy,\gamma}(\mathbf{z})Y(\mathbf{z}), \tag{3.74}$$

$$\mathbf{z}^{-\gamma}U(\mathbf{z}) = \hat{G}_{uy,\gamma}(\mathbf{z})Y(\mathbf{z}), \tag{3.75}$$

$$\mathbf{z}^{-\gamma+1}U(\mathbf{z}) = \hat{G}_{uy,\gamma-1}(\mathbf{z})Y(\mathbf{z}), \tag{3.76}$$

$$\vdots$$

$$\mathbf{z}^{-\eta}U(\mathbf{z}) = \hat{G}_{uy,\eta}(\mathbf{z})Y(\mathbf{z}). \tag{3.77}$$

Substituting $Y(\mathbf{z}) = G_{yu}(\mathbf{z})U(\mathbf{z})$ in (3.77) yields

$$\mathbf{z}^{-\eta}U(\mathbf{z}) = \hat{G}_{uy,\eta}(\mathbf{z})G_{yu}(\mathbf{z})U(\mathbf{z}). \tag{3.78}$$

It follows from (3.78) that

$$\hat{G}_{uy,\eta}(\mathbf{z})G_{yu}(\mathbf{z}) = \mathbf{z}^{-\eta}I_m, \tag{3.79}$$

which shows that $\hat{G}_{uy,\eta}$ is a deadbeat η-delay left inverse of G_{yu}.

3.6.2 Numerical Examples

The following example illustrates Theorem 4 for a system with rank-deficient Markov parameters and with no invariant zeros.

Example 3.6.1. Consider $G_{yu}(\mathbf{z}) = C(\mathbf{z}I - A)^{-1}B + D$ given by

$$G_{yu}(\mathbf{z}) = \frac{1}{\mathbf{z}^5}(H_5 + H_4\mathbf{z} + H_3\mathbf{z}^2 + H_2\mathbf{z}^3 + H_1\mathbf{z}^4), \tag{3.80}$$

where

$$H_1 = H_2 = H_3 = \begin{bmatrix} 1 & 1 \\ 0 & 0 \\ 0 & 0 \end{bmatrix}, \; H_4 = \begin{bmatrix} 1 & 2 \\ 0 & 0 \\ 1 & 1 \end{bmatrix}, \; H_5 = \begin{bmatrix} 1 & 2 \\ 1 & 0 \\ 1 & 1 \end{bmatrix}. \tag{3.81}$$

Note that H_0 is zero, (A, B, C, D) has no invariant zeros, $\mu = 4$, and $\eta = 5$. To apply Theorem 4 using (3.54), we choose $k = 0$ and $r = 20 \geq \max\{\mu, \eta\} = 5$. Let the unknown initial state $x(0) = [4\ 2\ 1\ 3\ 6\ 8\ 7\ 3\ 1\ 2]^{\mathrm{T}}$ and, for all $k \geq 0$, let the unknown input $u(k) = [u_{(1)}(k)\ u_{(2)}(k)]^{\mathrm{T}}$, where $u_{(1)}(k)$ and $u_{(2)}(k)$ are sampled Gaussian white noise with variance 1. Figure 3.4 shows that, for all $0 \leq k \leq r - \eta = 15$, the reconstructed input is equal to the actual input, which confirms (3.54). Furthermore, the reconstructed initial state (not shown in Fig. 3.4) is equal to $x(0)$. $\diamond$

Example 3.6.2. Reconsider Example 3.5.2 but now with the objective of reconstructing the unknown input u. Note that $\eta = 1$. To reconstruct u, we apply Theorem 4 in two different ways, namely, 1) by using (3.54), and 2) by using the filter $\hat{G}_{uy,1}$ given by (3.77). To apply (3.54), we choose $k = 0$ and $r = 40 \geq \max\{\mu, \eta\} = 2$. Using (3.77), the computed $\hat{G}_{uy,1}$ is given by

$$\hat{G}_{uy,1}(\mathbf{z}) = \begin{bmatrix} \frac{6.344\mathbf{z}^2 + 4.089\mathbf{z} - 0.4335}{\mathbf{z}^2} \\ \frac{6.623\mathbf{z}^2 - 0.2729\mathbf{z} - 0.04078}{\mathbf{z}^2} \end{bmatrix}. \tag{3.82}$$

Figure 3.5 shows that, for all $0 \leq k \leq 40 - \eta = 39$, the reconstructed input is equal to the actual input, which confirms (3.54). It also shows that, for all $\max(\mu - \eta, 0) = 1 \leq k \leq 40 - \eta = 39$, the reconstructed input is equal to the actual input, which confirms (3.77). $\diamond$

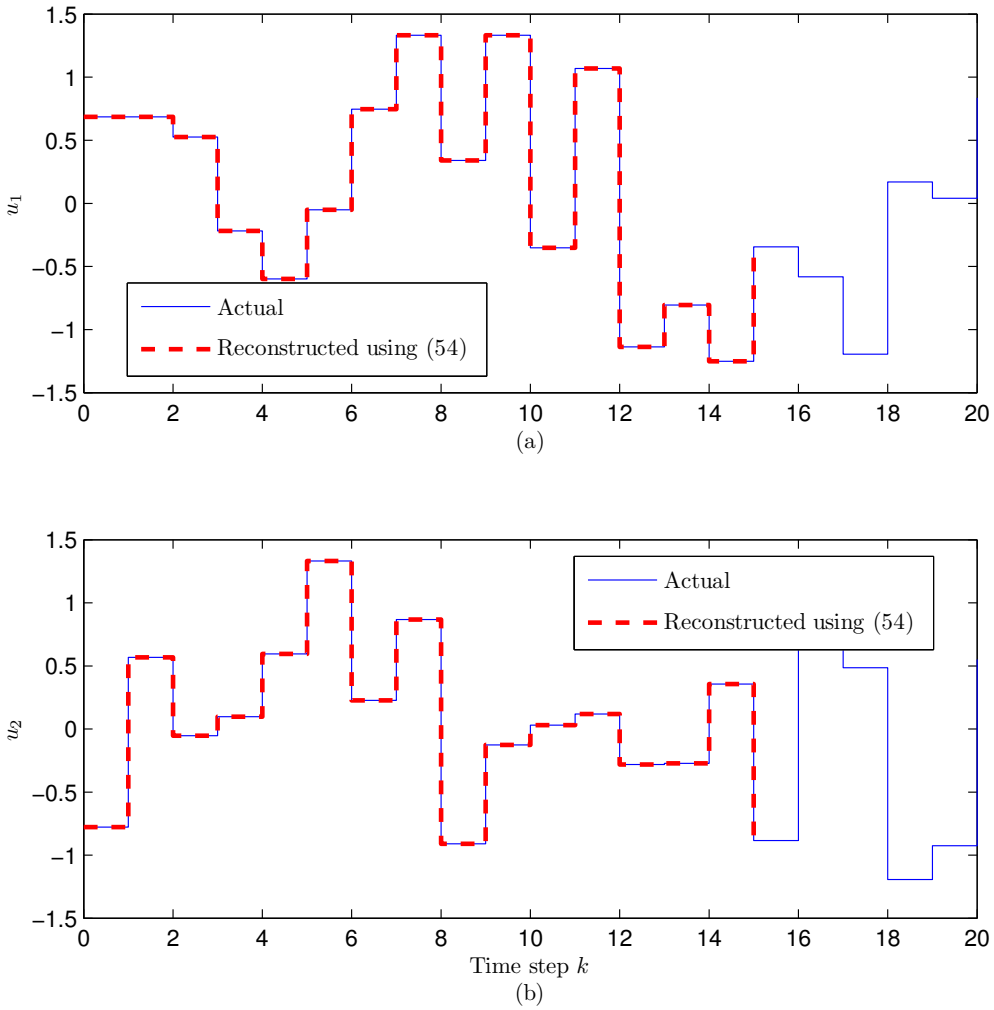

Figure 3.4: Application of Theorem 4 to Example 3.6.1. For all $0 \leq k \leq r - \eta = 15$, the reconstructed input is equal to the actual input, which confirms (3.54).

3.7 Effect of Disturbance and Sensor Noise

The following example illustrates Theorem 4 in the presence of an unknown disturbance that is not reconstructed.

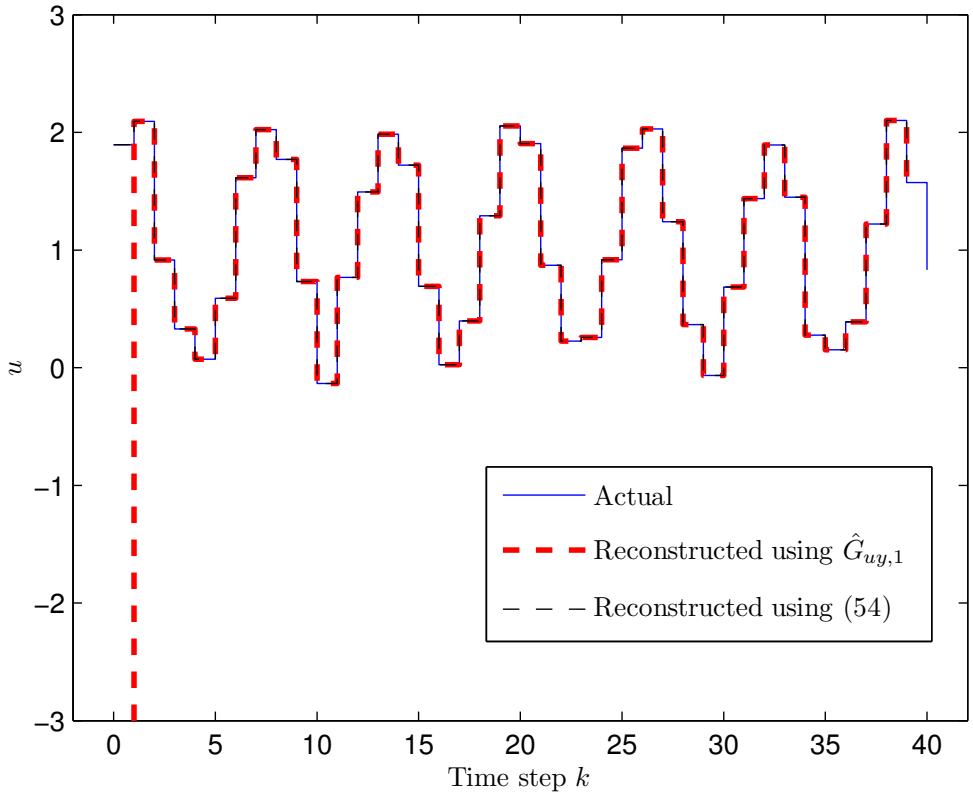

Figure 3.5: Application of Theorem 4 to Example 3.6.2. For all $0 \leq k \leq 40 - \eta = 39$, the reconstructed input is equal to the actual input, which confirms (3.54). For all $\max(\mu - \eta, 0) = 1 \leq k \leq 40 - \eta = 39$, the reconstructed input is equal to the actual input, which confirms (3.77).

Example 3.7.1. Let $G(\mathbf{z}) = C(\mathbf{z}I - A)^{-1}B + D$ be given by

$$G_{yu}(\mathbf{z}) = \frac{1}{(\mathbf{z} - 0.4)(\mathbf{z} - 0.6)^3} \begin{bmatrix} -4 & 1 & \mathbf{z}{-}0.5 \\ 1 & -3 & \mathbf{z}{-}0.1 \end{bmatrix}. \tag{3.83}$$

Note that $p = 2 < m = 3$, and thus *ii*) of Proposition 6 implies that η is infinite. Consequently, Theorem 4 is not applicable for reconstructing the unknown input u. Now, partition $B = [B_1\, B_2\, B_3]$, where B_i is the i^{th} column of B. Note that $(A, [B_1\, B_2], C, D)$ has no invariant zeros, $\eta = 4$, and $\mu = 3$. Let $u(k) = [u_1(k)\, u_2(k)\, u_3(k)]^{\mathrm{T}}$. Thus, if $u_3 \equiv 0$, then Theorem 4 can be used to exactly reconstruct u_1 and u_2 in $\eta = 4$

steps. Now suppose that u_3 is not zero. Since it is impossible to reconstruct all of the components of u, u_3 can be viewed as an unknown disturbance. In this case, we apply Theorem 4 to estimate u_1 and u_2 in the presence of u_3 and assess the resulting accuracy.

Let $u_1(k) = 1$, let $u_2(k) = \sin(k)$, and let $u_3(k)$ be sampled zero-mean Gaussian white noise with variance 0.1. Furthermore, let the available measurement be $[y^{\mathrm{T}}(0) \ \cdots \ y^{\mathrm{T}}(40)]^{\mathrm{T}}$. To reconstruct $[u_1(k)\, u_2(k)]^{\mathrm{T}}$, we apply Theorem 4 in two different ways, namely, 1) by using (3.54), and 2) by using $\hat{G}_{uy,4}$ given by (3.77). To apply (3.54), we choose $k = 0$ and $r = 40 \geq \max\{\mu, \eta\} = 4$. Furthermore, we use (3.77) to compute $\hat{G}_{uy,4}$. Figure 3.6 shows the estimates of u_1 and u_2 in the presence of the unknown disturbance u_3. Note that, for this example, the estimates obtained using $\hat{G}_{uy,4}$ and (3.54) are identical. $\diamond$

In the presence of measurement noise, the following example compares Theorem 4 with ULISE [29] for a system with full-column-rank H_1.

Example 3.7.2. Reconsider Example 3.5.2 but now with the objective of reconstructing the unknown input u in the presence of additive zero-mean Gaussian white sensor noise. The standard deviation of the additive noise in both measurements is 0.01. Figure 3.7 shows the input estimates for $\hat{G}_{uy,1}$, (3.54), and ULISE. For $5 \leq k \leq 39$, the error for $\hat{G}_{uy,1}$ has mean 0.027 N and standard deviation 0.11 N; the error for (3.77) has mean 0.026 N and standard deviation 0.094 N; and the error for ULISE has mean 0.027 N and standard deviation 0.10 N. $\diamond$

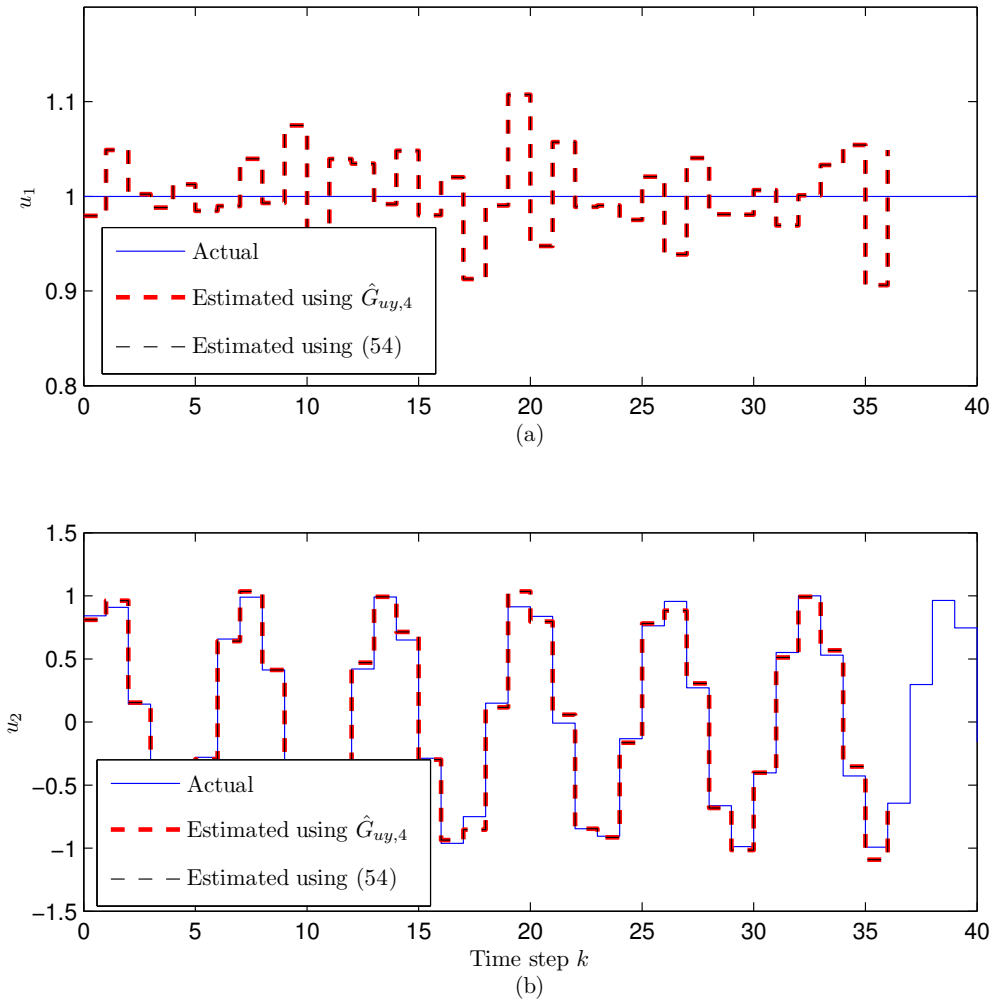

Figure 3.6: Application of Theorem 4 to Example 3.7.1 in the presence of white disturbance.

3.8 Theorem 4 as an Unbiased Input Estimator

Consider the additive sensor and disturbance noise as

$$x(k+1) = Ax(k) + Bu(k) + w(k), \tag{3.84}$$

$$y(k) = Cx(k) + Du(k) + v(k), \tag{3.85}$$

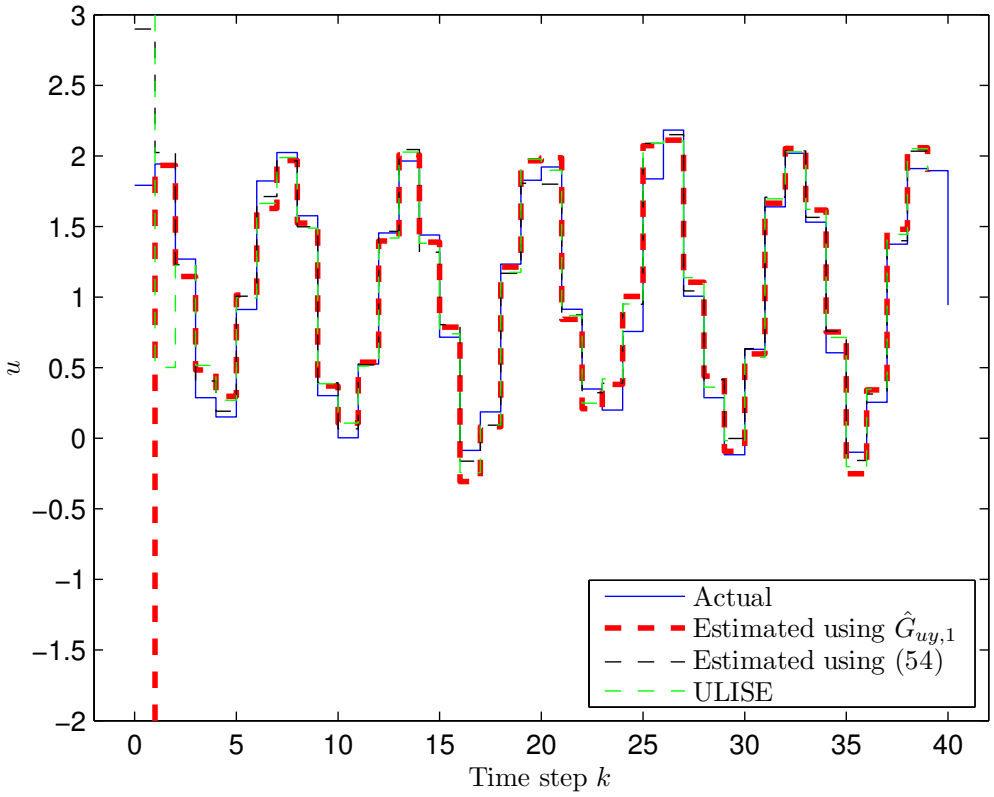

Figure 3.7: Comparison of Theorem 4 with ULISE for Example 3.7.2 in the presence of measurement noise.

where, $w(k) \in \mathbb{R}^n$, and $v(k) \in \mathbb{R}^p$ are zero mean, uncorrelated, white-noise sequences. It follows from (3.84), (3.85) that

$$\mathcal{Y}_r = \Psi_r \begin{bmatrix} x(0) \\ \mathcal{U}_r \end{bmatrix} + \mathcal{N}_r \mathcal{W}_r + \mathcal{V}_r, \tag{3.86}$$

where

$$\mathcal{W}_r \triangleq \begin{bmatrix} w(0) \\ w(1) \\ \vdots \\ w(r) \end{bmatrix}, \in \mathbb{R}^{(r+1)n}, \quad \mathcal{V}_r \triangleq \begin{bmatrix} v(0) \\ v(1) \\ \vdots \\ v(r) \end{bmatrix}, \in \mathbb{R}^{(r+1)p}, \tag{3.87}$$

$$\mathcal{N}_r \triangleq \begin{bmatrix} D & 0 & 0 & \cdots & 0 \\ C & D & 0 & \cdots & 0 \\ CA & C & D & \cdots & 0 \\ \vdots & \vdots & \ddots & \ddots & \vdots \\ CA^{r-1} & CA^{r-2} & \cdots & C & D \end{bmatrix} \in \mathbb{R}^{(r+1)p\times(r+1)n}. \tag{3.88}$$

Let the estimates of $x(0)$ and $\mathcal{U}_{r-\eta}$ given by

$$\begin{bmatrix} \hat{x}(0) \\ \hat{\mathcal{U}}_{r-\eta} \end{bmatrix} \triangleq P_{r,\eta,m,n}\Psi_r^+\mathcal{Y}_r. \tag{3.89}$$

Using (3.86) and (3.89), it follows from (54) of Theorem 4 with $k = 0$ that

$$\begin{bmatrix} \hat{x}(0) \\ \hat{\mathcal{U}}_{r-\eta} \end{bmatrix} = \begin{bmatrix} x(0) \\ \mathcal{U}_{r-\eta} \end{bmatrix} + P_{r,\eta,m,n}\Psi_r^+\mathcal{N}_r\mathcal{W}_r + P_{r,\eta,m,n}\Psi_r^+\mathcal{V}_r. \tag{3.90}$$

Since, by assumption, $w(k)$ and $v(k)$ are zero-mean white noise, (3.90) implies that

$$\mathbb{E}\begin{bmatrix} \hat{x}(0) \\ \hat{\mathcal{U}}_{r-\eta} \end{bmatrix} = \begin{bmatrix} x(0) \\ \mathcal{U}_{r-\eta} \end{bmatrix}, \tag{3.91}$$

and thus (3.89) is an unbiased estimate of $\begin{bmatrix} x(0) \\ \mathcal{U}_{r-\eta} \end{bmatrix}$. The variance of (3.89) is given by

$$\operatorname{var} \begin{bmatrix} \hat{x}(0) \\ \hat{\mathcal{U}}_{r-\eta} \end{bmatrix} = P_{r,\eta,m,n} \Psi_r^+ [N_r R_w N_r^{\mathrm{T}} + R_v] (P_{r,\eta,m,n} \Psi_r^+)^{\mathrm{T}}, \tag{3.92}$$

where $R_w \triangleq \mathbb{E}[\mathcal{W}_r \mathcal{W}_r^{\mathrm{T}}]$, and $R_v \triangleq \mathbb{E}[\mathcal{V}_r \mathcal{V}_r^{\mathrm{T}}]$.

3.9 Linear Time-Varying Systems

Consider the linear time-varying system

$$x(k+1) = A_k x(k) + B_k u(k), \tag{3.93}$$

$$y(k) = C_k x(k) + D_k u(k), \tag{3.94}$$

where, for all $k \geq 0$, $x(k) \in \mathbb{R}^n$, $u(k) \in \mathbb{R}^m$, and $y(k) \in \mathbb{R}^p$. The goal is to use knowledge of $y(k)$ to estimate the unknown state $x(k)$ and the unknown input $u(k)$.

Define

$$\mathcal{Y}_{k:k+r} \triangleq \begin{bmatrix} y(k) \\ y(k+1) \\ \vdots \\ y(k+r) \end{bmatrix} \in \mathbb{R}^{(r+1)p}, \quad \mathcal{U}_{k:k+r} \triangleq \begin{bmatrix} u(k) \\ u(k+1) \\ \vdots \\ u(k+r) \end{bmatrix} \in \mathbb{R}^{(r+1)m}, \tag{3.95}$$

$$\Gamma_{k\,:\,k+r} \triangleq \begin{bmatrix} C_k \\ C_{k+1}A_k \\ C_{k+2}A_{k+1}A_k \\ C_{k+3}A_{k+2}A_{k+1}A_k \\ \vdots \\ C_{k+r}A_{k+r-1}A_{k+r-2}\cdots A_k \end{bmatrix} \in \mathbb{R}^{(r+1)p\times n}, \tag{3.96}$$

$$M_{k\,:\,k+r} \triangleq \begin{bmatrix} D_k & 0 & 0 & 0 & \cdots & 0 \\ C_{k+1}B_k & D_{k+1} & 0 & 0 & \cdots & 0 \\ C_{k+2}A_{k+1}B_k & C_{k+2}B_{k+1} & D_{k+2} & 0 & \cdots & 0 \\ C_{k+3}A_{k+2}A_{k+1}B_k & C_{k+3}A_{k+2}B_{k+1} & C_{k+3}B_{k+2} & D_{k+3} & \cdots & 0 \\ \vdots & \vdots & \vdots & \ddots & \ddots & \vdots \\ C_{k+r}A_{k+r-1}\cdots A_{k+1}B_k & C_{k+r}A_{k+r-1}\cdots A_{k+2}B_{k+1} & C_{k+r}A_{k+r-1}\cdots A_{k+3}B_{k+2} & \cdots & C_{k+r}B_{k+r-1} & D_{k+r} \end{bmatrix}. \tag{3.97}$$

It follows from (3.93), (3.94) that

$$\mathcal{Y}_{k\,:\,k+r} = \Gamma_{k\,:\,k+r}\, x(k) + M_{k\,:\,k+r}\, \mathcal{U}_{k\,:\,k+r} = \Psi_{k\,:\,k+r} \begin{bmatrix} x(k) \\ \mathcal{U}_{k\,:\,k+r} \end{bmatrix}, \tag{3.98}$$

where

$$\Psi_{k\,:\,k+r} \triangleq \begin{bmatrix} \Gamma_{k\,:\,k+r} & M_{k\,:\,k+r} \end{bmatrix} \in \mathbb{R}^{(r+1)p\times[n+(r+1)m]}. \tag{3.99}$$

Let $\bar{\eta} \geq 0$ be the smallest integer, such that, for all $k \geq 0$

$$\mathrm{rank} M_{k+\bar{\eta}} = m + \mathrm{rank} M_{k+\bar{\eta}-1}. \tag{3.100}$$

Furthermore, let $\bar{\mu} \geq 0$ be the smallest integer, such that, for all $k \geq 0$

$$\text{rank}\Psi_{k+\bar{\mu}} = n + \text{rank}M_{k+\bar{\mu}}. \tag{3.101}$$

The following theorem provides deadbeat input and state estimates for linear time-varying systems. The proof of the following theorem is similar to Theorem 4.

Theorem 5. Assume that $\bar{\eta}$ and $\bar{\mu}$ are finite. Then, for all $k \geq 0$ and $r \geq \max\{\bar{\eta}, \bar{\mu}\}$,

$$\begin{bmatrix} x(k) \\ \mathcal{U}_{k:k+r-\bar{\eta}} \end{bmatrix} = \begin{bmatrix} I_{n+(r-\bar{\eta}+1)m} & 0_{[n+(r-\bar{\eta}+1)m]\times\bar{\eta}m} \end{bmatrix} \Psi^{+}_{k:k+r} \mathcal{Y}_{k:k+r}. \tag{3.102}$$

Example 3.9.1. Consider the following linear time-varying system

$$A_k = \begin{cases} \begin{bmatrix} 0 & 0.5 & 0 \\ 0 & 0 & 1 \\ 1.5 & 0 & 0 \end{bmatrix}, & k = 0, 2, 4, \ldots \\ \begin{bmatrix} 0 & 0.5 & 0 \\ 0 & 0 & 1 \\ 0.5 & 0 & 0 \end{bmatrix}, & k = 1, 3, 5, \ldots \end{cases} \tag{3.103}$$

and, for all $k \geq 0$

$$B_k = \begin{bmatrix} 0 & 0 & 1 \end{bmatrix}^{\mathrm{T}}, C_k = \begin{bmatrix} 1 & 0 & 0 \\ 0 & 0 & 1 \end{bmatrix}, D_k = \begin{bmatrix} 0 & 0 \end{bmatrix}^{\mathrm{T}}. \tag{3.104}$$

Note that $\bar{\eta} = \bar{\mu} = 1$. To apply Theorem 5 using (3.102), we choose $k = 0$ and

$r = 5 \geq \max\{\bar{\eta}, \bar{\mu}\} = 1$. Let the unknown initial state $x(0) = [4\ 6\ 10]^{\mathrm{T}}$ and, for all $k \geq 0$, let the unknown input $u(k)$ be sampled Gaussian white noise with variance 1. Figure 3.8 shows that, for all $0 \leq k \leq r - \eta = 4$, the reconstructed input is equal to the actual input, which confirms (3.102). Furthermore, the reconstructed initial state (not shown in Fig. 3.8) is equal to $x(0)$. $\diamond$

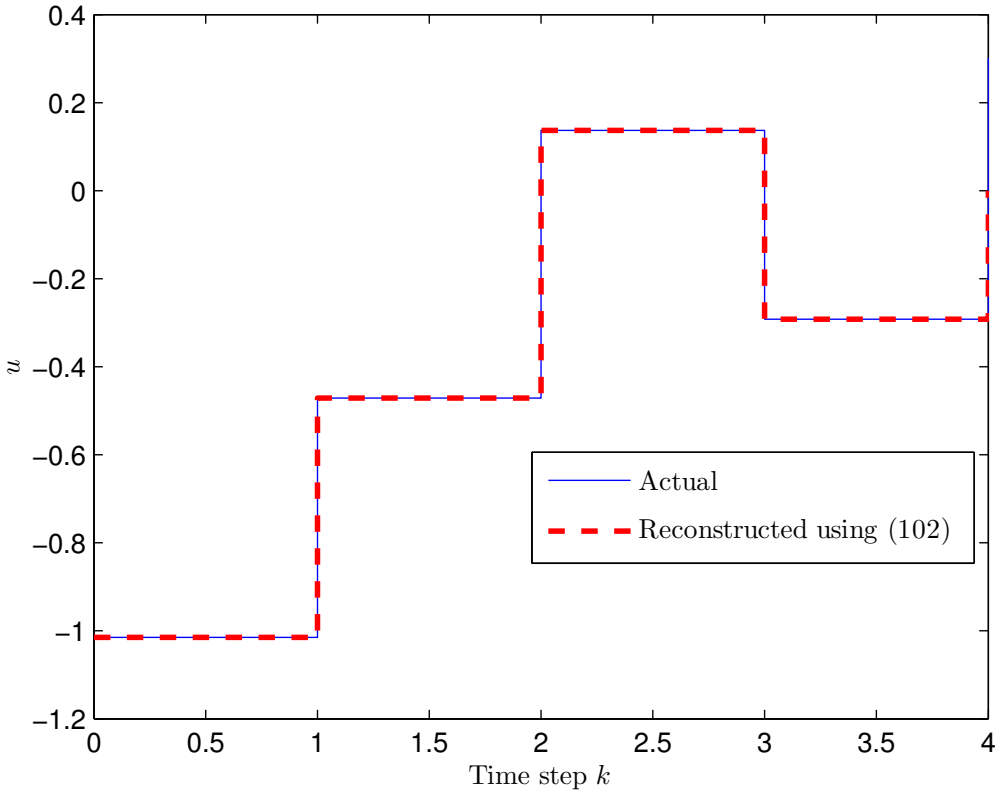

Figure 3.8: Application of Theorem 5 to Example 3.9.1. For all $0 \leq k \leq r-\eta = 4$, the reconstructed input is equal to the actual input, which confirms (3.102).

3.10 Conclusions

Using the generalized inverse of a block-Toeplitz matrix, this chapter presented simplified and unified algorithms for deadbeat input reconstruction and state estimation for MIMO systems that are d-delay invertible, that is, invertible with a delay of

d steps. These algorithms do not assume the existence of a full-column-rank Markov parameter.

The assumption that the system is d-delay invertible is equivalent to the finiteness of the index η, which is the smallest delay d such that the system is d-delay invertible. Various questions concerning η remain open. Although the finiteness of η can be verified by checking n rank conditions, an easily verifiable necessary and sufficient condition for the finiteness of η is lacking. Numerical examples suggest that the existence of at least one Markov parameter with full column rank implies that η is finite; however, (3.18) shows that this condition is not necessary. Since the finiteness of η is a necessary and sufficient condition for the existence of a d-delay inverse with smallest delay, it seems reasonable to view η as the relative degree of square or tall systems. This notion may have relevance to other areas such as adaptive control.

In the next chapter, we consider asymptotic input estimation for systems with invariant zeros and rank deficient Markov parameters.

CHAPTER 4

Asymptotic Input and State Estimation Based on the Projection onto the Complement of Unobservable Input Subspace

4.1 Introduction

Deadbeat input reconstruction for systems with at least one invariant zero and unknown initial condition is impossible. This can easily be seen by noting that if the system has an invariant zero, then it has a nontrivial unobservable input subspace [24]. In this case, asymptotic input reconstruction must be considered, with careful attention paid to the presence of nonmimimum-phase zeros.

This chapter first numerically investigates the effect of invariant zeros either inside or outside the unit circle on the projected input sequence onto the orthogonal complement of unobservable input subspace. Then, using the projection, we give Property 4.1 for asymptotic input estimation, and demonstrate it numerically in Example 4.4.1. Proof of this property is outside the scope of this dissertation.

4.2 Projection Onto the Orthogonal Complement of Unobservable Input Subspace

We now consider systems of the form [(2.1),(2.2)] that are not IISO due to the presence of invariant zeros. Theorem 1 implies that $\mathcal{N}(\Psi_r)$ is nonzero, where Ψ_r is given by (2.6). Thus, the initial state and input sequence cannot be determined uniquely. Consequently, we use the projector $\mathcal{P}_{r,\perp} \stackrel{\triangle}{=} \Psi_r^+\Psi_r$, where Ψ_r^+ is the genearlized inverse of Ψ_r, to estimate the projection of the state and input sequence onto $\mathcal{N}(\Psi_r)^\perp$. For an input sequence of length r starting at step $k \geq 0$, this projection is given by

$$\begin{bmatrix} x_{\perp,k,r}(k) \\ d_{\perp,k,r}(k) \\ \vdots \\ d_{\perp,k,r}(k+r-1) \end{bmatrix} \stackrel{\triangle}{=} \mathcal{P}_{r,\perp} \begin{bmatrix} x(k) \\ d(k) \\ \vdots \\ d(k+r-1) \end{bmatrix} = \Psi_r^+ \begin{bmatrix} y(k) \\ y(k+1) \\ \vdots \\ y(k+r) \end{bmatrix}. \tag{4.1}$$

The dimension of the nullspace of Ψ_r is given by the following proposition.

Proposition 9. Assume that η exists. Then, for all $r \geq \eta$,

$$\dim(\mathcal{N}(\Psi_r)) = \eta + \text{number of invariant zeros.} \tag{4.2}$$

The following example illustrates Proposition 9.

Example 4.2.1. Consider $\mathcal{G}(\mathrm{z}) = C(\mathrm{z}I - A)^{-1}G$ given by

$$\mathcal{G}(\mathrm{z}) = \frac{\mathrm{z} - 1.2}{(\mathrm{z} - 0.9)^2(\mathrm{z} - 0.6)^2} \begin{bmatrix} 1 \\ \mathrm{z} - 0.85 \end{bmatrix}. \tag{4.3}$$

Note that (A, G, C) has one invariant zero at 1.2, $H_0 = H_1 = 0_{2\times 1}$, and $\eta = 2$. It thus follows from Proposition 9 that, for all $r \geq \eta = 2$, $\dim(\mathcal{N}(\Psi_r)) = 2 + 1 = 3$,

which can be confirmed numerically. $\diamond$

4.3 Effect of an Invariant Zero on the Unobservable Input

Depending on the location of the invariant zero ξ, the unobservable input (2.13) has the following properties:

1. If ξ is inside the open unit disk, then $d(r)$ converges to zero.

2. If ξ is on the unit circle, then $d(r)$ is persistent.

3. If ξ is outside the closed unit disk, then $d(r)$ diverges.

The following example illustrates properties of the projection (4.1) for various locations of the invariant zero for a system with full-column-rank CG.

Example 4.3.1. Consider the 2×1 transfer function $\mathcal{G}(\mathrm{z}) = C(\mathrm{z}I - A)^{-1}G$ given by

$$\mathcal{G}(\mathrm{z}) = \frac{(\mathrm{z} - \xi)(\mathrm{z} - \mathrm{conj}(\xi))}{(\mathrm{z} - 0.9)(\mathrm{z} - 0.8)(\mathrm{z} - 0.7)(\mathrm{z} - 0.6)} \begin{bmatrix} 1 \\ \mathrm{z} - 0.85 \end{bmatrix}, \tag{4.4}$$

where $\xi \in \mathbb{C}$ is an invariant zero of (A, G, C) and $\mathrm{conj}(\xi)$ is the conjugate of ξ. Note that, since the relative degree of the $(2, 1)$ entry of $\mathcal{G}$ is 1, it follows that CG is nonzero and thus has full column rank, and thus, for all $r \geq 1$, M_r has full column rank. However, since (A, G, C) has two invariant zeros, Proposition 3 implies that [(2.1),(2.2)] is not IISO.

Now, let $\begin{bmatrix} \bar{x} \\ \bar{d} \end{bmatrix} \in \mathcal{N}(\mathcal{Z}(\xi))$ be nonzero with nonzero real part, and define $d(k) = d_{\mathrm{ob}}(k) + d_{\mathrm{uo}}(k)$, where, for all $k \geq 0$, $d_{\mathrm{ob}}(k) = 1$ and $d_{\mathrm{uo}}(k) = \mathrm{Re}(\xi^k \bar{d})$. Furthermore, let $x(0) = \mathrm{Re}(\bar{x})$, and let $\hat{d}_{\mathrm{ULISE}}$ denote the input estimate given by the ULISE filter

[29]. Therefore,

$$\begin{bmatrix} x(0) \\ \mathcal{D}_{r-1} \end{bmatrix} = \begin{bmatrix} 0 \\ \mathcal{D}_{\mathrm{ob},r-1} \end{bmatrix} + \begin{bmatrix} x(0) \\ \mathcal{D}_{\mathrm{uo},r-1} \end{bmatrix}, \tag{4.5}$$

where

$$\mathcal{D}_{\mathrm{ob},r-1} \triangleq \begin{bmatrix} d_{\mathrm{ob}}(0) \\ d_{\mathrm{ob}}(1) \\ \vdots \\ d_{\mathrm{ob}}(r) \end{bmatrix}, \quad \mathcal{D}_{\mathrm{uo},r-1} \triangleq \begin{bmatrix} d_{\mathrm{uo}}(0) \\ d_{\mathrm{uo}}(1) \\ \vdots \\ d_{\mathrm{uo}}(r) \end{bmatrix}. \tag{4.6}$$

It thus follows from Proposition 3 that

$$\mathcal{P}_{r,\perp} \begin{bmatrix} x(0) \\ \mathcal{D}_{\mathrm{uo},r-1} \end{bmatrix} = 0, \tag{4.7}$$

which, along with (4.1) and (4.5), yields

$$\mathcal{P}_{r,\perp} \begin{bmatrix} x(0) \\ \mathcal{D}_{r-1} \end{bmatrix} = \mathcal{P}_{r,\perp} \begin{bmatrix} 0 \\ \mathcal{D}_{\mathrm{ob},r-1} \end{bmatrix} = \Psi_r^+ \mathcal{Y}_r. \tag{4.8}$$

We choose $r = 200$ and $k = 0$ to compute Ψ_r^+ and $d_{\perp,k,r}$ in (4.1).

First, let $\xi = 0.6 + 0.6\jmath$, which lies in the open unit disk. In this case, Figure 4.1a shows that $d_{\perp,0,41}$ and $\hat{d}_{\mathrm{ULISE}}$ converge to d_{ob}. Furthermore, Figure 4.1a shows that $d - d_{\mathrm{ob}}$ converges to zero, which is consistent with the fact that $d_{\mathrm{uo}} = d - d_{\mathrm{ob}}$ converges to zero. Thus, $d - d_{\perp,0,41}$ and $d - \hat{d}_{\mathrm{ULISE}}$ also converge to zero. Figure 4.1b shows that, for $k \geq 30$, the input estimates obtained using (4.8) and the method of [29] closely follow d_{ob} and are essentially identical.

Next, let $\xi = 0.6 + 0.8\jmath$, which lies on the unit circle. In this case, Figure 4.1c

shows that, as r increases, $d_{\perp,0,r}$ converges to d for all k, whereas, $\hat{d}_{\text{ULISE}} \neq d_{\text{ob}}$. Furthermore, Figure 4.1c shows that $d - d_{\text{ob}}$ does not converge to zero, which is consistent with the fact that d_{uo} is harmonic. Figure 4.1d shows that the magnitude of the error $d_{\text{ob}} - \hat{d}_{\text{ULISE}}$ does not decrease, whereas, as r increases, the error $d_{\text{ob}} - d_{\perp,0,r}$ converges to zero for all k.

Finally, let $\xi = 0.8 + 0.7\jmath$, which lies outside the closed unit disk. Figure 4.1e shows that $\hat{d}_{\text{ULISE}}$ diverges from both d_{ob} and d. This divergence is consistent with the fact that Theorem 6 in [29] is confined to minimum-phase systems. On the other hand, Figure 4.1e shows that, $d_{\perp,0,61}(0)$ converges to $d_{\text{ob}}(0)$. Figure 4.1f shows that the error $d_{\perp,0,61} - d_{\text{ob}}$ converges to zero backward in time. $\diamond$

4.4 Input Estimation for Systems with Invariant Zeros

For a system with an invariant zero ξ, Example 4.3.1 illustrates that, as the length r of the data window increases, the projected input $d_{\perp,k,r}$ given by (4.1) converges to d. However, the convergence "direction" depends on the location of ξ relative to the unit circle. These observations are captured by the following property of the input sequence projected onto $\mathcal{N}(\Psi_r)^{\perp}$, which is demonstrated numerically in Example 4.4.1 below. Proof of this property is outside the scope of this dissertation.

Property 4.1. Assume that (A, G, C) has no zeros on the unit circle, d is bounded, and η is finite. Furthermore, for all $r > \eta$, let $\delta(r) \in [0,\, r - \eta]$, and assume that $\delta(r)$ satisfies the following conditions:

i) If (A, G, C) has all invariant zeros inside the open unit disk, then $\lim_{r\to\infty} \delta(r) = \infty$.

ii) If (A, G, C) has all invariant zeros outside the closed unit disk, then $\lim_{r\to\infty}[r - \delta(r)] = \infty$.

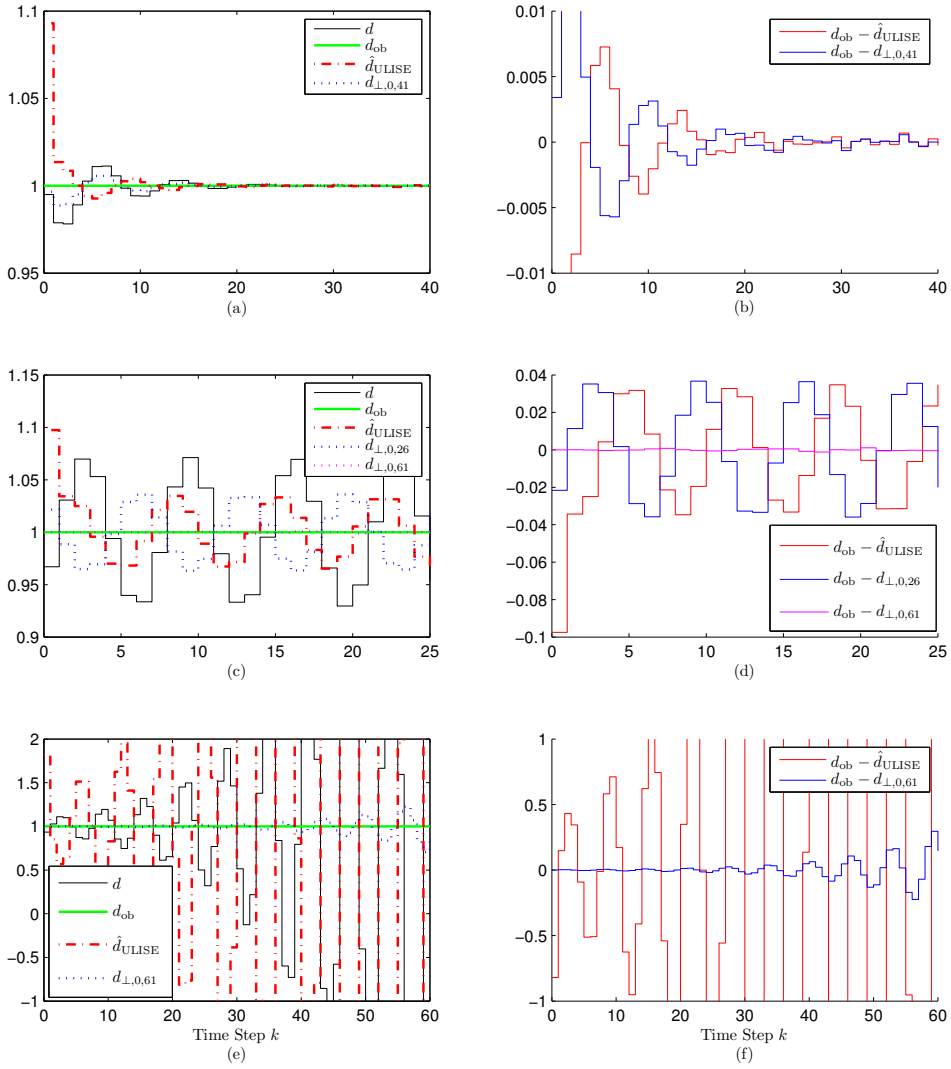

Figure 4.1: Comparison of the ULISE filter and the projection (4.8) in Example 4.3.1 for various locations of the invariant zero ξ. (a) $d_{\perp,0,41}$ and $\hat{d}_{\text{ULISE}}$ converge to d_{ob}. (b) For $k \geq 30$, the input estimates obtained using (4.8) and ULISE closely follow d_{ob} and are essentially identical. (c) As r increases, $d_{\perp,0,r}$ converges to d_{ob} for all k, whereas, $\hat{d}_{\text{ULISE}} \neq d_{\text{ob}}$. (d) The magnitude of the error $d_{\text{ob}} - \hat{d}_{\text{ULISE}}$ does not decrease, whereas, as r increases, the error $d_{\text{ob}} - d_{\perp,0,r}$ converges to zero for all k. (e) $\hat{d}_{\text{ULISE}}$ diverges from both d_{ob} and d. (f) The error $d_{\perp,0,61} - d_{\text{ob}}$ converges to zero backward in time.

iii) If (A, G, C) has at least one invariant zero inside the open unit disk and at least one invariant zero outside the closed unit disk, then $\lim_{r\to\infty} \delta(r) = \lim_{r\to\infty}[r -$

$\delta(r)] = \infty$.

Then, for all $k \geq 0$,

$$\lim_{r\to\infty} \{ \begin{bmatrix} 0_{l_d\times(l_x+\delta(r)l_d)} & I_{l_d} & 0_{l_d\times(r-\delta(r)-1)l_d} \end{bmatrix} \Psi_r^+ \begin{bmatrix} y(k) \\ y(k+1) \\ \vdots \\ y(k+r) \end{bmatrix} - d(k+\delta(r))\} = 0. \quad (4.9)$$

Using the notation (4.1), it follows that (4.9) can be written as

$$\lim_{r\to\infty} [d_{\perp,k,r}(k+\delta(r)) - d(k+\delta(r))] = 0. \quad (4.10)$$

The following example illustrates Property 4.1 for a system with invariant zeros and rank-deficient Markov parameters.

Example 4.4.1. Consider $\mathcal{G}(\mathrm{z}) = C(\mathrm{z}I - A)^{-1}G$ given by

$$\mathcal{G}(\mathrm{z}) = \frac{(\mathrm{z}-0.8)(\mathrm{z}-1.2)}{(\mathrm{z}-0.9)^2(\mathrm{z}-0.6)^3} \begin{bmatrix} 1 \\ \mathrm{z}-0.85 \end{bmatrix}. \quad (4.11)$$

The invariant zeros of (A, G, C) are 0.8 and 1.2, which corresponds to *iii*) of Property 1. Furthermore, $H_1 = 0$ and $\eta = 2$. Let the unknown initial state $x(0) = [1 \;\; 1 \;\; 2 \;\; 4 \;\; 5]^{\mathrm{T}}$ and, for all $k \geq 0$, let the unknown input $d(k)$ be sampled Gaussian white noise with variance 1. To apply Property 4.1, we choose $\delta(r) = \frac{r-1}{2}$, and hence $\delta(r)$ satisfies $\lim_{r\to\infty} \delta(r) = \lim_{r\to\infty}[r - \delta(r)] = \infty$. For the case k=0, Figure 4.2 shows that, as r increases, $|d_{\perp,0,r}(\delta(r)) - d(\delta(r))|$ converges to zero, which illustrates (4.10).

Next, for $l \geq 1$ and data $[y^{\mathrm{T}}(0) \;\; y^{\mathrm{T}}(1) \;\; \ldots \;\; y^{\mathrm{T}}(l)]^{\mathrm{T}}$, we use (4.9) to estimate the unknown input d. Let $r \leq l$ and, for all $k \in [0, l-r]$, let $d_{\perp,k,r}(k+\delta(r))$ be the estimate of $d(k+\delta(r))$. To illustrate (4.10), choose $r = 61 < l = 200$, and hence $\delta(r) = 30$. Figure 4.3(a) shows that, for all $k \in [0, 139]$, $d_{\perp,k,61}(k+30)$ follows $d(k+30)$

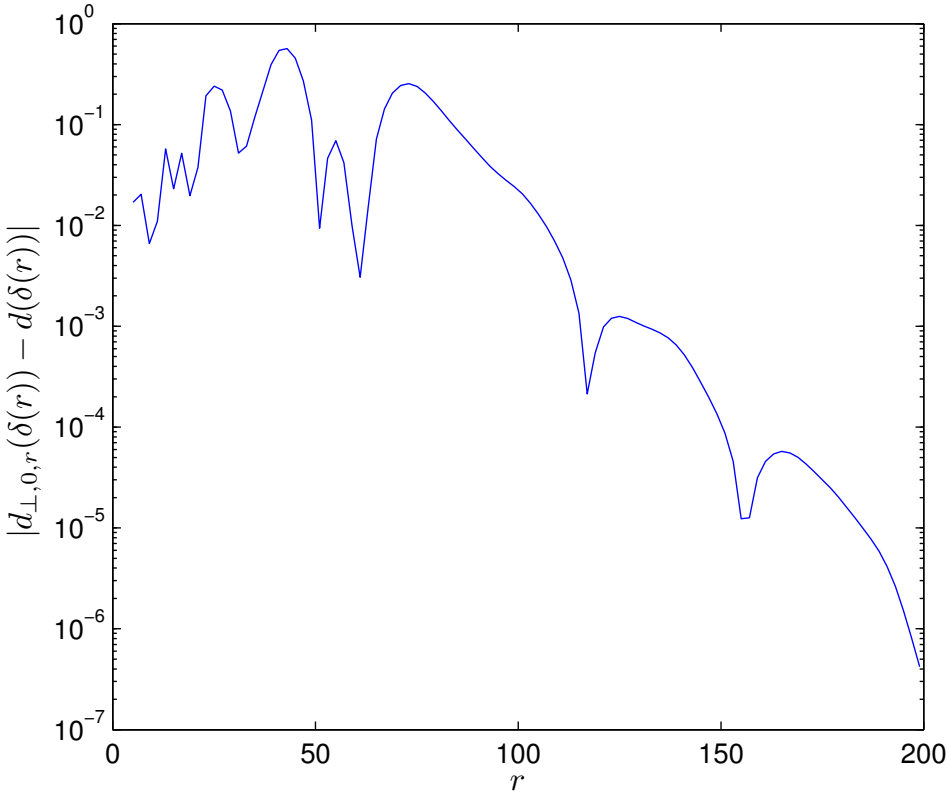

Figure 4.2: Illustration of Property 4.1 for Example 4.4.1. Note that, $|d_{\perp,0,r}(\delta(r)) - d(\delta(r))|$ decreases as r increases, which illustrates (4.10) and thus also (4.9).

with root-mean-squared-error (RMSE) 0.71. Next, we choose $r = 121 < l = 200$, and hence $\delta(r) = 60$. Figure 4.3(b) shows that, for all $k \in [0, 79]$, $d_{\perp,k,61}(k{+}30)$ follows $d(k{+}60)$ with RMSE 0.0027. Figures 4.3(a) and 4.3(b) show that, as r increases, the estimates improve; however, the length of the estimation window $l{-}r{+}1$ decreases as r increases. $\diamond$

4.5 Conclusions

This chapter presented Property 4.1 for system with zeros either inside or outside the unit disk. The property is based on a batch algorithm which requires the

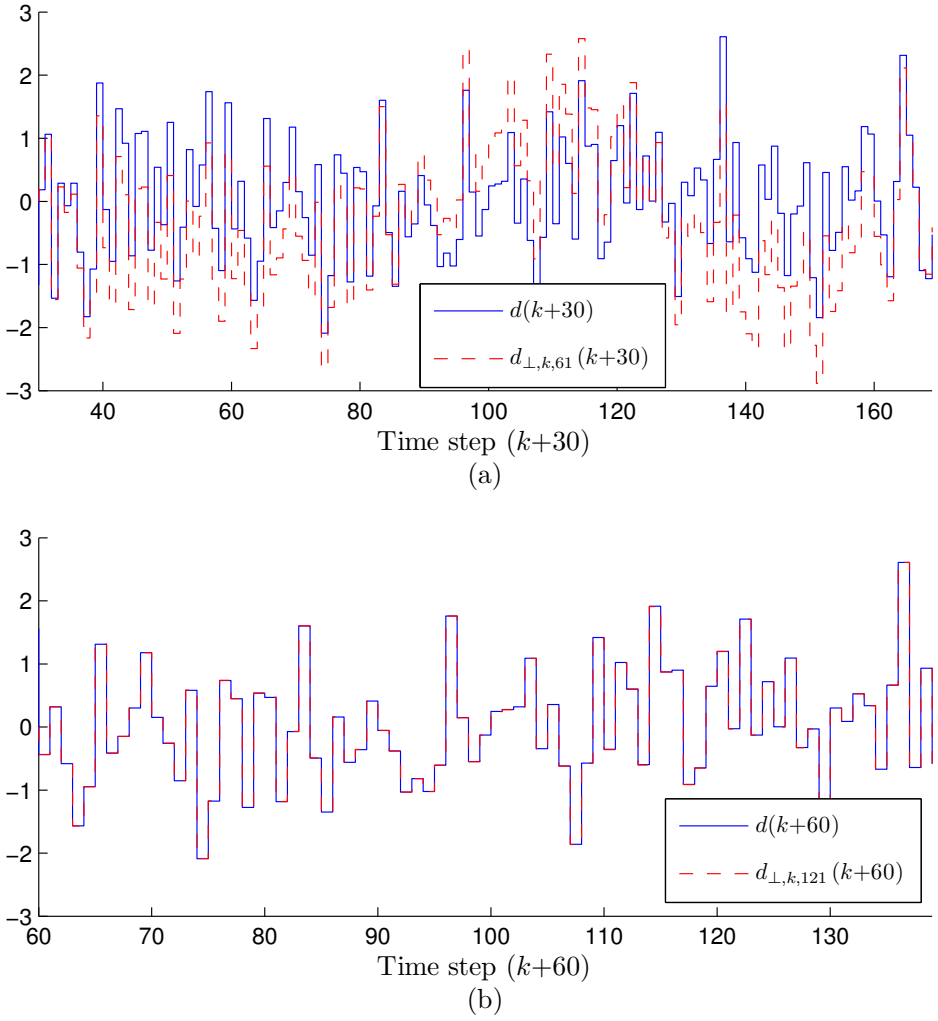

Figure 4.3: Estimation of the unknown input d for the system (4.11) in Example 4.4.1 using (4.9). (a) For all $k \in [0, 139]$, $d_{\perp,k,61}(k+30)$ follows $d(k+30)$ with RMSE of 0.71. (b) For all $k \in [0, 79]$, $d_{\perp,k,61}(k+30)$ closely follows $d(k+60)$ with RMSE of 0.0027. Note that, as r increases, the estimates improve; however, the length of the estimation window $l-r+1$ decreases as r increases.

computation of the generalized inverse Ψ_r^+. Thus, techniques that would avoid the need to compute Ψ_r^+ for large r is desirable. The next chapter presents an input and state estimation algorithm based on the retrospective cost and Kalman filter, which is recursive and effective for systems with zeros anywhere in the complex plane.

CHAPTER 5

Asymptotic Input and State Estimation Based on the Retrospective Cost and Kalman Filter

5.1 Introduction

The Kalman filter and its variants provide well-established techniques for estimating states that are not directly measured [1–3, 80, 81]. The goal of these techniques is to obtain optimal state estimates in the presence of process and sensor noise. These techniques typically assume that the sensor and process noise are stationary with zero mean. If, however, the process noise includes a known deterministic component, then estimator bias can be avoided by injecting this component into the estimator; this technique underlies the separation principle of linear-quadratic-Gaussian control. If, however, the process noise is biased, that is, has unknown, nonzero mean, or, more generally, it includes an unknown deterministic component, then it is of interest to obtain estimates that are unbiased, that is, unaffected by the deterministic-but-unknown input. This problem is addressed in [4–7, 82].

The advantages of injecting the known deterministic input signal into the estimator motivate the development of techniques for estimating not only the unmeasured states but also the unknown deterministic input. The value of this objective in practice resides in the fact that knowledge of the deterministic input and its injection

into the estimator can greatly increase the accuracy of the state estimates relative to the ad hoc technique of choosing the disturbance covariance matrix to overbound the deterministic input. The potential value of this approach is evident from the increasing literature on input estimation [12, 14–31, 35–39].

An alternative approach to input estimation is to assume that the unknown input is the output of an auxiliary linear/nonlinear system with known dynamics driven by white noise. The dynamics of the auxiliary system are appended to the dynamics of the physical system, and the augmented model is used to as the basis of the state estimator [83–85]. This approach may not be accurate, however, if the unknown input cannot be approximated by the output of a linear system driven by white noise. The approach of the present chapter can be viewed as an adaptive technique for learning suitable dynamics that capture the unknown input.

The motivation for the present chapter resides in the fact that most of the techniques for state and input estimation cited above are confined to minimum-phase systems, that is, systems with invariant zeros contained in the open unit disk. In particular, the approach of [29], which extends the method of [17], explicitly invokes a minimum-phase assumption.

The case of nonminimum-phase (NMP) zeros, that is, zeros that are either on the unit circle or outside the closed unit disk, is much more challenging. As shown in [24], a naive attempt to estimate the input for a NMP system with zeros outside the closed unit disk yields a reconstruction error that is unbounded; in the case of zeros on the unit circle, the input-reconstruction error is bounded but nonzero. In contrast, in the case of minimum-phase systems, the input-reconstruction error vanishes asymptotically. Unlike most of the references cited above, [39] considers the case of NMP zeros, but the method is not applicable to the case of zeros on the unit circle.

More generally, it is important to stress that exact input reconstruction for a

system with *any* zeros is impossible. This can easily be seen by noting that the presence of an invariant zero implies the existence of an initial condition and input for which the output is identically zero. These details are related to the *unobservable input subspace* [24]. Hence, in the case where the system has one or more invariant zeros, the goal is to achieve asymptotic input reconstruction of the component of the input that resides in the orthogonal complement of the unobservable input subspace.

The present chapter is aimed at the case where the system is NMP. In particular, the present chapter considers state and input estimation based on retrospective cost optimization [38, 40–45]. Based on this technique, the contribution of the present chapter is the development of retrospective cost input estimation (RCIE), which is a technique for state and input estimation that is effective for NMP systems. This approach uses an estimator whose coefficients are recursively updated at each time step so as to minimize a retrospective cost function. Motivation for this approach is discussed within the context of adaptive control in [47, 48].

The contents of this chapter are as follows. Section 5.2 introduces the state and input estimation problem along with the RCIE algorithm and details of the input-estimation subsystem. Section 5.3 shows how RCIE can asymptotically reconstruct the input to a NMP system by embedding an internal model of the unknown input in the input-estimation subsystem. Section 5.4 illustrates the effect of the unobservable input subspace. Finally, in Section 5.5, we compare RCIE with the filter presented in [29].

5.2 Input and State Estimation

Consider the linear discrete-time system

$$x(k) = A(k-1)x(k-1) + B(k-1)u(k-1) + G(k-1)d(k-1) + D_1(k-1)w(k-1), \tag{5.1}$$

$$y(k) = C(k)x(k) + D_2(k)v(k), \tag{5.2}$$

where $x(k) \in \mathbb{R}^{l_x}$ is the unknown state, $u(k) \in \mathbb{R}^{l_u}$ is the known input, $d(k) \in \mathbb{R}^{l_d}$ is the unknown input, $w(k) \in \mathbb{R}^{l_w}$ is unknown white process noise with zero mean and unit variance, $y(k) \in \mathbb{R}^{l_y}$ is the measured output, and $v(k) \in \mathbb{R}^{l_v}$ is unknown white measurement noise with zero mean and unit variance. This model may represent a sampled-data version of a continuous-time plant with sample time T_s, in which case $x(k)$ denotes the state at time $t = kT_\mathrm{s}$. The matrices $A(k) \in \mathbb{R}^{l_x \times l_x}$, $B(k) \in \mathbb{R}^{l_x \times l_u}$, $G(k) \in \mathbb{R}^{l_x \times l_d}$, $D_1(k) \in \mathbb{R}^{l_x \times l_w}$, $C(k) \in \mathbb{R}^{l_y \times l_x}$, and $D_2(k) \in \mathbb{R}^{l_y \times l_v}$ are assumed to be known. The process noise covariance is $V_1(k) \triangleq D_1(k)D_1(k)^{\mathrm{T}} \in \mathbb{R}^{l_x \times l_x}$, and the measurement noise covariance is $V_2(k) \triangleq D_2(k)D_2(k)^{\mathrm{T}} \in \mathbb{R}^{l_y \times l_y}$. The goal is to estimate the unknown input $d(k)$ and the unknown state $x(k)$.

5.2.1 Retrospective Cost Input Estimation (RCIE)

In order to estimate the unknown input $d(k)$, we consider the Kalman filter forecast step

$$x_{\mathrm{fc}}(k) = A(k-1)x_{\mathrm{da}}(k-1) + B(k-1)u(k-1) + G(k-1)\hat{d}(k-1), \tag{5.3}$$

$$y_{\mathrm{fc}}(k) = C(k)x_{\mathrm{fc}}(k), \tag{5.4}$$

$$z(k) = y_{\mathrm{fc}}(k) - y(k), \tag{5.5}$$

where $\hat{d}(k) \in \mathbb{R}^{l_d}$ is the input estimate, $x_{\mathrm{da}}(k) \in \mathbb{R}^{l_x}$ is the data-assimilation state, $x_{\mathrm{fc}}(k) \in \mathbb{R}^{l_x}$ is the forecast state, and $z(k) \in \mathbb{R}^{l_y}$ is the innovations. The goal is to develop an input estimator that minimizes $z(k)$ by estimating $d(k)$.

We obtain the input estimate $\hat{d}(k)$ as the output of the *input-estimation subsystem* of order n_{c} given by

$$\hat{d}(k) = \sum_{i=1}^{n_c} P_i(k)\hat{d}(k-i) + \sum_{i=0}^{n_c} Q_i(k)z(k-i), \tag{5.6}$$

where $P_i(k) \in \mathbb{R}^{l_d \times l_d}$ and $Q_i(k) \in \mathbb{R}^{l_d \times l_y}$. Note that (5.6) represents an exactly proper transfer function with direct feedthrough from the innovations $z(k)$ to the estimate $\hat{d}(k)$ of $d(k)$. RCIE minimizes $z(k)$ by updating $P_i(k)$ and $Q_i(k)$. The subsystem (5.6) can be reformulated as

$$\hat{d}(k) = \Phi(k)\theta(k), \tag{5.7}$$

where the regressor matrix $\Phi(k)$ is defined by

$$\Phi(k) \triangleq \begin{bmatrix} \hat{d}(k-1) \\ \vdots \\ \hat{d}(k-n_{\mathrm{c}}) \\ z(k) \\ \vdots \\ z(k-n_{\mathrm{c}}) \end{bmatrix}^{\mathrm{T}} \otimes I_{l_d} \in \mathbb{R}^{l_d \times l_\theta}$$

and

$$\theta(k) \triangleq \mathrm{vec} \begin{bmatrix} P_1(k) \cdots P_{n_{\mathrm{c}}}(k) \; Q_0(k) \cdots Q_{n_{\mathrm{c}}}(k) \end{bmatrix} \in \mathbb{R}^{l_\theta},$$

where $l_\theta \triangleq l_d^2 n_{\mathrm{c}} + l_d l_y(n_{\mathrm{c}}+1)$, "$\otimes$" is the Kronecker product, and "vec" is the column-

stacking operator. The order n_c of the input-estimation subsystem must be chosen large enough to accommodate an internal model of the unknown input. The action of the internal model is described in Section 5.3.

Define the $l_y \times l_d$ filter $G_{f,k}(\mathbf{q}) \triangleq D_{f,k}^{-1}(\mathbf{q})N_{f,k}(\mathbf{q})$, where $\mathbf{q}$ is the forward shift operator, $n_f \geq 1$ is the order of G_f,

$$N_{f,k}(\mathbf{q}) \triangleq K_1(k)\mathbf{q}^{n_f-1} + K_2(k)\mathbf{q}^{n_f-2} + \cdots + K_{n_f}(k), \tag{5.8}$$

$$D_{f,k}(\mathbf{q}) \triangleq I_{l_y}\mathbf{q}^{n_f} + A_1(k)\mathbf{q}^{n_f-1} + A_2(k)\mathbf{q}^{n_f-2} + \cdots + A_{n_f}(k), \tag{5.9}$$

and, for all $1 \leq i \leq n_f$ and $k \geq 0$, $K_i(k) \in \mathbb{R}^{l_y \times l_d}$ and $A_i(k) \in \mathbb{R}^{l_y \times l_y}$.

Next, for all $k \geq 0$, we define the *retrospective input*

$$d_{rc}(\hat{\theta}, k) \triangleq \Phi(k)\hat{\theta} \tag{5.10}$$

and the corresponding *retrospective performance variable*

$$z_{rc}(\hat{\theta}, k) \triangleq z(k) + G_{f,k}(\mathbf{q})[d_{rc}(\hat{\theta}, k) - \hat{d}(k)], \tag{5.11}$$

where the filter $G_{f,k}(\mathbf{q})$ is derived in Section 5.2.3 and the coefficient vector $\hat{\theta} \in \mathbb{R}^{l_\theta}$ is determined by optimization below. Defining

$$\Phi_f(k) \triangleq G_{f,k}(\mathbf{q})\Phi(k) \in \mathbb{R}^{l_y \times l_\theta}, \tag{5.12}$$

$$\hat{d}_f(k) \triangleq G_{f,k}(\mathbf{q})\hat{d}(k) \in \mathbb{R}^{l_y}, \tag{5.13}$$

it follows that $z_{rc}(\hat{\theta}, k)$ can be written as

$$z_{rc}(\hat{\theta}, k) = z(k) + \Phi_f(k)\hat{\theta} - \hat{d}_f(k). \tag{5.14}$$

For $k \geq 1$, we define the retrospective cost function

$$J(\hat{\theta}, k) \triangleq \sum_{i=0}^{k} \lambda^{k-i} \left(z_{\mathrm{rc}}(\hat{\theta}, i)^{\mathrm{T}} R_z z_{\mathrm{rc}}(\hat{\theta}, i) + [\Phi(i)\hat{\theta}]^{\mathrm{T}} R_d \Phi(i)\hat{\theta} \right)$$
$$+ \lambda^k [\hat{\theta} - \theta(0)]^{\mathrm{T}} R_\theta [\hat{\theta} - \theta(0)], \tag{5.15}$$

where $R_z \in \mathbb{R}^{l_y \times l_y}$, $R_d \in \mathbb{R}^{l_d \times l_d}$, and $R_\theta \in \mathbb{R}^{l_\theta \times l_\theta}$ are positive definite, and $\lambda \in (0, 1]$ is the forgetting factor. Let $P(0) = R_\theta^{-1}$ and $\theta(0) = \theta_0$. Then, for all $k \geq 1$, the cumulative cost function (5.15) has the unique global minimizer $\theta(k)$ given by the RLS update

$$\theta(k) = \theta(k-1) - P(k-1)\tilde{\Phi}(k)^{\mathrm{T}} \Gamma(k) [\tilde{\Phi}(k)\theta(k-1) + \tilde{z}(k)], \tag{5.16}$$
$$P(k) = \frac{1}{\lambda} [P(k-1) - P(k-1)\tilde{\Phi}(k)^{\mathrm{T}} \Gamma(k) \tilde{\Phi}(k) P(k-1)], \tag{5.17}$$

where

$$\tilde{\Phi}(k) \triangleq \begin{bmatrix} \Phi_{\mathrm{f}}(k) \\ \Phi(k) \end{bmatrix} \in \mathbb{R}^{(l_y + l_d) \times l_\theta}, \tag{5.18}$$
$$\tilde{R}(k) \triangleq \begin{bmatrix} R_z(k) & 0 \\ 0 & R_d(k) \end{bmatrix} \in \mathbb{R}^{(l_y + l_d) \times (l_y + l_d)}, \tag{5.19}$$
$$\tilde{z}(k) \triangleq \begin{bmatrix} z(k) - \hat{d}_{\mathrm{f}}(k) \\ 0 \end{bmatrix} \in \mathbb{R}^{l_y + l_d}, \tag{5.20}$$
$$\Gamma(k) \triangleq [\lambda \tilde{R}(k)^{-1} + \tilde{\Phi}(k) P(k-1) \tilde{\Phi}(k)^{\mathrm{T}}]^{-1}. \tag{5.21}$$

Note that RCIE uses RLS to estimate the coefficients θ of the input-estimation subsystem. Since the RLS equation is a quadratic matrix equation, its computational complexity is $O(n_c^2)$.

5.2.2 State Estimation

In order to estimate the state $x(k)$, we use $x_{\rm fc}(k)$ given by (5.3) to obtain the estimate $x_{\rm da}(k)$ of $x(k)$ given by the Kalman filter data-assimilation step

$$x_{\rm da}(k) = x_{\rm fc}(k) + K_{\rm da}(k)z(k), \tag{5.22}$$

where the state estimator gain $K_{\rm da}(k) \in \mathbb{R}^{l_x \times l_y}$ is given by

$$K_{\rm da}(k) = -P_{\rm f}(k)C(k)^{\rm T}[C(k)P_{\rm f}(k)C(k)^{\rm T} + V_2(k)]^{-1}, \tag{5.23}$$

and the forecast error covariance $P_{\rm f}(k) \in \mathbb{R}^{l_x \times l_x}$ and the data-assimilation error covariance $P_{\rm da}(k) \in \mathbb{R}^{l_x \times l_x}$ are given by

$$P_{\rm f}(k) = A(k-1)P_{\rm da}(k-1)A(k-1)^{\rm T} + V_1(k-1) + V_{\hat{d}}(k-1), \tag{5.24}$$

$$P_{\rm da}(k) = [I + K_{\rm da}(k)C(k)]P_{\rm f}(k), \tag{5.25}$$

where $V_{\hat{d}}(k)$ is the covariance of $\hat{d}(k)$. Note that, if $\hat{d}(k) = d(k)$ for all $k \geq 0$, then, for all $k \geq 0$, $V_{\hat{d}}(k) = 0$ and the state estimate $x_{\rm da}$ given by (5.22) is the standard Kalman filter estimate.

5.2.3 Filter Construction

For simplicity of presentation, the known input u and the process noise w are omitted in this subsection. By substituting (5.3) into (5.22), the forecast step is given as

$$x_{\rm fc}(k) = \bar{A}(k-1)x_{\rm fc}(k-1) + G(k-1)\hat{d}(k-1) + \bar{B}(k-1)y(k-1), \tag{5.26}$$

where

$$\bar{A}(k) \stackrel{\triangle}{=} A(k)[I+K_{\rm da}(k)C(k)],\ \bar{B}(k) \stackrel{\triangle}{=} -A(k)K_{\rm da}(k). \tag{5.27}$$

The forecast state estimate $x_{\rm fc}(k)$ given by (5.26) can be expanded as

$$\begin{aligned} x_{\rm fc}(k) = &\left(\prod_{i=1}^{n} \bar{A}(k-i)\right) x_{\rm fc}(k-n) \\ &+ \sum_{i=2}^{n} \left(\prod_{j=1}^{i-1} \bar{A}(k-j)\right) G(k-i)\hat{d}(k-i) + G(k-1)\hat{d}(k-1) \\ &+ \sum_{i=2}^{n} \left(\prod_{j=1}^{i-1} \bar{A}(k-j)\right) \bar{B}(k-i)y(k-i) + \bar{B}(k-1)y(k-1), \end{aligned} \tag{5.28}$$

where $\prod_{i=1}^{2} M_i \stackrel{\triangle}{=} M_2 M_1$. Using (5.4) and (5.28) yields

$$z(k) = C(k)\left(\prod_{i=1}^{n} \bar{A}(k-i)\right) x_{\rm fc}(k-n) + \sum_{i=1}^{n} H_i(k)\hat{d}(k-i) + \sum_{i=1}^{n} H_i'(k)y(k-i) - y(k), \tag{5.29}$$

where, for all $i \geq 1$,

$$H_i(k) \stackrel{\triangle}{=} \begin{cases} C(k)G(k-1), & i = 1, \\ C(k)\left(\prod_{j=1}^{i-1} \bar{A}(k-j)\right) G(k-i), & i \geq 2, \end{cases} \tag{5.30}$$

$$H_i'(k) \stackrel{\triangle}{=} \begin{cases} C(k)\bar{B}(k-1), & i = 1, \\ C(k)\left(\prod_{j=1}^{i-1} \bar{A}(k-j)\right) \bar{B}(k-i), & i \geq 2. \end{cases} \tag{5.31}$$

Furthermore, (5.10) and (5.29) imply

$$\begin{aligned} z_{\rm rc}(\hat{\theta}, k) = C(k)\left(\prod_{i=1}^{n} \bar{A}(k-i)\right) x_{\rm fc}(k-n) &+ \sum_{i=1}^{n} H_i(k) d_{\rm rc}(\hat{\theta}, k-i) \\ &+ \sum_{i=1}^{n} H_i'(k)y(k-i) - y(k). \end{aligned} \tag{5.32}$$

Subtracting (5.29) from (5.32) yields

$$z_{\rm rc}(\hat{\theta},k) = z(k) + \sum_{i=1}^{n} H_i(k)\frac{1}{\mathbf{q}^i}[d_{\rm rc}(\hat{\theta},k) - \hat{d}(k)]. \tag{5.33}$$

Hence, $G_{{\rm f},k}(\mathbf{q})$ in (5.11) is the FIR filter

$$G_{{\rm f},k}(\mathbf{q}) = \sum_{i=1}^{n_{\rm f}} H_i(k)\frac{1}{\mathbf{q}^i}, \tag{5.34}$$

and, thus, for all $k \geq 0$ and all $i = 1, \ldots, n_{\rm f}$, $A_i(k) = 0$ and $K_i(k) = H_i(k)$ in (5.9) and (5.8), respectively. Furthermore, $\Phi_{\rm f}$ and $\hat{d}_{\rm f}$ defined by (5.12) and (5.13) are given by

$$\Phi_{\rm f}(k) = \sum_{i=1}^{n_{\rm f}} H_i(k)\Phi(k-i), \quad \hat{d}_{\rm f}(k) = \sum_{i=1}^{n_{\rm f}} H_i(k)\hat{d}(k-i). \tag{5.35}$$

A pseudo algorithm for RCIE is given in Appendix C.

5.2.4 Transfer Function Representation of RCIE

The physical system $G_{yd,k}$, forecast subsystem $G_{{\rm fc},k}$, input-estimation subsystem $G_{\hat{d}z,k}$, and data-assimilation subsystem $G_{{\rm da},k}$ in Figure 5.1 represent [(5.1),(5.2)], (5.3), (5.6), and (5.22), respectively. For simplicity of presentation, the known input u and the process noise w are not shown in Figure 5.1 and are omitted for the remainder of this subsection.

By substituting (5.26) into (5.4), $y_{\rm fc}$ is given by

$$y_{\rm fc}(k) = G_{y_{\rm fc}y,k}(\mathbf{q})y(k) + G_{y_{\rm fc}\hat{d},k}(\mathbf{q})\hat{d}(k), \tag{5.36}$$

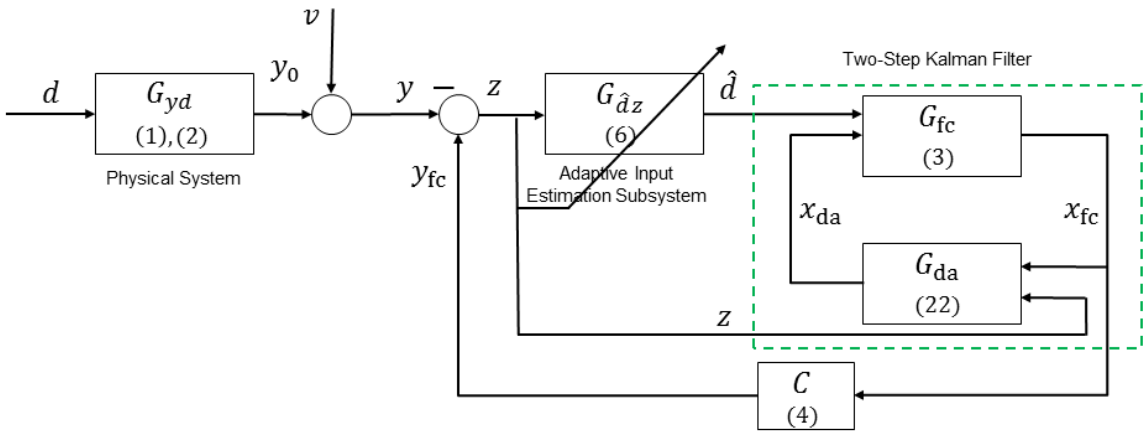

Figure 5.1: Block diagram of retrospective cost input estimation. The two-step Kalman filter consists of the forecast subsystem G_{fc} and the data-assimilation subsystem G_{da}. The innovations z and the output $\hat{d}$ of the input-estimation subsystem $G_{\hat{d}z}$ are the inputs of the two-step Kalman filter.

where

$$G_{y_{\mathrm{fc}}y,k}(\mathbf{q}) = C(k)[\mathbf{q}I - \bar{A}(k)]^{-1}\bar{B}(k), \tag{5.37}$$

$$G_{y_{\mathrm{fc}}\hat{d},k}(\mathbf{q}) = C(k)[\mathbf{q}I - \bar{A}(k)]^{-1}G(k). \tag{5.38}$$

Next, it follows from (5.6) that $\hat{d}$ is given by

$$\hat{d}(k) = G_{\hat{d}z,k}(\mathbf{q})z(k), \tag{5.39}$$

where

$$G_{\hat{d}z,k}(\mathbf{q}) = \left(I_{l_d} - P_1(k)\mathbf{q}^{-1} - \cdots - P_{n_c}(k)\mathbf{q}^{-n_c}\right)^{-1}\left(Q_0(k) + Q_1(k)\mathbf{q}^{-1} + \cdots + Q_{n_c}\mathbf{q}^{-n_c}\right). \tag{5.40}$$

Next, it follows from (5.1), (5.2) that y is given by

$$y(k) = G_{yd,k}(\mathbf{q})d(k) + D_2(k)v(k), \tag{5.41}$$

where

$$G_{yd,k}(\mathbf{q}) = C(k)[\mathbf{q}I - A(k)]^{-1}G(k). \tag{5.42}$$

Using (5.36), (5.39), and (5.41), the innovations z defined by (5.5) is given by

$$z(k) = G_{zd,k}(\mathbf{q})d(k) + G_{zy,k}(\mathbf{q})D_2(k)v(k), \tag{5.43}$$

where

$$G_{zy,k} = [I_{l_y} - G_{y_{\rm fc}\hat{d},k}G_{\hat{d}z,k}]^{-1}[G_{y_{\rm fc}y,k} - I_{l_y}], \tag{5.44}$$

$$G_{zd,k} = G_{zy,k}G_{yd,k}. \tag{5.45}$$

Using (5.39) and (5.43), $\hat{d}$ is given by

$$\hat{d}(k) = G_{\hat{d}d,k}(\mathbf{q})d(k) + G_{\hat{d}v,k}(\mathbf{q})v(k), \tag{5.46}$$

where

$$G_{\hat{d}d,k} = G_{\hat{d}z,k}G_{zd,k}, \tag{5.47}$$

$$G_{\hat{d}v,k} = G_{\hat{d}z,k}G_{zy,k}D_2(k). \tag{5.48}$$

Now, define the notation

$$G_{yd,k} \triangleq D_{yd,k}^{-1} N_{yd,k} \in \mathbb{R}^{l_y \times l_d}(\mathbf{q}), \tag{5.49}$$

$$G_{y_{\rm fc}y,k} \triangleq D_{y_{\rm fc}y,k}^{-1} N_{y_{\rm fc}y,k} \in \mathbb{R}^{l_y \times l_y}(\mathbf{q}), \tag{5.50}$$

$$G_{y_{\rm fc}\hat{d},k} \triangleq D_{y_{\rm fc}\hat{d},k}^{-1} N_{y_{\rm fc}\hat{d},k} \in \mathbb{R}^{l_y \times l_d}(\mathbf{q}), \tag{5.51}$$

$$G_{\hat{d}z,k} \triangleq D_{\hat{d}z,k}^{-1} N_{\hat{d}z,k} \in \mathbb{R}^{l_d \times l_y}(\mathbf{q}), \tag{5.52}$$

and note from (5.37) and (5.38) that $D_{y_{\rm fc}\hat{d},k} = D_{y_{\rm fc}y,k}$. Using (5.50), (5.52), it follows that (5.45) and (5.47) are given by

$$G_{zd,k} = (I_{l_y} - D_{y_{\rm fc}\hat{d},k}^{-1} N_{y_{\rm fc}\hat{d},k} D_{\hat{d}z,k}^{-1} N_{\hat{d}z,k})^{-1} (D_{y_{\rm fc}y,k}^{-1} N_{y_{\rm fc}y,k} - I_{l_y}) D_{yd,k}^{-1} N_{yd,k}, \tag{5.53}$$

$$G_{\hat{d}d,k} = D_{\hat{d}z,k}^{-1} N_{\hat{d}z,k} (I_{l_y} - D_{y_{\rm fc}\hat{d},k}^{-1} N_{y_{\rm fc}\hat{d},k} D_{\hat{d}z,k}^{-1} N_{\hat{d}z,k})^{-1} (D_{y_{\rm fc}y,k}^{-1} N_{y_{\rm fc}y,k} - I_{l_y}) D_{yd,k}^{-1} N_{yd,k}. \tag{5.54}$$

5.3 Analysis of the Input Estimation Subsystem

We now analyze the input-estimation subsystem $G_{\hat{d}z,k}$ in order to determine conditions on $G_{\hat{d}z,k}$ under which $z(k)$ and $\hat{d}(k) - d(k)$ converge to zero. We then show that RCIE adapts $G_{\hat{d}z,k}$ so as to satisfy these conditions.

In the following analysis, we assume for simplicity that A, C, G, $K_{\rm da}$, and $G_{\hat{d}z}$ are time invariant. Furthermore, as a special case, assume that $l_d = l_y = 1$ and $u = w = v = 0$. Then, using (5.53) and (5.54), it follows that (5.43) and (5.46) are given by

$$z(k) = G_{zd}(\mathbf{q})\, d(k) = \frac{N_{yd}(\mathbf{q})(N_{y_{\rm fc}y}(\mathbf{q}) - D_{y_{\rm fc}y}(\mathbf{q})) D_{y_{\rm fc}\hat{d}}(\mathbf{q}) D_{\hat{d}z}(\mathbf{q})}{D_{yd}(\mathbf{q}) D_{y_{\rm fc}y}(\mathbf{q}) (D_{y_{\rm fc}\hat{d}}(\mathbf{q}) D_{\hat{d}z}(\mathbf{q}) - N_{y_{\rm fc}\hat{d}}(\mathbf{q}) N_{\hat{d}z}(\mathbf{q}))}\, d(k), \tag{5.55}$$

$$\hat{d}(k) = G_{\hat{d}d}(\mathbf{q})\, d(k) = \frac{N_{\hat{d}z}(\mathbf{q})N_{yd}(\mathbf{q})(N_{y_{\rm fc}y}(\mathbf{q}) - D_{y_{\rm fc}y}(\mathbf{q}))D_{y_{\rm fc}\hat{d}}(\mathbf{q})}{D_{yd}(\mathbf{q})D_{y_{\rm fc}y}(\mathbf{q})(D_{y_{\rm fc}\hat{d}}(\mathbf{q})D_{\hat{d}z}(\mathbf{q}) - N_{y_{\rm fc}\hat{d}}(\mathbf{q})N_{\hat{d}z})(\mathbf{q})}\, d(k). \tag{5.56}$$

In the following analysis, we replace the forward shift operator $\mathbf{q}$ with the $\mathcal{Z}$-transform variable 'z' in order to use the final value theorem. The identity

$$\det(\mathrm{z}I - A - BC) = \det(\mathrm{z}I - A) - C\mathrm{adj}(\mathrm{z}I - A - BKC)B \tag{5.57}$$

implies that

$$\begin{aligned} &D_{y_{\rm fc}y}(\mathrm{z}) - N_{y_{\rm fc}y}(\mathrm{z}) = \det(\mathrm{z}I - \bar{A}) - C\mathrm{adj}(\mathrm{z}I - \bar{A})\bar{B} \\ &= \det(\mathrm{z}I - A - AK_{\rm da}C) + C\mathrm{adj}(\mathrm{z}I - A - AK_{\rm da}C)AK_{\rm da} \\ &= \det(\mathrm{z}I - A) - C\mathrm{adj}(\mathrm{z}I - A - AK_{\rm da}C)AK_{\rm da} + C\mathrm{adj}(\mathrm{z}I - A - AK_{\rm da}C)AK_{\rm da} \\ &= \det(\mathrm{z}I - A) = D_{yd}(\mathrm{z}). \end{aligned} \tag{5.58}$$

Since $\bar{A} = A + AK_{\rm da}C$, it follows from (5.37) and (5.42) that $N_{y_{\rm fc}\hat{d}} = N_{yd}$. Using (5.58), $D_{y_{\rm fc}\hat{d}} = D_{y_{\rm fc}y}$, and $N_{y_{\rm fc}\hat{d}} = N_{yd}$, it follows from (5.55) and (5.56) that

$$\mathcal{Z}\{z\}(\mathrm{z}) = G_{zd}(\mathrm{z})\,\mathcal{Z}\{d\}(\mathrm{z}) = \frac{N_{yd}(\mathrm{z})D_{\hat{d}z}(\mathrm{z})}{N_{y_{\rm fc}\hat{d}}(\mathrm{z})N_{\hat{d}z}(\mathrm{z}) - D_{y_{\rm fc}\hat{d}}(\mathrm{z})D_{\hat{d}z}(\mathrm{z})}\,\mathcal{Z}\{d\}(\mathrm{z}), \tag{5.59}$$

$$\mathcal{Z}\{\hat{d}\}(\mathrm{z}) = G_{\hat{d}d}(\mathrm{z})\,\mathcal{Z}\{d\}(\mathrm{z}) = \frac{N_{\hat{d}z}(\mathrm{z})N_{yd}(\mathrm{z})}{N_{y_{\rm fc}\hat{d}}(\mathrm{z})N_{\hat{d}z}(\mathrm{z}) - D_{y_{\rm fc}\hat{d}}(\mathrm{z})D_{\hat{d}z}(\mathrm{z})}\,\mathcal{Z}\{d\}(\mathrm{z}). \tag{5.60}$$

As an example, assume that $d(k) \equiv \bar{d}$ is constant and $G_{\hat{d}z}$ has an internal model of d, that is, $D_{\hat{d}z}(\mathrm{z}) = (\mathrm{z}-1)\bar{D}_{\hat{d}z}(\mathrm{z})$. Then,

$$\mathcal{Z}\{d\}(\mathrm{z}) = \frac{\bar{d}}{\mathrm{z}-1}, \quad G_{\hat{d}z}(\mathrm{z}) = \frac{N_{\hat{d}z}(\mathrm{z})}{(\mathrm{z}-1)\bar{D}_{\hat{d}z}(\mathrm{z})}. \tag{5.61}$$

Using (5.59) and assuming that $N_{y_{\rm fc}\hat{d}}(\mathrm{z})N_{\hat{d}z}(\mathrm{z}) - (\mathrm{z}-1)D_{y_{\rm fc}\hat{d}}(\mathrm{z})\bar{D}_{\hat{d}z}(\mathrm{z})$ is asymptotically

stable, it follows from the final value theorem that

$$\lim_{k\to\infty} z(k) = \lim_{\mathrm{z}\to 1}(\mathrm{z}-1)\frac{(\mathrm{z}-1)N_{yd}(\mathrm{z})\bar{D}_{\hat{d}z}(\mathrm{z})}{N_{y_{\mathrm{fc}}\hat{d}}(\mathrm{z})N_{\hat{d}z}(\mathrm{z}) - (\mathrm{z}-1)D_{y_{\mathrm{fc}}\hat{d}}(\mathrm{z})\bar{D}_{\hat{d}z}(\mathrm{z})} \cdot \frac{\bar{d}}{(\mathrm{z}-1)} = 0. \tag{5.62}$$

Similarly, using (5.60) and $N_{y_{\mathrm{fc}}\hat{d}} = N_{yd}$, it follows that

$$\lim_{k\to\infty} \hat{d}(k) = \left.\frac{N_{\hat{d}z}(\mathrm{z})N_{yd}(\mathrm{z})}{N_{y_{\mathrm{fc}}\hat{d}}(\mathrm{z})N_{\hat{d}z}(\mathrm{z}) - (\mathrm{z}-1)D_{y_{\mathrm{fc}}\hat{d}}(\mathrm{z})\bar{D}_{\hat{d}z}(\mathrm{z})}\right|_{\mathrm{z}=1} \bar{d} = \bar{d}. \tag{5.63}$$

To apply the above analysis, we assume that the unknown input $d(k)$ is generated by the discrete-time, linear time-invariant exogenous subsystem

$$x_d(k) = A_d x_d(k-1), \tag{5.64}$$

$$d(k) = C_d x_d(k), \tag{5.65}$$

where $A_d \in \mathbb{R}^{n\times n}$, $C_d \in \mathbb{R}^{l_d\times n}$, and the eigenvalues of A_d are simple and lie on the unit circle. Now, assume that the following conditions are satisfied:

P1. $G_{\hat{d}z}$ contains an internal model of d, that is, for all $\lambda \in \mathrm{spec}(A_d)$, $|G_{\hat{d}z}(\lambda)| = \infty$.

P2. $N_{y_{\mathrm{fc}}\hat{d}}N_{\hat{d}z} - D_{y_{\mathrm{fc}}\hat{d}}D_{\hat{d}z}$ is asymptotically stable.

P3. For all $\lambda \in \mathrm{spec}(A_d)$, $G_{\hat{d}d}(\lambda) = 1$.

Then it follows from the internal model principle [86] that, as $k \to \infty$, $z(k) \to 0$ and $\hat{d}(k) - d(k) \to 0$. The following examples show that RCIE adapts $G_{\hat{d}z,k}$ such that P1–P3 are asymptotically satisfied.

Example 5.3.1. Consider the minimum-phase (MP) system

$$G_{yd}(\mathrm{z}) = \frac{\mathrm{z}-0.9}{(\mathrm{z}-0.7)(\mathrm{z}-0.8)} \tag{5.66}$$

with the minimal realization

$$A = \begin{bmatrix} 1.5 & -0.56 \\ 1 & 0 \end{bmatrix}, \quad G = \begin{bmatrix} 1 \\ 0 \end{bmatrix}, \quad C = \begin{bmatrix} 1 & -0.9 \end{bmatrix}. \tag{5.67}$$

Let $n_c = 3$, $n_f = 24$, $\lambda = 1$, $R_\theta = 10^{-4} I_{l_\theta}$, $R_d = 10^{-6}$, $R_z = 1$, and $V_{\hat{d}} = 10^{-2} I_{l_x}$, and let B, V_1, and V_2 be zero. The unknown input is $d(k)$=1+ sin(0.3k), which consists of a step and a harmonic. Its $\mathcal{Z}$-transform is given by

$$\mathcal{Z}\{d\}(\mathrm{z}) = \frac{\mathrm{z}}{\mathrm{z}-1} + 0.29\frac{\mathrm{z}}{\mathrm{z}^2 - 1.91\mathrm{z} + 1}. \tag{5.68}$$

Note that, since the input d is unknown, the frequency of its harmonic component is unknown to RCIE. It thus is not possible to construct an auxiliary system that captures the spectrum of d.

After an initial transient of 10 time steps, $\hat{d}$ follows d, as shown in Fig. 5.2(a). The estimator coefficients $\theta(k)$ shown in Fig. 5.2(b) converge in 50 steps to

$$G_{\hat{d}z,50}(\mathrm{z}) = -2.91\frac{(\mathrm{z}+0.006)(\mathrm{z}^2 - 0.99\mathrm{z} + 0.34)}{(\mathrm{z}-1.004)(\mathrm{z}^2 - 1.909\mathrm{z} + 0.999)}. \tag{5.69}$$

The poles of $G_{\hat{d}z,50}$ at 1.004 and $0.95 \pm 0.29\jmath$ in (5.69) show that RCIE builds an internal model of d in $G_{\hat{d}z,50}$. Thus, P1 is satisfied. Furthermore, K_{da} (not shown in Fig. 5.2) also converges, and the poles of $G_{\hat{d}d,50}$ are shown in Fig. 5.2(c). Since the poles of $G_{\hat{d}d,50}$ are inside the open unit disk, P2 is satisfied. The magnitude and phase plots of $G_{\hat{d}d,50}$ in Fig. 5.2(d) show that, at both DC and the unknown input frequency 0.3 rad/sec, the magnitude is 1 and the phase is 0 deg. Hence, P3 is satisfied.

To test the robustness of RCIE to model error, we vary the (1,2) entry of A matrix while keeping G, C constant. The RCIE parameters are kept the same for all cases. Fig. 5.3 shows the mean and standard deviation of the error $|d - \hat{d}|$, after 50 time-steps, for a range of values of the (1,2) entry of A. Note that the mean and standard

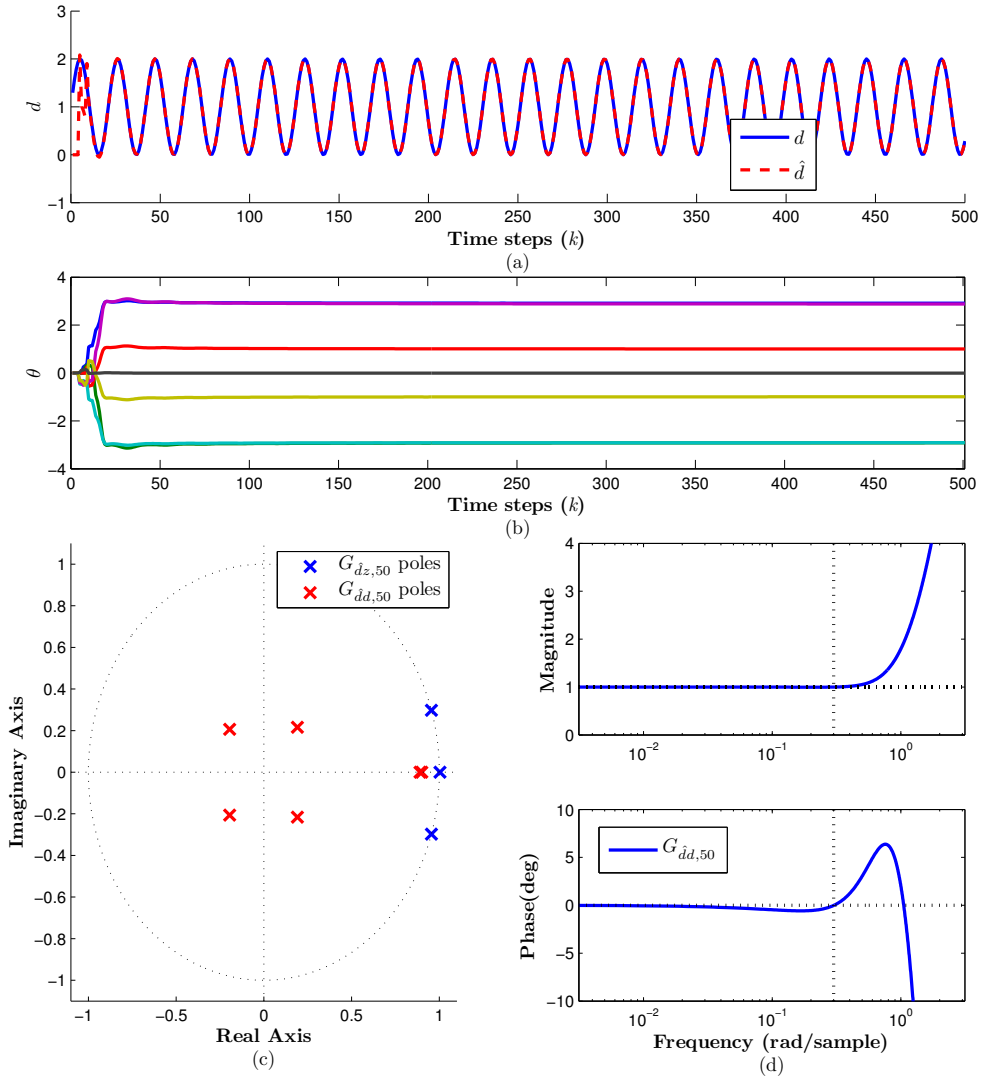

Figure 5.2: RCIE for the minimum-phase system (5.66). (a) After the initial transient, $\hat{d}$ follows d. (b) The estimator coefficients θ converge in about 50 steps. (c) The poles of $G_{\hat{d}z,50}$ at 1.004 and $0.95 \pm 0.29\jmath$ show that RCIE builds an internal model of d in $G_{\hat{d}z,50}$. The poles of $G_{\hat{d}d,50}$ are inside the open unit disk. (d) $G_{\hat{d}d,50}$ has magnitude 1 and phase 0 deg at both DC and the unknown input frequency 0.3 rad/sec.

deviation of the error increase linearly as the (1,2) entry of A varies from its true value 0.56. $\diamond$

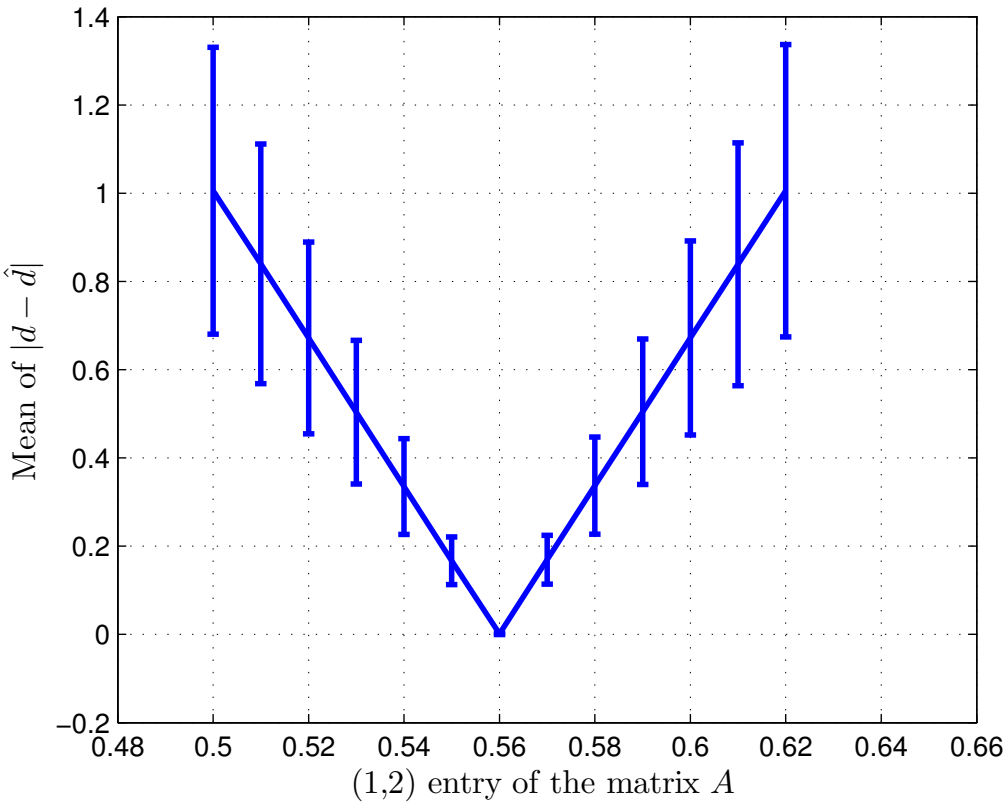

Figure 5.3: Robustness of RCIE to model error for the system (5.66). The (1,2) entry of A is varied while keeping the matrices G, C and RCIE parameters constant. Note that the mean and standard deviation of the error increase linearly as the (1,2) entry of A varies from its true value 0.56.

Example 5.3.2. Consider the nonminimum-phase (NMP) system

$$G_{yd}(\mathrm{z}) = \frac{\mathrm{z} - 1.2}{(\mathrm{z} - 0.7)(\mathrm{z} - 0.8)}. \tag{5.70}$$

with the minimal realization

$$A = \begin{bmatrix} 1.5 & -0.56 \\ 1 & 0 \end{bmatrix}, \quad G = \begin{bmatrix} 2 \\ 0 \end{bmatrix}, \quad C = \begin{bmatrix} 0.5 & -0.6 \end{bmatrix}. \tag{5.71}$$

The tuning parameters are same as in Example 5.3.1. The unknown input is $d(k) = \sin(0.3k)$.

After an initial transient of about 90 steps, $\hat{d}$ follows d, as shown in Fig. 5.4(a). The estimator coefficients $\theta(k)$ shown in Fig. 5.4(b) converge in about 450 steps to

$$G_{\hat{d}z,450}(\mathrm{z}) = 8.52\frac{(\mathrm{z}+0.01)(\mathrm{z}^2-1.908\mathrm{z}+0.91)}{(\mathrm{z}+10.46)(\mathrm{z}^2-1.903\mathrm{z}+0.99)}. \tag{5.72}$$

The poles of $G_{\hat{d}z,450}$ at $0.95 \pm 0.29\jmath$ in (5.72) show that RCIE builds an internal model of d in $G_{\hat{d}z,450}$. Thus, P1 is satisfied. Furthermore, K_{da} (not shown in Fig. 5.2) also converges, and the poles of $G_{\hat{d}d,450}$ are shown in Fig. 5.4(c). Since the poles of $G_{\hat{d}d,450}$ are inside the open unit disk, P2 is satisfied. The magnitude and phase plots of $G_{\hat{d}d,450}$ in Fig. 5.4(d) show that, at the unknown input frequency 0.3 rad/sec, the magnitude is 1 and the phase is 0 deg. Hence, P3 is satisfied. $\diamond$

Example 5.3.3. Consider the linear, time-varying system

$$G_{yd,k}(\mathbf{q}) = \frac{\mathbf{q}-\xi(k)}{(\mathbf{q}-0.8)(\mathbf{q}-0.9)}, \tag{5.73}$$

where

$$\xi(k) = \begin{cases} 0.95, & k < 100, \\ 0.95 + 0.001(k-100), & 100 \leq k \leq 300, \\ 1.15, & k > 300. \end{cases} \tag{5.74}$$

Note that, during the transition, G_{yd} is MP for $k < 150$, and NMP for $k \geq 150$. Let $n_{\mathrm{c}} = 8$, $n_{\mathrm{f}} = 48$, $\lambda = 0.998$, $R_\theta = 10^{-2} I_{l_\theta}$, $R_d = 10^{-6}$, $R_z = 1$, and $V_{\hat{d}} = 10^{-2} I_{l_x}$.

First, we consider the case where the unknown input $d(k)$ is constant. Fig. 5.5(a) shows that RCIE estimates d for both MP and NMP G_{yd} with an intervening transient. Fig. 5.5(b) shows that the estimator coefficients $\theta(k)$ readapt due to the transition of G_{yd} from MP to NMP dynamics in order to estimate d. Note that, at $k = 100$ and 600 steps, $G_{\hat{d}z,k}$ has a pole at 1, $G_{\hat{d}d,k}$ is asymptotically stable, and $G_{\hat{d}d,k}(1) \approx 1$. Hence, before and after the transition, P1-P3 are satisfied.

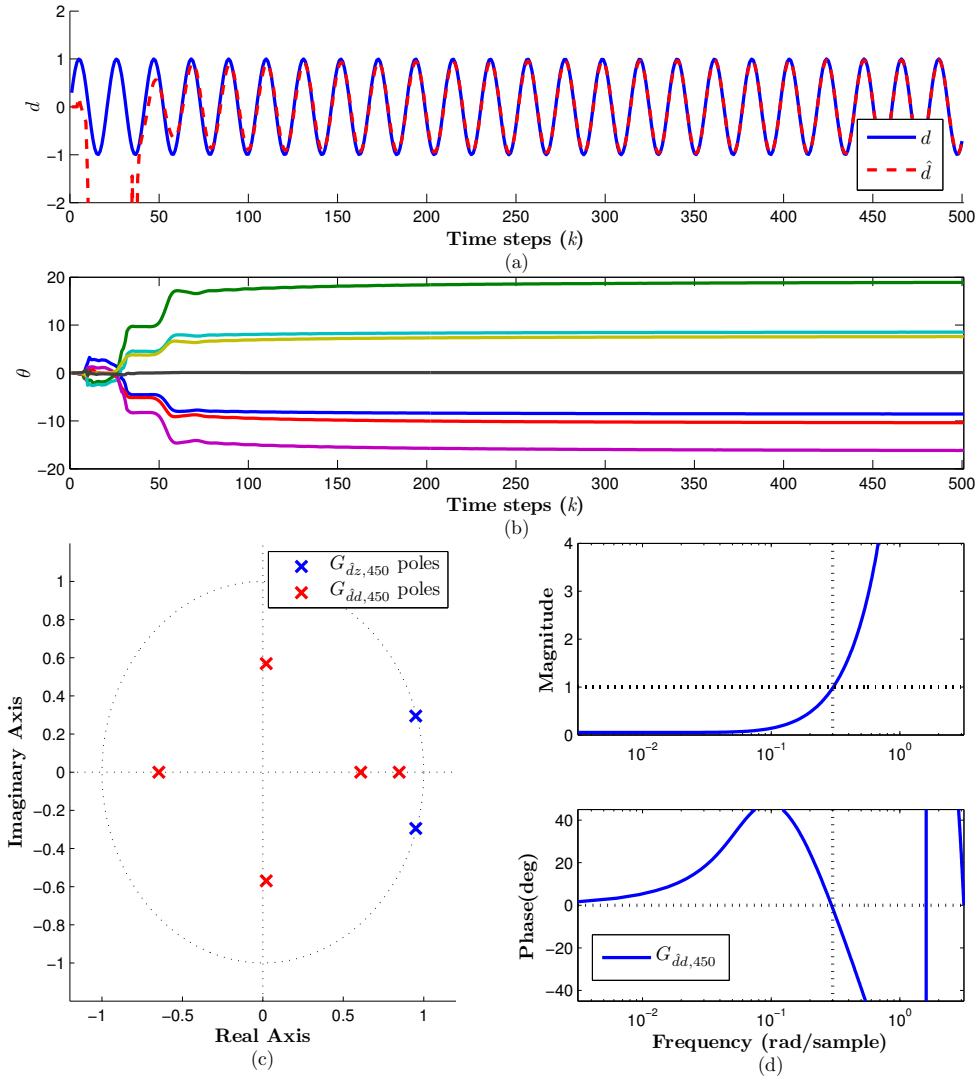

Figure 5.4: RCIE for the NMP system (5.70). (a) After the initial transient, $\hat{d}$ follows d. (b) The estimator coefficients θ converge in about 450 steps. (c) The poles of $G_{\hat{d}z,450}$ at $0.95 \pm 0.29\jmath$ show that RCIE builds an internal model of d in $G_{\hat{d}z}$. The poles of $G_{\hat{d}d,450}$ are inside the open unit disk. (d) $G_{\hat{d}d}$ has magnitude 1 and phase 0 deg at the unknown input frequency 0.3 rad/sec.

Next, we consider the case where $d(k) = \sin(0.1k)$. Fig. 5.5(c) shows that RCIE estimates d for both MP and NMP G_{yd} with an intervening transient. Fig. 5.5(d) shows that the estimator coefficients $\theta(k)$ readapt due to the transition of G_{yd} from

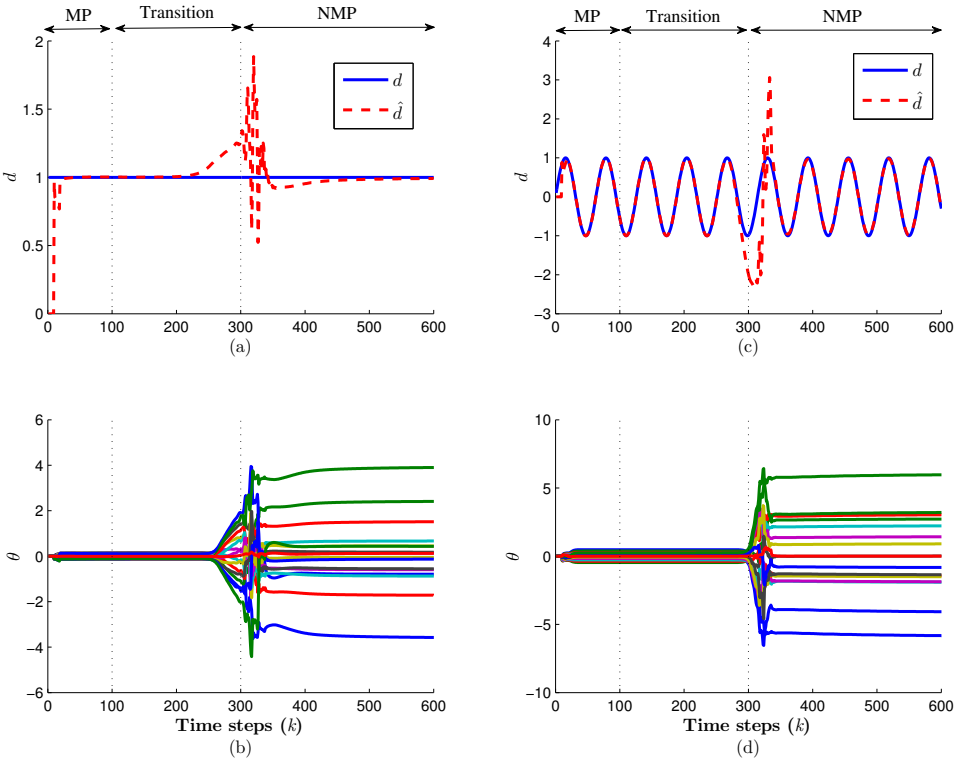

Figure 5.5: RCIE for the time-varying system (5.73). The transition begins at $k = 100$ steps and ends at $k = 300$ steps. (a) RCIE estimates constant d for both MP and NMP G_{yd} with an intervening transient response. (b) The estimator coefficients readpat due to the transition of G_{yd} from MP to NMP dynamics in order to estimate d. (c) RCIE estimates harmonic d for both MP and NMP G_{yd} with an intervening transient response. (d) The estimator coefficients readpat due to the transition of G_{yd} from MP to NMP dynamics in order to estimate d.

MP to NMP dynamics in order to estimate d. Note that, at $k = 100$ and 600 steps, $G_{\hat{d}z,k}$ has poles at 0.995 ± 0.099, $G_{\hat{d}d,k}$ is asymptotically stable, and $G_{\hat{d}d}(e^{0.1\jmath}) \approx 1$. Hence, before and after the transition, P1-P3 are satisfied. $\diamond$

5.4 Effect of the Unobservable Input Subspace

As shown in [24], if (A, G, C) has an invariant zero, then it has a nontrivial unobservable input subspace. In particular, an input of the form $d(k) = \mathrm{Re}(\xi^k \bar{d})$, where

$\xi \in \mathbb{C}$ is an invariant zero of (A, G, C) and $\bar{d} \in \mathbb{C}^{l_d}$ is specified in Example 5.4.1 below, is unobservable since there exists an initial condition $x(0) = \mathrm{Re}(\bar{x})$ such that the output is identically zero. Note that, for each example in Section 5.3, the input d was chosen so that its spectral content is disjoint from the zeros of (A, G, C). For instance, in Example 5.3.1, d is the sum of step and harmonic signals, but the zero of G_{yd} is 0.9. This section illustrates the effect of the unobservable input subspace in the case where the unknown input has spectral content that coincides with a zero of (A, G, C).

Example 5.4.1. Consider the system

$$G_{yd}(\mathrm{z}) = C(\mathrm{z}I - A)^{-1}G = \frac{\mathrm{z} - \xi}{(\mathrm{z} - 0.7)(\mathrm{z} - 0.8)}, \tag{5.75}$$

where $\xi \in \mathbb{C}$ is an invariant zero of (A, G, C). Let $\begin{bmatrix} \bar{x} \\ \bar{d} \end{bmatrix} \in \mathcal{N}\left(\begin{bmatrix} \xi I - A & -G \\ C & 0 \end{bmatrix}\right)$ be nonzero with nonzero real part, and define $d(k) = d_{\mathrm{ob}}(k) + d_{\mathrm{uo}}(k)$, where, for all $k \geq 0$, $d_{\mathrm{ob}}(k) = \sin(0.3k)$ and $d_{\mathrm{uo}}(k) = \mathrm{Re}(\xi^k \bar{d})$. Furthermore, let $x(0) = \mathrm{Re}(\bar{x})$. Note that d_{uo} is unobservable. Next, let $n_{\mathrm{c}} = 8$, $n_{\mathrm{f}} = 48$, $\lambda = 0.998$, $R_\theta = 10^{-2} I_{l_\theta}$, $R_d = 10^{-6}$, $R_z = 1$, and $V_{\hat{d}} = 10^{-2} I_{l_x}$.

First, let $\xi = 0.96$, which lies in the open unit disk. In this case, Fig. 5.6a shows that $\hat{d}$ converges to d_{ob}. Furthermore, Fig. 5.6a shows that $d - d_{\mathrm{ob}}$ converges to zero, which is consistent with the fact that $d_{\mathrm{uo}} = d - d_{\mathrm{ob}}$ converges to zero. Thus, $d - \hat{d}$ also converges to zero.

Next, let $\xi = 1$, which lies on the unit circle. In this case, Fig. 5.6b shows that $\hat{d}$ converges to d_{ob}. Furthermore, Fig. 5.6b shows that $d - d_{\mathrm{ob}}$ does not converge to zero, which is consistent with the fact that d_{uo} is constant. Thus, $d - \hat{d}$ converges to d_{uo}.

Finally, let $\xi = 1.08$, which lies outside the closed unit disk. In this case, Fig. 5.6c

shows that $\hat{d}$ converges to $d_{\rm ob}$. Furthermore, Fig. 5.6c shows that $d - d_{\rm ob}$ diverges, which is consistent with the fact that $d_{\rm uo}$ diverges. Thus, $d-\hat{d}$ also diverges, however, $d_{\rm ob} - \hat{d}$ converges to zero.

Note that, in all three cases, $\hat{d}$ converges to $d_{\rm ob}$ and z (not shown in Fig. 5.6) converges to zero after an initial transient. $\diamond$

5.5 Comparison of RCIE with ULISE

We now compare RCIE with the ULISE filter [29] in the presence of process and measurement noise. To assess the accuracy of the input estimate, we plot the error metrics

$$e_{\rm RCIE}(k) \triangleq \frac{1}{N_{\rm trial}} \sqrt{\sum_{i=1}^{N_{\rm trial}} \Big[\hat{d}_i(k) - d(k)\Big]^2}, \tag{5.76}$$

$$e_{\rm ULISE}(k) \triangleq \frac{1}{N_{\rm trial}} \sqrt{\sum_{i=1}^{N_{\rm trial}} \Big[\hat{d}_{{\rm ULISE},i}(k) - d(k)\Big]^2}, \tag{5.77}$$

where i denotes the $i^{\rm th}$ trial, $\hat{d}_i$ is the ith RCIE estimate of d, $\hat{d}_{{\rm ULISE},i}$ is the ith ULISE estimate of d, and $N_{\rm trial}$ is the number of trials. Each trial is based on a randomly generated realization of v and w.

Example 5.5.1. Consider the mass-spring-damper system with masses m_1, m_2, and input force d applied to m_1. The dynamics are given by

$$\dot{x} = A_{\rm c} x + G_{\rm c} d, \tag{5.78}$$

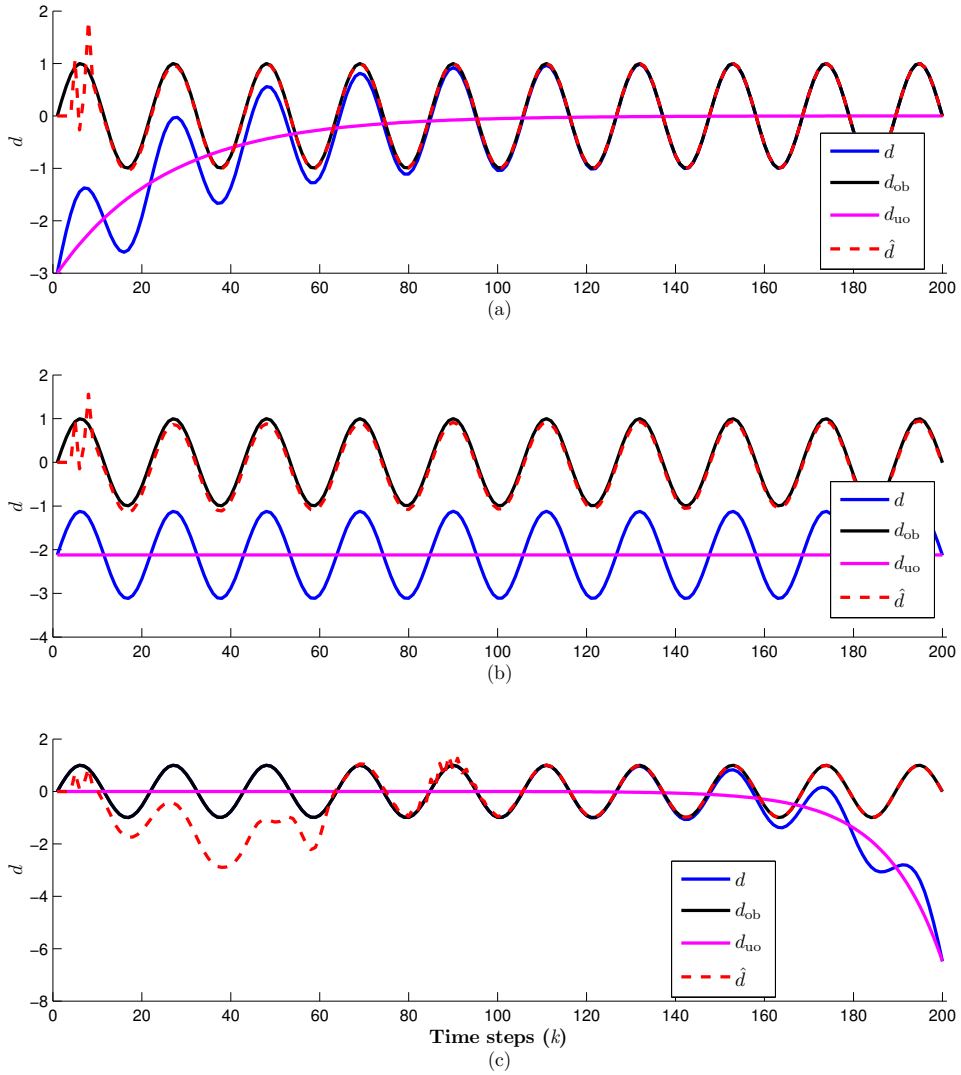

Figure 5.6: Effect of the unobservable input subspace on the estimate of the unknown input using RCIE for the system (5.75). (a) $\hat{d}$ converges to $d_{\rm ob}$, and $d_{\rm uo} = d - d_{\rm ob}$ converges to zero. (b) $\hat{d}$ converges to $d_{\rm ob}$, and $d_{\rm uo} = d - d_{\rm ob}$ is a nonzero constant. (c) $\hat{d}$ converges to $d_{\rm ob}$, and $d_{\rm uo} = d - d_{\rm ob}$ diverges.

where

$$A_{\rm c} \triangleq \begin{bmatrix} 0_{2\times 2} & I_{2\times 2} \\ \Omega_1 & \Omega_2 \end{bmatrix}, G_{\rm c} \triangleq \begin{bmatrix} 0_{2\times 1} \\ \Omega_3 \end{bmatrix}, \Omega_1 \triangleq \begin{bmatrix} -\frac{k_1+k_2}{m_1} & \frac{k_2}{m_1} \\ \frac{k_2}{m_2} & -\frac{k_2}{m_2} \end{bmatrix},$$

$$\Omega_2 \triangleq \begin{bmatrix} -\frac{c_1+c_2}{m_1} & \frac{c_2}{m_1} \\ \frac{c_2}{m_2} & -\frac{c_2}{m_2} \end{bmatrix}, \Omega_3 \triangleq \begin{bmatrix} \frac{1}{m_1} \\ 0 \end{bmatrix},$$

x_1 and x_2 are the displacements and x_3 and x_4 are the velocities of masses m_1 and m_2, respectively. We choose $m_1 = m_2 = 1\,\mathrm{kg}$, $k_1 = k_2 = 1\,\mathrm{N/m}$, and $c_1 = c_2 = 1\,\mathrm{kg/sec}$. We discretize (5.78) as

$$A = e^{A_\mathrm{c} T_\mathrm{s}}, \quad G = A_\mathrm{c}^{-1}(A_\mathrm{c} - I)G_\mathrm{c}, \tag{5.79}$$

where $T_\mathrm{s} = 0.1\,\mathrm{sec}$ is the sampling time. The discretized system has poles at $0.87 \pm 0.08\jmath$ and $0.97 \pm 0.05\jmath$. Letting

$$C = \begin{bmatrix} 1 & 0 & 0 & 0 \\ 0 & 1 & 0 & 0 \end{bmatrix},$$

we measure the positions and estimate the velocities and the unknown input force d on m_1. The system (A, G, C) has no invariant zeros. Let $N_\mathrm{trial} = 100$, $n_\mathrm{c} = 4$, $n_\mathrm{f} = 24$, $\lambda = 1$, $R_\theta = 10^{-2} I_{l_\theta}$, $R_d = 10^{-8}$, $R_z = I_{l_y}$, $V_{\hat{d}} = 0$, $D_1 = 10^{-2}\mathrm{diag}(1, 1, 2, 2)$, and $D_2 = 10^{-2}\mathrm{diag}(1, 1)$.

First, we consider the case where the unknown input force d is a multi-step. Fig. 5.7 shows that the error for RCIE has mean $0.2\,\mathrm{N}$ and standard deviation $0.3\,\mathrm{N}$, whereas the error for ULISE has mean $23.5\,\mathrm{N}$ and standard deviation $3.3\,\mathrm{N}$. Next, we consider the case where the unknown input force is a random walk. At each time step k, the random walk is modeled as an increase or decrease in the magnitude by 0.1N with equal probability. Fig. 5.8 shows that the RCIE error has mean $0.3\,\mathrm{N}$ and standard deviation $0.2\,\mathrm{N}$, whereas the ULISE error has mean $22.6\,\mathrm{N}$ and standard deviation $2.1\,\mathrm{N}$. $\diamond$

Example 5.5.2. Reconsider the system (5.78) but with zero damping, that is, $c_1 = c_2 = 0$. Hence (5.78) is Lyapunov stable but not asymptotically stable. The continuous-time system has no transmission zeros, but the discretized system (A, G, C) has one transmission zero at -1 due to the sampling.

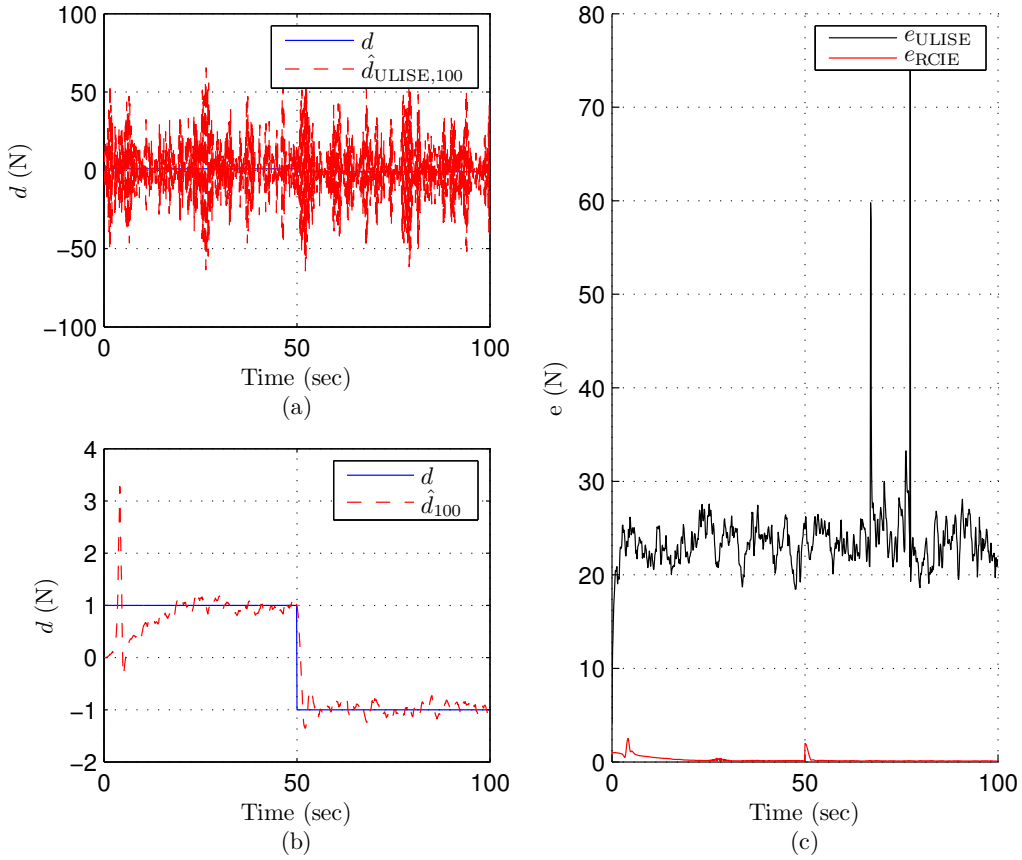

Figure 5.7: Estimation of a multi-step input for the lightly damped mass-spring-damper system (5.78). (a) UILSE estimate. (b) RCIE estimate. (c) Error in the input estimate. The error for RCIE has mean 0.2 N and standard deviation 0.3 N, whereas the error for ULISE has mean 23.5 N and standard deviation 3.3 N.

We consider the case where the unknown input force d is a multi-step. Fig. 5.9 shows that the RCIE error is 0.1 N at $t = 100$ sec, whereas the ULISE error diverges and is 282.7 N at $t = 100$ sec. The behavior of the error shown in Fig. 5.9c with ULISE for the NMP system is consistent with the fact that Theorem 6 in [29] is confined to minimum-phase systems. ◇

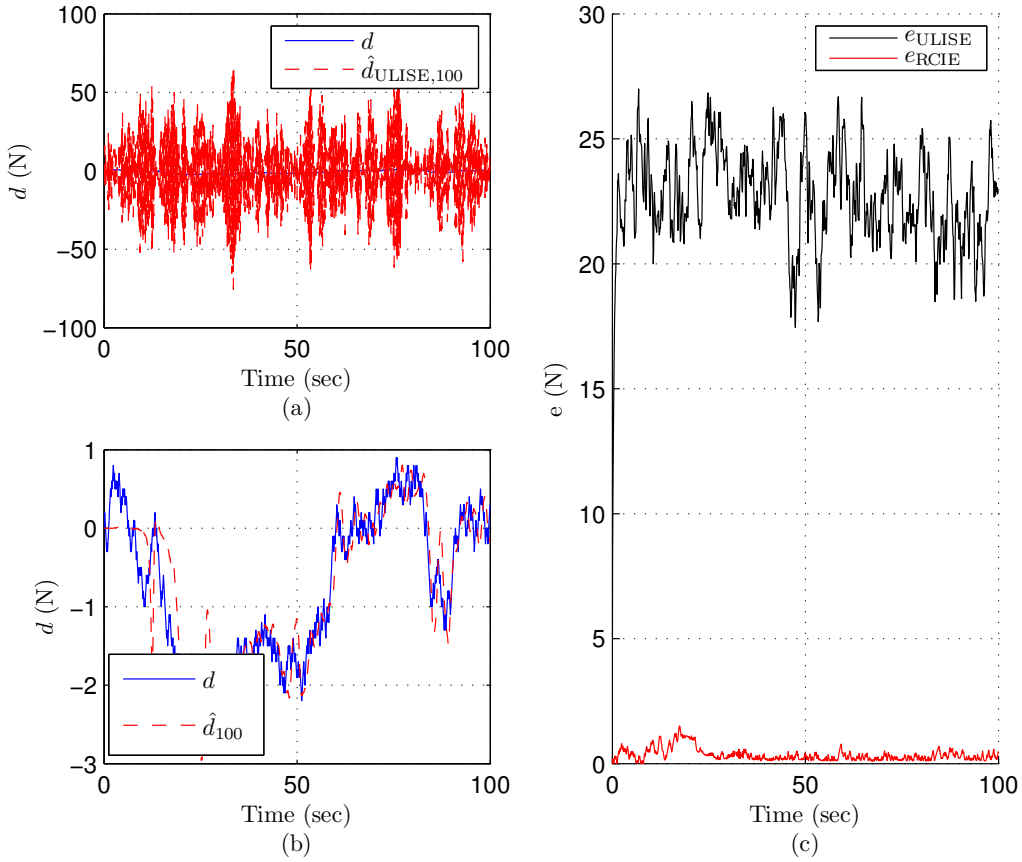

Figure 5.8: Estimation of an unknown random-walk input for the lightly damped, mass-spring-damper system (5.78). (a) ULISE estimate. (b) RCIE estimate. (c) Error in the input estimate. The RCIE error has mean 0.3 N and standard deviation 0.2 N, whereas the ULISE error has mean 22.6 N and standard deviation 2.1 N.

5.6 Conclusions

This chapter presented retrospective cost input estimation (RCIE) and showed that this algorithm is effective for asymptotically estimating the unknown input of a nonminimum-phase system. The mechanism underlying RCIE was explained in terms of an internal model of the unknown input. In particular, RCIE was shown to automatically construct an internal model of the unknown input d despite lack of knowledge of the spectrum of d and in the presence of arbitrary invariant zeros.

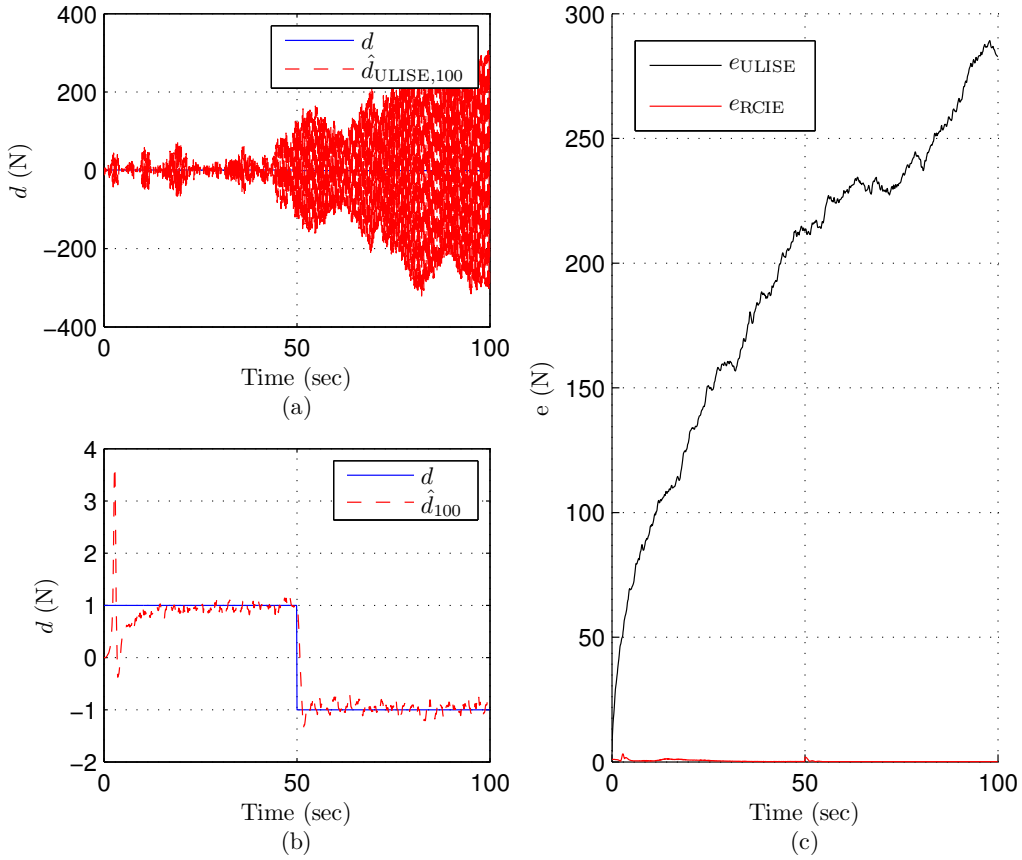

Figure 5.9: Estimation of an unknown multi-step input for the mass-spring system (5.78) with $c_1 = c_2 = 0$. (a) ULISE estimate. (b) RCIE estimate. (c) Error in the input estimate. The RCIE error is close to zero, whereas the ULISE error diverges.

In the subsequent chapters, we apply RCIE to the problems of target tracking, satellite drag estimation, and sensor fault detection.

CHAPTER 6

Target Tracking: Acceleration Estimation for a Maneuvering Vehicle

6.1 Introduction

The method developed in this chapter provides a novel approach to a longstanding problem in target tracking, namely, estimation of the inertial acceleration of a body using only position measurements. This problem is motivated by the need to estimate acceleration in order to predict future motion and distinguish ballistic vehicles from maneuvering vehicles. The extensive literature and diverse methods developed for this problem attests to its importance [20, 41, 55–60]. It turns out that, for this problem, the discretized kinematics have invariant zeros on the unit circle, and thus the approach of [39] is not applicable. A more restricted version of RCIE confined to LTI systems is applied to this problem for planar target tracking in [43]. The approach of [43], however, is not applicable to LTV systems, such as the kinematics of a 3D maneuvering vehicle resolved in the body frame. In addition, [43] does not recognize or address the NMP features of the problem.

The contents of the chapters are as follows. Section 6.2, based on kinematics, formulates the state space models for acceleration estimation. Section 6.3 describes the experimental setup, whereas, Sections 6.4 and 6.5 presents the application of

RCIE to estimation of inertial acceleration. Using optical position data for a UAV, RCIE estimates the inertial acceleration, which is modeled as an unknown input. The acceleration estimates are compared to IMU data from onboard sensors.

6.2 Problem Description

6.2.1 Kinematics

The Earth frame and body-fixed frame are denoted by $\mathrm{F_E}$ and $\mathrm{F_B}$, respectively. We assume that $\mathrm{F_E}$ is an inertial frame and the Earth is flat. The origin $\mathrm{O_E}$ of $\mathrm{F_E}$ is any convenient point fixed on the Earth. The axes $\hat{\imath}_{\mathrm{E}}$ and $\hat{\jmath}_{\mathrm{E}}$ are horizontal, while the axis $\hat{k}_{\mathrm{E}}$ points downward. $\mathrm{F_B}$ is defined with $\hat{\imath}_{\mathrm{B}}$, $\hat{\jmath}_{\mathrm{B}}$ and $\hat{k}_{\mathrm{B}}$ fixed relative to the body. $\mathrm{F_B}$ and $\mathrm{F_E}$ are related by

$$\mathrm{F_B} = \vec{R}_{\mathrm{B/E}}\, \mathrm{F_E}, \tag{6.1}$$

where $\vec{R}_{\mathrm{B/E}}$ is a physical rotation matrix represented by a 3-2-1 Euler rotation sequence, involving two intermediate frames $\mathrm{F_{E'}}$ and $\mathrm{F_{E''}}$. In particular,

$$\vec{R}_{\mathrm{B/E}} = \vec{R}_{\hat{\imath}_{\mathrm{E''}}}(\Phi)\, \vec{R}_{\hat{\jmath}_{\mathrm{E'}}}(\Theta)\, \vec{R}_{\hat{k}_{\mathrm{E}}}(\Psi), \tag{6.2}$$

where $\mathrm{F_{E'}} = \vec{\mathrm{R}}_{\mathrm{E'/E}}\, \mathrm{F_E}$, $\mathrm{F_{E''}} = \vec{\mathrm{R}}_{\mathrm{E''/E'}}\, \mathrm{F_{E'}}$, and $\vec{R}_{\hat{n}}(\kappa)$ is the Rodrigues rotation about the eigenaxis $\hat{n}$ through the eigenangle κ according to the right-hand rule.

Let p denote a point that is fixed on the body. The location of p relative to $\mathrm{O_E}$ is denoted by $\vec{r}_{\mathrm{p/O_E}}$ and is resolved in $\mathrm{F_E}$ as

$$\begin{bmatrix} X \\ Y \\ Z \end{bmatrix} \triangleq \vec{r}_{\mathrm{p/O_E}}\Big|_{\mathrm{E}}. \tag{6.3}$$

The velocity of p relative to O_E with respect to F_E is given by

$$\vec{v}_{p/O_E/E} = \overset{E\bullet}{\vec{r}}_{p/O_E}, \tag{6.4}$$

where E• denotes the derivative with respect to the time taken in Earth frame. The acceleration of p relative to O_E with respect to F_E is given by

$$\vec{a}_{p/O_E/E} = \overset{E\bullet}{\vec{v}}_{p/O_E/E} = \overset{E\bullet\bullet}{\vec{r}}_{p/O_E}. \tag{6.5}$$

We resolve $\vec{a}_{p/O_E/E}$ in F_E and F_B using the notation

$$\begin{bmatrix} A_x \\ A_y \\ A_z \end{bmatrix} \triangleq \vec{a}_{p/O_E/E}\Big|_E, \quad \begin{bmatrix} a_x \\ a_y \\ a_z \end{bmatrix} \triangleq \vec{a}_{p/O_E/E}\Big|_B. \tag{6.6}$$

Using (6.2) and (6.6), $\vec{a}_{p/O_E/E}$ in F_E is given by

$$\vec{a}_{p/O_E/E}\Big|_E = \mathcal{O}_{E/B}\, \vec{a}_{p/O_E/E}\Big|_B, \tag{6.7}$$

and thus,

$$\begin{bmatrix} A_x \\ A_y \\ A_z \end{bmatrix} = \mathcal{O}_{E/B} \begin{bmatrix} a_x \\ a_y \\ a_z \end{bmatrix}, \tag{6.8}$$

where

$$\mathcal{O}_{E/B} = \vec{R}_{E/B}\Big|_E.$$

Note that (6.1)–(6.8) are kinematic relations that are applicable to an arbitrary point p on a body and are independent of all modeling information.

6.2.2 State Space Models for Acceleration Estimation

For estimating the inertial acceleration of p relative to $\mathrm{O_E}$ with respect to $\mathrm{F_E}$, (6.4)–(6.8) are written in state space form

$$\dot{x} = A_{\mathrm{c}} x + G_{\mathrm{c}} d, \tag{6.9}$$

where

$$A_{\mathrm{c}} = \begin{bmatrix} 0_{3\times3} & I_{3\times3} \\ 0_{3\times3} & 0_{3\times3} \end{bmatrix}, \quad G_{\mathrm{c}} = \begin{bmatrix} 0_{3\times3} \\ I_{3\times3} \end{bmatrix}, \tag{6.10}$$

$$x = \begin{bmatrix} X & Y & Z & \dot{X} & \dot{Y} & \dot{Z} \end{bmatrix}^{\mathrm{T}}, \; d = \begin{bmatrix} A_x & A_y & A_z \end{bmatrix}^{\mathrm{T}}. \tag{6.11}$$

Note that (6.9) is an exact kinematic equations, and thus it does not include process noise. For estimating the inertial acceleration of p relative to $\mathrm{O_E}$ with respect to $\mathrm{F_B}$, (6.4)–(6.8) are written in state space form

$$\dot{x} = A_{\mathrm{c}} x + G_{\mathrm{c}} d + D_1 w, \tag{6.12}$$

where

$$A_{\mathrm{c}} = \begin{bmatrix} 0_{3\times3} & I_{3\times3} \\ 0_{3\times3} & 0_{3\times3} \end{bmatrix}, \quad G_{\mathrm{c}} = \begin{bmatrix} 0_{3\times3} \\ \mathcal{O}_{\mathrm{E/B}} \end{bmatrix}, \tag{6.13}$$

$$x = \begin{bmatrix} X & Y & Z & \dot{X} & \dot{Y} & \dot{Z} \end{bmatrix}^{\mathrm{T}}, \; d = \begin{bmatrix} a_x & a_y & a_z \end{bmatrix}^{\mathrm{T}}. \tag{6.14}$$

Likewise, (6.12) is an exact kinematic equation; however, process noise is now included to account for errors in the measurements of the matrix $\mathcal{O}_{\mathrm{E/B}}$ appearing in (6.13). Finally, notice that, due to $\mathcal{O}_{\mathrm{E/B}}$, (6.12) is a continuous-time linear, time-varying system, and therefore its discretization is linear, time-varying.

6.3 Experimental Setup

In the laboratory setup, we estimate the inertial acceleration of a quadrotor in $\mathrm{F_E}$ and $\mathrm{F_B}$ using (6.9) and (6.12), respectively, with $C = \begin{bmatrix} I_{3\times 3} & 0_{3\times 3} \end{bmatrix}$. The position $\vec{r}_{\mathrm{p/O_E}}\Big|_{\mathrm{E}}$ and attitude (Φ, Θ, Ψ) of the vehicle are obtained using the Vicon system and recorded for post-flight data analysis. To compare the estimated acceleration with the measured acceleration, data from the vehicle's inertial measurement unit (IMU) is recorded and time-stamped. Using knowledge of the vehicle attitude, IMU acceleration measurements are corrected to compensate for gravity offset for comparison with RCIE acceleration estimates.

6.4 Estimating inertial acceleration in the Earth frame

We discretize (6.9) with $T_{\mathrm{s}} = 0.01\,\mathrm{sec}$, which is the sample-rate of the recorded data. The system (A, G, C) is NMP with six poles at 1 and three invariant zeros at -1. Note that D_1 is zero. Let $n_{\mathrm{c}} = 2$, $n_{\mathrm{f}} = 6$, $\lambda = 1$, $R_\theta = 10^{-10} I_{l_\theta}$, $R_d = 10^{-2} I_{l_d}$, $R_z = I_{l_y}$, $V_{\hat{d}} = 10^{-4} I_{6\times 6}$, and $V_2 = 10^{-2} I_{3\times 3}$.

Fig. 6.1 shows the accuracy of the RCIE estimate of the inertial acceleration of the quadrotor in $\mathrm{F_E}$ using position measurements obtained from the Vicon system. For this setup, the estimates of d using filters [17] and [29] diverge in less than 2.5 sec (not shown).

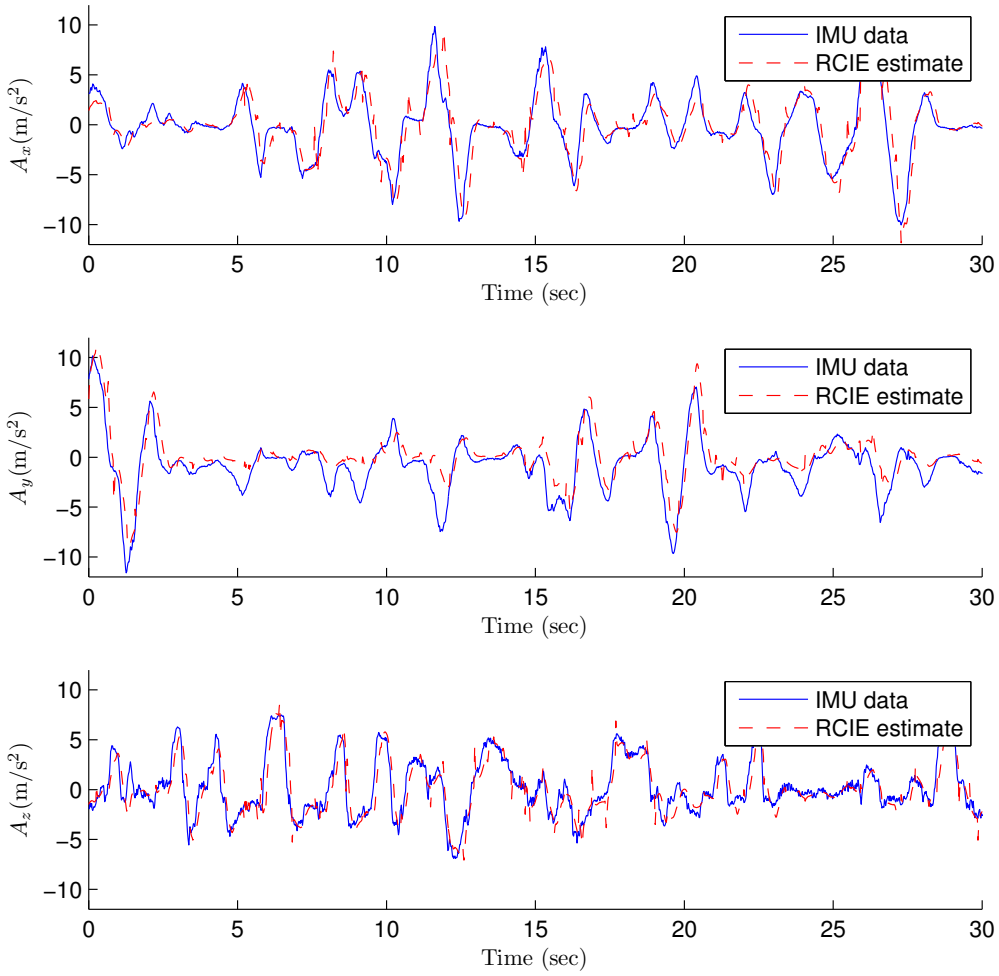

Figure 6.1: Estimation of the inertial acceleration of the quadrotor relative to $\mathrm{O_E}$ with respect to $\mathrm{F_E}$ using position measurements. RCIE estimates are compared with the IMU acceleration measurements transformed to $\mathrm{F_E}$ and corrected to compensate for gravity offset.

6.5 Estimating inertial acceleration in the body frame

Noting that G_c is time varying in (6.12), we discretize (6.12) at each time step k with $T_\mathrm{s} = 0.01\,\mathrm{sec}$, which is the sample-rate of the recorded data. Let $n_\mathrm{c} = 2$, $n_\mathrm{f} = 6$, $\lambda = 1$, $R_\theta = 10^{-10} I_{l_\theta}$, $R_d = 10^{-4} I_{l_d}$, $R_z = I_{l_y}$, $V_{\hat{d}} + V_1 = 10^{-4} I_{6\times 6}$, and $V_2 = 10^{-2} I_{3\times 3}$.

Fig. 6.2 shows the accuracy of the RCIE estimate of the inertial acceleration of

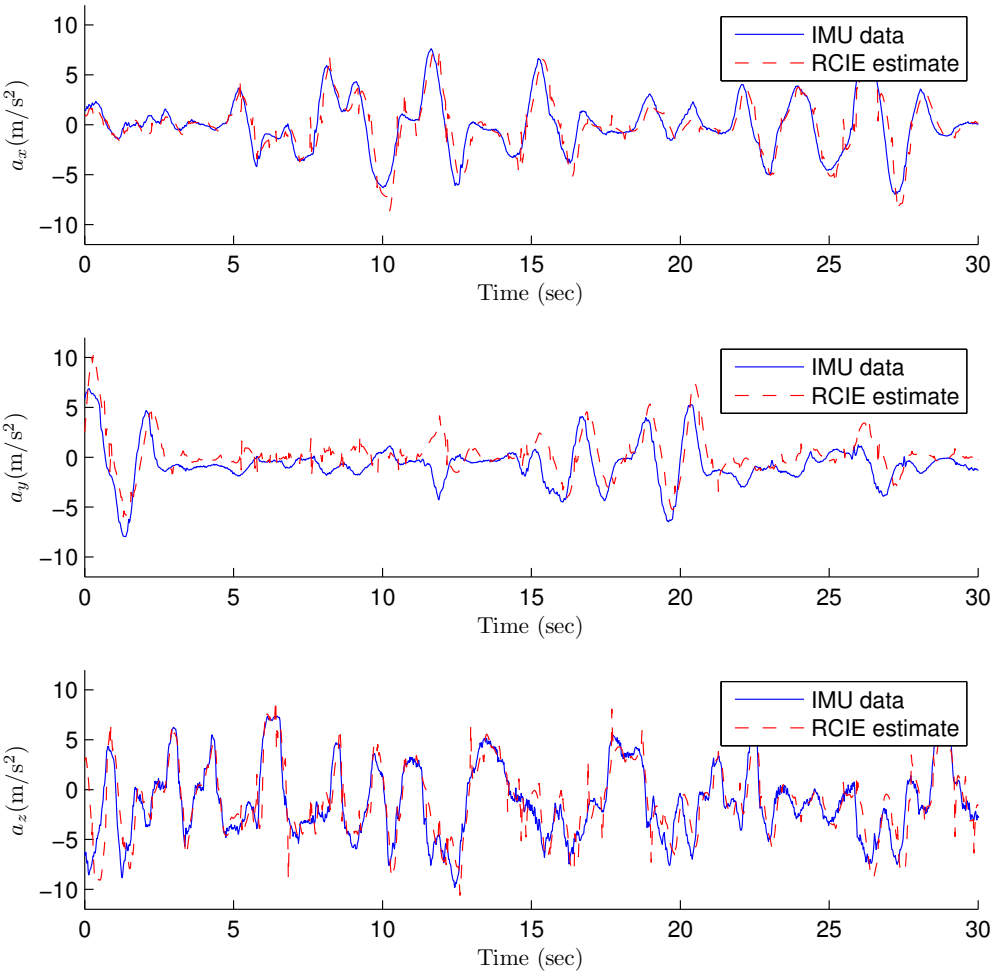

Figure 6.2: Estimation of the inertial acceleration of the quadrotor relative to $\mathrm{O_E}$ with respect to $\mathrm{F_B}$ using position and attitude measurements. RCIE estimates are compared with the IMU acceleration measurements with gravity correction.

the quadrotor in the body frame using position and attitude measurements obtained from the Vicon system. For this setup, the estimates of d using filters [17] and [29] diverge in less than 2.5 sec (not shown).

6.6 Conclusions

As an experimental application, RCIE was used to estimate the inertial acceleration of a UAV; these estimates were shown to be close to independent, onboard measurements provided by an IMU. In contrast, the techniques of [17] and [29] produced divergent estimates. In fact, the techniques in [17, 29, 39] are not applicable to this problem due to the presence of invariant zeros on the unit circle. In the next chapter, RCIE is applied to the problem of estimating drag acceleration of a satellite.

CHAPTER 7

Satellite Drag Estimation

7.1 Introduction

Orbit estimation is of increasing interest due to the need to avoid collisions between operational satellites and space debris. The number of derelict objects that can threaten satellites numbers in the tens of thousands, and measurements that can be used to track these objects are sparse. There is thus a pressing need for estimation algorithms that can use position and velocity measurements to obtain orbit estimates of the highest possible accuracy.

To address this problem, research has focused on nonlinear estimation techniques. Various classical techniques are applied to this problem in [87]. In [88], the extended Kalman filter (EKF) and the unscented Kalman filter (UKF) were applied to orbit estimation using range data. Optimal transport methods were applied to this problem in [89]. An alternative approach was taken in [90], where optimal control techniques were used to detect the motion of possibly maneuvering objects.

The present chapter focuses on the problem of drag estimation, where the goal is to estimate the drag acceleration of the body without assuming knowledge of the nominal orbit of the body. The estimation of satellite drag coefficients has been widely studied [91–94]. In the present chapter, drag acceleration is estimated by using *input estimation*. As an extension of state estimation, which uses knowledge

of the dynamics along with statistical information concerning the process and sensor noise to estimate states, input estimation uses the same information to estimate both states and inputs.

The contribution of the present chapter is the novel application of input estimation to the problem of estimating drag acceleration. The approach used in the present chapter is based on retrospective cost optimization. This technique is a variation of retrospective cost input estimation used in [44, 72, 95]. Related techniques have been applied to adaptive control [48].

7.2 Kinematics of a Satellite Orbiting the Earth

The Earth-Centered Inertial (ECI) frame is denoted by $\mathrm{F_E}$. The origin $\mathrm{O_E}$ of $\mathrm{F_E}$ is fixed at the center of the Earth. The axes $\hat{\imath}_{\mathrm{E}}$ points toward the vernal equinox, $\hat{k}_{\mathrm{E}}$ points North, and the axis $\hat{\jmath}_{\mathrm{E}} = \hat{k}_{\mathrm{E}} \times \hat{\imath}_{\mathrm{E}}$. Note that, $\hat{\imath}_{\mathrm{E}}$ and $\hat{\jmath}_{\mathrm{E}}$ lie in the equatorial plane.

Let p denote a point that is fixed on a satellite orbiting the Earth. The location of p relative to $\mathrm{O_E}$ is denoted by $\vec{r}_{\mathrm{p/O_E}}$ and is resolved in $\mathrm{F_E}$ as

$$\begin{bmatrix} X \\ Y \\ Z \end{bmatrix} \triangleq \vec{r}_{\mathrm{p/O_E}}\Big|_{\mathrm{E}}. \tag{7.1}$$

The velocity of p relative to $\mathrm{O_E}$ with respect to $\mathrm{F_E}$ is given by

$$\vec{v}_{\mathrm{p/O_E/E}} = \overset{\mathrm{E}\bullet}{\vec{r}}_{\mathrm{p/O_E}}, \tag{7.2}$$

where E$\bullet$ denotes the derivative with respect to the time taken in ECI frame. The

acceleration of p relative to O_E with respect to F_E is given by

$$\vec{a}_{p/O_E/E} = \overset{E\bullet}{\vec{v}}_{p/O_E/E} = \overset{E\bullet\bullet}{\vec{r}}_{p/O_E} . \tag{7.3}$$

Define

$$\hat{r} \triangleq \frac{\vec{r}_{p/O_E}}{|\vec{r}_{p/O_E}|}, \; \hat{v} \triangleq \frac{\vec{v}_{p/O_E/E}}{|\vec{v}_{p/O_E/E}|}, \; \hat{h} \triangleq \frac{\vec{r}_{p/O_E} \times \vec{v}_{p/O_E}}{|\vec{r}_{p/O_E} \times \vec{v}_{p/O_E}|}, \tag{7.4}$$

and $F_P \triangleq \begin{bmatrix} \hat{\imath}_P & \hat{\jmath}_P & \hat{k}_P \end{bmatrix} = \begin{bmatrix} \hat{v} \times \hat{h} & \hat{v} & \hat{h} \end{bmatrix}$. The frames F_P and F_E are related by

$$F_E = \vec{R}_{E/P} \, F_P, \tag{7.5}$$

where $\vec{R}_{E/P}$ is a physical rotation matrix. We resolve $\vec{R}_{E/P}$ in F_E as

$$\mathcal{O}_{E/P} \triangleq \vec{R}_{E/P}\Big|_E = \begin{bmatrix} \hat{\imath}_E \cdot \hat{\imath}_P & \hat{\imath}_E \cdot \hat{\jmath}_P & \hat{\imath}_E \cdot \hat{k}_P \\ \hat{\jmath}_E \cdot \hat{\imath}_P & \hat{\jmath}_E \cdot \hat{\jmath}_P & \hat{\jmath}_E \cdot \hat{k}_P \\ \hat{k}_E \cdot \hat{\imath}_P & \hat{k}_E \cdot \hat{\jmath}_P & \hat{k}_E \cdot \hat{k}_P \end{bmatrix}. \tag{7.6}$$

Note that $\mathcal{O}_{P/E} = \mathcal{O}_{E/P}^T$.

We resolve $\vec{v}_{p/O_E/E}$ and $\vec{a}_{p/O_E/E}$ in F_E and F_P using the notation

$$\begin{bmatrix} V_x \\ V_y \\ V_z \end{bmatrix} \triangleq \vec{v}_{p/O_E/E}\Big|_E, \quad \begin{bmatrix} v_x \\ v_v \\ v_h \end{bmatrix} \triangleq \vec{v}_{p/O_E/E}\Big|_P. \tag{7.7}$$

$$\begin{bmatrix} A_x \\ A_y \\ A_z \end{bmatrix} \triangleq \vec{a}_{p/O_E/E}\Big|_E, \quad \begin{bmatrix} a_x \\ a_v \\ a_h \end{bmatrix} \triangleq \vec{a}_{p/O_E/E}\Big|_P. \tag{7.8}$$

Using (7.6) and (7.8), $\vec{a}_{\mathrm{p/O_E/E}}$ in $\mathrm{F_E}$ is given by

$$\vec{a}_{\mathrm{p/O_E/E}}\Big|_{\mathrm{E}} = \mathcal{O}_{\mathrm{E/P}}\, \vec{a}_{\mathrm{p/O_E/E}}\Big|_{\mathrm{P}}, \tag{7.9}$$

and thus,

$$\begin{bmatrix} A_x \\ A_y \\ A_z \end{bmatrix} = \mathcal{O}_{\mathrm{E/P}} \begin{bmatrix} a_x \\ a_v \\ a_h \end{bmatrix}. \tag{7.10}$$

Note that (7.5)–(7.10) are exact kinematic relations that are applicable to an arbitrary point p on the satellite.

7.3 Dynamics of a Satellite Orbiting the Earth

The dynamics of a satellite moving in the Earth's gravity field is given by

$$\vec{F}_{\mathrm{gravity}} + \vec{F}_{\mathrm{pert}} = m_{\mathrm{sat}}\, \vec{a}_{\mathrm{p/O_E/E}}, \tag{7.11}$$

where F_{gravity} is the gravitational force acting on the satellite, F_{pert} is the perturbing force acting on the satellite, and m_{sat} is the mass of the satellite.

Gravity Model

We assume that the Earth is homogeneous and spherical. It thus follows from Newton's law of gravitation that

$$\underbrace{\frac{\vec{F}_{\mathrm{gravity}}}{m_{\mathrm{sat}}}}_{\vec{a}_{\mathrm{gravity}}} = -\mu \frac{\vec{r}_{\mathrm{p/O_E}}}{|\vec{r}_{\mathrm{p/O_E}}|^3}, \tag{7.12}$$

where $\mu = 398600.4405\,\mathrm{km}^3/\mathrm{sec}^2$. Substituting (7.3) and (7.12) into (7.11) yields

$$\overset{\mathrm{E}\bullet\bullet}{\vec{r}}_{\mathrm{p/O_E}} = -\mu \frac{\vec{r}_{\mathrm{p/O_E}}}{|\vec{r}_{\mathrm{p/O_E}}|^3} + \frac{F_{\mathrm{pert}}}{m_{\mathrm{sat}}}. \tag{7.13}$$

7.3.1 No Perturbing Force

If $\vec{F}_{\mathrm{pert}} = 0$, then using (7.1), (7.13) is given by

$$\ddot{X} = -\mu \frac{X}{(X^2+Y^2+Z^2)^{3/2}}, \tag{7.14}$$

$$\ddot{Y} = -\mu \frac{Y}{(X^2+Y^2+Z^2)^{3/2}}, \tag{7.15}$$

$$\ddot{Z} = -\mu \frac{Z}{(X^2+Y^2+Z^2)^{3/2}}. \tag{7.16}$$

Using (7.7), (7.14)–(7.16) can be written as the following first-order nonlinear ordinary differential equations

$$\dot{X} = V_x, \tag{7.17}$$

$$\dot{Y} = V_y, \tag{7.18}$$

$$\dot{Z} = V_z, \tag{7.19}$$

$$\dot{V}_x = -\mu \frac{X}{(X^2+Y^2+Z^2)^{3/2}}, \tag{7.20}$$

$$\dot{V}_y = -\mu \frac{Y}{(X^2+Y^2+Z^2)^{3/2}}, \tag{7.21}$$

$$\dot{V}_z = -\mu \frac{Z}{(X^2+Y^2+Z^2)^{3/2}}. \tag{7.22}$$

7.3.2 Drag as a Perturbing Force

Let the drag acting on the satellite be given by

$$\underbrace{\frac{\vec{F}_{\mathrm{pert}}}{m_{\mathrm{sat}}}}_{\vec{a}_{\mathrm{drag}}} = -\alpha \frac{\vec{v}_{\mathrm{p/O_E/E}}}{|\vec{v}_{\mathrm{p/O_E/E}}|}, \tag{7.23}$$

where $\alpha \in \mathbb{R}\,(\mathrm{kN/kg})$ is the magnitude of the acceleration due to drag. Using (7.1), (7.7), (7.13), and (7.23), the satellite dynamics are given by

$$\dot{X} = V_x, \tag{7.24}$$

$$\dot{Y} = V_y, \tag{7.25}$$

$$\dot{Z} = V_z, \tag{7.26}$$

$$\dot{V}_x = \underbrace{-\mu \frac{X}{(X^2+Y^2+Z^2)^{3/2}}}_{A_{x,\mathrm{gravity}}} \underbrace{-\alpha \frac{V_x}{(V_x^2+V_y^2+V_z^2)^{1/2}}}_{A_{x,\mathrm{drag}}}, \tag{7.27}$$

$$\dot{V}_y = \underbrace{-\mu \frac{Y}{(X^2+Y^2+Z^2)^{3/2}}}_{A_{y,\mathrm{gravity}}} \underbrace{-\alpha \frac{V_y}{(V_x^2+V_y^2+V_z^2)^{1/2}}}_{A_{y,\mathrm{drag}}}, \tag{7.28}$$

$$\dot{V}_z = \underbrace{-\mu \frac{Z}{(X^2+Y^2+Z^2)^{3/2}}}_{A_{z,\mathrm{gravity}}} \underbrace{-\alpha \frac{V_z}{(V_x^2+V_y^2+V_z^2)^{1/2}}}_{A_{z,\mathrm{drag}}}. \tag{7.29}$$

Note from (7.11), (7.12), and (7.23) that

$$\vec{a}_{\mathrm{drag}} = \vec{a}_{\mathrm{p/O_E/E}} - \vec{a}_{\mathrm{gravity}}. \tag{7.30}$$

Furthermore note that $\vec{a}_{\mathrm{drag}}|_{\mathrm{P}} = \begin{bmatrix} 0 & -\alpha & 0 \end{bmatrix}^{\mathrm{T}}$.

7.4 Model for Input Estimation

A continuous-time state-space model for input estimation can be formulated as

$$\dot{x}(t) = A_{\mathrm{c}}(t)x(t) + B_{\mathrm{c}}(t)u(t) + G_{\mathrm{c}}(t)d(t) + \bar{D}_1(t)w(t), \tag{7.31}$$

$$y(t) = C(t)x(t) + D_2(t)v(t), \tag{7.32}$$

where $x \in \mathbb{R}^{l_x}$ is the unknown state, $u \in \mathbb{R}^{l_u}$ is the known input, $d \in \mathbb{R}^{l_d}$ is the unknown input, $\bar{D}_1 w \in \mathbb{R}^{l_x}$ is the process noise with known covariance $\bar{V}_1 \triangleq \bar{D}_1 \bar{D}_1^{\mathrm{T}} \in$

$\mathbb{R}^{l_x \times l_x}$, $y \in \mathbb{R}^{l_y}$ is the measured output, and $D_2 \in \mathbb{R}^{l_v}$ is the measurement noise with known covariance $V_2 \triangleq D_2 D_2^{\mathrm{T}} \in \mathbb{R}^{l_y \times l_y}$. It is shown below that estimating acceleration is equivalent to estimating the unknown input d. We consider three scenarios for estimating the drag acceleration $\vec{a}_{\mathrm{drag}}$ by estimating the unknown input d using RCIE.

7.4.1 Indirect Estimation of Drag Acceleration in F_{E}

For indirect estimation of the drag acceleration, we first estimate $\vec{a}_{\mathrm{p/O_E/E}}$ resolved in $\mathrm{F_E}$. In doing so, we use (7.2), (7.7), (7.8), and write (7.3) in state space form

$$\dot{x} = A_{\mathrm{c}} x + G_{\mathrm{c}} d, \tag{7.33}$$

where

$$A_{\mathrm{c}} = \begin{bmatrix} 0_{3\times 3} & I_3 \\ 0_{3\times 3} & 0_{3\times 3} \end{bmatrix}, \quad G_{\mathrm{c}} = \begin{bmatrix} 0_{3\times 3} \\ I_3 \end{bmatrix}, \tag{7.34}$$

$$x = \begin{bmatrix} X & Y & Z & V_x & V_y & V_z \end{bmatrix}^{\mathrm{T}}, \; d = \begin{bmatrix} A_x & A_y & A_z \end{bmatrix}^{\mathrm{T}}. \tag{7.35}$$

Note that (7.33) is an exact kinematic equation, and thus it does not include process noise. Next, using (7.30) and the knowledge of gravity (7.12), the acceleration due to drag $\vec{a}_{\mathrm{drag}}$ resolved in F_{E} is given by

$$\vec{a}_{\mathrm{drag}}\Big|_{\mathrm{E}} = \vec{a}_{\mathrm{p/O_E/E}}\Big|_{\mathrm{E}} - \vec{a}_{\mathrm{gravity}}\Big|_{\mathrm{E}}, \tag{7.36}$$

$$\begin{bmatrix} A_{x,\mathrm{drag}} \\ A_{y,\mathrm{drag}} \\ A_{z,\mathrm{drag}} \end{bmatrix} = \begin{bmatrix} A_x \\ A_y \\ A_z \end{bmatrix} + \frac{\mu}{(X^2+Y^2+Z^2)^{3/2}} \begin{bmatrix} X \\ Y \\ Z \end{bmatrix}. \tag{7.37}$$

Note that (7.37) gives an indirect estimate of the drag acceleration. A direct estimate of drag acceleration is presented in the subsection below.

7.4.2 Direct Estimation of the Drag Acceleration in F_{E}

For a direct estimation of drag acceleration $\vec{a}_{\mathrm{drag}}$ resolved in $\mathrm{F_E}$, we use (7.2), (7.7), (7.8), (7.36), and write (7.3) in state space form

$$\dot{x} = A_{\mathrm{c}}x + B_{\mathrm{c}}u + G_{\mathrm{c}}d + \bar{D}_1 w, \tag{7.38}$$

where

$$A_{\mathrm{c}} = \begin{bmatrix} 0_{3\times3} & I_3 \\ 0_{3\times3} & 0_{3\times3} \end{bmatrix}, \quad B_{\mathrm{c}} = G_{\mathrm{c}} = \begin{bmatrix} 0_{3\times3} \\ I_3 \end{bmatrix}, \tag{7.39}$$

$$x = \begin{bmatrix} X & Y & Z & V_x & V_y & V_z \end{bmatrix}^{\mathrm{T}}, \tag{7.40}$$

$$u = \begin{bmatrix} A_{x,\mathrm{gravity}} & A_{y,\mathrm{gravity}} & A_{z,\mathrm{gravity}} \end{bmatrix}^{\mathrm{T}}, \tag{7.41}$$

$$d = \begin{bmatrix} A_{x,\mathrm{drag}} & A_{y,\mathrm{drag}} & A_{z,\mathrm{drag}} \end{bmatrix}^{\mathrm{T}}. \tag{7.42}$$

Likewise (7.33), (7.38) is an exact kinematic equation, but process noise is included to account for errors due to uncertainty in u.

7.4.3 Estimation of Drag Acceleration in F_{P}

For estimating the drag acceleration $\vec{a}_{\mathrm{drag}}$ resolved in $\mathrm{F_P}$, we use (7.2), (7.6), (7.7), (7.8), (7.36), (7.10), and write (7.3) in state space form

$$\dot{x} = A_{\mathrm{c}}x + B_{\mathrm{c}}u + G_{\mathrm{c}}d + \bar{D}_1 w, \tag{7.43}$$

where

$$A_{\mathrm{c}} = \begin{bmatrix} 0_{3\times3} & I_3 \\ 0_{3\times3} & 0_{3\times3} \end{bmatrix}, \; B_{\mathrm{c}} = \begin{bmatrix} 0_{3\times3} \\ I_3 \end{bmatrix}, \; G_{\mathrm{c}} = \begin{bmatrix} 0_{3\times1} \\ \hat{v}|_{\mathrm{E}} \end{bmatrix}, \tag{7.44}$$

$$x = \begin{bmatrix} X & Y & Z & V_x & V_y & V_z \end{bmatrix}^{\mathrm{T}}, \tag{7.45}$$

$$u = \begin{bmatrix} A_{x,\mathrm{gravity}} & A_{y,\mathrm{gravity}} & A_{z,\mathrm{gravity}} \end{bmatrix}^{\mathrm{T}}, \tag{7.46}$$

$$d = -\alpha. \tag{7.47}$$

Note that (7.43) is an exact kinematic equation, but process noise is now included to account for errors in the measurements of $\hat{v}|_{\mathrm{E}}$ appearing in (7.44). Finally, notice that, due to $\hat{v}|_{\mathrm{E}}$, (7.43) is a continuous-time linear, time-varying system, and therefore its discretization is linear, time-varying.

7.5 Numerical Results

7.5.1 Simulation Setup

Using retrospective cost input estimation (RCIE), we estimate the drag acceleration $\vec{a}_{\mathrm{drag}}$ of a satellite in $\mathrm{F_E}$ and $\mathrm{F_P}$ using [(7.33),(7.38)] and (7.43), respectively, and with $C = I_6$. We choose $\alpha = 10^{-5}\,\mathrm{kN/kg}$ in (7.23), which is unknown to RCIE. The position $\vec{r}_{\mathrm{p/O_E}}\Big|_{\mathrm{E}}$ and velocity $\vec{v}_{\mathrm{p/O_E}}\Big|_{\mathrm{E}}$ of the satellite are obtained by integrating (7.17)–(7.22) using the Matlab function ode45 with a numerical tolerance of 10^{-12}. The initial position and velocity are chosen such that the satellite orbit is circular with inclination 51.6 deg and radius 6731 km. The length of the simulation is set for 1 hr, and the noise-free position and velocity data are recorded using the sampling-time $T_{\mathrm{s}} = 0.1\,\mathrm{sec}$. Since RCIE is a discrete-time algorithm, we discretize (7.33), (7.38),

and (7.43) using the Matlab function c2d, which uses zero-order hold on the input for discretization. To assess the accuracy of the RCIE estimate, we define the relative error $e_d = |\frac{d-\hat{d}}{d}|$, where d is the actual input and $\hat{d}$ is the RCIE estimated input.

7.5.2 Indirect Estimation of the Drag Acceleration in $F_{\rm E}$

Let the RCIE parameters be $n_{\rm c} = 2$, $n_{\rm f} = 24$, $\lambda = 1$, $R_\theta = 10^{-12} I_{l_\theta}$, $R_d = 10^{-12} I_3$, $R_z = I_6$, $V_{\hat{d}} + V_1 = 10^{-8} I_6$, and $V_2 = 10^{-8} I_6$.

For indirect estimation of drag acceleration, we first use (7.33) to estimate the total inertial acceleration (A_x, A_y, A_z) of the satellite. Figure 7.1 shows that the RCIE estimates follow the actual acceleration (A_x, A_y, A_z). After the initial transient, the maximum relative errors in the directions x, y, z of $F_{\rm E}$ are $1.07, 3.52, 3.52$, respectively, whereas the minimum relative errors in the directions x, y, z of $F_{\rm E}$ are $1.05 \times 10^{-9}, 3.11 \times 10^{-9}, 3.11 \times 10^{-9}$, respectively.

Next, we use (7.37) to estimate the drag acceleration $(A_{x,\rm drag},\ A_{y,\rm drag},\ A_{z,\rm drag})$ acting on the satellite. Figure 7.2 shows that the drag acceleration estimates follow the actual acceleration $(A_{x,\rm drag},\ A_{y,\rm drag},\ A_{z,\rm drag})$. After the initial transient, the maximum relative errors in the directions x, y, z of $F_{\rm E}$ are $38.4, 81.2, 81.2$, respectively, whereas the minimum relative errors in the directions x, y, z of $F_{\rm E}$ are $2.6 \times 10^{-5}, 3.8 \times 10^{-5}, 3.8 \times 10^{-5}$, respectively.

7.5.3 Direct Estimation of Drag Acceleration in $F_{\rm E}$

Using the same RCIE parameters as in Section 7.5.2, we use (7.38) to obtain a direct estimation of the drag acceleration $(A_{x,\rm drag},\ A_{y,\rm drag},\ A_{z,\rm drag})$. Figure 7.3 shows that the drag acceleration estimates follow the actual acceleration $(A_{x,\rm drag},\ A_{y,\rm drag},\ A_{z,\rm drag})$. After the initial transient, the maximum relative errors in the directions x, y, z of $F_{\rm E}$ are $88.1, 6.5, 6.5$, respectively, whereas the minimum relative errors in the directions x, y, z of $F_{\rm E}$ are $6.1 \times 10^{-6}, 2.6 \times 10^{-4}, 2.6 \times 10^{-4}$, respectively.

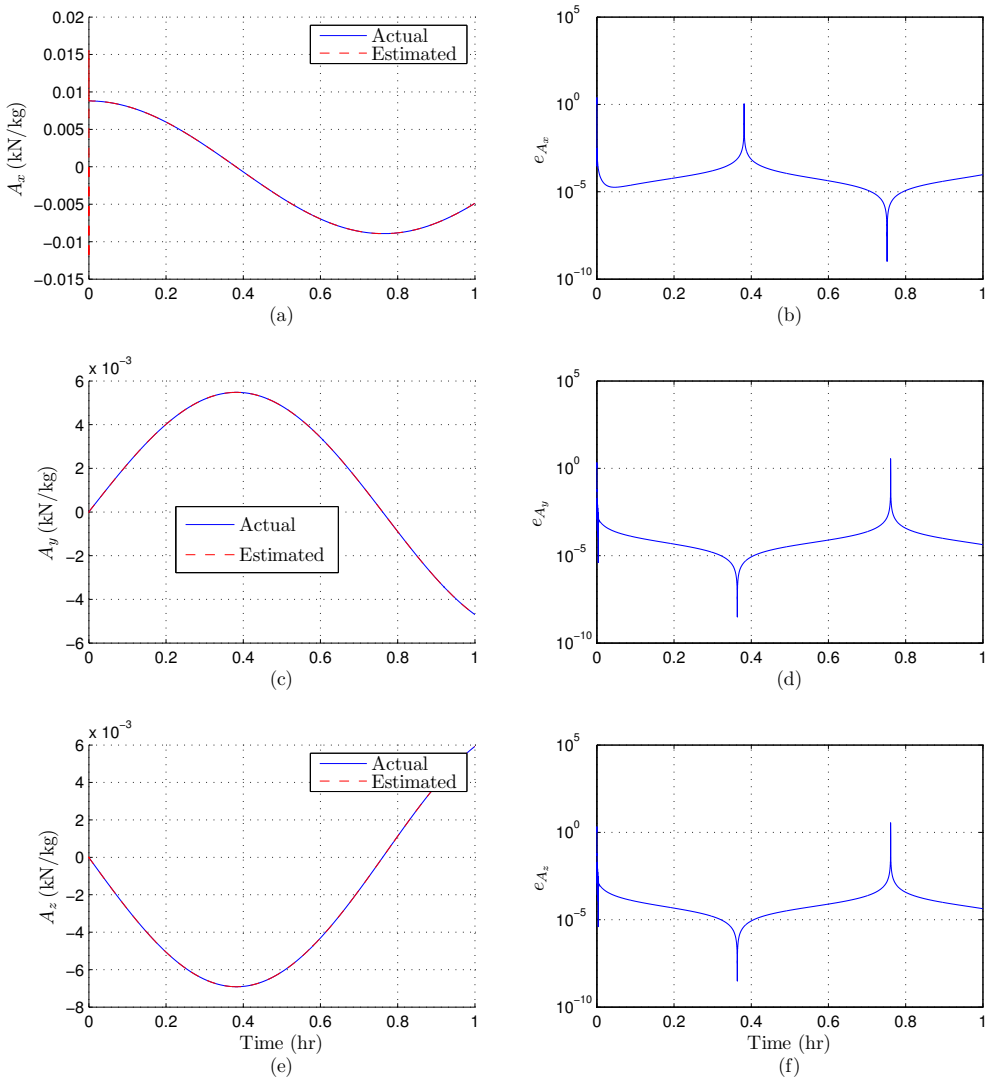

Figure 7.1: Estimation of the inertial acceleration (A_x, A_y, A_z) of the satellite using position and velocity measurements with $T_s = 0.1\,\text{sec}$. The RCIE estimates (dashed line) follow the actual acceleration (A_x, A_y, A_z) (solid line). After the initial transient, the maximum relative errors in the directions x, y, z of F_E are $1.07, 3.52, 3.52$, respectively, whereas the minimum relative errors in the directions x, y, z of F_E are $1.05 \times 10^{-9}, 3.11 \times 10^{-9}, 3.11 \times 10^{-9}$, respectively.

7.5.4 Estimation of Drag Acceleration in F_P

Let $n_c = 4$, $n_f = 4$, $\lambda = 1$, $R_\theta = 10^{-12} I_{l_\theta}$, $R_d = 10^{-8}$, $R_z = I_6$, $V_{\hat{d}} + V_1 = 10^{-12} I_6$, and $V_2 = 10^{-8} I_6$. To estimate the magnitude of drag acceleration α, we use (7.43).

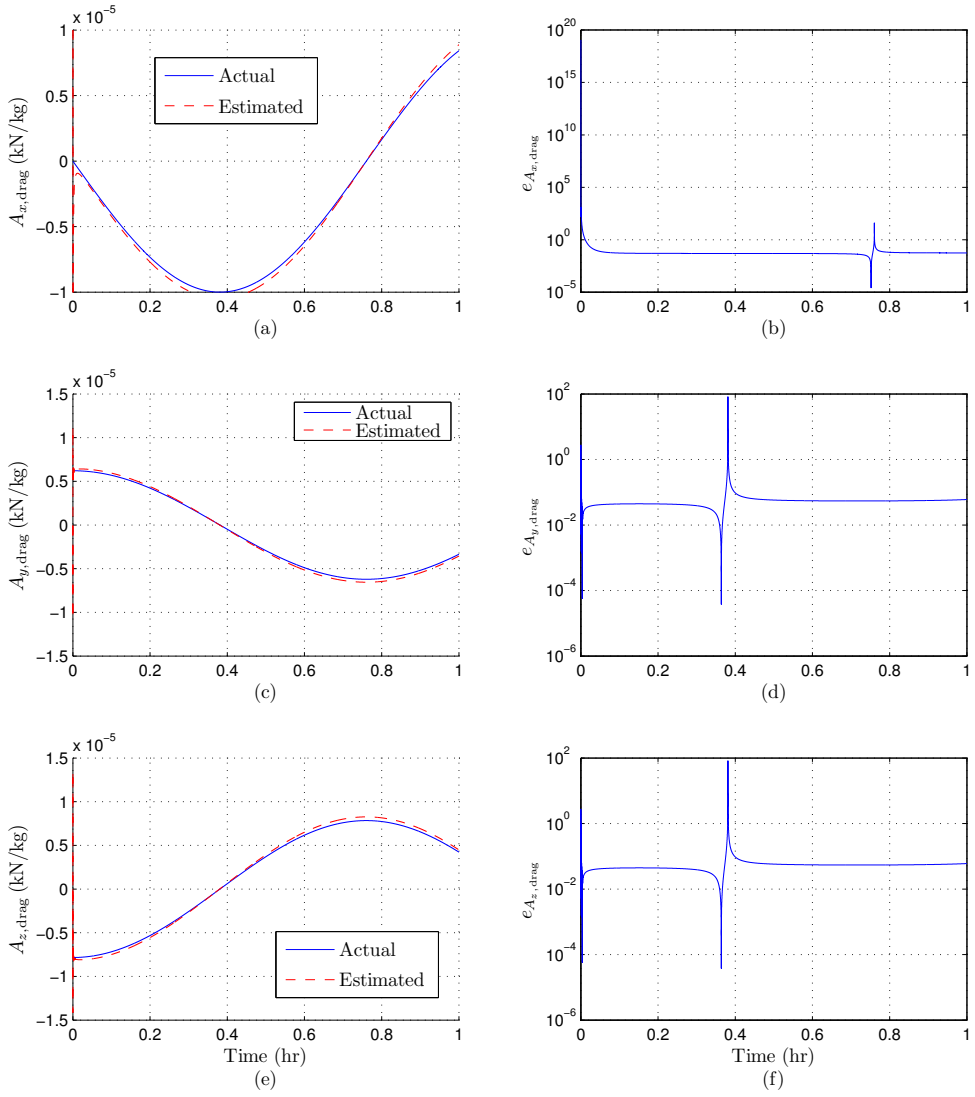

Figure 7.2: Indirect estimation of drag acceleration ($A_{x,\mathrm{drag}}$, $A_{y,\mathrm{drag}}$, $A_{z,\mathrm{drag}}$) of the satellite using the RCIE estimates of (A_x, A_y, A_z) shown in Figure 7.1. The drag acceleration estimates (dashed line) follow the actual acceleration ($A_{x,\mathrm{drag}}$, $A_{y,\mathrm{drag}}$, $A_{z,\mathrm{drag}}$) (solid line). After the initial transient, the maximum relative errors in the directions x, y, z of F_{E} are $38.4, 81.2, 81.2$, respectively, whereas the minimum relative errors in the directions x, y, z of F_{E} are $2.6 \times 10^{-5}, 3.8 \times 10^{-5}, 3.8 \times 10^{-5}$, respectively.

Figure 7.4 shows that the drag acceleration estimate follows the actual acceleration α.

After the initial transient, the maximum relative error is 0.1, whereas the minimum

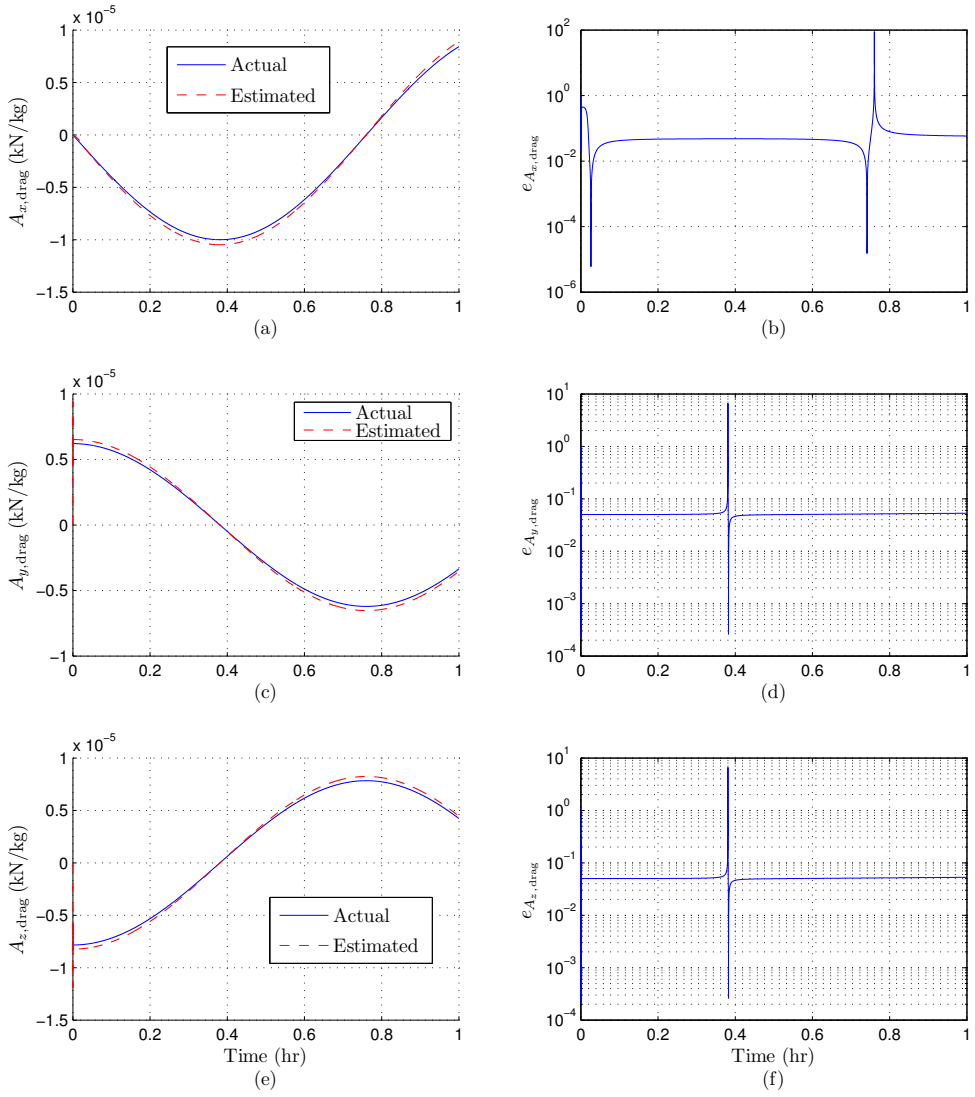

Figure 7.3: Direct estimation of drag acceleration ($A_{x,\text{drag}}$, $A_{y,\text{drag}}$, $A_{z,\text{drag}}$) of the satellite using gravity, position and velocity measurements with $T_\text{s} = 0.1\,\text{sec}$. The drag acceleration estimates (dashed line) follow the actual acceleration ($A_{x,\text{drag}}$, $A_{y,\text{drag}}$, $A_{z,\text{drag}}$) (solid line). After the initial transient, the maximum relative errors in the directions x, y, z of F_E are $88.1, 6.5, 6.5$, respectively, whereas the minimum relative errors in the directions x, y, z of F_E are $6.1 \times 10^{-6}, 2.6 \times 10^{-4}, 2.6 \times 10^{-4}$, respectively.

relative error is 6.3×10^{-6}.

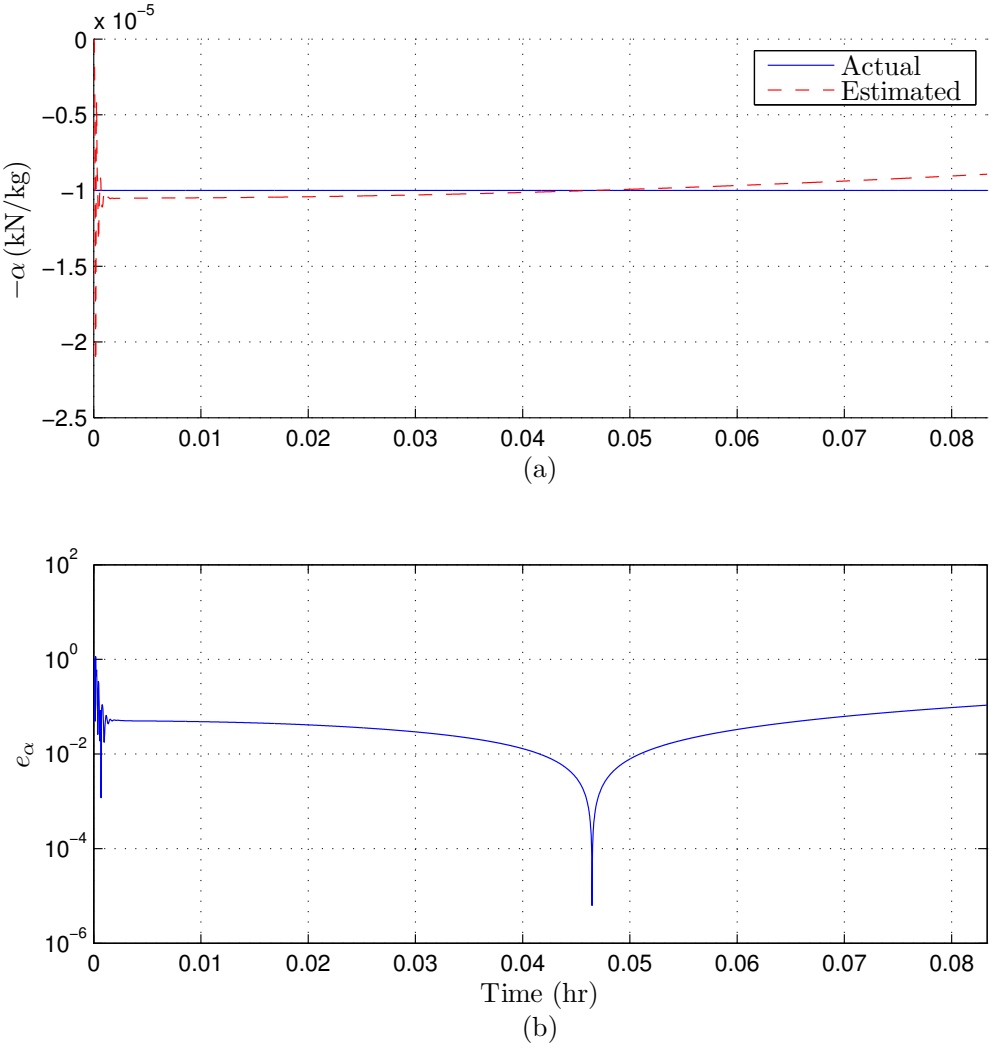

Figure 7.4: Estimation of the drag acceleration of the satellite in F_{P} using position and velocity measurements with $T_{\mathrm{s}} = 0.1\,\mathrm{sec}$. The drag acceleration estimate (dashed line) follows the actual acceleration α (solid line). After the initial transient, the maximum relative error is 0.1, whereas the minimum relative error is 6.3×10^{-6}.

7.6 Conclusion

Retrospective cost input estimation was used to estimate satellite drag. Three problem formulations were considered, namely, indirect estimation of the drag acceleration by estimating the total acceleration; direct estimation of the drag acceleration;

and estimation of the drag magnitude. These results, along with [72], show that input estimation can provide a viable approach to estimating acceleration modeled as an unknown input. In the next chapter, RCIE is applied to the problem of detecting sensor faults.

CHAPTER 8

Aircraft Sensor Fault Detection

8.1 Introduction

Sensor health is crucial to the operation of every feedback control system. Consequently, extensive research has been devoted to developing techniques for detecting and diagnosing sensor faults [61–70]. One approach is to search for anomalies in the sensor signal [67], while another approach is to compute sensor residuals based on the assumed model and measured input signals [61]. Yet another approach is to empirically identify transmissibilities between pairs of sensors under healthy conditions and then use these relations during subsequent operation to compute sensor residuals [71].

In the present chapter, we formulate the problem of diagnosing sensor faults for a flight vehicle as a problem of input and state estimation. In particular, we consider an exact model of the kinematics of the vehicle, which circumvents the need to measure forces and moments on the vehicle as well as the need to know the vehicle inertia and stability derivatives. Instead, the kinematics model views suspect sensor-measurement as the input or state. A related formulation is considered in [44, 45, 70].

Input estimation is an extension of state estimation where the goal is to estimate not only the states but also the inputs driving the system. In [72], we present an adap-

tive input estimation technique for nonminimum-phase-discrete-time linear systems based on the Kalman filter and retrospective-cost optimization. In the present chapter, we extend the approach in [72] to nonlinear systems by combining the unscented Kalman filter [73, 74] and retrospective cost input estimation [38, 44, 72].

To detect sensor faults using state and input estimation techniques, we use combinations of inertial and aerodynamic sensors. This work is motivated by [68, 70], which uses rate-gyro, accelerometer, GPS, angle-of-attack, and sideslip measurements to estimate forward velocity relative to the air in order to assess the health of the pitot tube. The present chapter extends the approach of [68, 70] in several ways. First, for pitot-tube fault detection, we apply the unscented Kalman filter with augmented bias states in order to deal with biased accelerometer measurements. Unlike [68, 70], we do not use GPS to assess the health of the pitot tube. Next, we consider four scenarios that are not considered in [68, 70], two of which depends on state estimation and the other two on input estimation.

In the first scenario, we use the pitot tube, rate gyros, accelerometers, α-sensor, and β-sensor to assess the health of the vertical gyros. In the second scenario, we use the pitot tube, vertical gyro, rate gyros, accelerometers, and β-sensor to assess the health of the α-sensor. In the third scenario, we use the pitot tube, rate gyros, vertical gyro, α-sensor, and β-sensor to assess the health of the accelerometers. In the fourth scenario, we use vertical gyro to assess the health of the rate gyros. For input estimation in the third and fourth scenarios, we use a variation of retrospective cost input estimation as described in [45, 72].

8.2 Aircraft Kinematics

8.2.1 Frames

The Earth frame and aircraft body-fixed frame are denoted by $\mathrm{F_E} = \begin{bmatrix} \hat{\imath}_\mathrm{E} & \hat{\jmath}_\mathrm{E} & \hat{k}_\mathrm{E} \end{bmatrix}$ and $\mathrm{F_{AC}} = \begin{bmatrix} \hat{\imath}_\mathrm{AC} & \hat{\jmath}_\mathrm{AC} & \hat{k}_\mathrm{AC} \end{bmatrix}$, respectively. We assume that $\mathrm{F_E}$ is an inertial frame and the Earth is flat. The origin $\mathrm{O_E}$ of $\mathrm{F_E}$ is any convenient point fixed on the Earth. The axes $\hat{\imath}_\mathrm{E}$ and $\hat{\jmath}_\mathrm{E}$ are horizontal, while the axis $\hat{k}_\mathrm{E}$ points downward. $\mathrm{F_{AC}}$ is defined with $\hat{\imath}_\mathrm{AC}$ pointing out the nose of the aircraft, $\hat{\jmath}_\mathrm{AC}$ pointing out the right wing, and $\hat{k}_\mathrm{AC}$ downward, that is, $\hat{k}_\mathrm{AC} = \hat{\imath}_\mathrm{AC} \times \hat{\jmath}_\mathrm{AC}$. $\mathrm{F_{AC}}$ and $\mathrm{F_E}$ are related by

$$\mathrm{F_{AC}} = \vec{R}_{\mathrm{AC/E}}\, \mathrm{F_E}, \tag{8.1}$$

where $\vec{R}_{\mathrm{AC/E}}$ is a physical rotation matrix represented by a 3-2-1 Euler rotation sequence involving two intermediate frames $\mathrm{F_{E'}}$ and $\mathrm{F_{E''}}$. In particular,

$$\vec{R}_{\mathrm{AC/E}} = \vec{R}_{\hat{\imath}_{\mathrm{E''}}}(\Phi)\, \vec{R}_{\hat{\jmath}_{\mathrm{E'}}}(\Theta)\, \vec{R}_{\hat{k}_\mathrm{E}}(\Psi), \tag{8.2}$$

where $\mathrm{F_{E'}} = \vec{\mathrm{R}}_{\mathrm{E'/E}}\, \mathrm{F_E}$, $\mathrm{F_{E''}} = \vec{\mathrm{R}}_{\mathrm{E''/E'}}\, \mathrm{F_{E'}}$, and

$$\vec{R}_{\hat{n}}\,(\kappa) \triangleq (\cos\kappa)\, \vec{U} + (1 - \cos\kappa)\hat{n}\hat{n}' + (\sin\kappa)\hat{n}^{\times}, \tag{8.3}$$

where $\vec{U}$ is the physical identity matrix. Note that (8.3) is the Rodrigues rotation about the eigenaxis $\hat{n}$ through the eigenangle κ according to the right-hand rule. Resolving (8.2) in $\mathrm{F_{AC}}$, we obtain

$$\mathcal{O}_{\mathrm{AC/E}} = \mathcal{O}_1(\Phi)\mathcal{O}_2(\Theta)\mathcal{O}_3(\Psi), \tag{8.4}$$

where

$$\mathcal{O}_1(\Phi) = \begin{bmatrix} 1 & 0 & 0 \\ 0 & \cos\Phi & \sin\Phi \\ 0 & -\sin\Phi & \cos\Phi \end{bmatrix}, \mathcal{O}_2(\Theta) = \begin{bmatrix} \cos\Theta & 0 & -\sin\Theta \\ 0 & 1 & 0 \\ \sin\Theta & 0 & \cos\Theta \end{bmatrix}, \mathcal{O}_3(\Psi) = \begin{bmatrix} \cos\Psi & \sin\Psi & 0 \\ -\sin\Psi & \cos\Psi & 0 \\ 0 & 0 & 1 \end{bmatrix}, \tag{8.5}$$

and thus

$$\mathcal{O}_{\mathrm{AC/E}} = \begin{bmatrix} (\cos\Theta)\cos\Psi & (\cos\Theta)\sin\Psi & -\sin\Theta \\ (\sin\Phi)(\sin\Theta)\cos\Psi - (\cos\Phi)\sin\Psi & (\sin\Phi)(\sin\Theta)\sin\Psi + (\cos\Phi)\cos\Psi & (\sin\Phi)\cos\Theta \\ (\cos\Phi)(\sin\Theta)\cos\Psi + (\sin\Phi)\sin\Psi & (\cos\Phi)(\sin\Theta)\sin\Psi - (\sin\Phi)\cos\Psi & (\cos\Phi)\cos\Theta \end{bmatrix}. \tag{8.6}$$

8.2.2 Rotational Kinematics

8.2.2.1 Poisson's Equation

The physical angular velocity $\vec{\omega}_{\mathrm{AC/E}}$ of $\mathrm{F_{AC}}$ relative to $\mathrm{F_E}$ is related to $\vec{R}_{\mathrm{AC/E}}$ by Poisson's equation

$$\overset{\mathrm{AC}\bullet}{\vec{R}}_{\mathrm{AC/E}} = \vec{R}_{\mathrm{AC/E}}\, \vec{\omega}^{\times}_{\mathrm{AC/E}}. \tag{8.7}$$

We resolve $\vec{\omega}_{\mathrm{AC/E}}$ and $\vec{R}_{\mathrm{AC/E}}$ in $\mathrm{F_{AC}}$ using the notation

$$\begin{bmatrix} P \\ Q \\ R \end{bmatrix} \triangleq \vec{\omega}_{\mathrm{AC/E}}\Big|_{\mathrm{AC}}, \quad \Omega \triangleq \vec{\omega}^{\times}_{\mathrm{AC/E}}\Big|_{\mathrm{AC}} = \begin{bmatrix} P \\ Q \\ R \end{bmatrix}^{\times}, \quad \mathcal{O}_{\mathrm{E/AC}} \triangleq \vec{R}_{\mathrm{AC/E}}\Big|_{\mathrm{AC}}, \tag{8.8}$$

where $\mathcal{O}_{\mathrm{E/AC}}$ is the orientation matrix of $\mathrm{F_E}$ relative to $\mathrm{F_{AC}}$. Using (8.8), (8.7) implies

$$\dot{\mathcal{O}}_{\mathrm{E/AC}} = \mathcal{O}_{\mathrm{E/AC}}\,\Omega, \tag{8.9}$$

and thus, since $\Omega^{\mathrm{T}} = -\Omega$,

$$\dot{\mathcal{O}}_{\mathrm{AC/E}} = -\Omega\,\mathcal{O}_{\mathrm{AC/E}}. \tag{8.10}$$

Using Kronecker algebra, (8.10) can be written as

$$\mathrm{vec}(\dot{\mathcal{O}}_{\mathrm{AC/E}}) = (I \otimes -\Omega)\,\mathrm{vec}(\mathcal{O}_{\mathrm{AC/E}}), \tag{8.11}$$

where "$\otimes$" is the Kronecker product and "vec" is the column-stacking operator. Note that (8.11) is a linear differential equation of the form $\dot{X}(t) = A(t)X(t)$, where $A(t) = (I \otimes -\Omega(t)) \in \mathbb{R}^{9\times 9}$ and $X(t) = \mathrm{vec}(\mathcal{O}_{\mathrm{AC/E}}(t)) \in \mathbb{R}^9$.

8.2.2.2 Euler-Angle Rate Equations

For the 3-2-1 (yaw-pitch-roll) Euler rotation sequence, we have

$$\vec{\omega}_{\mathrm{AC/E}}\Big|_{\mathrm{AC}} = \dot{\Phi}\hat{\imath}_{\mathrm{AC}} + \dot{\Theta}\hat{\jmath}_{\mathrm{E}''} + \dot{\Psi}\hat{k}_{\mathrm{E}'}. \tag{8.12}$$

Resolving (8.12) in $\mathrm{F_{AC}}$ using (8.8) yields

$$\begin{bmatrix} P \\ Q \\ R \end{bmatrix} = \begin{bmatrix} 1 & 0 & -\sin\Theta \\ 0 & \cos\Phi & (\cos\Theta)\sin\Phi \\ 0 & -\sin\Phi & (\cos\Theta)\cos\Phi \end{bmatrix} \begin{bmatrix} \dot{\Phi} \\ \dot{\Theta} \\ \dot{\Psi} \end{bmatrix}. \tag{8.13}$$

Assuming $\cos\Theta \neq 0$, the inverse transformation of (8.13) is given by

$$\begin{bmatrix} \dot{\Phi} \\ \dot{\Theta} \\ \dot{\Psi} \end{bmatrix} = N(\Phi, \Theta) \begin{bmatrix} P \\ Q \\ R \end{bmatrix}, \tag{8.14}$$

where

$$N(\Phi, \Theta) \stackrel{\triangle}{=} \begin{bmatrix} 1 & (\sin\Phi)\tan\Theta & (\cos\Phi)\tan\Theta \\ 0 & \cos\Phi & -\sin\Phi \\ 0 & (\sin\Phi)\sec\Theta & (\cos\Phi)\sec\Theta \end{bmatrix}. \tag{8.15}$$

8.2.2.3 Quaternion Rate Equations

Let $\mathrm{F_E}$ is rotated about the eigenaxis $\hat{n}$ by the angle ϕ according to the right-hand rule yielding $\mathrm{F_{AC}}$. Define

$$n \stackrel{\triangle}{=} \hat{n}\Big|_{\mathrm{E}} = \hat{n}\Big|_{\mathrm{AC}}. \tag{8.16}$$

Using Rodrigues rotation (8.3), the relationship between $\hat{n}, \phi$ and $\vec{R}_{\mathrm{AC/E}}$ is given by

$$\vec{R}_{\mathrm{AC/E}} = (\cos\phi)\ \vec{U} + (1 - \cos\phi)\hat{n}\hat{n}' + (\sin\phi)\hat{n}^{\times}. \tag{8.17}$$

Resolving (8.17) in $\mathrm{F_{AC}}$ yields

$$\mathcal{O}_{\mathrm{AC/E}} = (\cos\phi)I + (1 - \cos\phi)nn^{\mathrm{T}} - (\sin\phi)n^{\times}. \tag{8.18}$$

The quaternion vector of $\mathrm{F_{AC}}$ relative to $\mathrm{F_E}$ is defined by

$$q \triangleq \begin{bmatrix} \varepsilon \\ \eta \end{bmatrix} = \begin{bmatrix} n \sin \frac{\phi}{2} \\ \cos \frac{\phi}{2} \end{bmatrix} \in \mathbb{R}^4. \tag{8.19}$$

Note that and $\sqrt{q^{\mathrm{T}} q} = 1$. Using (8.19) and trigonometric identities, (8.18) can be written as

$$\mathcal{O}_{\mathrm{AC/E}} = (2\eta^2 - 1)I - 2\eta\varepsilon^{\times} + 2\varepsilon\varepsilon^{\mathrm{T}}. \tag{8.20}$$

The relationship between $\varepsilon, \eta, \dot{\varepsilon}, \dot{\eta}$ and $\vec{\omega}_{\mathrm{AC/E}}\Big|_{\mathrm{AC}}$ is

$$\begin{bmatrix} P \\ Q \\ R \end{bmatrix} = \begin{bmatrix} 2(\eta I - \varepsilon^{\times}) & -2\varepsilon \end{bmatrix} \begin{bmatrix} \dot{\varepsilon} \\ \dot{\eta} \end{bmatrix}. \tag{8.21}$$

The inverse transformation of (8.21) is given by

$$\begin{bmatrix} \dot{\varepsilon} \\ \dot{\eta} \end{bmatrix} = \frac{1}{2} \begin{bmatrix} \eta I + \varepsilon^{\times} \\ -\varepsilon^{\mathrm{T}} \end{bmatrix} \begin{bmatrix} P \\ Q \\ R \end{bmatrix}. \tag{8.22}$$

Note that (8.11), (8.14), and (8.22) are three different ways of computing attitude using angular velocity, given the initial attitude $\mathcal{O}_{\mathrm{AC/E}}(0)$, $[\Phi(0), \Theta(0), \Psi(0)]$, and $[\varepsilon(0), \eta(0)]$, respectively.

8.2.3 Translational Kinematics

At each time instant, let a denote the air particle located at a point that is fixed relative to the aircraft and upstream of the pitot tube. The location of the

aircraft center of mass c relative to the origin O_E of F_E at each time instant is given by

$$\vec{r}_{c/O_E} = \vec{r}_{c/a} + \vec{r}_{a/O_E}. \tag{8.23}$$

Differentiating (8.23) with respect to F_E yields

$$\vec{V}_c = \vec{V}_{AC} + \vec{V}_a, \tag{8.24}$$

where

$$\vec{V}_c \triangleq \overset{E\bullet}{\vec{r}}_{c/O_E}, \quad \vec{V}_{AC} \triangleq \overset{E\bullet}{\vec{r}}_{c/a}, \quad \vec{V}_a \triangleq \overset{E\bullet}{\vec{r}}_{a/O_E}. \tag{8.25}$$

The acceleration of the aircraft center of mass relative to O_E is given by

$$\vec{a}_{c/O_E/E} = \overset{E\bullet}{\vec{v}}_{c/O_E/E} = \overset{E\bullet}{\vec{v}}_{c/a/E} + \overset{E\bullet}{\vec{v}}_{a/O_E/E}. \tag{8.26}$$

We assume that the ambient wind is spatially uniform and constant with respect to F_E, i.e., $\overset{E\bullet}{\vec{v}}_{a/O_E/E} = 0$. Hence

$$\vec{a}_{c/O_E/E} = \overset{E\bullet}{\vec{v}}_{c/a/E} = \overset{E\bullet}{\vec{V}}_{AC}. \tag{8.27}$$

Using the transport theorem with (8.27) yields

$$\vec{a}_{c/O_E/E} = \overset{AC\bullet}{\vec{V}}_{AC} + \vec{\omega}_{AC/E} \times \vec{V}_{AC}, \tag{8.28}$$

which can be written as

$$\overset{AC\bullet}{\vec{V}}_{AC} = -\vec{\omega}_{AC/E} \times \vec{V}_{AC} + \vec{a}_{c/O_E/E}. \tag{8.29}$$

The accelerometer measurement $\vec{a}_{\text{meas}}$ with gravity offset is given by

$$\vec{a}_{\text{meas}} = \vec{a}_{\text{c/O}_\text{E}/\text{E}} - \vec{g}, \tag{8.30}$$

where the accelerometers are assumed to be located at the center of mass of the aircraft. Substituting (8.30) into (8.29) yields

$$\overset{\text{AC}\bullet}{\vec{V}}_{\text{AC}} = -\vec{\omega}_{\text{AC/E}} \times \vec{V}_{\text{AC}} + \vec{g} + \vec{a}_{\text{meas}}. \tag{8.31}$$

We resolve $\vec{V}_{\text{AC}}$ using the notation

$$\begin{bmatrix} U \\ V \\ W \end{bmatrix} \triangleq \vec{V}_{\text{AC}}\Big|_{\text{AC}}. \tag{8.32}$$

We resolve $\vec{a}_{\text{meas}}$ in F_{AC} using the notation

$$\begin{bmatrix} a_x \\ a_y \\ a_z \end{bmatrix} \triangleq \vec{a}_{\text{meas}}\Big|_{\text{AC}}. \tag{8.33}$$

We resolve the gravity vector $\vec{g}$ in F_{AC} using (8.6)

$$\vec{g}\Big|_{\text{AC}} = \mathcal{O}_{\text{AC/E}}\, \vec{g}\Big|_{\text{E}} = \mathcal{O}_{\text{AC/E}} \begin{bmatrix} 0 \\ 0 \\ g \end{bmatrix}, \tag{8.34}$$

where $g = 32.17\,\text{ft/s}^2$. Note that, by using the angular-velocity vector $\begin{bmatrix} P & Q & R \end{bmatrix}$, $\mathcal{O}_{\text{AC/E}}$ in (8.34) can be obtained by integrating either (8.11), (8.14), or (8.22). Alter-

natively, using (8.6), (8.34) is given by

$$\vec{g}\Big|_{\mathrm{AC}} = \begin{bmatrix} -(\sin\Theta)g \\ (\sin\Phi)(\cos\Theta)g \\ (\cos\Phi)(\cos\Theta)g \end{bmatrix}. \tag{8.35}$$

Resolving (8.31) in $\mathrm{F_{AC}}$ using (8.32), (8.33), and (8.34) yields

$$\begin{bmatrix} \dot{U} \\ \dot{V} \\ \dot{W} \end{bmatrix} = \begin{bmatrix} 0 & R & -Q \\ -R & 0 & P \\ Q & -P & 0 \end{bmatrix} \begin{bmatrix} U \\ V \\ W \end{bmatrix} + \mathcal{O}_{\mathrm{AC/E}} \begin{bmatrix} 0 \\ 0 \\ g \end{bmatrix} + \begin{bmatrix} a_x \\ a_y \\ a_z \end{bmatrix}. \tag{8.36}$$

Resolving (8.31) in $\mathrm{F_{AC}}$ using (8.32), (8.33), and (8.35) yields

$$\dot{U} = RV - QW - (\sin\Theta)g + a_x, \tag{8.37}$$

$$\dot{V} = -RU + PW + (\sin\Phi)(\cos\Theta)g + a_y, \tag{8.38}$$

$$\dot{W} = QU - PV + (\cos\Phi)(\cos\Theta)g + a_z. \tag{8.39}$$

Using the components of $\vec{V}_{\mathrm{AC}}$ resolved in $\mathrm{F_{AC}}$, the angle of attack α and sideslip β are given by

$$\alpha = \mathrm{atan2}(W, U), \tag{8.40}$$

$$\beta = \mathrm{atan2}(V, \sqrt{U^2 + W^2}). \tag{8.41}$$

Note that (8.1)–(8.41) are exact kinematic equations, and thus are applicable to all rigid aircraft.

8.3 Fault-Detection Scenarios

A continuous-time state-space model for input and state estimation can be formulated as

$$\dot{x} = f_{\mathrm{c}}\left(x, u, d\right) + \bar{D}_1 w, \tag{8.42}$$

$$y = h\left(x\right) + D_2 v, \tag{8.43}$$

where $x \in \mathbb{R}^{l_x}$ is the unknown state, $u \in \mathbb{R}^{l_u}$ is the known input, $d \in \mathbb{R}^{l_d}$ is the unknown input, $\bar{D}_1 w \in \mathbb{R}^{l_x}$ is the process noise with known covariance $\bar{V}_1 \triangleq \bar{D}_1 \bar{D}_1^{\mathrm{T}} \in \mathbb{R}^{l_x \times l_x}$, $y \in \mathbb{R}^{l_y}$ is the measured output, and $D_2 v \in \mathbb{R}^{l_v}$ is the measurement noise with known covariance $V_2 \triangleq D_2 D_2^{\mathrm{T}} \in \mathbb{R}^{l_y \times l_y}$. Table 8.1 lists the available on-board sensors for fault detection. In the following subsections, we show that a suspect sensor measurement can either be modeled as an unknown state x or an unknown input d. Comparing the estimates of x or d with the suspect sensor measurement provides the means for diagnosing sensor faults.

Sensor	**Measurements**	**Noise Standard Deviation**
Pitot Tube	U	σ_U
Rate Gyro	P, Q, R	σ_P, σ_Q, σ_R
Vertical Gyro	Θ, Φ	σ_Θ, σ_Φ
Magnetometer	Ψ	σ_Ψ
Accelerometers	a_x, a_y, a_z	σ_{a_x}, σ_{a_y}, σ_{a_z}
α-sensor	α	σ_α
β-sensor	β	σ_β

Table 8.1: On-board sensors for fault detection. The additive noise for each sensor is assumed to be white Gaussian.

8.3.1 Faulty Pitot Tube

For estimating the forward velocity U, the dynamics map f_c is given by (8.37)–(8.39), the output map h is given by (8.40)–(8.41), and x, u, and y in (8.42)–(8.43)

are given by

$$x = \begin{bmatrix} U \\ V \\ W \end{bmatrix}, \quad u = \begin{bmatrix} P & Q & R & \Phi & \Theta & a_x & a_y & a_z \end{bmatrix}^{\mathrm{T}}, \quad y = \begin{bmatrix} \alpha \\ \beta \end{bmatrix}. \tag{8.44}$$

Note that d is zero, $D_2 = \mathrm{diag}(\sigma_\alpha, \sigma_\beta)$, and $\bar{D}_1$ is given by

$$\bar{D}_1 = \begin{bmatrix} D_{PQR} & D_{\Phi\Theta} & D_{a_x a_y a_z} \end{bmatrix}, \tag{8.45}$$

where

$$D_{PQR} \triangleq \begin{bmatrix} 0 & -W & V \\ W & 0 & -U \\ -V & U & 0 \end{bmatrix} \begin{bmatrix} \sigma_P & 0 & 0 \\ 0 & \sigma_Q & 0 \\ 0 & 0 & \sigma_R \end{bmatrix},$$

$$D_{\Phi\Theta} \triangleq \begin{bmatrix} 0 & -\cos\Phi \\ -(\sin\Phi)\sin\Theta & (\cos\Phi)\cos\Theta \\ -(\cos\Phi)\sin\Theta & -(\sin\Phi)\cos\Theta \end{bmatrix} \begin{bmatrix} \sigma_\Phi & 0 \\ 0 & \sigma_\Theta \end{bmatrix},$$

$$D_{a_x a_y a_z} \triangleq \begin{bmatrix} \sigma_{a_x} & 0 & 0 \\ 0 & \sigma_{a_y} & 0 \\ 0 & 0 & \sigma_{a_z} \end{bmatrix}.$$

$D_{\Phi\Theta}$ is determined assuming $\sigma_\Phi, \sigma_\Theta$ are small and using the approximations

$$\sin w_\Phi \approx w_\Phi, \ \sin w_\Theta \approx w_\Theta,$$

$$\cos w_\Phi \approx 1, \ \cos w_\Theta \approx 1, w_\Phi w_\Theta = w_\Theta w_\Phi \approx 0,$$

where w_Φ and w_Θ are noise on the measurements of Φ and Θ, respectively.

In the absence of vertical gyro measurements (Φ, Θ), (8.36) can be used as the

dynamics f_c, where $\mathcal{O}_{\mathrm{AC/E}}$ can be estimated by either incorporating (8.11), (8.14), or (8.22) into the dynamics f_c.

8.3.2 Faulty Vertical Gyro

For estimating Euler angles (Φ, Θ, Ψ), the dynamics map f_c is given by (8.37)–(8.39) and (8.14), the output map h is given by (8.40)–(8.41), and x, u, and y in (8.42)–(8.43) are given by

$$x = \begin{bmatrix} U & V & W & \Phi & \Theta \end{bmatrix}^{\mathrm{T}}, \quad u = \begin{bmatrix} P & Q & R & a_x & a_y & a_z \end{bmatrix}^{\mathrm{T}}, \quad y = \begin{bmatrix} U & \alpha & \beta \end{bmatrix}^{\mathrm{T}}. \tag{8.46}$$

Note that d is zero, $D_2 = \mathrm{diag}(\sigma_U, \sigma_\alpha, \sigma_\beta)$, and $\bar{D}_1$ is given by

$$\bar{D}_1 = \begin{bmatrix} D_{PQR} & D_{a_x a_y a_z} & 0_{3\times 3} \\ 0_{2\times 3} & 0_{2\times 3} & -\bar{N}(\Phi,\Theta)\mathrm{diag}(\sigma_P, \sigma_Q, \sigma_R) \end{bmatrix}, \tag{8.47}$$

where

$$\bar{N}(\Phi,\Theta) \triangleq \begin{bmatrix} 1 & (\sin\Phi)\tan\Theta & (\cos\Phi)\tan\Theta \\ 0 & \cos\Phi & -\sin\Phi \end{bmatrix}.$$

8.3.3 Faulty α-sensor

For estimating angle of attack α, the dynamics map f_c is given by (8.37)–(8.39), the output map h is given by (8.41), and x, u, and y in (8.42)–(8.43) are given by

$$x = \begin{bmatrix} U \\ V \\ W \end{bmatrix}, \quad u = \begin{bmatrix} P & Q & R & \Phi & \Theta & a_x & a_y & a_z \end{bmatrix}^{\mathrm{T}}, \quad y = \begin{bmatrix} U \\ \beta \end{bmatrix}. \tag{8.48}$$

Note that d is zero, $\bar{D}_1$ is given by (8.45) and $D_2 = \text{diag}\left(\sigma_{\text{U}}, \sigma_\beta\right)$. Using the estimates $\hat{U}$, $\hat{W}$, the estimate of angle of attack $\hat{\alpha}$ is given by

$$\hat{\alpha} = \text{atan2}(\hat{W}, \hat{U}). \tag{8.49}$$

8.3.4 Faulty Accelerometer

For estimating accelerometer measurements (a_x, a_y, a_z), the dynamics map f_c is given by (8.37)–(8.39), the output map h is given by (8.40)–(8.41), and x, u, d, and y in (8.42)–(8.43) are given by

$$x = \begin{bmatrix} U \\ V \\ W \end{bmatrix}, \quad u = \begin{bmatrix} P & Q & R & \Phi & \Theta \end{bmatrix}^{\text{T}}, \quad d = \begin{bmatrix} a_x \\ a_y \\ a_z \end{bmatrix}, \quad y = \begin{bmatrix} U \\ \alpha \\ \beta \end{bmatrix}. \tag{8.50}$$

Note that $\bar{D}_1 = \begin{bmatrix} D_{PQR} & D_{\Phi\Theta} \end{bmatrix}$, and $D_2 = \text{diag}(\sigma_U, \sigma_\alpha, \sigma_\beta)$.

8.3.5 Faulty Rate Gyro

Estimation of Angular Velocity

For estimating angular velocity, the dynamics map f_c is given by (8.14), and x, d, and y in (8.42)–(8.43) are given by

$$x = \begin{bmatrix} \Phi \\ \Theta \\ \Psi \end{bmatrix}, \quad d = \begin{bmatrix} P \\ Q \\ R \end{bmatrix}, \quad y = \begin{bmatrix} \Phi \\ \Theta \\ \Psi \end{bmatrix}. \tag{8.51}$$

Note that u, w and $\bar{D}_1$ are zero in (8.14), and $D_2 = \text{diag}(\sigma_\Phi, \sigma_\Theta, \sigma_\Psi)$. Comparing the estimates of angular velocity to the actual rate-gyro measurements provides the means for assessing the health of the rate gyro.

Estimation of Rate-Gyro Noise

Consider additive noise in the angular velocity measurements $P_{\rm m}, Q_{\rm m}, R_{\rm m}$ of the form

$$P_{\rm m} = P + n_P + w_P, \tag{8.52}$$

$$Q_{\rm m} = Q + n_Q + w_Q, \tag{8.53}$$

$$R_{\rm m} = R + n_R + w_R, \tag{8.54}$$

where n_P, n_Q, n_R denote deterministic or non-white stochastic signals, and w_P, w_Q, w_R denote zero-mean white noise with known covariance $\bar{D}_{1w}$. Candidate deterministic signals include bias, drift, and harmonics. Substituting (8.52)–(8.54) into (8.14) yields

$$\begin{bmatrix} \dot{\Phi} \\ \dot{\Theta} \\ \dot{\Psi} \end{bmatrix} = N(\Phi,\Theta) \begin{bmatrix} P_{\rm m} \\ Q_{\rm m} \\ R_{\rm m} \end{bmatrix} - N(\Phi,\Theta) \begin{bmatrix} n_P \\ n_Q \\ n_R \end{bmatrix} - N(\Phi,\Theta) \begin{bmatrix} w_P \\ w_Q \\ w_R \end{bmatrix}. \tag{8.55}$$

In the case of (8.55), for estimating rate-gyro noise, x, u, d, w, y and $\bar{D}_1$ in (8.42)–(8.43) are given by

$$x = \begin{bmatrix} \Phi \\ \Theta \\ \Psi \end{bmatrix}, \; u = \begin{bmatrix} P_{\rm m} \\ Q_{\rm m} \\ R_{\rm m} \end{bmatrix}, \; d = \begin{bmatrix} n_P \\ n_Q \\ n_R \end{bmatrix}, \; y = \begin{bmatrix} \Phi \\ \Theta \\ \Psi \end{bmatrix}, \; \bar{D}_1 = -N(\Phi,\Theta)\mathrm{diag}(\sigma_P, \sigma_Q, \sigma_R), \tag{8.56}$$

and $D_2 = \mathrm{diag}(\sigma_\Phi, \sigma_\Theta, \sigma_\Psi)$. Analysis of the noise estimate provides an alternative means for assessing the health of the rate gyro.

8.4 Input and State Estimation for Nonlinear Systems

The state-space model (8.42)–(8.43) can be discretized to first order as

$$x(k) = f\left(x(k-1), u(k-1), d(k-1)\right) + D_1(k-1)w(k-1), \tag{8.57}$$

$$y(k) = h\left(x(k)\right) + D_2 v(k), \tag{8.58}$$

where k is the time step, $D_1(k) \triangleq T_{\mathrm{s}} \bar{D}_1(kT_{\mathrm{s}})$,

$$f\left(x(k), u(k), d(k)\right) = x(k) + T_{\mathrm{s}} f_{\mathrm{c}}\left(x(k), u(k), d(k)\right),$$

and T_{s} is the sampling time. $D_1(k)w(k)$ is the process noise with known covariance $V_1(k) \triangleq D_1(k)D_1(k)^{\mathrm{T}}$, and $D_2(k)v(k)$ is the measurement noise with known covariance $V_2(k) \triangleq D_2(k)D_2(k)^{\mathrm{T}}$. The goal is to estimate the unknown input $d(k)$ and the unknown state $x(k)$. To do so, we first estimate the unknown input using extended retrospective cost input estimation (ERCIE), and then estimate the unknown state using the unscented Kalman filter. Note that ERCIE is an extension of RCIE algorithm given by [72].

8.4.1 Extended Retrospective Cost Input Estimation (ERCIE)

In order to estimate the unknown input $d(k)$, we consider the forecast step

$$x_{\mathrm{fc}}(k) = f(x_{\mathrm{da}}(k-1), u(k-1), \hat{d}(k-1)), \tag{8.59}$$

$$y_{\mathrm{fc}}(k) = h(x_{\mathrm{fc}}(k)), \tag{8.60}$$

$$z(k) = y_{\mathrm{fc}}(k) - y(k), \tag{8.61}$$

where $x_{\mathrm{fc}}(k) \in \mathbb{R}^{l_x}$ is the forecast state, $\hat{d}(k) \in \mathbb{R}^{l_d}$ is the input estimate, $x_{\mathrm{da}}(k) \in \mathbb{R}^{l_x}$ is the data assimilation state, and $z(k) \in \mathbb{R}^{l_y}$ is the innovations. The goal is to

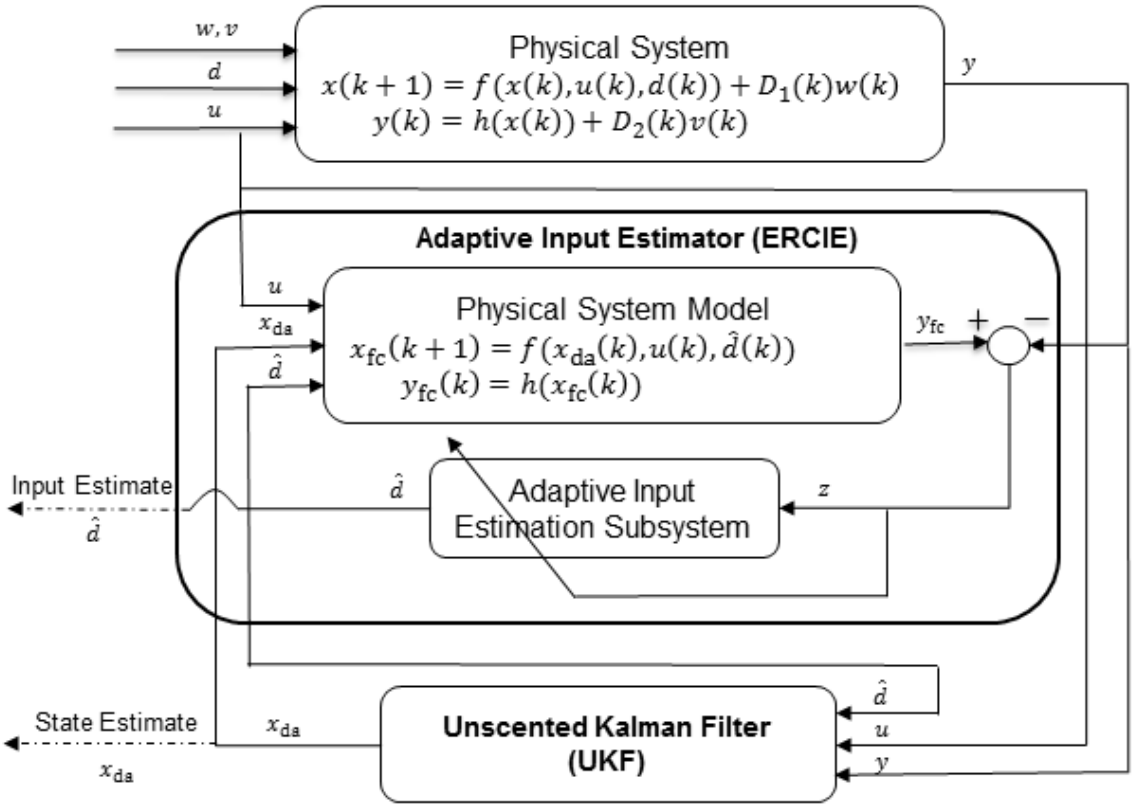

Figure 8.1: Input and state estimation architecture. ERCIE uses the innovations z to update the adaptive input estimation subsystem in order to generate the estimated input $\hat{d}$. The unscented Kalman filter uses the estimated input $\hat{d}$ in place of d to estimate the unknown state x of the physical system.

develop an adaptive input estimator that minimizes $z(k)$ by estimating $d(k)$.

We obtain the input estimate $\hat{d}(k)$ as the output of the *adaptive input-estimation subsystem* of order n_c given by

$$\hat{d}(k) = \sum_{i=1}^{n_c} P_i(k)\hat{d}(k-i) + \sum_{i=0}^{n_c} Q_i(k)z(k-i), \tag{8.62}$$

where $P_i(k) \in \mathbb{R}^{l_d \times l_d}$, $Q_i(k) \in \mathbb{R}^{l_d \times l_y}$. ERCIE minimizes $z(k)$ by updating $P_i(k)$ and $Q_i(k)$. Fig. 8.1 shows the structure of (8.57)–(5.6). The subsystem in (8.62) can be

reformulated as

$$\hat{d}(k) = \Phi(k)\theta(k), \tag{8.63}$$

where the regressor matrix $\Phi(k)$ is defined by

$$\Phi(k) \triangleq \begin{bmatrix} \hat{d}(k-1) \\ \vdots \\ \hat{d}(k-n_{\mathrm{c}}) \\ z(k) \\ \vdots \\ z(k-n_{\mathrm{c}}) \end{bmatrix}^{\mathrm{T}} \otimes I_{l_d} \in \mathbb{R}^{l_d \times l_\theta},$$

and

$$\theta(k) \triangleq \mathrm{vec} \begin{bmatrix} P_1(k) \cdots P_{n_{\mathrm{c}}}(k) \; Q_0(k) \cdots Q_{n_{\mathrm{c}}}(k) \end{bmatrix} \in \mathbb{R}^{l_\theta},$$

where $l_\theta \triangleq l_d^2 n_{\mathrm{c}} + l_d l_y (n_{\mathrm{c}}+1)$, "$\otimes$" is the Kronecker product, and "vec" is the column-stacking operator.

Define the $l_y \times l_d$ filter $G_{\mathrm{f},k}(\mathbf{q}) \triangleq D_{\mathrm{f},k}^{-1}(\mathbf{q}) N_{\mathrm{f},k}(\mathbf{q})$, where $\mathbf{q}$ is the forward shift operator, $n_{\mathrm{f}} \geq 1$ is the order of G_{f},

$$N_{\mathrm{f},k}(\mathbf{q}) \triangleq K_1(k)\mathbf{q}^{n_{\mathrm{f}}-1} + K_2(k)\mathbf{q}^{n_{\mathrm{f}}-2} + \cdots + K_{n_{\mathrm{f}}}(k), \tag{8.64}$$

$$D_{\mathrm{f},k}(\mathbf{q}) \triangleq I_{l_y}\mathbf{q}^{n_{\mathrm{f}}} + A_1(k)\mathbf{q}^{n_{\mathrm{f}}-1} + A_2(k)\mathbf{q}^{n_{\mathrm{f}}-2} + \cdots + A_{n_{\mathrm{f}}}(k), \tag{8.65}$$

and, for all $1 \leq i \leq n_{\mathrm{f}}$ and $k \geq 0$, $K_i(k) \in \mathbb{R}^{l_y \times l_d}$ and $A_i(k) \in \mathbb{R}^{l_y \times l_y}$.

Next, for all $k \geq 0$, we define the *retrospective input*

$$d_{\mathrm{rc}}(\hat{\theta}, k) \triangleq \Phi(k)\hat{\theta} \tag{8.66}$$

and the corresponding *retrospective performance variable*

$$z_{\mathrm{rc}}(\hat{\theta}, k) = z(k) + \Phi_{\mathrm{f}}(k)\hat{\theta} - \hat{d}_{\mathrm{f}}(k), \tag{8.67}$$

where

$$\Phi_{\mathrm{f}}(k) \triangleq G_{\mathrm{f},k}(\mathbf{q})\Phi(k), \quad \hat{d}_{\mathrm{f}}(k) \triangleq G_{\mathrm{f},k}(\mathbf{q})\hat{d}(k), \tag{8.68}$$

and $\hat{\theta} \in \mathbb{R}^{l_\theta}$ is determined by optimization below.

To construct G_{f}, we define the following matrices

$$A(k) \triangleq \left.\frac{\partial f}{\partial x}\right|_{x_{\mathrm{da}}(k),u(k),\hat{d}(k)}, \tag{8.69}$$

$$G(k) \triangleq \left.\frac{\partial f}{\partial d}\right|_{x_{\mathrm{da}}(k),u(k),\hat{d}(k)}, \tag{8.70}$$

$$C(k+1) \triangleq \left.\frac{\partial h}{\partial x}\right|_{x_{\mathrm{fc}}(k)}, \tag{8.71}$$

$$\bar{A}(k) \triangleq A(k)[I + K_{\mathrm{da}}(k)C(k)], \tag{8.72}$$

where K_{da} is defined by (8.98) in Section 8.4.2. $G_{\mathrm{f},k}$ in (8.67) is the FIR filter

$$G_{\mathrm{f},k}(\mathbf{q}) = \sum_{i=1}^{n_{\mathrm{f}}} H_i(k)\frac{1}{\mathbf{q}^i}, \tag{8.73}$$

where, for all $i \geq 1$,

$$H_i(k) \triangleq \begin{cases} C(k)G(k-1), & i = 1, \\ C(k)\left(\prod_{j=1}^{i-1} \bar{A}(k-j)\right) G(k-i), & i \geq 2. \end{cases} \tag{8.74}$$

For $k \geq 1$, we define the retrospective cost function

$$J(\hat{\theta}, k) \triangleq \sum_{i=0}^{k} \lambda^{k-i} \left(z_{\mathrm{rc}}(\hat{\theta}, i)^{\mathrm{T}} R_z z_{\mathrm{rc}}(\hat{\theta}, i) + [\Phi(i)\hat{\theta}]^{\mathrm{T}} R_d \Phi(i)\hat{\theta} \right) + \lambda^k [\hat{\theta} - \theta(0)]^{\mathrm{T}} R_\theta [\hat{\theta} - \theta(0)], \tag{8.75}$$

where $R_z \in \mathbb{R}^{l_y \times l_y}$, $R_d \in \mathbb{R}^{l_d \times l_d}$, and $R_\theta \in \mathbb{R}^{l_\theta \times l_\theta}$ are positive definite, and $\lambda \in (0, 1]$ is the forgetting factor. Let $P(0) = R_\theta^{-1}$ and $\theta(0) = \theta_0$. Then, for all $k \geq 1$, the cumulative cost function (8.75) has the unique global minimizer $\theta(k)$ given by the RLS update

$$\theta(k) = \theta(k-1) - P(k-1)\tilde{\Phi}(k)^{\mathrm{T}} \Gamma(k)[\tilde{\Phi}(k)\theta(k-1) + \tilde{z}(k)], \tag{8.76}$$

$$P(k) = \frac{1}{\lambda}[P(k-1) - P(k-1)\tilde{\Phi}(k)^{\mathrm{T}} \Gamma(k)\tilde{\Phi}(k)P(k-1)], \tag{8.77}$$

where

$$\tilde{\Phi}(k) \triangleq \begin{bmatrix} \Phi_{\mathrm{f}}(k) \\ \Phi(k) \end{bmatrix} \in \mathbb{R}^{(l_y + l_d) \times l_\theta}, \tag{8.78}$$

$$\tilde{R}(k) \triangleq \begin{bmatrix} R_z(k) & 0 \\ 0 & R_d(k) \end{bmatrix} \in \mathbb{R}^{(l_y + l_d) \times (l_y + l_d)}, \tag{8.79}$$

$$\tilde{z}(k) \triangleq \begin{bmatrix} z(k) - \hat{d}_{\mathrm{f}}(k) \\ 0 \end{bmatrix} \in \mathbb{R}^{l_y + l_d}, \tag{8.80}$$

$$\Gamma(k) \triangleq [\lambda \tilde{R}(k)^{-1} + \tilde{\Phi}(k)P(k-1)\tilde{\Phi}(k)^{\mathrm{T}}]^{-1}. \tag{8.81}$$

8.4.2 Unscented Kalman Filter for State Estimation (UKF)

Let S be a set of sigma points consisting of $2l_x + 1$ vectors and their associated weights

$$S = \{(x_i, W_i) : i = 0, \ldots, 2l_x\}. \tag{8.82}$$

To provide an unbiased state estimate, the weights W_i satisfy

$$\sum_{i=0}^{2l_x} W_i = 1. \tag{8.83}$$

Define

$$\lambda \triangleq \alpha^2(l_x + \mu) - l_x, \tag{8.84}$$

$$c \triangleq l_x + \lambda, \tag{8.85}$$

where $\alpha \in \mathbb{R}$ and $\mu \in \mathbb{R}$ are tunable. The sigma points and their associated weights are chosen as

$$x_0(k-1) = x_{\mathrm{da}}(k-1), \tag{8.86}$$

$$x_i(k-1) = x_{\mathrm{da}}(k-1) + (\sqrt{cP_{\mathrm{da}}(k-1)})_i, \quad i = 1, \ldots, l_x, \tag{8.87}$$

$$x_{i+l_x}(k-1) = x_{\mathrm{da}}(k-1) - (\sqrt{cP_{\mathrm{da}}(k-1)})_i, \quad i = 1, \ldots, l_x, \tag{8.88}$$

$$W_0 = \frac{\lambda}{c}, \tag{8.89}$$

$$W_i = \frac{1}{2c}, \; i = 1, \ldots, 2l_x. \tag{8.90}$$

where $x_{\mathrm{da}}(k) \in \mathbb{R}^{l_x}$ is the data assimilation state. $P_{\mathrm{da}}(k) \in \mathbb{R}^{l_x \times l_x}$ is the data assimilation error covariance, and $(\sqrt{cP_{\mathrm{da}}(k-1)})_i$ is the i^{th} column of the positive semi-definite square root of $cP_{\mathrm{da}}(k-1)$.

Each sigma point is transformed through (8.59) as

$$x_{\mathrm{fc},i}(k) = \ f(x_i(k-1), u(k-1), \hat{d}(k-1)). \tag{8.91}$$

We use the transformed points obtained from (8.91) to compute their mean and covariance as

$$\bar{x}_{\mathrm{fc}}(k) = \sum_{i=0}^{2l_x} W_i x_{\mathrm{fc},i}(k), \tag{8.92}$$

$$P_{\mathrm{fc}}(k) = \sum_{i=0}^{2l_x} W_i \tilde{x}_{\mathrm{fc},i}(k)(\tilde{x}_{\mathrm{fc},i}(k))^{\mathrm{T}} + (1+\beta-\alpha^2)\tilde{x}_{\mathrm{fc},0}(k)(\tilde{x}_{\mathrm{fc},0}(k))^{\mathrm{T}} + V_1(k-1) + V_{\hat{d}}(k-1), \tag{8.93}$$

where $\tilde{x}_{\mathrm{fc},i}(k) \stackrel{\triangle}{=} x_{\mathrm{fc},i}(k) - \bar{x}_{\mathrm{fc}}(k)$, $V_{\hat{d}}(k)$ is the covariance of $\hat{d}(k)$, and $\beta \in \mathbb{R}$ is tunable. We then transform sigma points through the observation model

$$y_{\mathrm{fc},i}(k) = \ h(x_i(k-1)). \tag{8.94}$$

and calculate their mean and covariance as

$$\bar{y}_{\mathrm{fc}}(k) = \sum_{i=0}^{2l_x} W_i y_{\mathrm{fc},i}(k), \tag{8.95}$$

$$P_{y_{\mathrm{fc}}}(k) = \sum_{i=0}^{2l_x} W_i \tilde{y}_{\mathrm{fc},i}(k)(\tilde{y}_{\mathrm{fc},i}(k))^{\mathrm{T}} + (1+\beta-\alpha^2)\tilde{y}_{\mathrm{fc},0}(k)(\tilde{y}_{\mathrm{fc},0}(k))^{\mathrm{T}} + V_2(k), \tag{8.96}$$

where $\tilde{y}_{\mathrm{fc},i}(k) \stackrel{\triangle}{=} y_{\mathrm{fc},i}(k) - \bar{y}_{\mathrm{fc}}(k)$. The cross covariance between the two errors $\tilde{x}_{\mathrm{fc},i}(k)$

and $\tilde{y}_{\mathrm{fc},i}(k)$ is

$$P_{\tilde{x}_{\mathrm{fc}}\tilde{y}_{\mathrm{fc}}}(k) = \sum_{i=0}^{2l_x} W_i \tilde{x}_{\mathrm{fc},i}(k)(\tilde{y}_{\mathrm{fc},i}(k))^{\mathrm{T}} + (1+\beta-\alpha^2)\tilde{x}_{\mathrm{fc},0}(k)(\tilde{y}_{\mathrm{fc},0}(k))^{\mathrm{T}}. \tag{8.97}$$

The data assimilation step is given by

$$K_{\mathrm{da}}(k) = P_{\tilde{x}_{\mathrm{fc}}\tilde{y}_{\mathrm{fc}}}(k)P_{y_{\mathrm{fc}}}^{-1}(k), \tag{8.98}$$

$$P_{\mathrm{da}}(k) = P_{\mathrm{fc}}(k) - K_{\mathrm{da}}(k)P_{\tilde{x}_{\mathrm{fc}}\tilde{y}_{\mathrm{fc}}}^{\mathrm{T}}(k), \tag{8.99}$$

$$x_{\mathrm{da}}(k) = x_{\mathrm{fc}}(k) + K_{\mathrm{da}}(k)\left[y(k) - \bar{y}_{\mathrm{fc}}(k)\right], \tag{8.100}$$

where $K_{\mathrm{da}}(k) \in \mathbb{R}^{l_x \times l_y}$ is the state estimator gain.

8.5 Fault Detection Setup

The formulation in Section 8.3 is applicable to all rigid aircraft. In this chapter, we use the NASA Generic Transport Model (GTM) to illustrate sensor fault detection. GTM is a high-fidelity six-degree-of-freedom nonlinear aircraft model with aerodynamic lookup tables [96–99].

8.5.1 Types of Sensor Faults

We consider the following types of sensor faults:

- *Bias*. The sensor measurement has a constant offset from the true measurement.
- *Drift*. The sensor measurement has a constant-slope deviation from the true measurement.
- *Deadzone*. The sensor reads zero within a specific range.
- *Stuck*. The sensor reading is fixed.

8.5.2 Procedure for Sensor Fault Detection

For sensor fault detection using input and state estimation, rich sensor signals are needed. This can be achieved either by exciting the dynamics of the aircraft using its control surfaces or it can arise naturally from the atmosphere, e.g., wind gusts. For this chapter, the dynamics of the aircraft are excited using a saturated harmonic elevator input.

For detecting a fault in one of the sensors listed in Table 8.1, we assume that the remaining sensors are functional. We then define the *true residual*

$$e_{\text{true}}(k) \triangleq \sqrt{\sum_{i=k}^{k+k_{\text{w}}} [s(i) - \hat{s}(i)]^2} \tag{8.101}$$

and the *sensor residual*

$$e_{\text{sens}}(k) \triangleq \sqrt{\sum_{i=k}^{k+k_{\text{w}}} [s_{\text{sens}}(i) - \hat{s}(i)]^2}, \tag{8.102}$$

where s is the true value of the signal that the sensor measures, $\hat{s}$ is the estimate of s, s_{sens} is the sensor measurement of s, and k_{w} is the data-window size. Note that, depending on the formulation in Section 8.3, $\hat{s}$ is either a state estimate or an input estimate given by the algorithm in Section 8.4. As shown in Section 8.6, by examining the sensor residual, sensor faults can be detected. For each numerical example, $k_{\text{w}} = 1000$ data points, and $x_{\text{da}}(0) = 0.9x(0)$.

8.6 GTM Examples

We set the sampling time $T_{\text{s}} = 0.01\,\text{sec}$ and consider a scenario where GTM is initially trimmed for level flight at an altitude of 8000 ft. We excite the aircraft dynamics using the elevator deflection $\delta e(k) = \text{sat}_2\,[4\,\sin(60kT_{\text{s}} + 45)]$ deg, which is

a saturated sinusoid with amplitude 4 deg, maximum deflection of ±2 deg, and a period of 6 sec. The ambient wind is constant with magnitude of 16.88 ft/sec.

To emulate sensor noise, we add zero-mean white noise to all of the sensor measurements with standard deviations $\sigma_{a_x} = \sigma_{a_y} = \sigma_{a_z} = 0.01g$, $\sigma_P = \sigma_Q = \sigma_R = 0.01$ rad/sec, $\sigma_\Phi = \sigma_\Theta = \sigma_\Psi = 0.01$ rad, $\sigma_\alpha = \sigma_\beta = 0.01$ rad, and $\sigma_U = 0.1$ ft/sec. Unless stated otherwise, the noise level is fixed for all the examples in this section.

To show the fault and noise level, we plot the true measurement and sensor measurement together. We also present the true residual to show the accuracy of the estimates. Note that in practical application, the true measurement and thus the true residual are not available. However, the sensor residual can be used in practice for fault detection.

8.6.1 Fault Detection for Pitot-Tube Failure

In the following cases, the pitot tube fails by becoming stuck at the constant value of 160 ft/s, beginning at 100 sec. Fig. 8.2 shows that the true residual decreases to 1 ft/sec, indicating that UKF is operating correctly. However, the sensor residual jumps after the sensor fails.

Next, to see the effect of accelerometer bias, we consider the case with accelerometer bias $b_{a_x} = b_{a_y} = b_{a_z} = 0.01g$. Fig. 8.3 shows that the estimated pitot-tube measurement drifts due to the biased accelerometers. In order to deal with these biases, the dynamics in (8.42) are augmented as

$$\dot{x} = f_{\mathrm{c}}(x, u, d) + \hat{b} + \bar{D}_1 w, \quad \dot{\hat{b}} = 0, \tag{8.103}$$

where $\hat{b} \in \mathbb{R}^3$ is the estimated bias in the accelerometers. Fig. 8.4 shows that, with the augmented states, the true residual is less than 2 ft/s, thus indicating no drift in the estimate of U. Consequently, $\hat{b}$ converges to the accelerometer bias as shown in Fig. 8.5.

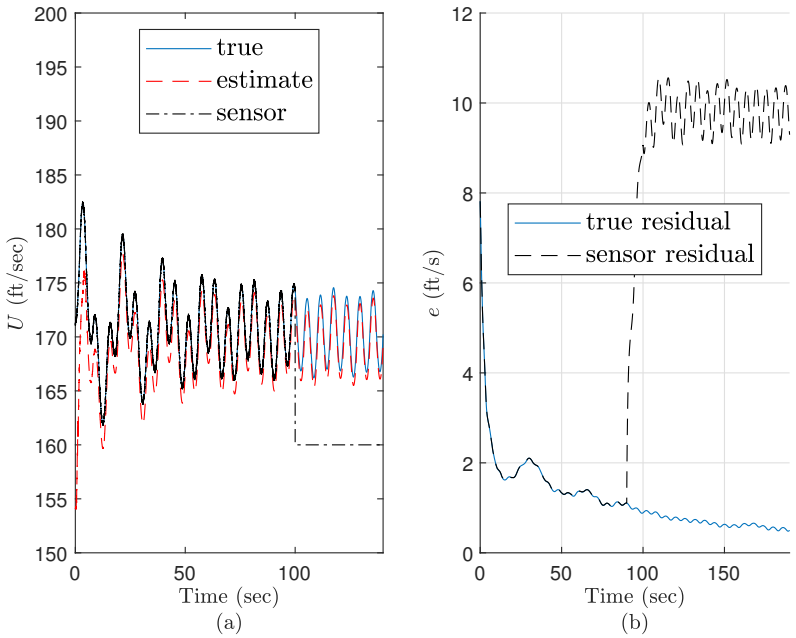

Figure 8.2: Stuck pitot tube. (a) At 100 sec, the sensor measurement is stuck at 160 ft/sec. (b) The sensor residual jumps to a mean value of 9.5 ft/sec indicating pitot-tube failure.

8.6.2 Fault Detection for Vertical-Gyro Failure

We consider cases where the vertical gyro has either a bias, deadzone, or drift beginning at 100 sec. Fig. 8.6 shows the estimate of Φ and Θ. Figs. 8.7a and 8.8a show cases where Φ and Θ have biases of 2 deg. Note that the sensor residuals have offsets due to these biases. Next, we consider the deadzone case where the Φ-sensor reads zero within ± 2 deg. Fig. 8.7b shows that the sensor residual has an offset due to the deadzone. Finally, Fig. 8.8b shows a case where the measurement of Θ drifts with a slope of 0.01 deg/sec. Note that the sensor residual also drifts from the true residual.

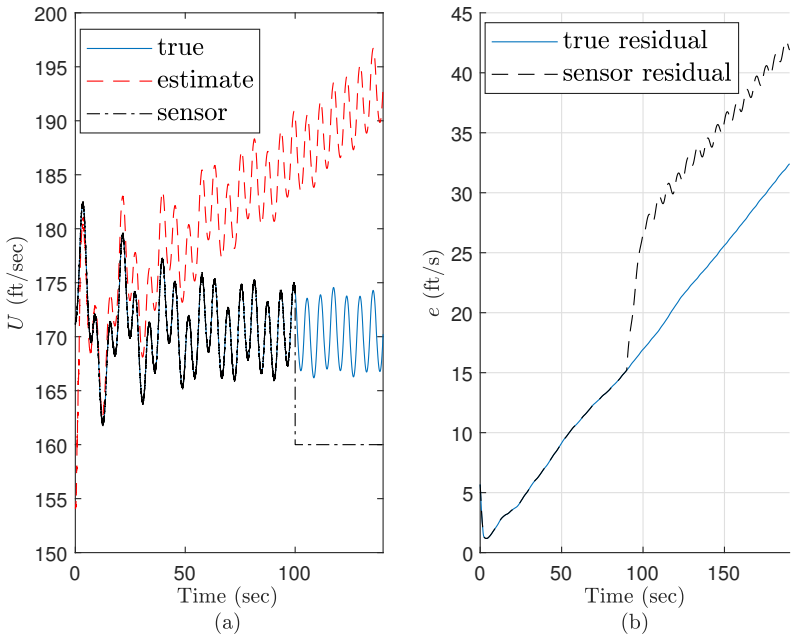

Figure 8.3: Estimation of U with biased accelerometers. (a) The estimate of U drifts from the true measurement. Beginning at 100 sec, the sensor measurement is stuck at 160 ft/sec. (b) The true and sensor residuals are both increasing, and therefore it is not possible to detect the sensor fault. This shortcoming is overcome in Fig. 8.4.

8.6.3 Fault Detection for α-sensor Failure

We now present cases where the α-sensor has either a bias or deadzone beginning at $t = 100$ sec. First, we consider the case where the α-sensor has a bias of 4 deg. Fig. 8.9 shows that the true residual is less than 0.6 deg, and the sensor residual jumps to 3.5 deg due to the bias. Next, we consider the deadzone case where the α-sensor reads zero within ± 2 deg. Fig. 8.10 shows that the sensor residual has an offset due to the deadzone.

8.6.4 Fault Detection for Accelerometer Failure

For accelerometer fault detection, we use ERCIE to estimate acceleration. Specifically, we estimate a_x and a_z separately, that is, when a_x is estimated, (a_y, a_z) are

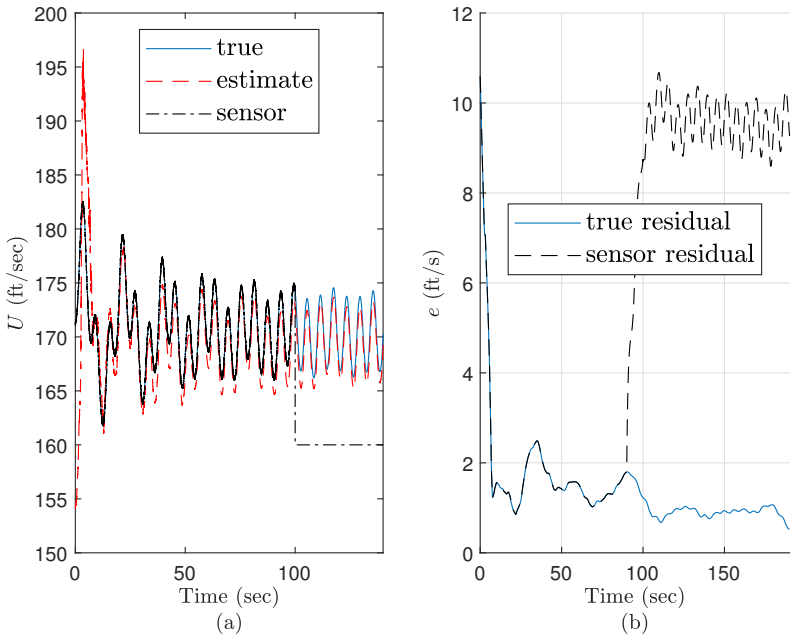

Figure 8.4: Estimation of U with augmented bias states. (a) The estimate of U indicates no drift. Beginning at 100 sec, the sensor measurement is stuck at 160 ft/sec. (b) The true residual is less than 2 ft/sec, whereas the sensor residual has an offset due to the stuck fault.

assumed to be functional, whereas, when a_z is estimated, (a_x, a_y) are assumed to be functional. For ERCIE, we choose $V_{\hat{d}} = 10^{-4} I_{3\times 3}$, $n_{\mathrm{c}} = 2$, $n_{\mathrm{f}} = 6$, $\lambda = 1$, $R_\theta = 10^{-8} I_{l_\theta}$, and $R_z = I_{l_y}$. For estimating a_x, $R_d = 10^{-2}$, and for estimating a_z, $R_d = 10^{-4}$.

Next, we consider cases where the accelerometer has either a bias or drift beginning at 100 sec. Fig. 8.11 shows that ERCIE is able to estimate a_x and a_z. Figs. 8.12a and 8.13a show cases where a_x and a_z have biases of $0.05g$ and $0.1g$, respectively. Note that the sensor residuals have offsets due to these biases. Figs. 8.12b and 8.13b show cases where the measurements of a_x and a_z drift with a slope of 0.001 g/sec. Note that the sensor residuals also drift from the respective true residuals.

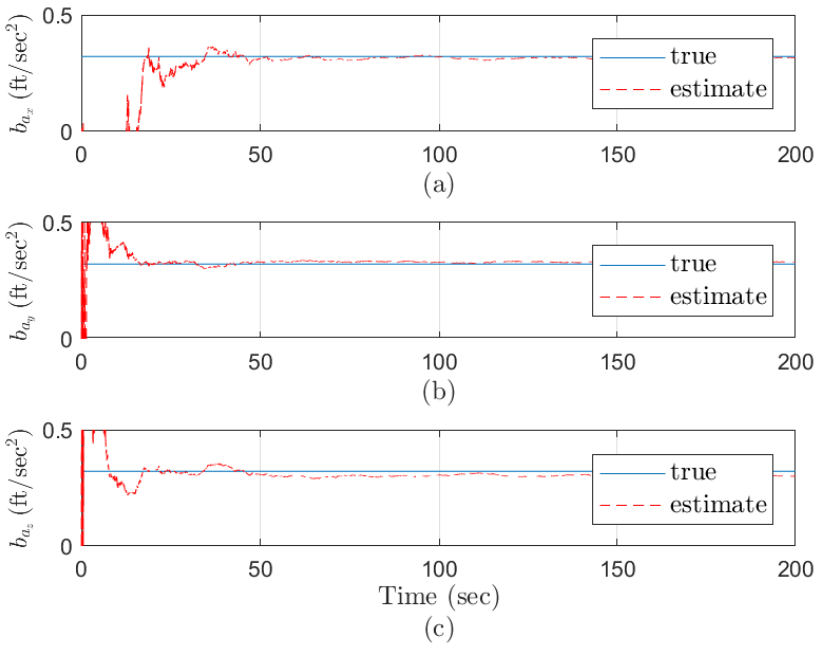

Figure 8.5: Estimate of accelerometer bias. (a) b_{a_x} estimate. (b) b_{a_y} estimate. (c) b_{a_z} estimate.

8.6.5 Fault Detection for Rate-Gyro Failure

An alternative method to examining the sensor-residual for detecting a sensor fault, is to directly estimate the noise in the sensor measurement. In this subsection, we estimate the noise in rate-gyros measurements.

For all of the examples in this subsection, we choose the standard deviation of w_P, w_Q, w_R in (8.52)–(8.54) to be 1 deg/sec. For ERCIE, we choose $V_{\hat{d}} = 10^{-6} I_{3\times 3}$, $n_{\rm c} = 6$, $n_{\rm f} = 36$, $\lambda = 1$, $R_\theta = 10^{-2} I_{l_\theta}$, $R_d = 0$, and $R_z = I_{l_y}$. We first consider cases where the Euler-angle measurements (Φ, Θ, Ψ) have no noise, and choose $V_2 = 10^{-4} I_{3\times 3}$.

Fig. 8.14 shows the case where the rate-gyro measurements have bias. The magnitudes of the bias are $2, -4$ and 4 deg/sec in P, Q, and R measurements, respectively. The Root-Mean-Squared-Error (RMSE) of the bias estimates after $t = 5$ sec in P, Q, and R measurements are $0.11, 0.21$ and 0.19 deg/sec, respectively.

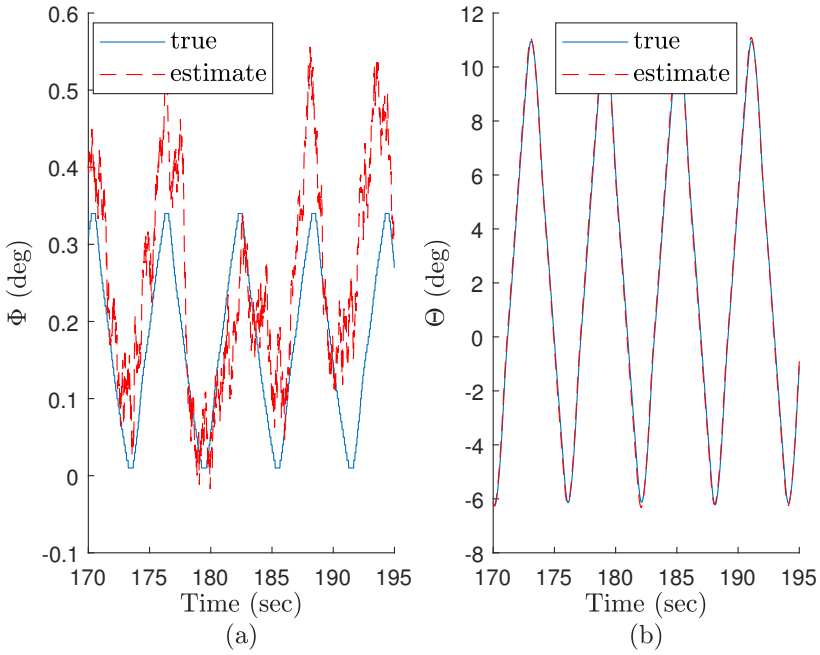

Figure 8.6: Estimation of Euler angles Φ and Θ. (a) Estimate of Φ. (b) Estimate of Θ.

Fig. 8.15 shows the case where the rate-gyro measurements have both bias and drift. The bias magnitudes are the same as in Fig. 8.14. The drift begins at $t = 20\,\text{sec}$ with a slope of 0.1 and $-0.1\,\text{deg/sec}^2$ in Q and R measurements, respectively. The RMSE of the rate-gyro noise estimates after $t = 5\,\text{sec}$ in P, Q, and R measurements are $0.61, 0.26$ and 0.26 deg/sec, respectively.

Fig. 8.16 shows the case where the noise in rate-gyro measurements is a random walk. At each time step k, the random walk is modeled as an increase or decrease in the noise magnitude by $0.1\,\text{deg/sec}$ with equal probabilities. The RMSE of the random walk noise estimates after $t = 5\,\text{sec}$ in P, Q, and R measurements are $1.0, 1.2$ and 0.8 deg/sec, respectively.

We now consider the case where the Euler angle-measurements (Φ, Θ, Ψ) are corrupted by white noise with standard deviation $0.5\,\text{deg/sec}$ and hence $V_2 = 0.0045 I_{3\times 3}$. Fig. 8.17 shows the case where the rate-gyro measurements have bias. The magni-

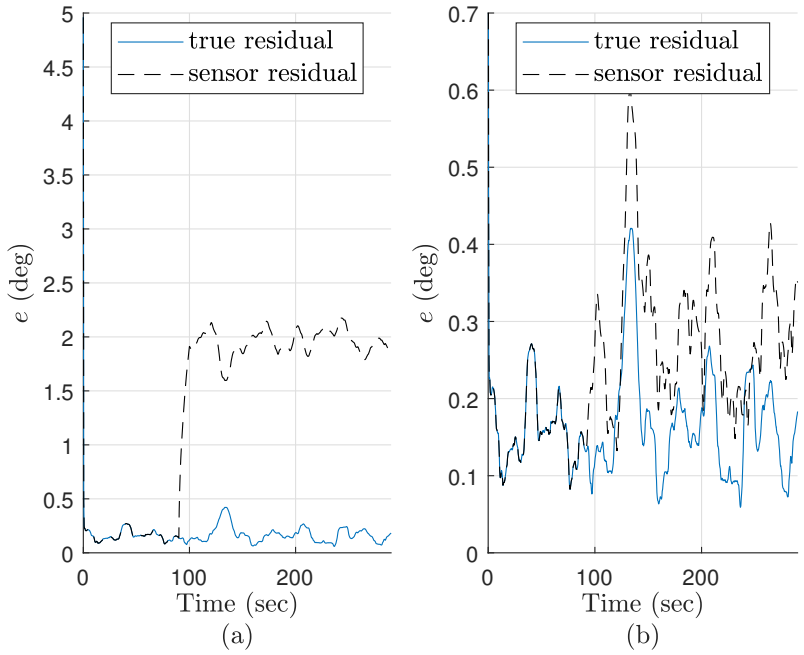

Figure 8.7: Φ-sensor. (a) The measurement of Φ is subject to a bias. Note that the sensor residual jumps at 100 sec when the bias begins. (b) Beginning at 100 sec, the Φ-sensor reads zero within ±2 deg. Note that the sensor residual indicates an offset due to the deadzone.

tudes of the bias are the same as in Fig. 8.14. The RMSE of the bias estimates after $t = 5\,\text{sec}$ in P, Q, and R measurements are $0.24, 0.40$ and 0.40 deg/sec, respectively.

8.7 Experimental Result: Estimation of Angular Velocity of a Maneuvering Vehicle

In the laboratory setup, we estimate the angular velocity of a quadrotor resolved in $\mathrm{F_{AC}}$ using the formulation in Section 8.3.8.3.5.8.3.5. The attitude (Φ, Θ, Ψ) of the vehicle is obtained using a Vicon system and recorded for post-flight data analysis. To compare the estimated angular velocity with the measured angular velocity, data from the vehicle's rate-gyro is recorded and time-stamped.

We discretize (8.42) using (8.57) with $T_\text{s} = 0.01\,\text{s}$, which is the sample rate of the

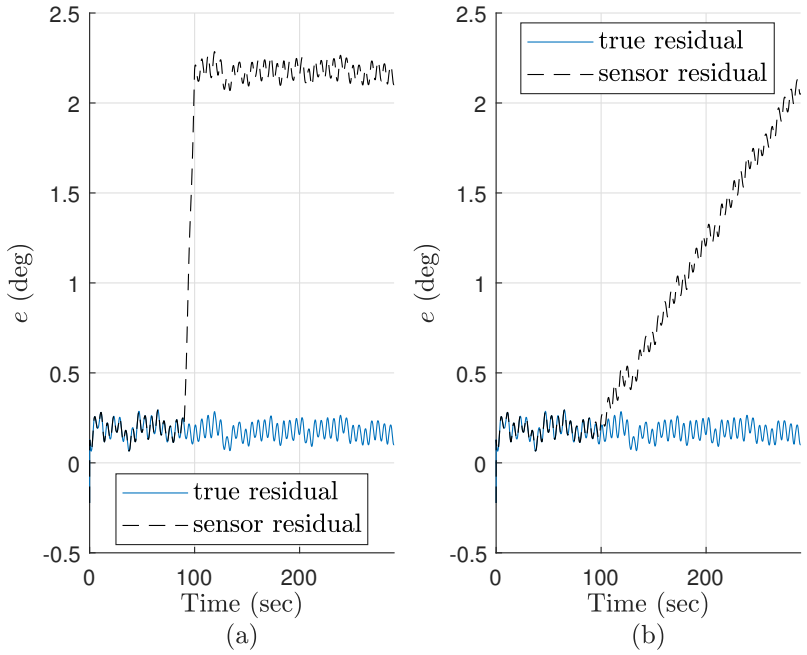

Figure 8.8: Θ-sensor. (a) The measurement of Θ is subject to a bias. Note that the sensor residual jumps at 100 sec when the bias begins. (b) The measurement of Θ is subject to a drift. Note that the sensor residual begins to increase at 100 sec when the drift begins.

recorded data. We choose $V_{\hat{d}} = 10^{-4} I_{3\times 3}$, $V_2 = 10^{-2} I_{3\times 3}$, $n_{\mathrm{c}} = 6$, $n_{\mathrm{f}} = 36$, $\lambda = 1$, $R_\theta = 10^{-2} I_{l_\theta}$, $R_d = 10^{-4} I_{l_d}$, and $R_z = I_{l_y}$.

Fig. 8.18 shows the accuracy of the ERCIE estimate of the angular velocity of the quadrotor using the attitude measurement obtained from the Vicon system.

8.8 Conclusion

This chapter showed that sensor fault diagnosis for aircraft is feasible using either state estimation alone or state estimation in conjunction with input estimation. Since the aircraft kinematics are nonlinear, the unscented Kalman filter (UKF) was used for sensor fault diagnosis in cases where the sensor measurement is modeled as an unknown state variable. In cases where the sensor measurement is modeled as an unknown input, extended retrospective cost input estimation (ERCIE) was used in

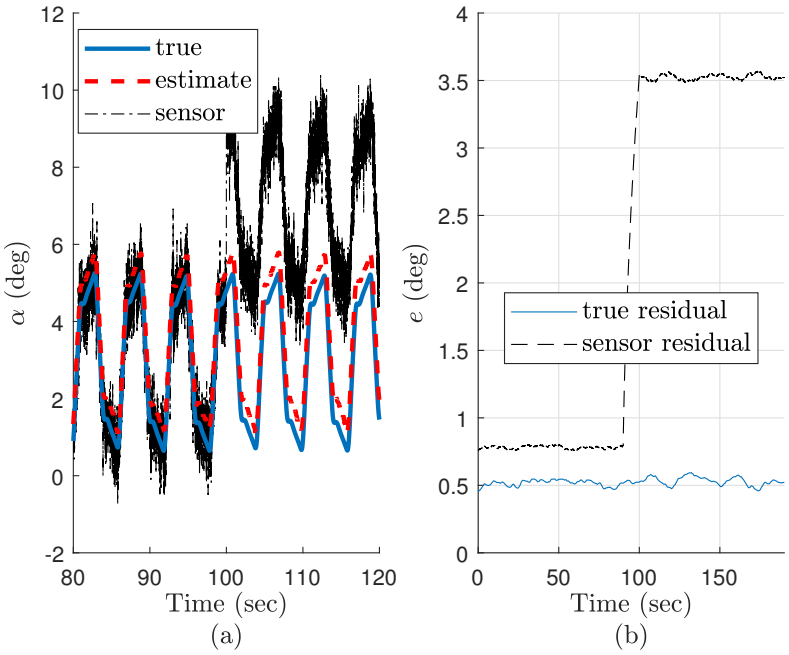

Figure 8.9: α-sensor with a bias. (a) Beginning at 100 sec, the α-sensor has a bias of 4 deg. (b) The sensor residual indicates an offset due to the bias.

conjunction with UKF to provide a combined input and state estimation technique for sensor fault diagnosis for nonlinear systems.

Five fault-detection scenarios, in particular, faulty pitot tube, vertical gyros, angle-of-attack sensor, accelerometers, and rate gyros were investigated. We used UKF for pitot tube, vertical gyro, and angle-of-attack sensor fault detection, and UKF/ERCIE for rate gyros and accelerometer fault detection. In order to illustrate sensor fault detection, we used the NASA Generic Transport Model and presented cases for detecting stuck, bias, drift, and deadzone sensor faults. For all cases, we showed that the sensor residual can be used to detect sensor faults. Furthermore, for diagnosing rate gyros, we demonstrated the method on laboratory data, where camera measurements were used to estimate the angular velocity of a quadrotor with validation based on onboard rate-gyros.

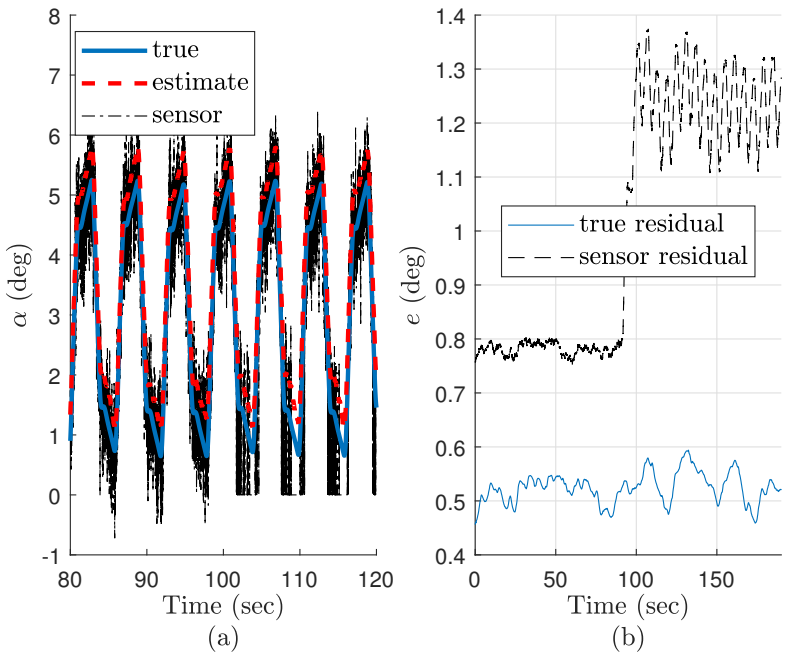

Figure 8.10: α-sensor with a deadzone. (a) Beginning at 100 sec, the α-sensor reads zero within ± 2 deg. (b) The sensor residual indicates an offset due to the deadzone.

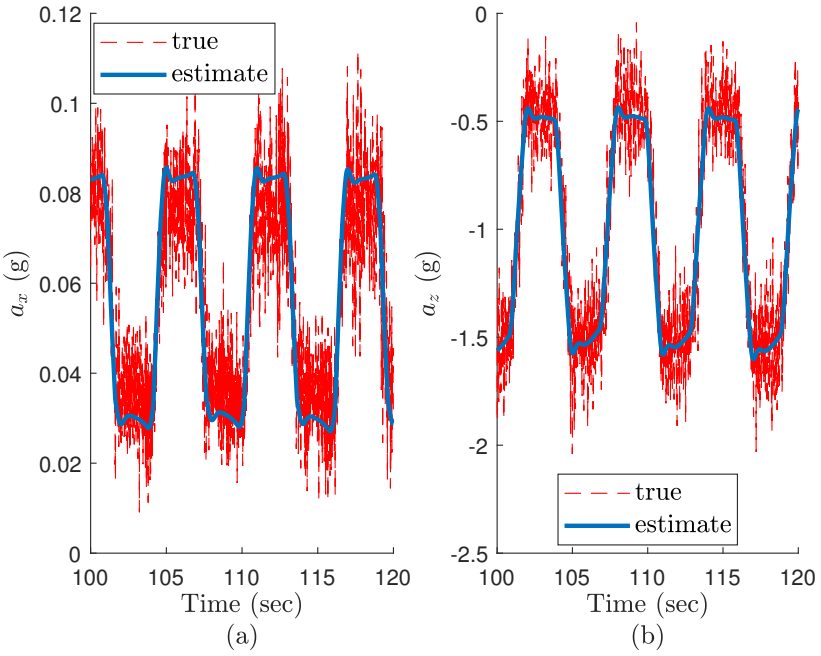

Figure 8.11: Acceleration estimation using ERCIE. Note that, ERCIE is able to estimate a_x and a_z. (a) Estimate of a_x. (b) Estimate of a_z.

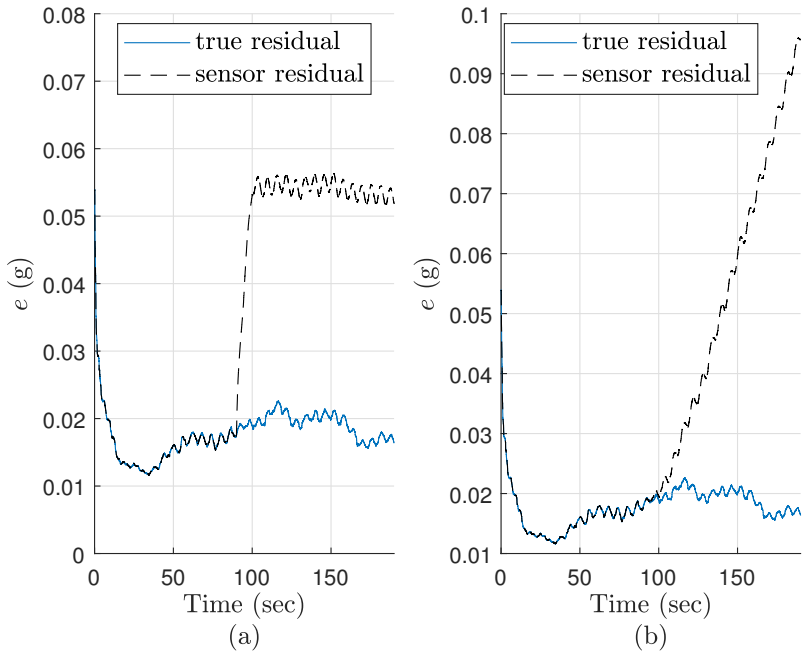

Figure 8.12: a_x-sensor. (a) The measurement of a_x is subject to a bias. Note that the sensor residual jumps at 100 sec when the bias begins. (b) The measurement of a_x is subject to a drift. Note that the sensor residual begins to increase at 100 sec when the drift begins.

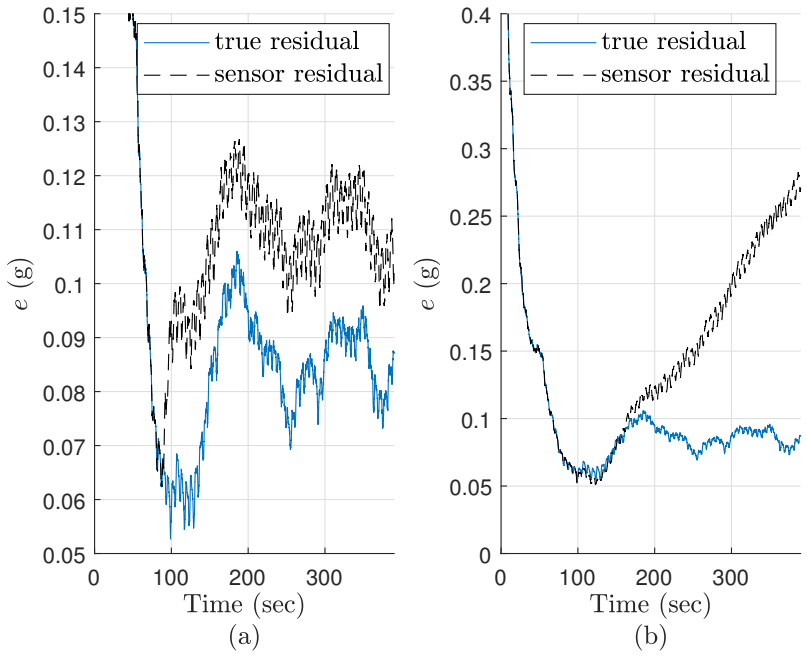

Figure 8.13: a_z-sensor. (a) The measurement of a_z is subject to a bias. Note that the sensor residual jumps at 100 sec when the bias begins. (b) The measurement of a_z is subject to a drift. Note that the sensor residual begins to increase at 100 sec when the drift begins.

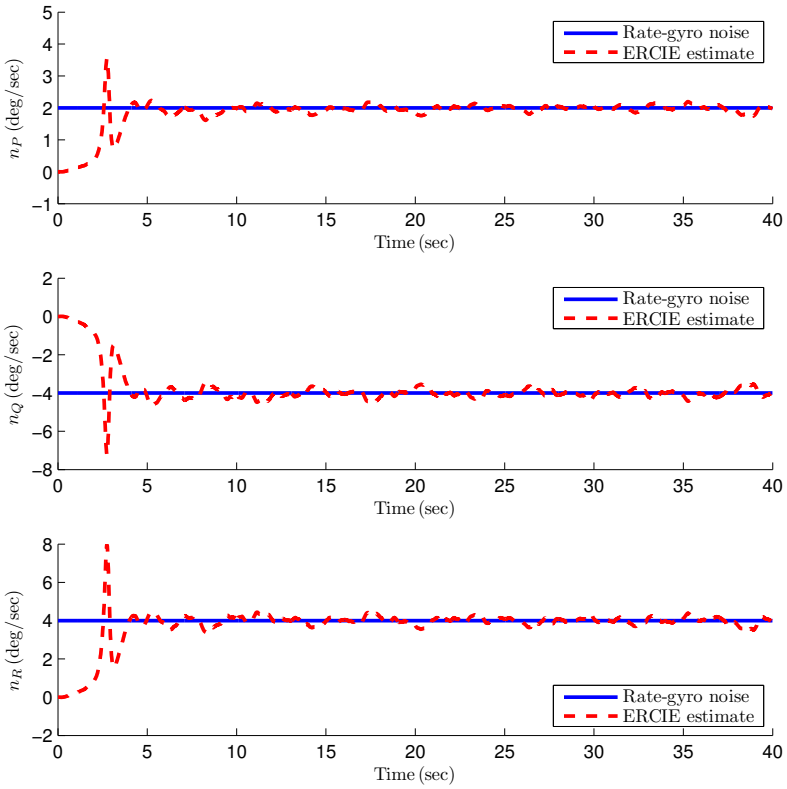

Figure 8.14: Estimation of bias. The RMSE of the bias estimates after $t = 5\,\text{sec}$ in P, Q, and R measurements are $0.11, 0.21$ and 0.19 deg/sec, respectively.

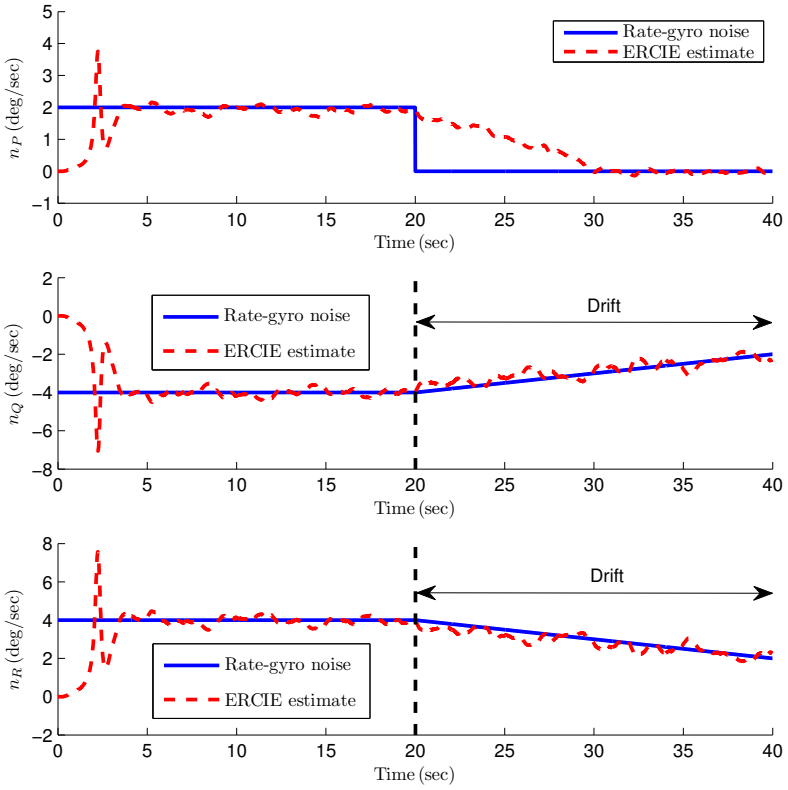

Figure 8.15: Estimation of bias and drift. The drift begins at $t = 20\,\text{sec}$ with a slope of 0.1 and $-0.1\,\text{deg/sec}^2$ in Q and R measurements, respectively. The RMSE of the rate-gyro noise estimates after $t = 5\,\text{sec}$ in P, Q, and R measurements are $0.61, 0.26$ and 0.26 deg/sec, respectively.

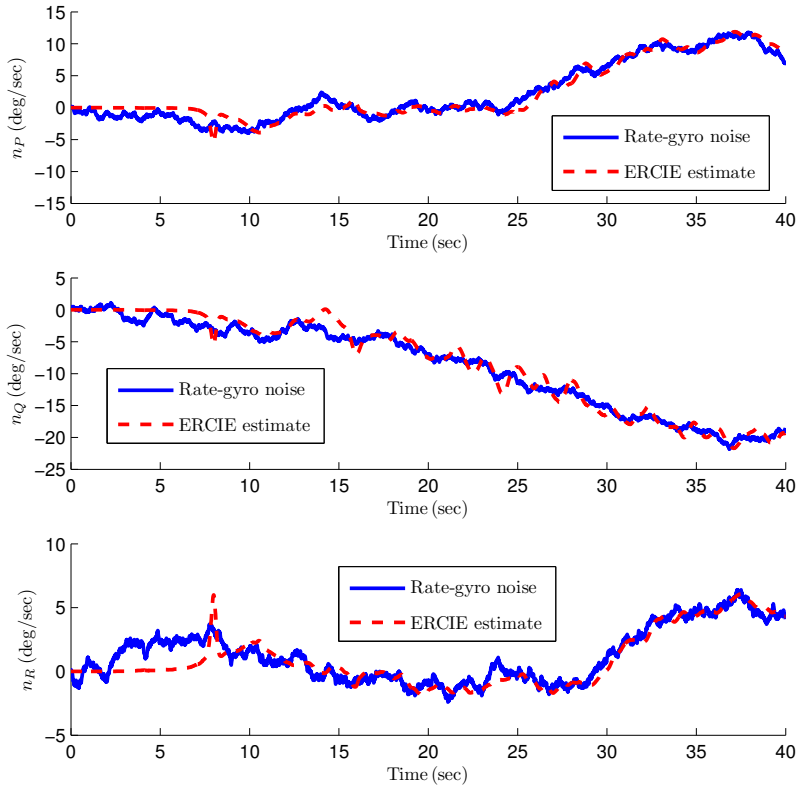

Figure 8.16: Estimation of random walk in rate-gyro measurements. The RMSE of the noise estimates after $t = 5\,\text{sec}$ in P, Q, and R measurements are $1.0, 1.2$ and 0.81 deg/sec, respectively.

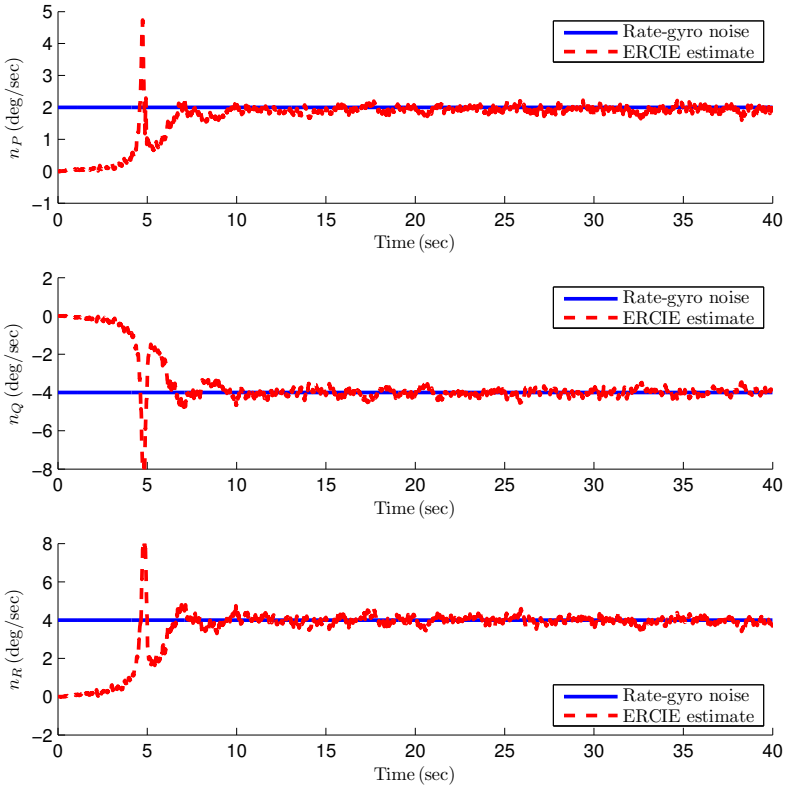

Figure 8.17: Estimation of bias in rate-gyro measurements using noisy Euler-angle measurements. The magnitudes of the bias are the same as in Fig. 8.14. The RMSE of the bias estimates after $t = 5\,\text{sec}$ in P, Q, and R measurements are $0.24, 0.40$ and 0.40 deg/sec, respectively.

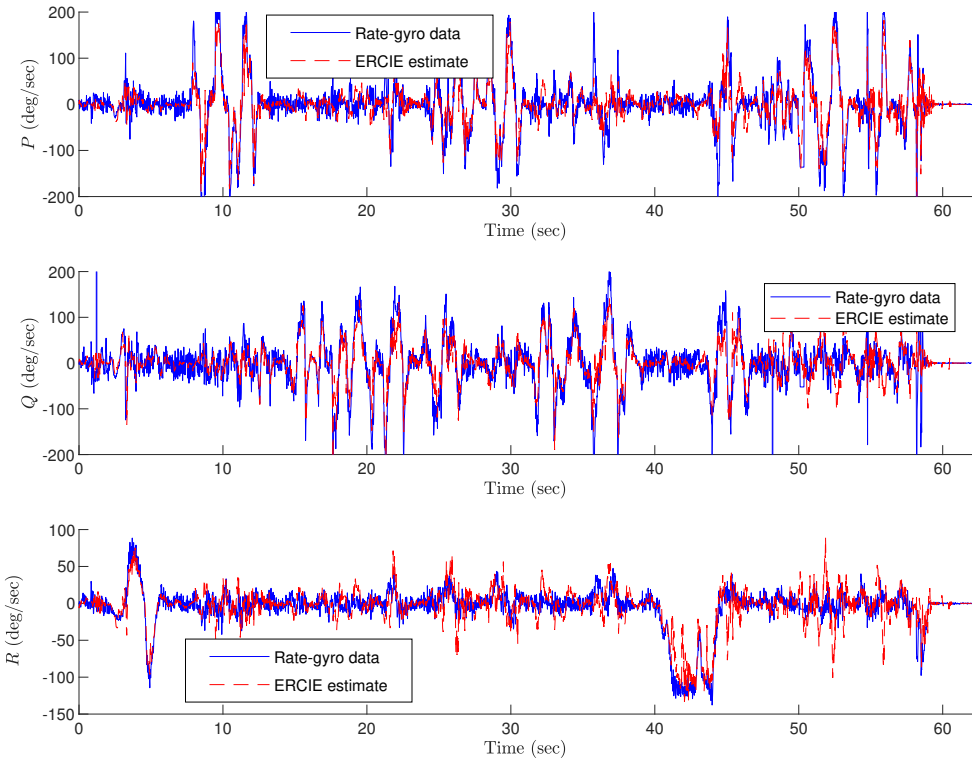

Figure 8.18: Estimation of the angular velocity of the quadrotor resolved in $\mathrm{F_{AC}}$ using attitude measurements. ERCIE estimates are compared with the vehicle's rate-gyro measurements.

CHAPTER 9

Conclusions and Future Work

9.1 Conclusions

Using the generalized inverse of a block-Toeplitz matrix, this dissertation presented simplified and unified algorithms for deadbeat input reconstruction and state estimation for MIMO systems that are d-delay invertible, that is, invertible with a delay of d steps. These algorithms do not assume the existence of a full-column-rank Markov parameter.

The assumption that the system is d-delay invertible is equivalent to the finiteness of the index η, which is the smallest delay d such that the system is d-delay invertible. Various questions concerning η remain open. Although the finiteness of η can be verified by checking n rank conditions, an easily verifiable necessary and sufficient condition for the finiteness of η is lacking. Numerical examples suggest that the existence of at least one Markov parameter with full column rank implies that η is finite; however, (3.18) shows that this condition is not necessary. Since the finiteness of η is a necessary and sufficient condition for the existence of a d-delay inverse with smallest delay, it seems reasonable to view η as the relative degree of square or tall systems. This notion may have relevance to other areas such as adaptive control.

Next, this dissertation presented retrospective cost input estimation (RCIE) and showed that this algorithm is effective for asymptotically estimating the unknown in-

put of a nonminimum-phase system. The mechanism underlying RCIE was explained in terms of an internal model of the unknown input. In particular, RCIE was shown to automatically construct an internal model of the unknown input d despite lack of knowledge of the spectrum of d and in the presence of arbitrary invariant zeros.

As an experimental application, RCIE was used to estimate the inertial acceleration of a UAV; these estimates were shown to be close to independent, onboard measurements provided by an IMU. In contrast, the techniques of [17] and [29] produced divergent estimates. In fact, the techniques in [17, 29, 39] are not applicable to this problem due to the presence of invariant zeros on the unit circle.

Finally, this dissertation showed that sensor fault diagnosis for aircraft is feasible using either state estimation alone or state estimation in conjunction with input estimation. Since the aircraft kinematics are nonlinear, the unscented Kalman filter (UKF) was used for sensor fault diagnosis in cases where the sensor measurement is modeled as an unknown state variable. In cases where the sensor measurement is modeled as an unknown input, extended retrospective cost input estimation (ERCIE) was used in conjunction with UKF to provide a combined input and state estimation technique for sensor fault diagnosis for nonlinear systems.

Five fault-detection scenarios, in particular, faulty pitot tube, vertical gyros, angle-of-attack sensor, accelerometers, and rate gyros were investigated. UKF was used for diagnosing pitot tube, vertical gyros, and angle-of-attack sensor fault detection, whereas, UKF/ERCIE was used for diagnosing rate gyros and accelerometers. In order to illustrate sensor fault detection, this dissertation used the NASA Generic Transport Model and presented cases for detecting stuck, bias, drift, and deadzone sensor faults. For all cases, it was shown that the sensor residual can be used to detect sensor faults. Furthermore, for diagnosing rate gyros, the method was demonstrated on laboratory data, where camera measurements were used to estimate the angular velocity of a quadrotor with validation based on onboard rate-gyros.

9.2 Future Work

9.2.1 Deadbeat Input Reconstruction and State Estimation

Extensions for future research include *i*) numerical techniques that avoid the need to compute Ψ_r^+ for large r; and the *ii*) development of a fully stochastic treatment of input estimation that accounts for sensor noise as well as disturbances whose reconstruction would violate the requirement $m \leq p$, as demonstrated in Example 3.6.1. Finally, extensions to nonlinear systems present a future challenge and fruitful research direction.

9.2.2 Retrospective Cost Input Estimation

Extensions for future research include the following questions. First, the covariance $V_{\hat{d}}(k)$ of $\hat{d}(k)$ is required to update the forecast error covariance P_{f} given by (5.24). An online technique for setting this covariance is desirable. Second, analysis of properties P1–P3 can provide guidelines for choosing a minimum value of n_c, which can reduce the RCIE computations. Next, alternative techniques for constructing G_{f} that are simpler than the method given in Section 5.2.3 could simplify the implementation of RCIE. Finally, stochastic analysis of RCIE remains a future objective.

9.2.3 Sensor Fault Detection

Extensions for future research include the following. Methods for detecting faults in pitot tube, vertical gyros, rate gyros, accelerometers, and angle-of-attack sensor were presented. Formulating methods for diagnosing faults for magnetometer and sideslip sensors remain open. Finally, the analysis in this dissertation did not include, however, statistical tests to determine the presence of a sensor fault in cases where the level of noise is sufficiently high that the sensor fault is not apparent. The development of such statistical measures is a candidate for future research.

APPENDICES

APPENDIX A

Rank of a Block-Toeplitz Matrix

The following result is used in the proofs of Lemma 2 and Proposition 8.

Lemma 1. Let $A \in \mathbb{R}^{n\times m}$, $B \in \mathbb{R}^{l\times m}$, $C \in \mathbb{R}^{n\times p}$, $D \in \mathbb{R}^{l\times p}$, and $E \in \mathbb{R}^{l\times q}$. Assume that A has full column rank, and $\mathcal{R}(A) \cap \mathcal{R}(C) = \{0\}$. Then

$$\mathcal{R}\left(\begin{bmatrix} A \\ B \end{bmatrix}\right) \cap \left(\begin{bmatrix} C & 0 \\ D & E \end{bmatrix}\right) = \{0\}. \tag{A.1}$$

Proof. Let

$$\begin{bmatrix} x \\ y \end{bmatrix} \in \mathcal{R}\left(\begin{bmatrix} A \\ B \end{bmatrix}\right) \cap \left(\begin{bmatrix} C & 0 \\ D & E \end{bmatrix}\right).$$

Therefore, $x \in \mathcal{R}(A)\cap\mathcal{R}(C) = \{0\}$, and thus $x = 0$. Furthermore, there exists $z \in \mathbb{R}^m$ such that $\left[\begin{smallmatrix} 0 \\ y \end{smallmatrix}\right] = \left[\begin{smallmatrix} A \\ B \end{smallmatrix}\right] z$, and thus $Az = 0$ and $y = Bz$. Since A has full column rank, it follows that $z = 0$, and thus $y = 0$. □

The following result is used in the proof of Proposition 7.

Lemma 2. Let $r \geq 2$, for all $i \in \{0, 1, \ldots, r\}$, let $H_i \in \mathbb{R}^{n \times m}$, and define the block-Toeplitz matrix

$$T_r = \begin{bmatrix} H_0 & 0 & \cdots & 0 & 0 \\ H_1 & H_0 & \ddots & 0 & 0 \\ \vdots & \ddots & \ddots & \ddots & \vdots \\ H_{r-1} & H_{r-2} & \ddots & H_0 & 0 \\ H_r & H_{r-1} & \cdots & H_1 & H_0 \end{bmatrix} = \begin{bmatrix} C_r & C_{r-1} & \cdots & C_1 & C_0 \end{bmatrix}, \tag{A.2}$$

where, for all $i \in \{0, \ldots, r\}$, C_i denotes the $(i+1)^{\text{th}}$ block column of T_r labeled from right to left. Furthermore, let $l \in \{1, \ldots, r\}$, and assume that C_l has full column rank and

$$\mathcal{R}(C_l) \cap \mathcal{R}([C_{l-1} \ \cdots \ C_0]) = \{0\}. \tag{A.3}$$

Then, $[C_r \ \cdots \ C_l]$ has full column rank, and

$$\mathcal{R}([C_r \ \cdots \ C_l]) \cap \mathcal{R}([C_{l-1} \ \cdots \ C_0]) = \{0\}. \tag{A.4}$$

Proof. Noting

$$T_l = \left[\begin{array}{c|c} & 0 \\ C_l & \\ & T_{l-1} \end{array}\right] = \left[\begin{array}{ccc|c} & T_{l-1} & & 0 \\ \hline H_l & \cdots & H_1 & H_0 \end{array}\right] \tag{A.5}$$

and using rank$C_l = m$, (A.3), and Fact 2.11.9 in [79, p. 131], it follows that

$$\begin{aligned}\text{rank}T_l &= \text{rank}C_l + \text{rank}\left[\begin{smallmatrix} 0 \\ T_{l-1} \end{smallmatrix}\right] - \dim(\mathcal{R}(C_l) \cap \mathcal{R}(\left[\begin{smallmatrix} 0 \\ T_{l-1} \end{smallmatrix}\right]) \\ &= m + \text{rank}T_{l-1} - \dim(\mathcal{R}(C_l) \cap \mathcal{R}([C_{l-1} \ \cdots \ C_0]) \\ &= m + \text{rank}T_{l-1}. \end{aligned} \tag{A.6}$$

Similarly, since

$$T_{l+1} = \left[\begin{array}{c|c} C_{l+1} & \begin{matrix} 0 \\ T_l \end{matrix} \end{array}\right] = \left[\begin{array}{c|c|c} C_l & \begin{matrix} 0 \\ T_{l-1} \end{matrix} & 0 \\ \hline H_{l+1} & H_l \ \cdots \ H_1 & H_0 \end{array}\right], \tag{A.7}$$

it follows from rank$C_{l+1} = m$, (A.6), and (A.7) that

$$\begin{aligned}\text{rank}T_{l+1} &= \text{rank}C_{l+1} + \text{rank}T_l - \dim\left(\mathcal{R}(C_{l+1}) \cap \mathcal{R}\left(\begin{bmatrix} 0 \\ T_l \end{bmatrix}\right)\right) \\ &= 2m + \text{rank}T_{l-1} - \dim\left(\mathcal{R}\left(\begin{bmatrix} C_l \\ H_{l+1} \end{bmatrix}\right) \cap \mathcal{R}\left(\left[\begin{array}{c|c} \begin{matrix} 0 \\ T_{l-1} \end{matrix} & \begin{matrix} 0 \\ 0 \end{matrix} \\ \hline H_l \ \cdots \ H_1 & H_0 \end{array}\right]\right)\right). \end{aligned} \tag{A.8}$$

Since $\mathcal{R}(C_l) \cap \mathcal{R}(\left[\begin{smallmatrix} 0 \\ T_{l-1} \end{smallmatrix}\right]) = \{0\}$ and C_l has full column rank, it follows from Lemma 1 that

$$\mathcal{R}\left(\begin{bmatrix} C_l \\ H_{l+1} \end{bmatrix}\right) \cap \mathcal{R}\left(\left[\begin{array}{c|c} \begin{matrix} 0 \\ T_{l-1} \end{matrix} & \begin{matrix} 0 \\ 0 \end{matrix} \\ \hline H_l \ \cdots \ H_1 & H_0 \end{array}\right]\right) = \{0\}. \tag{A.9}$$

Combining (A.9) with (A.8) yields

$$\text{rank}T_{l+1} = 2m + \text{rank}T_{l-1}. \tag{A.10}$$

Similarly, since

$$T_{l+2} = \left[\begin{array}{c|c} C_{l+2} & \begin{array}{c} 0 \\ T_{l+1} \end{array} \end{array}\right] = \left[\begin{array}{c|c|c} \begin{array}{c} C_{l+1} \\ \\ \hline H_{l+2} \end{array} & \begin{array}{c} 0 \\ T_l \\ \hline H_{l+1} \quad \cdots \quad H_1 \end{array} & \begin{array}{c} 0 \\ \\ \hline H_0 \end{array} \end{array}\right], \tag{A.11}$$

it follows from $\text{rank}C_{l+2} = m$ and (A.10) that

$$\begin{aligned} \text{rank}T_{l+2} &= \text{rank}C_{l+2} + \text{rank}T_{l+1} - \dim\left(\mathcal{R}(C_{l+2}) \cap \mathcal{R}\left(\begin{bmatrix} 0 \\ T_{l+1} \end{bmatrix}\right)\right) \\ &= 3m + \text{rank}T_{l-1} - \dim\left(\mathcal{R}\left(\begin{bmatrix} C_{l+1} \\ H_{l+2} \end{bmatrix}\right) \cap \mathcal{R}\left(\left[\begin{array}{c|c} \begin{array}{c} 0 \\ T_l \\ \hline H_{l+1} \quad \cdots \quad H_1 \end{array} & \begin{array}{c} 0 \\ 0 \\ \hline H_0 \end{array} \end{array}\right]\right)\right). \end{aligned} \tag{A.12}$$

It follows from (A.7) and (A.9) that $\mathcal{R}(C_{l+1}) \cap \mathcal{R}(\left[\begin{smallmatrix} 0 \\ T_l \end{smallmatrix}\right]) = \{0\}$, and, since C_{l+1} has full column rank, it follows from Lemma 1 that

$$\mathcal{R}\left(\begin{bmatrix} C_{l+1} \\ H_l \end{bmatrix}\right) \cap \mathcal{R}\left(\left[\begin{array}{c|c} \begin{array}{c} 0 \\ T_l \\ \hline H_{l+1} \quad \cdots \quad H_1 \end{array} & \begin{array}{c} 0 \\ 0 \\ \hline H_0 \end{array} \end{array}\right]\right) = \{0\}. \tag{A.13}$$

Combining (A.13) with (A.12) yields

$$\text{rank}T_{l+2} = 3m + \text{rank}T_{l-1}. \tag{A.14}$$

By similar arguments, it follows that, for all $k \geq 1$,

$$\text{rank}T_{l+k} = (k+1)m + \text{rank}T_{l-1}, \tag{A.15}$$

which, with $k = r - l$, yields

$$\text{rank}T_r = (r-l+1)m + \text{rank}T_{l-1}. \tag{A.16}$$

Noting

$$T_r = \left[\begin{array}{ccc|c} C_r & \cdots & C_l & 0 \\ & & & T_{l-1} \end{array}\right] = \left[\begin{array}{ccc|ccc} C_r & \cdots & C_l & C_{l-1} & \cdots & C_0 \end{array}\right], \tag{A.17}$$

it follows that

$$\text{rank}T_r = \text{rank}\left[C_r \ \cdots \ C_l\right] + \text{rank}T_{l-1} - \dim\left(\mathcal{R}([C_r \ \cdots \ C_l]) \cap \mathcal{R}([C_{l-1} \ \cdots \ C_0])\right). \tag{A.18}$$

Combining (A.18) with (A.16) yields

$$0 \leq \dim\left(\mathcal{R}([C_r \ \cdots \ C_l]) \cap \mathcal{R}([C_{l-1} \ \cdots \ C_0])\right) = \text{rank}\left[C_r \ \cdots \ C_l\right] - (r-l+1)m \leq 0,$$

which implies that $[C_r \ \cdots \ C_l]$ has full column rank and (A.4) holds. □

APPENDIX B

Generalized Inverse of a Partitioned Matrix

The following result is used in the proofs of Theorem 2, Theorem 3, and Theorem 4.

Lemma 3. Let $A \in \mathbb{R}^{n\times m}$ and $B \in \mathbb{R}^{n\times l}$, define $C \triangleq (I - AA^{+})B$ and $D \triangleq (I - BB^{+})A$, and assume that $\mathcal{R}(A) \cap \mathcal{R}(B) = \{0\}$. Then, $C^{+}A = 0$, $D^{+}B = 0$, $C^{+}B = B^{+}B$, $D^{+}A = A^{+}A$,

$$[A\ B]^{+} = \begin{bmatrix} D^{+} \\ C^{+} \end{bmatrix}, \quad [A\ B]^{+}[A\ B] = \begin{bmatrix} A^{+}A & 0 \\ 0 & B^{+}B \end{bmatrix}. \tag{B.1}$$

Proof. The result follows from Theorem 1, line 6 on page 21, and line 7 on page 22 of [100]. □

APPENDIX C

Pseudo Algorithm for Retrospective Cost Input Estimation

Choose $n_c \geq 1$, $n_\mathrm{f} \geq 1$, $0 < \lambda \leq 1$, R_z, R_d, R_θ, and $V_{\hat{d}}$.
$k_n = \max(n_c, n_\mathrm{f})$;
Initialize: $\hat{d}(0) = 0$; $x_\mathrm{da}(0) = \mathbf{E}[x(0)]$; $P_\mathrm{da}(0) = \mathbf{E}[(x(0) - x_\mathrm{da}(0))^\mathrm{T}(x(0) - x_\mathrm{da}(0))]$; $\theta(k_n) = 0_{l_\theta}$; $P(k_n - 1) = R_\theta^{-1}$;
for $k = 1$ **to** N **do**
▷ Forecast Step
    $x_\mathrm{fc}(k) = A(k-1)x_\mathrm{da}(k-1) + B(k-1)u(k-1) + G(k-1)\hat{d}(k-1)$;
    $z(k) = C(k)x_\mathrm{fc}(k) - y(k)$;
▷ Input Estimation
    if $k \geq k_n$ **do**
        $\Phi(k) = \left[\hat{d}(k-1)^\mathrm{T} \cdots \hat{d}(k-n_\mathrm{c})^\mathrm{T}\, z(k)^\mathrm{T} \cdots z(k-n_\mathrm{c})^\mathrm{T}\right] \otimes I_{l_d}$;
        $\bar{A}(k-1) = A(k-1)[I_{l_x} + K_\mathrm{da}(k-1)C(k-1)]$;
        $\tilde{H}(k) = \begin{bmatrix} C(k)G(k-1) & H_2(k) & \cdots & H_{n_\mathrm{f}}(k) \end{bmatrix}$, where $H_i(k) = C(k)\left(\prod_{j=1}^{i-1} \bar{A}(k-j)\right) G(k-i)$;
        $\Phi_\mathrm{f}(k) = \tilde{H}(k)\left[\Phi(k-1)^\mathrm{T} \quad \cdots \quad \Phi(k-n_\mathrm{f})^\mathrm{T}\right]^\mathrm{T}$;
        $\hat{d}_\mathrm{f}(k) = \tilde{H}(k)\left[\hat{d}(k-1)^\mathrm{T} \quad \cdots \quad \hat{d}(k-n_\mathrm{f})^\mathrm{T}\right]^\mathrm{T}$;
        $\tilde{\Phi}(k) = \begin{bmatrix} \Phi_\mathrm{f}(k)^\mathrm{T} & \Phi(k)^\mathrm{T} \end{bmatrix}^\mathrm{T}$;
        $\tilde{R}(k) = \mathrm{blockdiag}(R_z, R_d)$;
        $\tilde{z}(k) = \begin{bmatrix} [z(k) - \hat{d}_\mathrm{f}(k)]^\mathrm{T} & 0_{1\times l_d} \end{bmatrix}^\mathrm{T}$;
        $\Gamma(k) = [\lambda\tilde{R}(k)^{-1} + \tilde{\Phi}(k)P(k-1)\tilde{\Phi}(k)^\mathrm{T}]^{-1}$;
        $P(k) = \lambda^{-1}[P(k-1) - P(k-1)\tilde{\Phi}(k)^\mathrm{T}\Gamma(k)\tilde{\Phi}(k)P(k-1)]$;
        $\theta(k) = \theta(k-1) - P(k-1)\tilde{\Phi}(k)^\mathrm{T}\Gamma(k)[\tilde{\Phi}(k)\theta(k-1) + \tilde{z}(k)]$;
        $\hat{d}(k) = \Phi(k)\theta(k)$; ▷ Input estimate.
    else do
        $\hat{d}(k) = \hat{d}(0)$;
    end if
▷ Data-Assimilation Step
        $P_\mathrm{f}(k) = A(k-1)P_\mathrm{da}(k-1)A(k-1)^\mathrm{T} + V_1(k-1) + V_{\hat{d}}(k-1)$;
        $K_\mathrm{da}(k) = -P_\mathrm{f}(k)C(k)^\mathrm{T}[C(k)P_\mathrm{f}(k)C(k)^\mathrm{T} + V_2(k)]^{-1}$;
    $P_\mathrm{da}(k) = [I_{l_x} + K_\mathrm{da}(k)C(k)]P_\mathrm{f}(k)$;
    $x_\mathrm{da}(k) = x_\mathrm{fc}(k) + K_\mathrm{da}(k)z(k)$; ▷ State estimate.
end for

BIBLIOGRAPHY

BIBLIOGRAPHY

[1] D. Simon, *Optimal State Estimation: Kalman, H_∞, and Nonlinear Approaches*. John Wiley & Sons, 2006.

[2] F. L. Lewis, L. Xie, and D. Popa, *Optimal and Robust Estimation: With an Introduction to Stochastic Control Theory*. CRC Press, 2007.

[3] J. L. Crassidis and J. L. Junkins, *Optimal Estimation of Dynamic Systems*. CRC Press, 2011.

[4] J. D. Glover, "The Linear Estimation of Completely Unknown Signals," *IEEE Trans. Autom. Contr.*, vol. 14, no. 6, pp. 766–767, 1969.

[5] P. K. Kitanidis, "Unbiased Minimum-Variance Linear State Estimation," *Automatica*, vol. 23, no. 6, pp. 775–778, 1987.

[6] M. Darouach and M. Zasadzinski, "Unbiased Minimum Variance Estimation for Systems with Unknown Exogenous Inputs," *Automatica*, vol. 33, no. 4, pp. 717–719, 1997.

[7] M. Hou and R. J. Patton, "Optimal Filtering for Systems with Unknown Inputs," *IEEE Trans. Autom. Contr.*, vol. 43, no. 3, pp. 445–449, 1998.

[8] M. E. Valcher, "State Observers for Discrete-Time Linear Systems with Unknown Inputs," *IEEE Trans. Autom. Contr.*, vol. 44, no. 2, pp. 397–401, 1999.

[9] M. Sain and J. L. Massey, "Invertibility of Linear Time-Invariant Dynamical Systems," *IEEE Trans. Autom. Contr.*, vol. 14, pp. 141–149, 1969.

[10] J. L. Massey and M. Sain, "Inverses of Linear Sequential Circuits," *IEEE Trans. Computers*, vol. 17, pp. 330–337, 1968.

[11] A. Willsky, "On the Invertibility of Linear Systems," *IEEE Trans. Autom. Contr.*, vol. 19, pp. 272–274, 1974.

[12] M. Corless and J. Tu, "State and Input Estimation for a Class of Uncertain Systems," *Automatica*, vol. 34, no. 6, pp. 757–764, 1998.

[13] M. Hou and R. J. Patton, "Input Observability and Input Reconstruction," *Automatica*, vol. 34, no. 6, pp. 789–794, 1998.

[14] C.-S. Hsieh, "Robust Two-Stage Kalman Filters for Systems with Unknown Inputs," *IEEE Trans. Autom. Contr.*, vol. 45, no. 12, pp. 2374–2378, 2000.

[15] Y. Xiong and M. Saif, "Unknown Disturbance Inputs Estimation Based on a State Functional Observer Design," *Automatica*, vol. 39, pp. 1389–1398, 2003.

[16] T. Floquet and J. P. Barbot, "State and Unknown Input Estimation for Linear Discrete-Time Systems," *Automatica*, vol. 42, pp. 1883–1889, 2006.

[17] S. Gillijns and B. De Moor, "Unbiased Minimum-Variance Input and State Estimation for Linear Discrete-Time Systems," *Automatica*, vol. 43, no. 1, pp. 111–116, 2007.

[18] C.-C. Ho and C.-K. Ma, "Active Vibration Control of Structural Systems by a Combination of the Linear Quadratic Gaussian and Input Estimation Approaches," *J. Sound Vibr.*, vol. 301, no. 3, pp. 429–449, 2007.

[19] C.-S. Hsieh, "Extension of Unbiased Minimum-Variance Input and State Estimation for Systems with Unknown Inputs," *Automatica*, vol. 45, no. 9, pp. 2149–2153, 2009.

[20] H. Khaloozadeh and A. Karsaz, "Modified Input Estimation Technique for Tracking Manoeuvring Targets," *Radar, Sonar & Navigation, IET*, vol. 3, no. 1, pp. 30–41, 2009.

[21] R. Orjuela, B. Marx, J. Ragot, and D. Maquin, "On the Simultaneous State and Unknown Input Estimation of Complex Systems via a Multiple Model Strategy," *Contr. Th. & App., IET*, vol. 3, no. 7, pp. 877–890, 2009.

[22] H. Palanthandalam-Madapusi and D. S. Bernstein, "A Subspace Algorithm for Simultaneous Identification and Input Reconstruction," *Int. J. Adaptive Contr. Sig. Proc.*, vol. 23, pp. 1053–1069, 2009.

[23] M.-S. Chen and C.-C. Chen, "Unknown Input Observer for Linear Non-Minimum Phase Systems," *J. Franklin Inst.*, vol. 347, no. 2, pp. 577–588, 2010.

[24] S. Kirtikar, H. Palanthandalam-Madapusi, E. Zattoni, and D. S. Bernstein, "l-Delay Input and Initial-State Reconstruction for Discrete-Time Linear Systems," *Cir., Sys., Sig. Proc.*, vol. 30, no. 1, pp. 233–262, 2011.

[25] H. Fang, Y. Shi, and J. Yi, "On Stable Simultaneous Input and State Estimation for Discrete-Time Linear Systems," *Int. J. Adaptive Contr. Sig. Proc.*, vol. 25, no. 8, pp. 671–686, 2011.

[26] H. Fang, R. A. de Callafon, and J. Cortes, "Simultaneous Input and State Estimation for Nonlinear Systems with Applications to Flow Field Estimation," *Automatica*, vol. 49, no. 9, pp. 2805–2812, 2013.

[27] J. Yang, F. Zhu, and X. Sun, "State Estimation and Simultaneous Unknown Input and Measurement Noise Reconstruction Based on Associated Observers," *Int. J. Adaptive Contr. Sig. Proc.*, vol. 27, no. 10, pp. 846–858, 2013.

[28] J. Sanchez and H. Benaroya, "Review of Force Reconstruction Techniques," *J. Sound Vibr.*, vol. 333, no. 14, pp. 2999–3018, 2014.

[29] S. Z. Yong, M. Zhu, and E. Frazzoli, "A Unified Filter for Simultaneous Input and State Estimation of Linear Discrete-Time Stochastic Systems," *Automatica*, vol. 63, pp. 321–329, 2016.

[30] P. Lu, E.-J. van Kampen, C. C. de Visser, and Q. Chu, "Framework for State and Unknown Input Estimation of Linear Time-Varying Systems," *Automatica*, vol. 73, pp. 145–154, 2016.

[31] A. Chakrabarty, R. Ayoub, S. H. Żak, and S. Sundaram, "Delayed Unknown Input Observers for Discrete-Time Linear Systems with Guaranteed Performance," *Sys. Contr. Lett.*, vol. 103, pp. 9–15, 2017.

[32] R. Rajamani, Y. Wang, G. D. Nelson, R. Madson, and A. Zemouche, "Observers with Dual Spatially Separated Sensors for Enhanced Estimation: Industrial, Automotive, and Biomedical Applications," *IEEE Contr. Sys. Mag.*, vol. 37, no. 3, pp. 42–58, 2017.

[33] L. Silverman, "Inversion of Multivariable Linear Systems," *IEEE Trans. Autom. Contr.*, vol. 14, pp. 270–276, 1969.

[34] Y. S. Shmaliy, S. Zhao, and C. K. Ahn, "Unbiased Finite Impulse Response Filtering," *IEEE Contr. Sys. Mag.*, vol. 37, no. 5, pp. 70–89, 2017.

[35] C.-S. Hsieh and F.-C. Chen, "Optimal Solution of the Two-Stage Kalman Estimator," *IEEE Trans. Autom. Contr.*, vol. 44, no. 1, pp. 194–199, 1999.

[36] H. J. Palanthandalam-Madapusi and D. S. Bernstein, "Unbiased Minimum-Variance Filtering for Input Reconstruction," *Proc. Amer. Contr. Conf.*, pp. 11–13, NewYork, 2007.

[37] A. Termehchy and A. Afshar, "A Novel Design of Unknown Input Observer for Fault Diagnosis in Non-minimum Phase Systems," *IFAC Proceedings Volumes, 19th IFAC World Congress*, vol. 47, no. 3, pp. 8552–8557, 2014.

[38] A. Ansari and D. S. Bernstein, "Adaptive Input Estimation for Nonminimum-Phase Discrete-Time Systems," *Proc. Contr. Dec. Conf.*, pp. 1159–1164, Las Vegas, 2016.

[39] G. Marro and E. Zattoni, "Unknown-State, Unknown-Input Reconstruction in Discrete-Time Nonminimum-Phase Systems: Geometric Methods," *Automatica*, vol. 46, no. 5, pp. 815–822, 2010.

[40] A. M. D'Amato and D. S. Bernstein, "Adaptive Forward-Propagating Input Reconstruction for Nonminimum-Phase Systems," *Proc. Amer. Conf. Contr.*, pp. 598–603, Montreal, 2012.

[41] R. Gupta, A. M. D'Amato, A. A. Ali, and D. S. Bernstein, "Retrospective-Cost-Based Adaptive State Estimation and Input Reconstruction for a Maneuvering Aircraft with Unknown Acceleration," in *AIAA Guid. Nav. Contr. Conf.*, 2012, AIAA-2012-4600-398.

[42] A. A. Ali, A. Goel, A. J. Ridley, and D. S. Bernstein, "Retrospective-Cost-Based Adaptive Input and State Estimation for the Ionosphere–Thermosphere," *J. Aerosp. Infor. Sys.*, vol. 12, pp. 767–783, 2015.

[43] L. Han, Z. Ren, and D. S. Bernstein, "Maneuvering target tracking using retrospective-cost input estimation," *IEEE Trans. Aerosp. Elec. Sys.*, vol. 52, no. 5, pp. 2495–2503, 2016.

[44] A. Ansari and D. S. Bernstein, "Aircraft Sensor Fault Detection Using State and Input Estimation," *Proc. Amer. Contr. Conf.*, pp. 5951–5956, Boston, 2016.

[45] ——, "Estimation of Angular Velocity and Rate-Gyro Noise for Sensor Health Monitoring," *Proc. Amer. Contr. Conf.*, pp. 128–133, Seattle, 2017.

[46] ——, "Adaptive non-Bayesian state estimation," *Proc. Amer. Contr. Conf.*, pp. 6977–6982, Boston, 2016.

[47] Y. Rahman, A. Xie, J. B. Hoagg, and D. S. Bernstein, "A Tutorial and Overview of Retrospective Cost Adaptive Control," in *Proc. Amer. Contr. Conf.*, Boston, MA, July 2016, pp. 3386–3409.

[48] Y. Rahman, A. Xie, and D. S. Bernstein, "Retrospective Cost Adaptive Control: Pole Placement, Frequency Response, and Connections with LQG Control," *IEEE Contr. Sys. Mag.*, vol. 37, pp. 28–69, October 2017.

[49] A. Ansari and D. S. Bernstein, "Retrospective Cost Adaptive Control of the Generic Transport Model Under Uncertainty and Failure," *Journal of Aerospace Information Systems*, vol. 14, no. 3, pp. 123–174, 2017.

[50] A. Ansari, N. Zhang, and D. Bernstein, "Retrospective Cost Adaptive PID Control of Quadcopter/Fixed-Wing Mode Transition in a VTOL Aircraft," in *2018 AIAA Guidance, Navigation, and Control Conference*, 2018, p. 1838.

[51] A. Ansari and D. Bernstein, "Retrospective Cost Adaptive Control of the Generic Transport Model under Abrupt Faults," in *2018 AIAA Guidance, Navigation, and Control Conference*, 2018, p. 1125.

[52] A. Ansari, A. Prach, and D. S. Bernstein, "Adaptive Trim and Trajectory Following for a Tilt-Rotor Tricopter," in *American Control Conference (ACC), 2017*. IEEE, 2017, pp. 1109–1114.

[53] A. Ansari and D. S. Bernstein, "Adaptive Control of an Aircraft with Uncertain Nonminimum-Phase Dynamics," in *Proc. Amer. Contr. Conf.*, Chicago, IL, July 2015, pp. 844–849.

[54] A. Ansari, M. J. Yu, and D. S. Bernstein, "Exploration and Mapping of an Unknown Flight Envelope," in *Proc. Dyn. Sys. Contr. Conf.*, Los Angeles, CA, 2014, pp. 523–528.

[55] Y. T. Chan, A. G. C. Hu, and J. B. Plant, "A Kalman Filter Based Tracking Scheme with Input Estimation," *IEEE Trans. Aerosp. Elec. Sys.*, vol. AES-15, no. 2, pp. 237–244, 1979.

[56] P. Bogler, "Tracking a Maneuvering Target Using Input Estimation," *IEEE Trans. Aerosp. Elec. Sys.*, vol. AES-23, no. 3, pp. 298–310, 1987.

[57] B. W. Ahn, J. W. Choi, T. H. Fang, and T. L. Song, "A Modified Variable Dimension Filter with Input Estimation for Maneuvering Target Tracking," in *Proc. Amer. Contr. Conf.*, 2003, pp. 1266–1271.

[58] C. Yang and E. Blasch, "Characteristic Errors of the IMM Algorithm under Three Maneuver Models for an Accelerating Target," in *11th Int. Conf. Infor. Fusion*. IEEE, 2008, pp. 1–8.

[59] X. R. Li and V. P. Jilkov, "Survey of Maneuvering Target Tracking. Part II: Motion Models of Ballistic and Space Targets," *IEEE Trans. Aerosp. Elec. Sys.*, vol. 46, no. 1, pp. 96–119, 2010.

[60] Y. Wang, S. Sun, and L. Li, "Adaptively Robust Unscented Kalman Filter for Tracking a Maneuvering Vehicle," *J. Guid. Contr. Dyn.*, vol. 37, pp. 1696–1701, 2014.

[61] R. Isermann, "Process fault detection based on modeling and estimation methods-a survey," *Automatica*, vol. 20, pp. 387–404, 1984.

[62] A. M. Agogino, S. Srinivas, and K. M. Schneider, "Multiple sensor expert system for diagnostic reasoning, monitoring and control of mechanical systems," *Mech. Sys. Sig. Proc.*, vol. 2, pp. 165–185, 1988.

[63] D. Zhou and P. Frank, "Fault diagnostics and fault tolerant control," *IEEE Trans. Aerosp. Elec. Sys.*, vol. 34, pp. 420–427, 1998.

[64] J. Gertler, *Fault Detection and Diagnosis in Engineering Systems*. CRC press, 1998.

[65] R. Isermann, *Fault-Diagnosis Systems: An Introduction from Fault Detection to Fault Tolerance*. Springer, 2006.

[66] Y. Zhang and J. Jiang, "Bibliographical review on reconfigurable fault-tolerant control systems," *Ann. Rev. Contr.*, vol. 32, pp. 229–252, 2008.

[67] P. Freeman, P. Seiler, and G. J. Balas, "Air data system fault modeling and detection," *Contr. Engr. Pract.*, vol. 21, pp. 1290–1301, 2013.

[68] S. Gururajan, M. Fravolini, M. Rhudy, A. Moschitta, and M. Napolitano, "Evaluation of sensor failure detection, identification and accommodation (SFDIA) performance following common-mode failures of pitot tubes," *SAE Technical Paper*, Sept 2014.

[69] M. L. Fravolini, M. Rhudy, S. Gururajan, S. Cascianelli, and M. Napolitano, "Experimental evaluation of two pitot free analytical redundancy techniques for the estimation of the airspeed of an uav," *SAE Int. Jr. of Aerosp.*, vol. 7, pp. 109–116, 2014.

[70] M. B. Rhudy, M. L. Fravolini, Y. Gu, M. R. Napolitano, S. Gururajan, and H. Chao, "Aircraft model-independent airspeed estimation without pitot tube measurements," *Aerosp. and Elec. Sys., IEEE Transactions on*, vol. 51, pp. 1980–1995, 2015.

[71] K. F. Aljanaideh and D. S. Bernstein, "Aircraft Sensor Health Monitoring Based on Transmissibility Operators," *Journal of Guidance, Control, and Dynamics*, vol. 38, no. 8, pp. 1492–1495, 2015.

[72] A. Ansari and D. S. Bernstein, "Input Estimation for Nonminimum-Phase Systems with Application to Acceleration Estimation for a Maneuvering Vehicle," *IEEE Trans. Contr. Sys. Tech.*, 2018, available online.

[73] E. A. Wan and R. Van Der Merwe, "The Unscented Kalman filter for Nonlinear Estimation," in *Adaptive Systems for Signal Processing, Communications, and Control Symposium 2000. AS-SPCC. The IEEE 2000.* IEEE, 2000, pp. 153–158.

[74] S. J. Julier and J. K. Uhlmann, "Unscented Filtering and Nonlinear Estimation," *Proceedings of the IEEE*, vol. 92, no. 3, pp. 401–422, 2004.

[75] S. Z. Yong, M. Zhu, and E. Frazzoli, "Simultaneous input and state estimation with a delay," in *Decision and Control (CDC), 2015 IEEE 54th Annual Conference on.* IEEE, 2015, pp. 468–475.

[76] C.-S. Hsieh, "Unbiased minimum-variance input and state estimation for systems with unknown inputs: A system reformation approach," *Automatica*, vol. 84, pp. 236–240, 2017.

[77] S. Sundaram and C. N. Hadjicostis, "Delayed Observers for Linear Systems with Unknown Inputs," *IEEE Transactions on Automatic Control*, vol. 52, no. 2, pp. 334–339, 2007.

[78] C.-T. Chen, *Linear System Theory and Design.* Oxford University Press, Inc., 1998.

[79] D. S. Bernstein, *Matrix Mathematics: Theory, Fact, and Formulas*, 2nd ed. Princeton: Princeton University Press, 2009.

[80] R. E. Kalman, "A New Approach to Linear Filtering and Prediction Problems," *J. Basic Eng.*, vol. 82, no. 1, pp. 35–45, 1960.

[81] R. E. Kalman and R. S. Bucy, "New Results in Linear Filtering and Prediction Theory," *J. Basic Eng.*, vol. 83, no. 1, pp. 95–108, 1961.

[82] B. Friedland, "Treatment of Bias in Recursive Filtering," *IEEE Trans. Autom. Contr.*, vol. 14, no. 4, pp. 359–367, 1969.

[83] K. C. Veluvolu and Y. C. Soh, "High-Gain Observers with Sliding Mode for State and Unknown Input Estimations," *IEEE Trans. Ind. Elec.*, vol. 56, no. 9, pp. 3386–3393, 2009.

[84] B. Xiao, S. Yin, and O. Kaynak, "Tracking Control of Robotic Manipulators with Uncertain Kinematics and Dynamics," *IEEE Trans. Ind. Elec.*, vol. 63, no. 10, pp. 6439–6449, 2016.

[85] B. Xiao and S. Yin, "Velocity-Free Fault-Tolerant and Uncertainty Attenuation Control for a Class of Nonlinear Systems," *IEEE Trans. Ind. Elec.*, vol. 63, no. 7, pp. 4400–4411, 2016.

[86] B. A. Francis and W. M. Wonham, "The Internal Model Principle of Control Theory," *Automatica*, vol. 12, no. 5, pp. 457–465, 1976.

[87] J. L. Crassidis and J. L. Junkins, *Optimal Estimation of Dynamic Systems*, 2nd ed. Chapman and Hall, 2011.

[88] B. O. S. Teixeira, M. A. Santillo, R. S. Erwin, and D. S. Bernstein, "Spacecraft Tracking Using Sampled-Data Kalman Filters: An Illustrative Application of Extended and Unscented Estimators," *IEEE Contr. Sys. Mag.*, vol. 28, pp. 78–94, August 2017.

[89] N. Das, R. Bhattacharya, R. P. Ghosh, N. Buha, and B. Mallick, "Optimal Transport Based Tracking of Space Objects in Cylindrical Manifolds," preprint.

[90] D. P. Lubey, D. J. Scheeres, and R. S. Erwin, "Maneuver detection and reconstruction of stationkeeping spacecraft at geo using the optimal control-based estimator," in *Proc. IFAC Workshop Adv. Contr. Nav. Autonomous Aero. Veh.*, 2015, pp. 216–221.

[91] M. M. Moe, S. D. Wallace, and K. Moe, "Refinements in determining satellite drag coefficients-method for resolving density discrepancies," *Journal of guidance, control, and dynamics*, vol. 16, no. 3, pp. 441–445, 1993.

[92] E. M. Gaposchkin, "Calculation of satellite drag coefficients," MASSACHUSETTS INST OF TECH LEXINGTON LINCOLN LAB, Tech. Rep., 1994.

[93] C. A. McLaughlin, S. Mance, and T. Lichtenberg, "Drag coefficient estimation in orbit determination," *The Journal of the Astronautical Sciences*, vol. 58, no. 3, pp. 513–530, 2011.

[94] D. A. Vallado and D. Finkleman, "A critical assessment of satellite drag and atmospheric density modeling," *Acta Astronautica*, vol. 95, pp. 141–165, 2014.

[95] L. Han, A. Xie, Z. Ren, and D. S. Bernstein, "Maneuvering Target Tracking with Unknown Acceleration Using Retrospective-Cost-Based Adaptive Input and State Estimation," in *Proc. 34th Chinese Contr. Conf.*, 2015, pp. 5029–5034.

[96] T. Jordan, W. Langford, C. Belcastro, J. Foster, G. Shah, G. Howland, and R. Kidd, "Development of a Dynamically Scaled Generic Transport Model Testbed for Flight Research Experiments," *AUVSI Unmanned Unlimited, Arlington, VA*, 2004.

[97] R. M. Bailey, R. W. Hostetler, K. N. Barnes, C. M. Belcastro, and C. M. Belcastro, "Experimental Validation: Subscale Aircraft Ground Facilities and Integrated Test Capability," in *Proc. AIAA Guid. Nav. Cont. Conf.*, San Francisco, CA, 2005, p. 110, AIAA-2005-6433.

[98] T. L. Jordan and R. M. Bailey, "NASA Langleys AirSTAR Testbed: A Subscale Flight Test Capability for Flight Dynamics and Control System Experiments," in *Proc. AIAA Guid. Nav. Cont. Conf.*, Honolulu, HI, 2008, pp. 18–21, AIAA-2008-6660.

[99] K. Cunningham, D. E. Cox, D. G. Murri, and S. E. Riddick, "A Piloted Evaluation of Damage Accommodating Flight Control Using a Remotely Piloted Vehicle," in *Proc. AIAA Guid. Nav. Cont. Conf.*, Portland, OR, 2011, AIAA-2011-6451.

[100] J. K. Baksalary and O. M. Baksalary, "Particular Formulae for the Moore–Penrose Inverse of a Columnwise Partitioned Matrix," *Lin. Alg. Appl.*, vol. 421, no. 1, pp. 16–23, 2007.